UNIVERSITY OF PALERMO
PHD JOINT PROGRAM:
UNIVERSITY OF CATANIA - UNIVERSITY OF MESSINA
XXXVII CYCLE

DOCTORAL THESIS

Non-linear heat transfer beyond Fourier's Law: analytical and numerical investigations

Author:
Carmelo Filippo MUNAFÓ

Supervisor:
Prof. Patrizia ROGOLINO

A thesis submitted in fulfillment of the requirements for the degree of Doctor of Mathematics

in

Mathematics and Computational Sciences

Declaration of Authorship

I, Carmelo Filippo MUNAFÓ, declare that this thesis titled, "Non-linear heat transfer beyond Fourier's Law: analytical and numerical investigations" and the work presented in it are my own. I confirm that:

- This work was done wholly or mainly while in candidature for a research degree at this University.
- Where any part of this thesis has previously been submitted for a degree or any other qualification at this University or any other institution, this has been clearly stated.
- Where I have consulted the published work of others, this is always clearly attributed.
- Where I have quoted from the work of others, the source is always given. With the exception of such quotations, this thesis is entirely my own work.
- I have acknowledged all main sources of help.
- Where the thesis is based on work done by myself jointly with others, I have made clear exactly what was done by others and what I have contributed myself.

Signed: 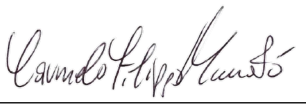

Date: 12/11/2024

"Great is the confusion under the sky, so the situation is excellent!"

Mao Zedong

UNIVERSITY OF PALERMO

Abstract

Department of Mathematics and Computer Sciences

Doctor of Mathematics

Non-linear heat transfer beyond Fourier's Law: analytical and numerical investigations

by Carmelo Filippo MUNAFÓ

Recent advances in modern engineering technology have highlighted the limitations of classical models traditionally applied in various fields, such as Fourier's law for heat conduction, Fick's law for diffusion, and Newton's law for viscous flow. These models, while widely accepted, may no longer be adequate for describing certain phenomena, especially in light of the technological progress in micro- and nano-scale devices. At low temperatures, and for processes with very short time scales, deviations from classical laws become increasingly evident. For instance, heat conduction in heterogeneous materials—such as rocks, layered structures, foams, and 3D-printed samples—can be better described using models that go beyond Fourier's law.

The necessity of explaining these phenomena has led to the development of alternative models, a process that began in the mid-20th century and continues to evolve today. Numerous experimental studies have revealed considerable discrepancies between classical laws and observed results. One notable issue with classical theories is that they lead to parabolic-type partial differential equations, which imply that perturbations propagate at infinite velocity—a result that contradicts both experimental evidence and theoretical expectations, as perturbations should propagate at finite speeds. This inconsistency can be addressed by considering the relaxation times of fluxes (such as thermal, diffusion, and momentum fluxes), often referred to as dissipative fluxes. However, the evolution equations for such fluxes are incompatible with classical thermodynamic theories, as they may lead to negative entropy production under certain conditions. To resolve this, the field of Extended Thermodynamics provides a thermodynamically consistent framework for these extended models. This dissertation focuses on heat conduction models that extend beyond Fourier's law, specifically non-Fourier heat conduction models. The primary aim is to explore generalizations of Fourier's law by introducing temperature-dependent material parameters, such as thermal conductivity and relaxation time. These assumptions are crucial for accurately modeling phenomena at low temperatures or for small-scale systems, where thermal conductivity is known to vary with temperature. The physical and mathematical foundations of these extended heat conduction models—such as the Cattaneo and Guyer-Krumhansl models—are discussed within the framework of non-equilibrium thermodynamics, providing a powerful basis for non-linear extensions. The study of these non-linear effects is driven by the rapid advancement of technology, which increasingly demands a description of fast and high-frequency processes where such effects become significant. As a result, the design of future micro- and nano-scale devices poses considerable challenges. Understanding heat transport at these scales and proposing modified versions of classical

equations—consistent with the second law of thermodynamics—is crucial for facilitating the design of these devices.

The deviation from Fourier's law is also evident at low temperatures and in micro/nano-devices, where phenomena such as second sound behavior emerge. Under these extreme conditions, both thermal conductivity and relaxation time become temperature-dependent, necessitating their inclusion in the Maxwell-Cattaneo-Vernotte model. The effects of these nonlinearities are explored through numerical solutions of one- and two-dimensional heat pulse experiments, using a staggered field finite difference method.

Furthermore, deviations from Fourier's law are also observed in inhomogeneous materials, such as rocks and metal foams. The Fourier hierarchy derived from the Guyer-Krumhansl equation provides a physical interpretation of these observed phenomena. Initially, we investigate the impact of nonlinear thermal conductivity and relaxation time by solving the one-dimensional Guyer-Krumhansl equation. We then focus on the implications of whirling heat current density, solving the two-dimensional Guyer-Krumhansl equation with space- and time-dependent heat pulse boundary conditions, again using a staggered scheme. Special emphasis is placed on the transient evolution, which reveals unique local temperature reduction effects due to heat current vorticity. These effects are only observable during the transient phase, where the evolving heat current vorticity induces a local temperature decrease relative to the initial state. The numerical resolution of this problem introduces additional challenges, particularly regarding boundary conditions, for which we propose a specific extrapolation method. Additionally, using Helmholtz decomposition, we establish an analogy with the linearized acoustics of Newtonian fluids, illustrating how the heat flux density mirrors the role of the velocity field. Our solutions also uncover an unexpected temperature behavior induced by the whirling heat flux density: under certain conditions, the temperature can locally decrease for a short period when the curl of the heat flux density dominates the heat conduction process.

Finally, we explore potential applications of non-Fourier-type equations, ranging from biological tissue modeling to laser welding processes. In particular, we present a hyperbolic heat transport model for homogeneously perfused biological tissue irradiated by a laser beam. This non-Fourier-like bioheat equation is solved analytically using the Laplace transform method. Subsequently, we present numerical results obtained from a welding laser process on a metal plate, modeled using Fourier's law. Special attention is given to possible future extensions of this model by incorporating relaxation times and temperature-dependent material parameters.

In this work, we apply the same modeling framework to heat propagation phenomena at both low and room temperatures, covering artificial and natural test samples, as well as biological tissues.

Keywords: Non-equilibrium Thermodynamics, Extended Thermodynamics, heat pulse experiments, heat conduction, heat transfer, Cattaneo equation, Guyer-Krumhansl equation, whirling heat flux density, vortices

Acknowledgements

The first person I wish to thank is Professor Patrizia Rogolino, who has supported me since our first meeting (even though it was initially online, via Teams, from Turin). She has helped me grow tremendously and has always been available, at any time – on Saturdays, Sundays, late at night, and even during holidays – showing extreme patience towards me. I was truly fortunate to have such a wonderful person as my supervisor, someone I would even dare to call a "mother" for all that she has done for me. I will never stop thanking her. I owe the pleasure of having met her to Professor Annunziata Palumbo, to whom I would also like to express my gratitude for the support I have received since my undergraduate studies

A special thanks goes to Professor Maria Carmela Lombardo, for her great availability, professionalism, and kindness over these three years of my PhD. Thanks also to Robert Kovacs, who welcomed me in Budapest; working with him was invaluable, and I hope this collaboration will continue in the future. I would also like to thank Professor Francesco Oliveri for his professionalism and willingness to support me throughout this journey, as well as for our conversations during our trips to Boccetta.

I would like to thank the reviewers, Prof. David Jou and Prof. Christina Papenfuss, for their suggestions, which have contributed significantly to the improvement of this work, as well as for their comments on potential future developments.

A special thought goes to my colleagues and friends: Carmelo Cisto, a person of a thousand talents; Emanuele, my dear "uncle" who patiently endured my "provocations"; Alessandra, and Ernesto. I want to thank my friend Guglielmo, with whom I have shared so much: he is a special person whom I met in Prof. Oliveri's course, and he has become a true friend. We even won the "best friends" award together during an edition of the Summer School of Mathematical Physics in Ravello. Our friendship has become solid and precious. I am also grateful to another dear friend I met during my PhD, Aldo, who has since become incredibly important to me: even if our paths may diverge, I am sure we will always be there for each other. A warm thanks goes to Antonella, who with her unique morning greetings and her marachelles gave me moments of carefree and support. I am also grateful to Antonino, with whom I have shared every step of my journey, from our university studies to this doctorate. Thanks also to Marco Menale, with whom I had the pleasure of collaborating and who has become a great friend, and to Matteo Gorgone, one of the most supportive and available people, always ready to clarify any doubt.

A special thanks goes to Salvo Rotuletti, a friend with exceptional values, someone everyone would want by their side. I have shared everything with him: from university to aperitifs, from challenging times to lighthearted ones. I truly hope our friendship will continue to bring us many wonderful experiences.

Lastly, I want to thank my family, to whom I dedicate this thesis. If I am here today defending this thesis, it is thanks to the sacrifices of my father, Concetto, who always ensured that I could study and that I never lacked anything (and he still does… you're a pro at this now, Dad, keep going! haha!)-

And then there's my mother, an exceptional woman, the mother everyone would want, to whom I dedicate in particular this thesis. She taught me what it means to love unconditionally and to give without expecting anything in return. She was my first example of determination and kindness, and I am immensely grateful for her constant support and affection. She was the first to believe in me, even when I doubted myself, and she always knew how to give me the right advice, the unconditional support, and the smile I needed in difficult times. Thank you for being a

shining example of strength, goodness, and boundless patience. If I've made it this far, it's also because of everything you taught me (though not the neurons – those are from Dad… just imagine if I had stayed in the womb one more month, what might have come out hahaha!). You have been, and continue to be, my guide and role model. Thank you, Mom, for being the rock that supports me every day.

Thank you all; I could never have reached this milestone without you.

Oops, now someone might be wondering if "he forgot about me". Who could it be?

I almost forgot the most important person of all: my little brother, Antonino. There are no words to describe him, only a big THANK YOU (written in capital letters, of course!). He has always been there for me, and I know he always will be. You'll still have to put up with me… We lived together in Turin, sharing every moment, every challenge, and every laugh, including those times you'd lose it when "Rogo" would call me at 10 p.m., and you'd say, "I need to sleep!" but understood how much it meant to me. He teases me about my "missions" to the university, saying I never actually work haha! He calls me "Doctor" (probably to make fun), and we have our own little routine now: every day, at the same time, I call him, and he jokes that he has to take "his daily pill." We don't need many words; just a look is enough to understand each other, and having a brother like him is the greatest gift my parents could have given me… or maybe it was a gift from someone who swapped me in the incubator haha! Thank you from the bottom of my heart, little brother, for always being by my side. Now that you're far away, know that I miss you tremendously.

Italian version

La prima persona che desidero ringraziare è la Professoressa Patrizia Rogolino, che mi ha sostenuto sin dal nostro primo incontro (anche se inizialmente solo online, su Teams, da Torino). Mi ha aiutato a crescere moltissimo, ed è sempre stata disponibile, in qualsiasi momento – anche di sabato, di domenica, a tarda sera, e persino durante le vacanze – mostrando un'estrema pazienza nei miei confronti. Sono stato davvero fortunato ad avere come supervisore una persona meravigliosa, che oserei definire una "mamma" per tutto ciò che ha fatto per me. Non smetterò mai di ringraziarla. Devo il piacere di averla conosciuta alla Professoressa Annunziata Palumbo, alla quale desidero esprimere anche la mia gratitudine per il supporto ricevuto fin dai tempi della laurea triennale.

Un ringraziamento speciale va anche alla Professoressa Maria Carmela Lombardo, per la sua grande disponibilità, professionalità e cortesia durante questi tre anni di dottorato. Grazie anche a Robert Kovacs, che mi ha accolto a Budapest: lavorare con lui è stato fondamentale e spero che questa collaborazione possa proseguire in futuro. Desidero ringraziare anche il Professore Francesco Oliveri, per la sua professionalità e disponibilità che ha sempre messo a disposizione in questo mio percorso e per le chiacchierate durante i nostri viaggi verso Boccetta.

Ringrazio i revisori, prof. David Jou e prof. Christina Papenfuss, per i loro suggerimenti, che hanno contribuito in modo significativo al miglioramento di questo elaborato, e per i loro commenti sui possibili sviluppi futuri.

Un pensiero speciale va ai miei colleghi e amici: Carmelo Cisto, una persona dalle mille qualità; Emanuele, il mio caro zio che ha sopportato con pazienza le mie "provocazioni"; Alessandra, ed Ernesto. Ringrazio il mio amico Guglielmo, con cui ho condiviso moltissimo: una persona speciale che ho conosciuto seguendo un corso del Prof. Oliveri e che è diventato un vero amico, al punto da vincere insieme il premio "migliori amici" durante un'edizione della scuola estiva di fisica matematica a Ravello. La nostra amicizia è ormai solida e preziosa. Ringrazio anche un altro caro amico conosciuto grazie al dottorato, Aldo, che da quel primo incontro nello studio del Professor Oliveri è diventato per me importantissimo: anche se le nostre strade potrebbero divergere, sono sicuro che saremo sempre presenti l'uno per l'altro. Un affettuoso grazie va ad Antonella, che con il suo particolare modo di salutare ogni mattina e le sue marachelle mi ha regalato momenti di spensieratezza e supporto. Ringrazio anche Antonino, con cui ho condiviso ogni tappa del mio percorso, dalla triennale al dottorato. Grazie anche a Marco Menale, con cui ho avuto il piacere di collaborare e che è diventato un grande amico, e a Matteo Gorgone, una delle persone più presenti e disponibili a chiarire qualsiasi dubbio.

Un ringraziamento speciale va anche a Salvo Rotuletti, un amico dai valori eccezionali con cui ho condiviso tutto: dall'università agli aperitivi, dai momenti difficili a quelli spensierati. Spero che la nostra amicizia continui a regalarci tante belle esperienze.

Per ultimo desidero ringraziare la mia famiglia, a cui dedico questa tesi. Se oggi sono qui a difendere questa tesi, lo devo ai sacrifici di mio padre, Concetto, che ha sempre fatto in modo che io potessi studiare e non mi ha mai fatto mancare nulla (e continua ancora a farlo… striscia tu lo fai meglio, orami sei rodato ahaha!).

E poi c'è la mia mamma, una persona eccezionale, la mamma che tutti vorrebbero e alla quale dedico questa tesi. Mi ha insegnato cosa significa amare senza riserve e dare senza aspettarsi nulla in cambio. È stata il mio primo esempio di determinazione e gentilezza, e sono immensamente grato per il suo supporto e il suo affetto, sempre presente e costante. Lei è stata la prima a credere in me, anche quando io

stesso avevo dei dubbi, e ha sempre saputo darmi il consiglio giusto, il sostegno incondizionato e il sorriso che mi serviva nei momenti più difficili. Grazie per il tuo esempio di forza, di bontà e di pazienza infinita. Se sono arrivato fino a qui, è anche grazie a tutto quello che mi hai trasmesso (non i neuroni però, quelli solo da papà... e pensa se stavo ancora un mese in pancia cosa ti usciva ahahaha!). Sei stata, e continui a essere, la mia guida e il mio modello. Grazie, mamma, per essere la roccia che mi sostiene ogni giorno.

Grazie a tutti, senza di voi non ce l'avrei mai fatta a raggiungere questo traguardo.

Ops, arrivati qui, qualcuno starà dicendo si è "scordato di me". Chi sarà?

Stavo quasi dimenticando il più importante di tutti: il mio fratellino, Antonino. Per lui non ci sono parole, solo un grande GRAZIE (scritto grande, eh!). C'è sempre stato, e so che ci sarà sempre. Ancora mi dovrà sopportare... Abbiamo vissuto insieme a Torino, condividendo ogni momento, ogni difficoltà e ogni risata, anche le tue sclerate quando la "Rogo" mi chiamava alle 22 e tu dicevi "Io devo dormire!", sapendo però quanto ci tenevo. Mi prende in giro per le "missioni" all'università dicendo che non lavoro mai ahaha! Mi chiama "Dottore o Medico" (forse per prendermi in giro), e ormai abbiamo una nostra piccola routine: ogni giorno, allo stesso orario, lo chiamo e lui scherza dicendo che deve prendersi "la pillola". Tra noi non servono molte parole, ci basta uno sguardo per capirci, e avere un fratello come lui è il dono più grande che i miei genitori potevano farmi... o forse è un regalo di chi mi ha scambiato nell'incubatrice ahaha! Grazie di cuore, fratellino, per essere sempre al mio fianco. Ora che sei lontano, sappi che mi manchi tremendamente.

Contents

List of Figures

List of Tables

List of Abbreviations

CIT	**C**lassical **I**rreversible **T**hermodynamics
TIP	**T**hermodynamics of **I**rreversible **P**rocess
RT	**R**ational **T**hermodynamics
RET	**R**ational **E**xtended **T**hermodynamics
EIT	**E**xtended **I**rreversible **T**hermodynamics
NET-IV	**N**on-**E**quilibrium **T**hermodynamic with **I**nternal **V**ariables
F	**F**ourier
MCV	**M**axwell-**C**attaneo-**V**ernotte
CE-MCV	**C**onjugate-**E**xtension-**M**axwell-**C**attaneo-**V**ernotte
GK	**G**uyer-**K**rumhansl
L-F	**L**inear-**F**ourier
NL-F	**N**on-**F**ourier
L-MCV	**L**inear-**M**axwell-**C**attaneo-**V**ernotte
NL-MCV	**N**on-**L**inear-**M**axwell-**C**attaneo-**V**ernotte
L-CE-MCV	**L**inear-**C**onjugate-**E**xtension-**M**axwell-**C**attaneo-**V**ernotte
NL-CE-MCV	**N**on-**L**inear-**C**onjugate-**E**xtension-**M**axwell-**C**attaneo-**V**ernotte
L-GK	**L**inear-**G**uyer-**K**rumhansl
NL-GK	**N**on-**L**inear-**G**uyer-**K**rumhansl
FDM	**F**inite-**D**ifference-**M**ethod
1D	**O**ne-**D**imension
2D	**T**wo-**D**imension
BC/BCs	**B**oundary-**C**onditions
IC/ICs	**I**nitial-**C**onditions
IBVP	**I**nitial-**B**oundary-**V**alue-**P**roblem
PDE	**P**artial-**D**ifferential-**E**quation

Dedicated to my mum . . .

Chapter 1

Introduction

Experimentally, many years ago it was discovered that the classical laws, such as Fourier's law for heat conduction, Fick law for diffusion and Newton law for viscous flow could be wrong certain circumstances. This is mainly due to the advent of technological development in the field of micro/nano-devices, in fact the characteristic time and duration of processes at low temperature become increasingly shorter. It is thus important to explain phenomena which go beyond classical laws. However, it is known that after the introduction of these classical relations in the balance laws, one arrives at the partial differential equations of parabolic type, that implies that the perturbations are propagated with infinite velocity. This behaviour is sometimes not in agreement with experimental tests, it seems strange even from a theoretical point of view, because the effects of perturbations should propagate at finite velocity, not only from the relativistic frame, but also in the non-relativistic point of view. This could be avoided taking into account the relaxation times of the respective fluxes, e.g. thermal flux, diffusion flux, moment flux, usually known as **dissipative fluxes**. However, in classical thermodynamics (Classical Irreversible thermodynamics and Rational thermodynamics) the evolution equations necessary for such dissipative fluxes, are not compatible with these theories, because these leads, in some circumstances, a negative entropy production.

For some researchers it is unexpected that the thermodynamics can be used as a framework to extend the classical equations. Since, historically, the classical thermodynamics has allowed the temperature of a gas to be calculated or the pressure to be predicted etc, but not to understand nanoscale phenomena, or low temperature phenomena in which different laws are required. In addition, the second law should be universal and general. How is it possible to incorporate the new equations that extend the classical constitutive laws? The question is whether, from a practical point of view, such relaxation times exist for dissipative fluxes. In many systems it has been found that dissipative fluxes are characterized by not negligible relaxation times, for example thermal and electrical conductors at low temperature, superconductors and so on. So in real situations, these systems are out of local equilibrium, how can they be incorporated into classical theories?

As a result, new theories of the non-equilibrium were needed, including Rational Extended Thermodynamics, Extended Irreversible Thermodynamics, Thermodynamics with Internal Variables, GENERIC (GEneral Non equilibrium Equation of Reversible Irreversible Coupling) and many others. For this reason, a thorough understanding of these new theories, whether linear or not, may be important not only from a theoretical point of view but also for practical and application purposes. These theories introduce as new independent variables the dissipative fluxes and aim to obtain for them evolution equations compatible with the second law of thermodynamics. However, the main quantity is a generalized non-equilibrium entropy, dependent both classical variables and dissipative fluxes.

In this dissertation we will focus on heat conduction problems beyond the Fourier's law. In particular, the aim is to investigate generalization of Fourier's law by introducing material parameters that are not constant but depend on temperature. As numerous experiments show (see the next section), there are considerable discrepancies with classical laws. However, these effects have been studied, because of the rapid technological development has made it is necessary to describe fast and high-frequency processes in which such effects emerge. These latter make the design phase of future micro/nano devices very difficult, for this reason to understand the transport of heat at these scales and propose modified versions of the classical equations (compatible with the second law of thermodynamics) is a central point to facilitate its design.

Several theories have been developed in the context of irreversible thermodynamics. A brief historical summary of the possible engineering applications opportunities of these phenomena are presented.

1.1 Historical summary

Most of the heat conduction engineering problems, in agreement with the classical hermodynamics are based on the well known Fourier's law, which states that the heat flux $\mathbf{q}(\mathbf{x}, t)$ is proportional to the temperature gradient $\nabla T(\mathbf{x}, t)$.

$$\mathbf{q} = -\lambda(T)\nabla T$$

wherein the coefficient $\lambda(T)$ represents the thermal conductivity for an isotropic material, that in general, is non-constant but can depend on the temperature. This model is applied for calculations in engineering practice.

As is commonly known this law has limits, so it is inevitable to find the correct extension and determine the possibilities of practical implementations. In fact this constitutive relation for the heat flux leads together to energy balance law

$$\rho c\, \partial_t T + \nabla \cdot \mathbf{q} = \rho r$$

where the quantities c and ρ are the specific heat capacity and the mass density of the rigid conductor, respectively; $r(\mathbf{x}, t)$ represents the specific internal heat source, to the classical form of the heat equation,

$$\rho c\, \partial_t T + \nabla \cdot (\lambda \nabla T) = \rho r \tag{1.1}$$

which has been successfully used to model the temperature in materials for over many years. But this equation leads to an infinite speed of heat propagation, which means that any initial heat pulse is felt instantly (for any little time instant $t > 0$) at any point in the whole medium. This behaviour is known as the 'Paradox of Heat Conduction', and contradicts the so called 'strong principle of causality' , i.e. that information cannot travel faster than a finite speed, in classical physics, while in relativistic field, the information cannot travel faster than light speed.

During the 20th century, several experiments have shown that there are heat conduction phenomena which are unexplainable with Fourier's law and require generalized equations to be predicted and described. In the literature several generalizations of Fourier's law have been suggested such as the Maxwell-Cattaneo-Vernotte equation (MCV) [1–3], Dual-Phase-Lag (DPL), Guyer-Krumhansl (GK) [4–6], Jeffrey (JF) [7], Green-Naghdi (GN) [8]. This study began with the theoretical predictions of

Onsager, Tisza and Landau. While the first, he discussed the likely microstructural reasons for deviation from Fourier's law [9], as happens for example with heterogeneous materials; Tisza and Landau predicted a heat conduction behaviour in helium II, where the temperature shows a dissipation but also wave propagation, which cannot be explained by Fourier's law [10, 11]. This phenomenon is known as **second sound** and has been observed under extreme conditions (low temperatures or ideal materials). The first experimental results, which led to the detection of the second sound, were carried out in superfluid helium II by Peshkov nel 1944 [12], which applies heat pulse excitation (see Figure 1.1).

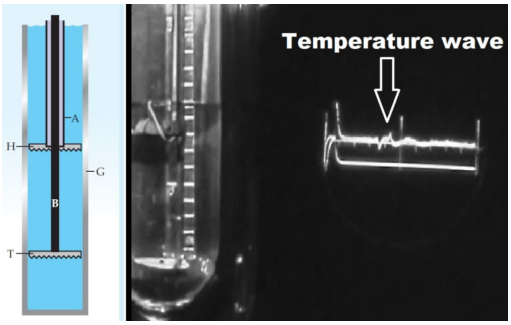

(a)

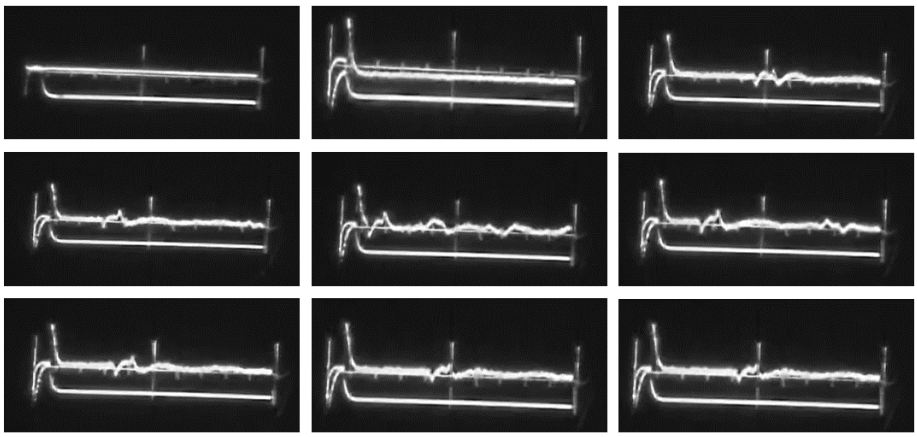

(b)

FIGURE 1.1: Top panel (a): A simplified schematic picture about Peshkov's experiment [12–15]. In a glass tube (G), heat pulse signals are generated by the heater (H), and temperature is measured by the thermometer (T). A and B denote tubes with adjustable positions, which ensured better observability of the temperature waves. Bottom panel (b): A screenshot from Alfred Leitner's video. A 1963 film by Alfred Leitner demonstrating the wave-like propagation of temperature of liquid helium II when cooled below the lambda point (the superfluid state). Heat is conducted at $20\,m/s$ in a totally different way from traditional heat conduction. [1]

This non-Fourier type behavior has been investigated in several experiments, in particular, from 1970s, after the discovery of the second sound in low-temperature solids [16–21] and subsequently several predictions of similar phenomena were carried out for heterogeneous materials at room temperature [22–24]. Other researchers

[1] Source of the picture: https://www.youtube.com/watch?v=NjPFfT2EyxQ

have analyzed the relaxational phenomena in granular and biological media, but unfortunately these measurements have not been confirmed because the related experimental results have proved to be contradictory and unclear [25–28].

Several questions arise about the propagation speed of the second sound : its modelling requires, for example, the Maxwell-Cattaneo-Vernotte equation [1–3], the first - hyperbolic - extension of the Fourier law

$$\tau(T)\frac{\partial \mathbf{q}}{\partial t} + \mathbf{q} = -\lambda(T)\nabla T,$$

where τ is the relaxation time of the heat flux that in general together the thermal conductivity can depend on the temperature, when these non linearities are introduced appear futher terms into the evolution equation, see [29]. This model includes a relaxation mechanism to adapt the heat flux gradually (i.e. the presence of time derivative term represents the memory effect), to a change in temperature gradient. This is an extension of classical diffusion theory and can lead to a hyperbolic diffusion equation, that is, a wave with finite velocity. The predicted characteristic wave speed is $v = \sqrt{\alpha/\tau}$ in which $\alpha = \lambda/(\rho c)$ is thermal diffusivity. Their ratio characterizes the observed wave and therefore thermophysical properties.

However, as many authors have highlighted [13–15], the propagation velocity is highly non-linear. Therefore, the material and thermal parameters must depend on temperature, such as thermal conductivity, specific heat capacity, relaxation time and mass density (here we are assuming it is constant, since we study the propagation of heat in a rigid conductor). This explains the aim of this thesis, which is to study the effects on heat propagation caused by the introduction of such non-linearity. In particular, we want to understand the induced effects by assuming thermal conductivity and relaxation time not constant but temperature-dependent through particular laws. Determining what are the qualitative and quantitative changes in the observed temperature distribution, in one or two spatial dimensions.

On the other hand, the inclusion of such nonlinear behaviour in heat conduction models is only possible with a well-established and consolidated thermodynamic framework, since the coefficients are not independent of each other [29, 30]. The onsagerian relationships connect them, for example the temperature dependence of thermal conductivity influences the other parameters, you will see in the demonstrations of the compatibility of non-Fourier heat conduction models in the various thermodynamic theories [29, 30]. It was found that the temperature dependence of relaxation time necessarily implies the temperature dependence of mass density [29, 30]. This means that the physical phenomenon requires a complete thermomechanical framework, or the inclusion of mechanical effects. This leads to ballistic propagation, i.e. an elastic wave that carries heat. From a continuum point of view, it is induced by thermal expansion [31, 32] and always propagated at the speed of sound [33]. In addition, beyond the temperature dependence of parameters (both thermal and mechanical), an explicit coupling between the thermal field and the mechanical field could occur [34]. In the present thesis, mechanical effects are neglected and will be the aim of future work.

Subsequently, Guyer and Krumhansl derived from the microscopic point of view, through linearization of the Boltzmann equation [4–6], a more general heat conduction equation than Cattaneo's. This equation, in addition to including memory effects, takes into account non-local effects, so much so that the non-local generalization of Cattaneo is defined. It is expressed by the following partial differential

equation

$$\tau(T)\frac{\partial \mathbf{q}}{\partial t} + \mathbf{q} = -\lambda(T)\nabla T + \eta_1(T)\Delta\mathbf{q} + \eta_2(T)\nabla(\nabla\cdot\mathbf{q})$$

where η_1, η_2 represent the phenomenological coefficients in isotropic media and in general can be a function of temperature. Also, here, we observe when η_1, η_2 go to zero, the GK equation returns to the MCV form. Under a particular condition known as *resonance condition* ($l^2/\tau = \alpha$ this in the one-dimensional case, with $l^2 = \eta_1 + \eta_2$), the solution of the Fourier equation is recovered [35], and no deviation occurs. However, when this condition is not satisfy (i.e. the ratio of l^2/τ differs from thermal diffusivity α), the two conduction channels differ from each other, the Fourier resonance ceases, and the deviation becomes observable. This reflects the existence of different time and space scales of constituents.

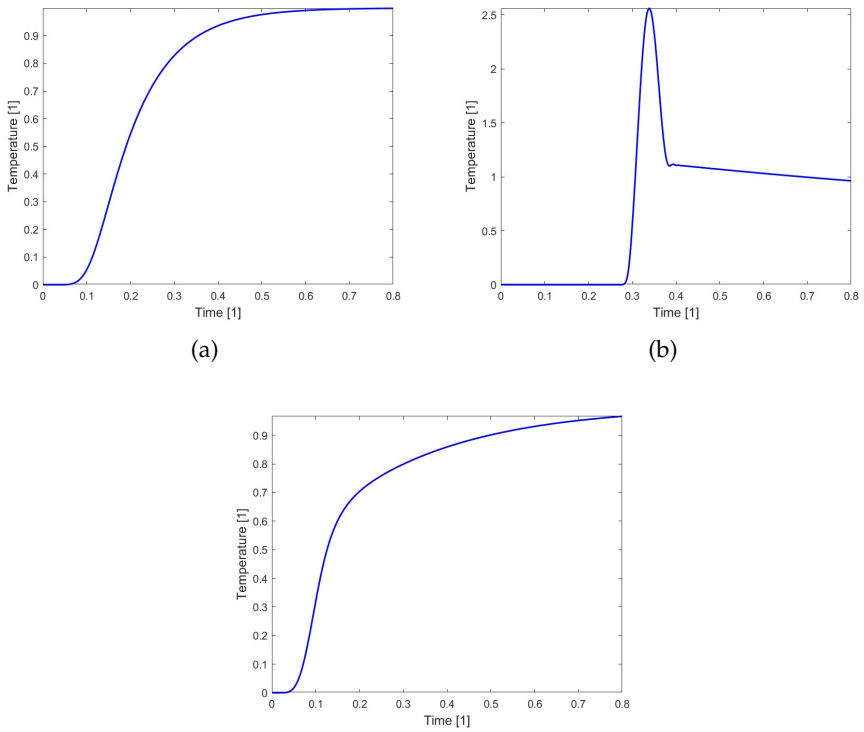

FIGURE 1.2: A typical solution for Fourier, MCV and GK equations respectively.

This equation can describe the second sound, in fact, it has significantly helped experimental research to determine the optimal frequency for making visible this wave phenomenon of heat propagation even in solids [5, 6]. Unfortunately, such a condition for ballistic propagation, known as window condition, does not exist. In fact, as reflected by the thesis of Ph.D of McNelly [33], it is difficult to observe the ballistic propagation experimentally. Despite these difficulties, there are remarkable observations that are based on pure crystals [36], mostly NaF, LiF or solid He. Ballistic propagation has been demonstrated in sodium fluoride crystals, NaF, by Jackson, Walker and McNelly [20, 21, 33] (see the Figure 1.3). In addition, Kovacs and Van [37], using the internal variable framework, quantitatively reproduced two sets of experiments modelling ballistic propagation, together with the second sound.

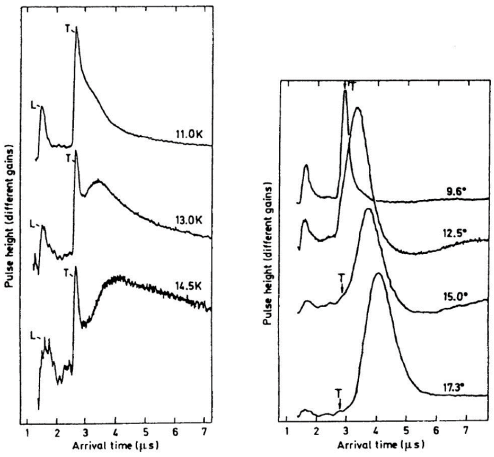

FIGURE 1.3: McNelly experiments on Naf: Ballistic heat propagation

However, it seemed that non-Fourier heat conduction theories could explain non-classical behaviour only under particular conditions: the materials studied were "perfect" or "ideal" (for NaF experiments, for example) and at low-temperature. These situations in the engineering field appear very rarely. Note that every real material, not "ideal", in a certain sense, is heterogeneous, for example due to the presence of porosity, composition of the material and inclusions created artificially. So it differs strongly from the materials mentioned above. Although in the literature, there are some famous experiments on such materials at room temperature, as those performed by Mitra et al. [38] and Kaminski [39], such data could not be reproduced by anyone else and therefore widely criticized [25, 40, 41]. Given the non-reproducibility, we can say that the second sound was not observed unambiguously in macroscopic samples at room temperature. More recently, in this direction, an experimental and theoretical study was conducted to detect non-Fourier thermal conduction in heterogeneous macroscopic samples at room temperature [42]. Such experiments were conducted at the Department of Energy Engineering of the University of Technology and Economics[2] in Budapest have shown that the deviation from heat conduction Fourier-type conduction can also be observed at room temperature and on several heterogeneous samples. To carry out such experiments, as usual in engineering practice, the heat-pulse experiment set-up was applied (see Figure 1.4 and [43, 44]). However, these deviations are not as marked as the second sound phenomenon, but their behavior can be detected, measured and cannot be explained by Fourier's law.

Contrary to what was expected, namely the wave-like deviation from the Fourier law (similar to the second sound) modelled with the Maxwell-Cattaneo-Vernotte equation; any ambient temperature experiments show such temperature waves and in most cases, neither Fourier nor Cattaneo equations were able to fit/explain the results. When the MCV equation is not good, dual-phase-lag (DPL) models are usually used. The DPL concept is based on a Taylor expansion of Fourier's law. However, DPL models violate fundamental physical principles for various reasons [45–48]. Despite its popularity, especially in the biological literature, the DPL model cannot become the standard equation in engineering practice to replace Fourier's law, this due to its numerous shortcomings. From a continuum point of view, the approach

[2]Finf here: http://irrev.energia.bme.hu/

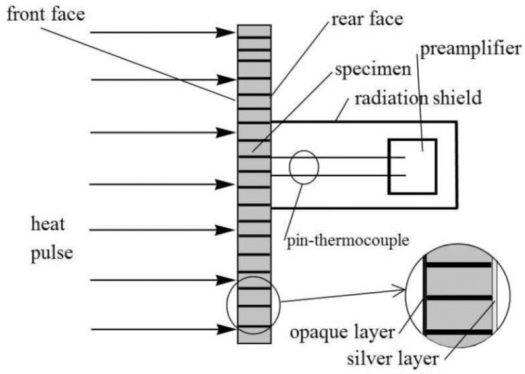

FIGURE 1.4: Setup of the heat-pulse experiment. The front face of the specimen is excited by a heat pulse and rear-side temperature is measured.

recently used by Kovacs is based on the use of the Guyer-Krumhansl equation. Initially this equation was derived based on kinetic theory with detailed microscopic modeling of phonons or heat carriers (quasiparticle describing a quantum of vibration in a rigid crystal lattice) and applied to low temperature problems. However, this kinetic approach is limited by the heat conduction mechanisms described in phonons, so it is not possible to apply this approach to more general questions (as phenomena at room temperature).

However, by virtue of the flexibility of the coefficients, which is a feature of the continuum approach of the GK equation, these are found experimentally without any hypothesis on the particular mechanism of heat transfer, unlike the kinetic approach. Thus, without using the hydrodynamics of phonons, it has been possible to successfully explain and model several experiments at room temperature in which no waves are detected, as shown in Figure 1.5, where the Fourier fit deviates strongly from the measured data, while the Guyer-Krumhansl fit follows the measured data very well.

This type of non-Fourier thermal conduction, as shown in [42], from measuring thermal pulses on various artificial and natural heterogeneous materials, such as foams, rocks or other porous materials is common for heterogeneous materials. Apparently, this is not a wave-like phenomenon but a diffusive phenomenon with multiple conduction channels. In particular, the mechanism that seems to accumulate, the two kinetic and continuum approaches, is presumably the presence of several "heat conduction channels". In hydrodynamic phonon transport, the two relaxation terms (resistive and normal collisions) represent two different propagation mechanisms for the phonon within spatially homogeneous samples. In the artificial sample, aluminium and polystyrene (in case of the capacitor, see [42]), aluminium and air (in case of a metallic foam, see [42]) are the two conduction channels. In the case of natural samples, such as rock samples (see [42]) there are no simple explanations due to the lack of "components" and the heat conduction coefficients are very different.

The Guyer-Krumhansl heat equation has many important practical applications, although it has a more complex structure than Fourier's law. It is an excellent candidate to replace Fourier's law in engineering problems because of its modeling capabilities which can include a wide range of phenomena, from low temperature to room temperature problems. For this reason, its mathematical properties must be

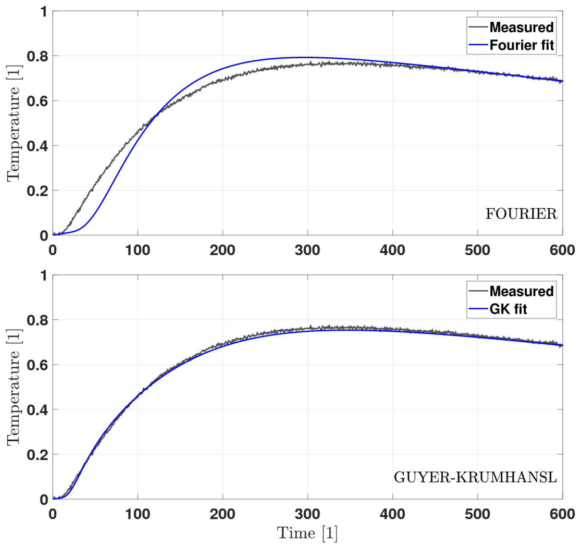

FIGURE 1.5: Result of a heat-pulse experiment: measured and fitted rear-side temperature of carbon foam samples. The measurement and fitting procedure have been performed by Anna Fehér and Róbert Kovács [22, 23, 42]. This phenomenon is called over-diffusive.

studied and understood. Recently, these properties have been the subject of intensive studies [49–53], both analytical and numerical.

For this reason, in this thesis we propose to continue these studies, focusing on the induced nonlinear effects not only in the equation of MCV but also for GK, because it has a very strong background and is of key importance in engineering applications.

Unfortunately, there is no general physical picture of the phenomenon that causes this deviation from the Fourier law at room temperature. For example, rocks are exceptional materials because of the different porosities, the distribution of microcracks, the variable composition, cracks and discontinuities can strongly modify the heat conduction, since there are several parallel mechanisms of heat transfer, for example, heat conduction in bulk material and convective heat transfer between bulk material and inclusions. The detailed modelling of experimental results is therefore not possible due to our limited knowledge, but only in particular situations. In Budapest, a research group [3] deals with the derivation and application of an effective thermal model with the technique of measuring the heat-pulse in various types of materials,includingd 3D printed samples. In this direction, a possible next step is to transfer such knowledge into engineering applications. It was found that the thermal properties depend not only on the material but also on its internal structure. Modern technologies make it possible to produce objects with a well-designed internal structure (for example, 3D printing) for specific tasks. Since these metamaterials are also layered structures, the transfer of experiences and conclusions reached in non-Fourier behaviour can contribute to such research. This means that if you identify relationships between the internal structure and thermal properties, you can develop a higher level thermal design methodology. At the same time, neither physical explanations nor modelling techniques or computational methods are fully developed, so further theoretical investigations are also needed.

[3] Finf here: http://irrev.energia.bme.hu/

1.2 An overview of the dissertation

The structure of the dissertation is as follows:

Chapter 1 provides a brief introduction to non-linear and non-Fourier thermal models, highlighting the motivation such extensions are needed.

Chapter 2 provides the historical background and derives Fourier's law along with its generalizations within various thermodynamic frameworks.

Chapter 3 introduces the Fourier equation, presents some classical analytical results, and discusses numerical solutions of the heat pulse experiment. Special attention is given to the temperature dependence of thermal conductivity.

Chapter 4 explores the Maxwell-Cattaneo-Vernotte evolution equation for heat flux, which modifies Fourier's law by incorporating thermal relaxation time as a key parameter. This chapter also includes numerical solutions, and we propose an alternative extension of the Cattaneo equation, inspired by analogies with linear optics.

Chapter 5 focuses on the effects of nonlinear thermal conductivity and relaxation time by solving the one-dimensional Guyer-Krumhansl equation. We then examine the implications of heat current vorticity by solving the two-dimensional Guyer-Krumhansl equation under space- and time-dependent heat pulse boundary conditions using a staggered numerical scheme. Particular emphasis is placed on the transient evolution, where local temperature reduction effects are linked to the presence of whirling heat currents. Additionally, we investigate the role of slip boundary conditions in the Guyer-Krumhansl model.

Chapter 6 explores potential applications of non-Fourier heat conduction equations, ranging from biological tissue modeling to laser welding processes.

Finally, the Conclusion chapter summarizes the key findings, offers a discussion, and outlines future research directions.

Chapter 2

Thermodynamic compatibility : Second law

The heat conduction is based on the energy balance law and on the constitutive equation, describing the material properties. Let us consider a rigid heat conductor at rest w.r.t. a reference frame, where the mass density ρ is constant, the velocity field is null (the material/substantial time derivative is equal to partial time derivative),the deformation in negligible($\sigma = 0$, $F = 0$). Our starting point is the balance of internal energy:

$$\rho \dot{e} + \nabla \cdot \mathbf{q} - \tau : L = \rho r$$

Being $L = \nabla \mathbf{v} = \mathbf{0}$ and assuming negligible the source term, i.e. $r = 0$, we obtain

$$\rho \dot{e} + \nabla \cdot \mathbf{q} = 0 \tag{2.1}$$

where ρ is the mass density, $\mathbf{q}$ is the heat flux, e denotes the internal specific energy and it can be expressed by $e = c\,T$, in case of constant specific heat c with T represents the temperature. The overdot denotes the substantial or total time derivative, i.e. $\frac{d}{dt} = \frac{\partial}{\partial t} + \mathbf{v} \cdot \nabla$, in this case it coincides with the partial derivative, indicated with ∂_t (because $\mathbf{v} = \mathbf{0}$) and $\nabla \cdot$ denotes the divergence operator.

This problem require a closure, i.e. is necessary to assign the costitutive equation for the the heat flux. The classical costitutive equation is the Fourier's law.

In classical irreversible thermodynamics (CIT) for heat conduction, the entropy density s is the function of the internal energy only. The assumption of local equilibrium of thermal interaction leads to Fourier's equation in the continuum case.

As mentioned in the introduction, several generalizations in order to reproduce and explain experiments [10–21, 27, 28, 33, 37, 42] are necessary. In this case, the generalization means the extension of the constitutive equation, this extension can be done in the :

- time direction ,
- space direction.

The first one is called memory extension when the history of the material is considered, it is represented by extra time derivatives in the constitutive equation. The second one is called non-local extension, where states are considered not only in a spatial point but in its neighborhood, it is realized by extra space derivatives in the constitutive equation.

The inertial, memory and non-local effects are best introduced by the extension of the state space with new fields:

- dissipative fluxes,

- internal variables.

or with the space derivatives of the state variables, i.e. its gradients (first order, second order, ...).

There are several theories that extend the validity of Fourier's law by additional terms in the constitutive equation and that obtain generalizations of the Fourier's law. Some of them are consistent with thermodynamics workbench, others are not.

Non-equilibrium thermodynamics can characterize the deviation from local equilibrium both in the entropy density and in the entropy flux by introducing dissipative fluxes, internal variables. However, one needs to derive an evolution equation for them.

This led to the possibility of deriving the evolution equations for non-Fourier heat flux, considering the evolution equations for thermomechanical variables as well as the evolution equations for the fluxes of these thermomechanical variables. Since for the latter they are not required to be assigned by means of a constitutive equation, but being considered as unknowns on a par with the thermomechanical variables, they must be added to the space of the states and equations of evolution must be assigned.

In particular these new theoretical frameworks extend the classical thermodynamic state space with these additional fields, as Rational Extended Thermodynamics (RET) [54–57], Extended Irreversible Thermodynamics (EIT) [58–60], Non-Equilibrium Thermodynamics with Internal Variables (NET-IV) [61–65] and GENERIC [66–70]. The relation of these theories to the previously mentioned requirements (well-posedness and second law) and benchmarks (experimental, kinetic theory compatibility) are very different, and also, their applicability is not the same (see also [71]). In particular RET, EIT, and NET-IV are constructive. RT is capable of checking the second law compatibility of the suggested constitutive equations. RET, EIT, and NET-IV pay attention to the compatibility with the microscopic world, i.e. kinetic theory of gases, where RET is the most strictly compatible, NET-IV is the least compatible, and EIT is situated between them. In addition, another point on which there are differences is the hyperbolic symmetrical structure of equations. In RET it is essential and we exploit, in the method of construction, the thermodynamic potentials to obtain equations of hyperbolic symmetric evolution. The EIT is open to the possibility of hyperbolic equations but does not make them a postulate. On the contrary, these approaches may be compatible under certain conditions.

The variety of the methods and aspects is wide. In general, we expect the compatibility with the second law of thermodynamics. the space-time evolution and the micro-scale background. The second law is the most important tool in the thermodynamic theories, to study the thermodynamic compatibity, to derive the constrains on the constitutive equations and to obtain asymptotically stable equilibrium. It is expressed by

$$\Sigma_s = \rho \dot{s} + \nabla \cdot \mathbf{J_s} - \rho \frac{r}{\theta} \geq 0 \tag{2.2}$$

where s, $\mathbf{J}_s$, Σ_s represents the specific entropy, the entropy flux and the entropy production, respectively; ρ is the mass density, T the absolute temperature and r the heat specific source. The operator "$\nabla \cdot$" represents the divergence.

In Rational Thermodynamics (RT), Coleman and Noll formulated the principle of entropy as:

The constitutive equations, which characterize the material properties of continuous media, must be assigned so that the second law of thermodynamics (2.2) is automatically satisfied (a priori).

The entropy principle, formulated by Coleman-Noll, can seem to be an arbitrary assumption, in that it seems to restrict processes rather than provide limitations on constitutive equations. But Muschik and Ehrentrant proved that:

For the classical solutions of equations governing the thermomechanical of a continuum, the second law of thermomechanical (2.2) *imposes restrictions only on the constitutive equations and not on the thermodynamic processes.*

However, Coleman and Noll, presented an rigorous method to investigate the second law of thermodynamics, called *Coleman-Noll procedure* [72]. After, Liu developed an alternative method [73], based on Lagrange multiplier, which today is known as the *Liu method* and which was extended by Cimmelli, Oliveri and Triani who introduced as constraints beyond the balance equations their differential consequences [74, 75], called *Metodo delle estese*. We observe that the Coleman-Noll and Liu procedures, when to consider a non-local state space, i.e. it is considered a state space that in addition to containing the thermomechanical variables also contains their gradients, lead to incompatibility with the second law of thermodynamics, for example for the Kortweg fluid. In the latter category of fluids, it must be assumed that the classical entropy flow proposed by Coleman-Noll, $\mathbf{q}/T$, contains an additional term $\mathbf{K}$, of an exclusively mechanical and non-thermal nature, called extraflux, as I. Muller had already guessed during his PhD,

$$\mathbf{J_s} = \frac{\mathbf{q}}{T} + \mathbf{K}.$$

In this way the entropy flux becomes the sum of the classical Coleman-Noll part plus a non-equilibrium contribution due to higher order flows.

Another method of analysis of (2.2), introduced under the Classical Irreversible Thermodynamics (CIT) theroy, is a phenomenological method called *Onsager procedure*, in which the production of entropy Σ_s is expressed as a bilinear form of generalized forces and flows, i.e. sum of products between generalized forces and flows

$$\Sigma_s = \sum_{\alpha=1}^{n} \mathbf{F}_\alpha \cdot \mathbf{J}_\alpha \geq 0. \tag{2.3}$$

In this chapter, we will present the derivation of Fourier's law and its extensions, Cattaneo and Guyer-Krumhansl, within the various thermodynamic theories: CIT, RT, RET, EIT; focusing in particular on the derivation within the Extended Irreversible Thermodynamics theory, highlighting how phenomenological coefficients are modified to include the presence of non-linear effects, i.e. non constant material parameters. This last assumption becomes necessary because in engineering applications, for example thermal conductivity, specific heat capacity, relaxation time, are temperature dependent and taking them constant becomes too strong an assumption [13–15]

2.1 Classical Irreversible Thermodynamics (CIT)

This section is dedicated to the derivation of Fourier's law in classical irreversible thermodynamics (CIT).

The classical irreversible thermodynamics, developed by Onsager and Prigogine, is based on the local equilibrium hypothesis. Outside equilibrium, it is assumed that any system depends locally on the same set of variables as when it is in equilibrium.

This leads to a formal thermodynamic structure identical to that of equilibrium: the intensive parameters such as temperature, pressure and chemical potentials are the Legendre transformations determine definite quantities while maintaining their usual meaning, the thermodynamic potentials are derived and all equilibrium thermodynamic relationships retain their validity.

The **Classical Irreversible Thermodynamics (CIT)** is the oldest thermodynamic theory, which dates back to the 40-50's and is based on semi-empirical methods, thus defined as they are not mathematical methods hypothetical-deductive, but phenomenological methods that are based on experiments that were conducted in the laboratory [76]. It is a macroscopic theory and uses the Onsager method to analyze the second law of thermodynamics.

The fundamental assumption underlying the CIT is that of local equilibrium. It postulates that the relations, local and instantaneous, between the thermal and mechanical properties of a physical system are the same as those of a uniform system in equilibrium, i.e. the system is globally out of equilibrium, it remains locally in equilibrium. This assumption implies that

- all the variables defined in equilibrium thermodynamics remain significant, in particular variables such as temperature and entropy are strictly defined at equilibrium, the value of these variables varies from one subsystem to another. So these quantities remain uniform but take different values from subsystem to subsystem, the system under consideration is assumed to be mentally divided into a series of subsystems large enough to be treated as thermodynamic subsystems macroscopic, but small enough that the equilibrium is very close to being achieved;
- relationships between state variables to equilibrium remain valid outside of equilibrium provided that they are declared locally at every instant of time. Therefore, entropy outside of equilibrium will depend on the same state variables as equilibrium;

From this hypothesis it follows that entropy depends only on the state variables and not on their gradients, therefore it is a local function, i.e. $s = s(e, z_\alpha)$ and in differential form is

$$ds = \left(\frac{\partial s}{\partial e}\right)_{z_\alpha} de + \left(\frac{\partial s}{\partial z_\alpha}\right)_{e,z_\beta} dz_\alpha \qquad \text{with } \beta \neq \alpha$$

Defining, as in equilibrium thermodynamics, the absolute temperature T (and other quantities as, the pressure, and the chemical potential and so on)

$$\frac{1}{T} = \left(\frac{\partial s}{\partial e}\right)_{z_\alpha} \qquad \frac{1}{T} m_\alpha = \left(\frac{\partial s}{\partial z_\alpha}\right)_{e,z_\beta} \tag{2.4}$$

one obtains from this definition the local form of the Gibbs relation

$$Tds = de + m_\alpha dz_\alpha \tag{2.5}$$

Our objective is to explicitly calculate the entropy production of the system and also the entropy flux, in order to obtain this relation, we compute the time derivative of the Gibbs relation

$$T\dot{s} = \dot{e} + m_\alpha \dot{z_\alpha} \tag{2.6}$$

by multiplying for the mass density ρ and replacing the energy balance law and the other balance law for z_α we obtain the following expression for the rate of change of the entropy

$$\rho \dot{s} = -\frac{1}{T} \nabla \cdot \mathbf{q} + ... \tag{2.7}$$

A comparison of this expression and the general balance equation of entropy permits to determine the expression for the entropy flux, $\mathbf{J_s}$, and for the entropy production, Σ_s.

Now, is possible to see the expression for the entropy production is a sum of products of thermodynamic flux $\mathbf{J}^\beta$ and thermodynamic force $\mathbf{F}_\alpha$. In terms of them the rate of entropy production presents the bilinear structure

$$\Sigma_s = \sum_{\beta=1}^{N} \mathbf{F}^\beta \cdot \mathbf{J}^\beta \tag{2.8}$$

therefore the production of entropy is expressed as products of generalized forces and flows and this theory uses the Onsager method to analyze the second law of thermodynamics, or to ensure that this entropy production is not negative.

A solution that leads to a production of non-negative entropy, is to assume that the flows are a linear combination of forces, as formalized with the following theorems

Theorem 1 (Onsager 1937)**.**
Sufficient condition for the (2.3) *to apply is that the generalized flows are linear combination of the generalized forces*

$$\mathbf{J}^\beta = \sum_{\alpha=1}^{N} \mathbf{L}_{\beta\alpha} \mathbf{F}^\alpha$$

where $\mathbf{L}_{\beta\alpha}$ *is a symmetric and positive definite matrix, called* ***matrix of the phenomenological coefficients*** *[9].*

In addition, for isotropic materials, the following principle is used

Principle 1 (Curie principle)**.**
Only forces and flows of the same tensor order are coupled.

This principle is empirical, but it has been discovered that it is a mathematical consequence of isotropic bodies, and it states that they couple scalars with scalars, vectors with vectors, rank tensors 2 with rank tensors 2, and so on... Therefore, in the case of non-isotropic bodies this principle loses its validity.

In general the fluxes and forces are not necessarily scalar quantities: they represent vectorial and tensorial quantities. Also, it should be noted that each individual flow and force has the property of vanishing at equilibrium. It should be stressed that the identification of thermodynamic flows and forces is arbitrary, in fact one could, for example, include the factor $1/T$ in flow instead of force and in the same way, The definitions of flows and forces could be exchanged. However, these different choices are not crucial and have no direct consequences on the interpretation of the final results. This is a little the limit of such a theory.

Observation 1 (CRITICISMS OF CIT)**.** *The criticisms of this method were:*

What is meant by generalized forces and flows? Is there a rigorous mathematical definition?

To answer these questions Onsager made an analogy with the conservative mechanical forces, which as we know are the gradient of a potential $mathbfF = nablaU$*, if the gradient is different from zero, then the particle subject to this field of force starts moving. So, you can imagine, for example*

$$z_\alpha = \rho \Rightarrow \nabla(z_\alpha) = \nabla\rho$$
$$z_\alpha = \theta \Rightarrow \nabla(z_\alpha) = \nabla T$$

where $\nabla\rho$ *and* ∇T *represent a mass density and temperature gradient, respectively. If the temperature gradient is different from zero, i.e.* $\nabla T \neq \mathbf{0}$*, means that the state of the thermodynamic system is not homogeneous. However, there are hottest and coldest zones of the system (less dense and denser areas), then the heat, according to the second principle of thermodynamics flows spontaneously from the hottest zones to the coldest ones (particles flow from denser to less dense areas). Thus, the temperature gradient,* $\nabla\theta$*, is interpreted as a thermodynamic force that "pushes' heat heat from hot to cold zones, similarly the density gradient,* $\nabla\rho$*, is interpreted as a thermodynamic force that "pushes' particles from denser zones to less dense zones.*

Onsager's interpretation, by analogy with the conservative mechanical forces, is not a strict definition of what is a thermodynamic force, of what is a thermodynamic flux, and this problem has not yet been solved. Therefore a criticism already made by Truesdell in the '50s is the lack of rigorous mathematical foundations, The method proposed by Onsager is also the opposite of what a rigorous mathematics must do. He said:

"I want a mathematical definition of generalized forces and fluxes"

He also highlighted that the theorem 1 only considers thermodynamic processes in which the fluxes are linear combinations of forces. Consequently, all those processes where this assumption is not valid are cut off, but there is also a production of non-negative entropy, $\Sigma_s \geq 0$*. So a series of processes are left out, the number of which we do not even know.*

However, even if the method of Onsager does not enjoy the mathematical rigor that instead enjoy the methods of Colemann-Noll and Liu, it is not to be discarded but must be seen as an additional possibility, to determine certain processes.

2.1.1 Fourier's Law

This Section describes is shown the derivation of Fourier's law for a rigid conductor, by the Onsager method which ensures compatibility with the second law of thermodynamics. The Fourier's law is a classical prototype of the constitutive equations leading to a parabolic partial differential equation, its simple classical derivation in Classical Irreversible Thermodynamics is based on the second law of thermodynamics.

We begin by considering a non-local space of the state

$$\mathbb{Z} =< e, \nabla e >$$

and in order to close (2.1), we need a costitutive relations for the heat flux, entropy flux and specific entropy as

$$\mathbf{q} = \mathbf{q}(e, \nabla e)$$
$$\mathbf{J_s} = \mathbf{J_s}(e, \nabla e)$$
$$s = s(e)$$

where, we observe in the classical local equilibrium situation the entropy depends only on the internal energy e (not on ∇e), and from the Gibbs relation

$$T\,ds = de$$

its derivative respect to the internal energy is the reciprocal absolute temperature

$$\frac{ds(e)}{de} = \frac{1}{T}.$$

Then the temperature depends on the internal energy and $T : e \to T(e)$ is the caloric equation of state, generally $e = c_v\,T$ with $c_v = \frac{de}{dT}$ the specific heat capacity.

Taking into account these considerations, the entropy production became

$$\begin{aligned}\Sigma_s = \rho\dot{s} + \operatorname{div}\mathbf{J_s} &= \rho\frac{ds}{de}\frac{\partial e}{\partial t} + \frac{\partial \mathbf{J_s}}{\partial e}\cdot\nabla e + \frac{\partial \mathbf{J_s}}{\partial \nabla e} : \nabla^2 e \\ &= -\frac{ds}{de}\operatorname{div}\mathbf{q} + \frac{\partial \mathbf{J_s}}{\partial e}\cdot\nabla e + \frac{\partial \mathbf{J_s}}{\partial \nabla e} : \nabla^2 e\end{aligned}$$

but the heat flux $\mathbf{q}$ is not a indipendent variable, therefore a constitutive equation of the form must be assigned $\mathbf{q} = \mathbf{q}(e, \nabla e)$, from which

$$\operatorname{div}\mathbf{q} = \frac{\partial \mathbf{q}}{\partial e}\cdot\nabla e + \frac{\partial \mathbf{q}}{\partial \nabla e} : \nabla^2 e$$

and substituting it, we have

$$\begin{aligned}\Sigma_s &= -\frac{ds}{de}\frac{\partial \mathbf{q}}{\partial e}\cdot\nabla e - \frac{ds}{de}\frac{\partial \mathbf{q}}{\partial \nabla e} : \nabla^2 e + \frac{\partial \mathbf{J_s}}{\partial e}\cdot\nabla e + \frac{\partial \mathbf{J_s}}{\partial \nabla e} : \nabla^2 e \\ &= \left(\frac{\partial \mathbf{J_s}}{\partial e} - \frac{ds}{de}\frac{\partial \mathbf{q}}{\partial e}\right)\cdot\nabla e + \left(\frac{\partial \mathbf{J_s}}{\partial \nabla e} - \frac{ds}{de}\frac{\partial \mathbf{q}}{\partial \nabla e}\right) : \nabla^2 e\end{aligned}$$

We assume that the entropy flux is

$$\mathbf{J_s} = \frac{ds}{de}\mathbf{q} = \frac{\mathbf{q}}{T}$$

so its derivatives are

$$\begin{aligned}\frac{\partial \mathbf{J_s}}{\partial e} &= \frac{d^2 s}{de^2}\mathbf{q} + \frac{ds}{de}\frac{\partial \mathbf{q}}{\partial e} \\ \frac{\partial \mathbf{J_s}}{\partial \nabla e} &= \frac{ds}{de}\frac{\partial \mathbf{q}}{\partial \nabla e}\end{aligned}$$

and substituting

$$\Sigma_s = \left(\frac{d^2 s}{de^2}\mathbf{q} + \frac{ds}{de}\frac{\partial \mathbf{q}}{\partial e} - \frac{ds}{de}\frac{\partial \mathbf{q}}{\partial e}\right)\cdot\nabla e + \left(\frac{ds}{de}\frac{\partial \mathbf{q}}{\partial \nabla e} - \frac{ds}{de}\frac{\partial \mathbf{q}}{\partial \nabla e}\right) : \nabla^2 e = \frac{d^2 s}{de^2}\mathbf{q}\cdot\nabla e$$

Then

$$\Sigma_s = \frac{d^2 s}{de^2}\mathbf{q}\cdot\nabla e \geq 0 \tag{2.9}$$

the simplest solution of this inequality is linear, in fact using the Onsager procedure, we identify the generalized fluxes and forces as in Table 2.1

Then the relation (2.9) may be interpreted as the product between a generalized

	Classical thermal
Forces	$\frac{d^2s}{de^2}\nabla e$
Fluxes	$\mathbf{q}$

TABLE 2.1: Thermodynamic 'forces' and 'fluxes'.

force and flow, for the theorem 1 and for the Curie principle 1 for the isotropic material, the generalized flux is expressed as a linear function of the generalized force, as follow

$$\mathbf{q} = l\,\frac{d^2s}{de^2}\nabla e = l\,\nabla\left(\frac{1}{T}\right) = -\frac{l}{T^2}\nabla T = -\lambda(T)\,\nabla T$$

where l represents the phenomenological coefficient, it is expressed by

$$l = \lambda(T)\,T^2$$

where $\lambda(T) > 0$ represent the thermal conductivity, that in general is a function on the temperature. Then we obtained the **Fourier's law**

$$\mathbf{q} = -\lambda(T)\,\nabla T \tag{2.10}$$

with the Onsager procedure in CIT which guarantees that the entropy inequality is automatically satisfied.

Now we observe that the non-linearity is introduced through the phenomenological coefficient, because the fraction l/T^2 describes the thermal conductivity. In order to obtain the linear case, i.e. the thermal conductivity is considered constant, we must assume that $l(T) = \lambda_0 T^2$ or simply T becomes T_0 in $\lambda(T)$. While, if the thermal conductivity is temperature dependent, for example let us suppose (in first approximation) it is a linear function of temperature [19, 20, 33], as follows

$$\lambda(T) = \lambda_0 + a(T - T_0) \tag{2.11}$$

where λ_0 is the thermal conductivity at the initial or reference temperature, a is a material coefficient and could be positive or negative according to the increase or decrease in thermal conductivity in relation to the temperature rise (non-zero value of coefficient a induces a non-linearity of thermal conductivity), is necessary the following constraint

$$l = [\lambda_0 + a(T - T_0)]\,T^2.$$

in order to guarantee the compatibility with the linear relation (2.11).

Hence the Fourier's nonlinear heat model can be written as

$$\rho\,\frac{\partial e}{\partial t} + \nabla\cdot\mathbf{q} = 0,$$
$$\mathbf{q} = -\lambda(T)\nabla T.$$

Replacing the Fourier law into the energy balance law, you get

$$\rho\frac{\partial e}{\partial t} + \nabla\cdot(-\lambda(T)\nabla T) = 0.$$

wherein the thermal conductivity λ is expressed by (2.11). However, substituting

the caloric equation of state, $T(e)$, we obtain the well-known parabolic partial differential heat equation

$$\rho\, c_v \frac{\partial T}{\partial t} - \nabla \cdot (\lambda(T)\nabla T) = 0.$$

Remark 1. *It is possible to obtain the same entropy production (2.9) with the following straightforward calculation*

$$\Sigma_s = \rho \dot{s} + \nabla \cdot \mathbf{J_s} = \frac{1}{T}\rho\, \dot{e} + \nabla \cdot \mathbf{J_s} = \nabla \cdot \left(\mathbf{J_s} - \frac{\mathbf{q}}{T}\right) + \mathbf{q} \cdot \nabla\left(\frac{1}{T}\right) \geq 0$$

and the entropy flux is fixed by eliminating the first term in the last inequality, that is

$$\mathbf{J_s} = \frac{\mathbf{q}}{T}$$

thus the entropy production simplifies to

$$\Sigma_s = \mathbf{q} \cdot \nabla\left(\frac{1}{T}\right) \geq 0$$

obviously as in (2.9). In fact, from $e = e(T)$ we have $T = T(e)$ and

$$\frac{d^2 s}{de^2} = \frac{d}{de}\left(\frac{ds}{de}\right) = \frac{d}{de}\left(\frac{1}{T}\right) = -\frac{1}{T^2}\frac{dT}{de}$$

from which

$$\Sigma_s = \frac{d^2 s}{de^2}\mathbf{q} \cdot \nabla e = -\frac{1}{T^2}\frac{dT}{de}\mathbf{q} \cdot \nabla e = -\frac{1}{T^2}\mathbf{q} \cdot \nabla T = \mathbf{q} \cdot \nabla\left(\frac{1}{T}\right)$$

2.2 Rational Thermodynamics (RT)

The **Rational Thermodynamics** was born with the school of Truesdell (1984) [77] and and has the starting point in the fundamental document of Coleman (1964) and Noll (1974) [72], its main purpose was to provide a rigorous method for the derivation of constitutive equations, thus in high contrast with CIT. To close the system of balance laws, constitutive equations are necessary. The idea of Coleman and Noll was to consider the law of entropy as a criterion for selecting a priori the class of constitutive equations that satisfy this inequality for any process. The limitation of this idea, as we will see, consists in the postulation that the flux of entropy is in the form of Clausius, that is the relationship between the flux of heat and temperature. Müller noted with the help of kinetic considerations that this requirement is too restrictive and proposed to extend the principle of entropy with a general flow of entropy as constitutive quantity [78] as we shall see in the theory of extended rational thermodynamics.

The key points on which this theory is based are briefly presented below

- Absolute temperature and entropy are assumed as primitive concepts and are introduced a priori.
- The principle of local equilibrium is not valid, so it is assumed that the behavior of a system at a certain time instant can depend not only on the values in that time instant but also on all past history.

- The mathematical formulation of the second law of thermodynamics, which essentially serves as a restriction on the form of constitutive equations is a crucial point. The starting point is the Clausius-Planck inequality, which states that between two equilibrium states A and B

$$\Delta S \geq \int_A^B \frac{dQ}{T}$$

that becomes

$$\frac{d}{dt}\int_\Omega \rho s\, dV + \int_{\partial\Omega} \mathbf{J_s}\cdot\mathbf{n}\, d\sigma + \int_\Omega \frac{\rho r}{T}\, dV \geq 0$$

and in local form

$$\rho\dot{s} + \operatorname{div}(\mathbf{J_s}) + \frac{\rho r}{T} \geq 0$$

In particular, the entropy flux $\mathbf{J_s}$ is taken by Coleman and Noll in the form $\mathbf{q}/T$ which in the following years is known as the classical form of the flow of entropy.

Introducing also the free energy of Helmholtz $\psi = e - T\,s$ and replacing the energy balance law, which leads to the elimination of the source term, we get the following inequality

$$-\rho(\dot{\psi} + s\dot{T}) + \sigma : L - \frac{1}{T}\nabla T\cdot\mathbf{q} \geq 0 \tag{2.12}$$

Such inequality (2.12) is known as the Clausius-Duhem inequality and for a thermomechanical process to be admissible any solution of the balance laws must satisfy such inequality. Originally they were looking for solutions of the laws of equilibrium and only later it was verified if these were compatible with the Clausius-Duhem inequality, but obviously this was not an effective approach. In fact, with the advent of this theory, we passed to another point of view, that is, we make the entropy inequality satisfied a priori, or assign the constituent relations to close the system of balance laws that meet the restrictions given by the second law. In this approach the important problem which follows is the choice of independent variables, field variables such as mass density, velocity, temperature, ... as there are further variables, which appear within the (2.12), internal energy, heat flow, stress tensor, entropy...) which are expressed in terms of the former by constitutive equations.

- The principle of equipresence. This principle states that if a variable is present in a constituent equation, will a priori be present in all constitutive equations and the conditions for the presence or absence of such independent variables in a constitutive relation results from the Clausius-Duhem inequality.

- The principle of local action. This principle states that the behaviour of a material point should be influenced only by points close to it. In other words, the values assumed by the constitutive relations at a given point do not take into account what happens at distant points; consequently, in a first order theory, In order to be able to calculate the number of orders, the spatial derivatives shall be omitted.

- The principle of material indifference requires that the constituent equations be independent from the observer. This principle implies, first of all, that the constitutive equations should be objective, i.e. form-invariant under arbitrary

time-dependent rotations and translations of the reference frames as expressed by the Euclidean transformation. This means that the form of the constitutive relations is not influenced by the superposition of any arbitrary and rigid movement of the body. Secondly, the constituent equations must be independent of reference system, in particular of its angular velocity. Of course, before examining the effect of a change in structure on a constituent equation, it is necessary to specify how the basic variables such as temperature, Energy, entropy, thermal flux, stress tensor... behave under such transformation and are expected to be objective.

2.2.1 Fourier's Law

This Section describes the derivation of Fourier's law, by the Coleman-Noll method to guarantee compatibility with the second law of thermodynamics.

Let us consider the Clausius-Duhem inequality (2.12) in the case of rigid conductor

$$-\rho(\dot{\psi} + s\dot{T}) - \frac{1}{T}\nabla T \cdot \mathbf{q} \geq 0 \tag{2.13}$$

We define a generic constitutive function Ψ on the state space $\mathbb{Z} = \{e, \nabla e\}$, i.e. $\Psi = \Psi(e, \nabla e)$ and after some calculation from (2.13), where we use $e = c\,T$, we get

$$\rho\left(\frac{\partial \Psi}{\partial e} + \frac{s}{c}\right)\dot{e} + \rho\frac{\partial \Psi}{\partial \nabla e} \cdot \dot{\nabla} e + \frac{1}{T}\nabla T \cdot \mathbf{q} \leq 0$$

then the thermodynamic restrictions are obtained

$$\begin{aligned}
&\dot{e} \notin \mathbb{Z}\rho\left(\frac{\partial \Psi}{\partial e} + \frac{s}{c}\right) = 0\\
&\dot{\nabla} e \notin \mathbb{Z}\rho\frac{\partial \Psi}{\partial \nabla e} = \mathbf{0}\\
&\nabla T, \mathbf{q} \in \mathbb{Z} \Rightarrow \frac{1}{T}\nabla T \cdot \mathbf{q} \leq 0
\end{aligned}$$

from which

$$\frac{\partial \Psi}{\partial e} = -\frac{s}{c} \tag{2.14}$$

$$\Psi = \Psi(e) \tag{2.15}$$

$$\frac{1}{T}\nabla T \cdot \mathbf{q} \leq 0 \tag{2.16}$$

A possible solution of (2.16) is Fourier's Law

$$\mathbf{q} = -\lambda \nabla T$$

in fact $-\lambda\,\mathbf{q} \cdot \mathbf{q} \leq 0$ which is trivially satisfied. This implies that the Fourier's Law is thermodynamical compatible in RT.

2.3 Rational Extended Thermodynamics (RET)

The first approach to an extended thermodynamic theory was carried out in a classical context by Ingo Müller [79], this is based on the modification of the Gibbs equation which also incorporates the effects of dissipative fluxes. This point of view has

been adopted over the years by several authors and was the starting point of the Extended Irreversible Thermodynamics (EIT) [58, 59].

Muller also criticized in [78] the RT because he did not agree with having to assign the entropy flux in the classical form of Coleman-Noll

$$\mathbf{J_S} = \frac{\mathbf{q}}{T}$$

and an additional term **K**, called **entropy extraflux** was added

$$\mathbf{J_S} = \frac{\mathbf{q}}{T} + \mathbf{K}$$

Furthermore, Muller thought that a thermodynamic theory should be constructed in agreement with the kinetic theory.

The introduction of dissipative fluxes as independent variables, in addition to the usual thermodynamic state variables, has profound implications: first, it goes beyond the local equilibrium hypothesis because dissipative fluxes play an essential role in the characterization of a state of non-equilibrium; secondly, the range of applicability of this extended theory (Extended thermodynamics ET) becomes wider than that of CIT and RT. In other words, the extended thermodynamic theory is applicable to phenomena far from equilibrium such as micro/nano fluxes, second sounds, shock waves, and so on.

This approach has been criticized by Ruggeri [80] because the entropy production depends largely on the choice of the entropy flux, and there are several field equations for a different entropy flux. Moreover, the differential system is not a priori in the form of balance laws. This implies, from a mathematical point of view, that it is not possible to define weak solutions and therefore impossible to study, in particular, shock waves. On the other hands this request, which involves assuming hyperbolic systems, eliminates many physical processes.

Later, a new approach was proposed by Liu and Müller in the classical context [81] and by Liu, Müller and Ruggeri in a relativistic framework [82], which gave rise to the so-called **Rational Extended Thermodynamics (RET)**. The main results were summarized in [54, 56].

The RET theory is a phenomenological theory which aims to reduce the gap between the macroscopic world (RT) and the microscopic world (kinetic theory)

Indeed, if one a gas is considered, two complementary approaches can be adopted to describe its behaviour: the continuous and the kinetic approaches. The first, the macroscopic approach, is to describe of a gas behaviour by means of a system of macroscopic equations, for example fluid dynamics, which are closed when appropriate constitutive relations are assigned. This is the classical context of CIT and RT, in which the Navier-Stokes-Fourier (NSF) theory has played a fundamental role. This theory has its limits : the nature of the resulting system is parabolic, it implies that signals are propagated at infinite speed. Furthermore, these classical macroscopic theories are intrinsically limited to a state of non-equilibrium characterized by a small value of the Knudsen number Kn, which represents a measure of gas rarefaction:

$$\mathrm{Kn} = \frac{\text{mean free path of molecule}}{\text{macroscopic characteristic length}}. \tag{2.17}$$

The second one, the microscopic approach, is based on kinetic theory where it is postulated that the state of gas is described by a distribution function, whose evolution is governed by the Boltzmann equation (2.18). Kinetic theory is applicable to

a non-equilibrium state characterized by a large value of the Knudsen number Kn. However, this approach presents considereble problems in the analytic resolution of the Boltzmann equation, this is the reason because the RET's aims is to reduce the gap between these two approaches: macroscopic and microscopic,

The mathematical framework of RET consists of a hierarchy of balance laws that it is the same hierarchical structure as that seen in the system of momentum equations in kinetic theory with truncation to a certain arbitrary order of moments. However, in the RET theory the closure of hierarchical system is achieved thorough the universal principles of physics: principle of objectivity, entropy, causality and stability.

In fact, this theory is based on the work published by a mathematician of New York, Harnold Grad in 1949, *On the kinetic theory of rarefied gases* [83], which leads to the

The stress tensor and heat flux are not necessarily constitutive equations, but they have their balance law.

This has brought to an end the foundations of rational thermodynamics (RT) according to which for for the stress tensor σ and for the heat flux were assigned constitutive equations, that were in agreement with the second law of thermodynamics. These were used to characterize the material and to close the system. Like this

There is obviously an exact set of equations that are satisfied by the thermodynamic variables, i.e. all conservation laws (conservation of mass, momentum, energy) but these do not form a determined system, because there are additional variables, namely stress σ and heat flux $\mathbf{q}$, for which a special form is assumed in terms of thermodynamic variables and their gradients. In particular, there is no universal relation which gives stress and heat flux in terms of thermodynamic variables and their gradients of all orders.

H. GRAD

2.3.1 Guidelines of RET : Boltzmann Equation and the Moments, closure

The theory of **Rational Extended Thermodynamics** is based on an infinite system of hierarchical balance laws, which must be satisfied by the moments of the distribution function f. Since a system consists of infinite equations, they must be truncated to a certain order N and the resulting system to be solved needs a "closure' which is obtained by taking into account:

- the entropy principle,
- strong causuality principle,
- the principle of objectivity.

Strictly using the *kinetic theory* of a monoatomic gas, which is based on the assumption that the condition of the gas is described by a distribution function:

$$f = f(\mathbf{x}, \boldsymbol{\xi}, t) = f(x_1, x_2, x_3, \xi_1, \xi_2, \xi_3, t)$$

which represents the probability of finding a gas particle, at instant t, in the point $\mathbf{x} = (x_1, x_2, x_3)$ with velocity $\boldsymbol{\xi} = (\xi_1, \xi_2, \xi_3)$. However, with $f(\mathbf{x}, \boldsymbol{\xi}, t)d\boldsymbol{\xi}$ we indicate the number density of (monatomic) molecules at the point $\mathbf{x}$ and time t that have velocities between $\boldsymbol{\xi}$ and $\boldsymbol{\xi} + d\boldsymbol{\xi}$.

In absence of external forces the time-evolution of the distribution function f is governed by the Boltzmann equation:

$$\frac{\partial f}{\partial t} + \xi_i \frac{\partial f}{\partial x_i} = Q(f) \quad \Leftrightarrow \quad \partial_t f + \xi_i \partial_i f = Q(f) \tag{2.18}$$

vector form

$$\underbrace{\frac{\partial f}{\partial t} + \boldsymbol{\xi} \cdot \nabla f}_{\frac{df}{dt}\ \text{material derivative}} = Q(f) \tag{2.19}$$

where $Q(f)$ represents the collision operator, it describes the effect of collisions between molecules of gas.

As is well known, all macroscopic thermodynamic quantities are identified as **moments of the distribution function**, obtained by averaging f on the space of the velocities:

$$F = \int_{\mathbb{R}^3} m f d\boldsymbol{\xi}$$
$$F_{i_1 i_2 i_3 \ldots i_k} = \int_{\mathbb{R}^3} m\, \xi_{i_1} \xi_{i_2} \xi_{i_3} \ldots \xi_{i_k} f d\boldsymbol{\xi} \text{ con } i_1, i_2, \ldots i_k \in 1,2,3 \text{ ed } k \in \mathbb{N}^+$$

where m is the mass of a molecule and $d\boldsymbol{\xi} = d\xi_1 d\xi_2 d\xi_3$.

In particular

0th moment	$F = \int_{\mathbb{R}^3} m f d\boldsymbol{\xi}$
1th moment	$F_{i_1} = \int_{\mathbb{R}^3} m \xi_{i_1} f d\boldsymbol{\xi}$
2th moment	$F_{i_1 1_2} = \int_{\mathbb{R}^3} m \xi_{i_1} \xi_{i_2} f d\boldsymbol{\xi}$
3th moment	$F_{i_1 1_2 i_3} = \int_{\mathbb{R}^3} m \xi_{i_1} \xi_{i_2} \xi_{i_3} f d\boldsymbol{\xi}$
$\vdots$	$\vdots$
kth moment	$F_{i_1 1_2 i_3 \ldots i_k} = \int_{\mathbb{R}^3} m \xi_{i_1} \xi_{i_2} \xi_{i_3} \ldots \xi_{i_k} f d\boldsymbol{\xi}$

As mentioned above, the collisional operator $Q(f)$ has a very complicated' expression, which makes it almost impossible to solve the Boltzmann equation analytically. Determination of the distribution function f, after an integration on the space of velocities, allows the resolution of the macroscopic quantity. A way to solve the Boltmann equation is to approximate it as did Grad in [83] giving rise to a hierarchical system that satisfies moments.

In fact, it is easy to note that the moments of function satisfy a hierarchy of the balance laws where the flux of one density becomes the density in the next one

$$\begin{aligned}
&\partial_t F + \partial_k F_k = P \\
&\qquad \swarrow \\
&\partial_t F_{i_1} + \partial_k F_{ki_1} = P_{i_1} \\
&\qquad \swarrow \\
&\partial_t F_{i_1 i_2} + \partial_k F_{ki_1 i_2} = P_{i_1 i_2} \\
&\qquad \swarrow \\
&\partial_t F_{i_1 i_2 i_3} + \partial_k F_{ki_1 i_2 i_3} = P_{i_1 i_2 i_3} \\
&\quad \vdots \qquad\quad \vdots \qquad\quad \vdots \\
&\partial_t F_{i_1 i_2 i_3 \ldots i_j} + \partial_k F_{ki_1 i_2 i_3 \ldots i_j} = P_{i_1 i_2 i_3 \ldots i_j} \\
&\quad \vdots \qquad\quad \vdots \qquad\quad \vdots \\
&\quad \vdots \qquad\quad \vdots \qquad\quad \vdots
\end{aligned} \tag{2.20}$$

where $P_{i_1 i_2 i_3 \ldots i_j}$ represent the productions

$$P_{i_1 i_2 \ldots i_j} = \int_{\mathbb{R}^3} m\, Q \xi_{i_1} \xi_{i_2} \cdots \xi_{i_j} d\boldsymbol{\xi}.$$

Taking $P_{ii} = 0$, we note that the first five equations are exactly the conservation laws, and correspond to the conservation laws of mass, momentum and energy, respectively.

However, if we define the following quantities

$$\begin{aligned}
h^0 &= -k_B \int_{\mathbb{R}^3} f \log f d\boldsymbol{\xi} \\
h^i &= -k_B \int_{\mathbb{R}^3} f \log f \xi_i d\boldsymbol{\xi}
\end{aligned}$$

with k_B being the Boltzmann constant, it is possible to prove the famous H-theorem:

$$\partial_t h^0 + \partial_i h^i = \Sigma \geqslant 0. \tag{2.21}$$

If we identify h^0, h^i and Σ as the entropy density, the entropy flux, and the entropy production, respectively, the previous theorem represents the balance law of entropy.

A fundamental postulate of the RET is based on the idea that a hierarchical system of balance laws (2.20) truncated but with tensorial density of some arbitrary order N, is interpreted as a phenomenological system describing some thermomechanical system. On this basis the following postulate has been formulated

Postulate 1. *Each thermodynamic system must be described by a truncated hierarchical system at tensor density of order N*

$$\begin{aligned}
&\partial_t F + \partial_k F_k = P \\
&\partial_t F_{i_1} + \partial_k F_{ki_1} = P_{i_1} \\
&\partial_t F_{i_1 i_2} + \partial_k F_{ki_1 i_2} = P_{i_1 i_2} \\
&\partial_t F_{i_1 i_2 i_3} + \partial_k F_{ki_1 i_2 i_3} = P_{i_1 i_2 i_3} \\
&\quad \vdots \qquad\qquad \vdots \qquad\qquad \vdots \\
&\partial_t F_{i_1 i_2 i_3 \ldots i_N} + \partial_k F_{ki_1 i_2 i_3 \ldots i_N} = P_{i_1 i_2 i_3 \ldots i_N}
\end{aligned} \tag{2.22}$$

where

$$\mathbf{U} = (F, F_{i_1}, F_{i_1 i_2}, F_{i_1 i_2 i_3}, ..., F_{i_1 i_2 i_3 \ldots i_N})$$

is the field of tensor densities, while

$$P, P_{i_1}, P_{i_1 i_2}, P_{i_1 i_2 i_3}, ..., P_{i_1 i_2 i_3 \ldots i_N}$$

are the productions.

As can be seen, the truncate system (2.22) is not a closed system, since the last flux and all productions do not satisfied balance laws. The idea of RET ([56]) is to assign the local constitutive equations for all productions and for the last flux:

$$\begin{aligned}
F_{i_1 i_2 i_3 \ldots i_N i_{N+1}} &= F_{i_1 i_2 i_3 \ldots i_N i_{N+1}}(F, F_{j_1}, F_{j_1 j_2}, F_{j_1 j_2 j_3}, ..., F_{j_1 j_2 j_3 \ldots j_N}) \\
\sigma_{i_1 i_2 i_3 \ldots i_k} &= \sigma_{i_1 i_2 i_3 \ldots i_k}(F, F_{j_1}, F_{j_1 j_2}, F_{j_1 j_2 j_3}, ..., F_{j_1 j_2 j_3 \ldots j_N}) \qquad \forall k = 0, 1 \ldots N
\end{aligned} \tag{2.23}$$

where if $k = 0$, then $\sigma_{i_0} = \sigma$.

Particular attention should be paid to the definition of the temperature of the non-equilibrium. If the study is limited to non-equilibrium thermodynamics under the local equilibrium hypothesis, there are no conceptual difficulties in the temperature of the non-equilibrium. In fact, CIT or RT do not have such difficulty. However, beyond the local equilibrium hypothesis to study highly nonequilibrium phenomena, we encounter an extremely difficult problem. The definition of an appropriate non-equilibrium temperature has always been a great challenge. In the RET (and also kinetic theory), the so-called kinetic temperature, which is defined by the thermal mean of the kinetic energy of a molecule, the equilibrium temperature has been adopted as the non-equilibrium temperature.

Observation 2. *We observe that the choice of the number of equations of the hierarchical system is arbitrary, that is the choice of the order N of the tensor density to which the system is to be truncated apparently arbitrary. So N you can choose large at will, and since increase in N leads to an increase in the number of equations, the physical interpretation of the various tensor densities becomes very difficult. Therefore, the choice of N should be made so that there is agreement with the experimental data.*

2.3.2 Cattaneo equation compatibility

The RET approach, unlike the RT and CIT theories, allows to demonstrate that the evolution equation for heat flux proposed by Cattaneo [1], Vernotte [2] and Maxwell [3] is compatible with the second law of thermodynamics.

Consider a hierarchical system truncated to tensor density of order 2, that is containing 4 scalar equations

$$\partial_t F + \partial_k F_k = P \tag{2.24}$$
$$\partial_t F_{i_1} + \partial_k F_{ki_1} = P_{i_1} \tag{2.25}$$

Now consider a rigid conductor, so with out deformation, density is constant and then the two equations of the system (2.24)-(2.25) cannot be interpreted as, respectively, the conservation law of mass and the balance law of momentum. However, since the equation (2.24) is scalar it is interpreted as the energy balance law, whereas the equation (2.25) being vector is interpreted as the balance law of a vector field, the heat flux Taking this into account, by identifying

$$\begin{aligned} F &= \rho\, e \\ F_k &= q_k \\ F_{ki_1} &= Q_{ki_1} \\ P &= 0 \\ P_{i_1} &= (\mathbf{r_q})_{i_1} \end{aligned}$$

one gets

$$\begin{aligned} \rho\, \partial_t e + \partial_k q_k &= 0 \\ \partial_t q_{i_1} + \partial_k Q_{ki_1} &= (\mathbf{r_q})_{i_1} \end{aligned}$$

and in vector form

$$\rho\, \partial_t e + \nabla \cdot \mathbf{q} = 0 \tag{2.26}$$
$$\partial_t \mathbf{q} + \nabla \cdot \mathbf{Q} = \mathbf{r_q} \tag{2.27}$$

For the system consisting of (2.26)-(2.27) to be closed, it is necessary to assign the constitutive relations for the last flux and for all productions. Let as consider a local state space

$$\mathbb{Z} =< e, \mathbf{q} >$$

where the clear difference with RT is observed, in fact it assumes the dissipative fluxes are in the state space, in this case the heat flux, for which a constitutive equation is no longer necessary but, in agreement with the guidelines of the RET, being an unknown field it also needs an evolution equation. Then the constitutive relations, all defined in the same way (i.e. depend of all field variables), are

$$\begin{aligned} \mathbf{Q} &= \mathbf{Q}(e, \mathbf{q}) \\ \mathbf{r_q} &= \mathbf{r_q}(e, \mathbf{q}) \\ s &= s(e, \mathbf{q}) \\ \mathbf{J_s} &= \mathbf{J_s}(e, \mathbf{q}) \end{aligned}$$

Introducing the entropy inequality

$$\Sigma_s = \rho\, \dot{s} + \operatorname{div} \mathbf{J_s} \geq 0$$

wherein the entropy flux is expressed in the classical form $\mathbf{J_s} = \mathbf{q}/T$, therefore the inequality assumed the following form

$$\Sigma_s = \rho\,\dot{s} + \operatorname{div}\frac{\mathbf{q}}{T} = \rho\,\dot{s} + \frac{1}{T}\operatorname{div}\mathbf{q} - \frac{1}{T^2}\,\mathbf{q}\cdot\nabla T \geq 0$$

and after the time derivative of entropy has been explained, replacing the energy balance law (2.26) and balance law of heat flux (2.27), we get

$$\begin{aligned}\Sigma_s &= \rho\,\frac{\partial s}{\partial e}\dot{e} + \rho\,\frac{\partial s}{\partial \mathbf{q}}\cdot\dot{\mathbf{q}} + \frac{1}{T}\operatorname{div}\mathbf{q} - \frac{1}{T^2}\mathbf{q}\cdot\nabla T \\ &= \left(\frac{\partial s}{\partial e} - \frac{1}{T}\right)\operatorname{div}\mathbf{q} + \rho\,\frac{\partial s}{\partial \mathbf{q}}\cdot\left(-\operatorname{div}\mathbf{Q} + \mathbf{r_q}\right) - \frac{1}{T^2}\mathbf{q}\cdot\nabla T \geq 0\end{aligned}$$

Moreover, substituting the divergence of $\mathbf{Q} = \mathbf{Q}(e, \mathbf{q})$ the inequality becomes

$$\Sigma_s = \left(\frac{\partial s}{\partial e} - \frac{1}{T}\right)\operatorname{div}\mathbf{q} - \left(\rho\,\frac{\partial s}{\partial \mathbf{q}}\cdot\frac{\partial \mathbf{Q}}{\partial e}\right)\cdot\nabla e - \left(\rho\,\frac{\partial s}{\partial \mathbf{q}}\cdot\frac{\partial \mathbf{Q}}{\partial \mathbf{q}}\right) : \nabla\mathbf{q} + \rho\,\frac{\partial s}{\partial \mathbf{q}}\cdot\mathbf{r_q} - \frac{1}{T^2}\mathbf{q}\cdot\nabla T \geq 0$$

and assuming $e = c_v\,T$ with c_v the specific heat capacity (assumed constant) we obtain the final form of the entropy production

$$\Sigma_s = \left(\frac{\partial s}{\partial e} - \frac{1}{T}\right)\operatorname{div}\mathbf{q} - \left(\rho\,c_v\frac{\partial s}{\partial \mathbf{q}}\cdot\frac{\partial \mathbf{Q}}{\partial e} + \frac{1}{T^2}\mathbf{q}\right)\cdot\nabla T - \left(\rho\,\frac{\partial s}{\partial \mathbf{q}}\cdot\frac{\partial \mathbf{Q}}{\partial \mathbf{q}}\right) : \nabla\mathbf{q} + \rho\,\frac{\partial s}{\partial \mathbf{q}}\cdot\mathbf{r_q} \geq 0.$$

Therefore, the thermodynamic restrictions are:

$$\begin{aligned}&\operatorname{div}\mathbf{q} \notin \mathbb{Z} \Rightarrow \frac{\partial s}{\partial e} - \frac{1}{T} = 0 \\ &\nabla T \notin \mathbb{Z} \Rightarrow \rho\,c_v\frac{\partial s}{\partial \mathbf{q}}\cdot\frac{\partial \mathbf{Q}}{\partial e} + \frac{1}{T^2}\mathbf{q} = \mathbf{0} \\ &\nabla\mathbf{q} \notin \mathbb{Z} \Rightarrow \rho\,\frac{\partial s}{\partial \mathbf{q}}\cdot\frac{\partial \mathbf{Q}}{\partial \mathbf{q}} = \mathbf{0} \\ &\mathbf{r_q} \in \mathbb{Z} \Rightarrow \rho\,\frac{\partial s}{\partial \mathbf{q}}\cdot\mathbf{r_q} \geq 0\end{aligned}$$

from which

$$\frac{\partial s}{\partial e} = \frac{1}{T} \tag{2.28}$$

$$\rho\,c_v\frac{\partial s}{\partial \mathbf{q}}\cdot\frac{\partial \mathbf{Q}}{\partial e} + \frac{1}{T^2}\mathbf{q} = \mathbf{0} \tag{2.29}$$

$$\frac{\partial \mathbf{Q}}{\partial \mathbf{q}} = \mathbf{0} \tag{2.30}$$

$$\rho\,\frac{\partial s}{\partial \mathbf{q}}\cdot\mathbf{r_q} \geq 0 \tag{2.31}$$

A possible solution to the (2.30) is given

$$\mathbf{Q} = \frac{\lambda}{\tau}TI$$

where λ and τ represent the thermal conductivity and the relaxation time of the heat flux, respectively. Now assuming

$$s(e, \mathbf{q}) = s_{eq}(e) + \tilde{s}(\mathbf{q})$$

by using the restriction (2.29) one has

$$\mathbf{0} = \rho\, c_v \frac{\partial s}{\partial \mathbf{q}} \cdot \frac{\partial \mathbf{Q}}{\partial e} + \frac{1}{T^2}\mathbf{q} = \frac{\rho\,\lambda}{\tau}\frac{\partial \tilde{s}}{\partial \mathbf{q}} \cdot I + \frac{1}{T^2}\mathbf{q} = \frac{\rho\,\lambda}{\tau}\frac{\partial \tilde{s}}{\partial \mathbf{q}} + \frac{1}{T^2}\mathbf{q}$$

from which

$$\frac{\partial \tilde{s}}{\partial \mathbf{q}} = -\frac{\tau}{\rho\lambda T^2}\,\mathbf{q} \tag{2.32}$$

after integrating

$$\tilde{s}(\mathbf{q}) = -\frac{\tau}{2\rho\lambda T^2}\,\mathbf{q}\cdot\mathbf{q}.$$

Then the entropy assumes the following form

$$s(e, \mathbf{q}) = s_{eq}(e) - \frac{\tau}{2\rho\lambda T^2}\mathbf{q}\cdot\mathbf{q}$$

where

$$\frac{\partial s_{eq}(e)}{\partial e} = \frac{1}{T}$$

from (2.28). Finally, by replacing what was previously obtained in the reduced inequality (2.31) we have

$$-\frac{\tau}{2\rho\lambda T^2}\mathbf{q}\cdot\mathbf{r_q} \geq 0$$

if the source term as the following form

$$\mathbf{r_q} = -\frac{\mathbf{q}}{\tau} \tag{2.33}$$

the reduced inequality is trivially satisfied, in fact it results

$$\frac{1}{2\rho\lambda T^2}\mathbf{q}\cdot\mathbf{q} \geq 0$$

In conclusion, the second principle of thermodynamics is automatically satisfied if the following constitutive equations are assigned

$$\mathbf{Q} = \frac{\lambda}{\tau}TI \tag{2.34}$$

$$\mathbf{r_q} = -\frac{\mathbf{q}}{\tau} \tag{2.35}$$

$$s(e, \mathbf{q}) = s_{eq}(e) - \frac{\tau}{2\rho\lambda T^2}\mathbf{q}\cdot\mathbf{q} = s_{eq}(e) - \frac{\tau c_v^2}{2\rho\lambda e^2}\,|\mathbf{q}|^2 \tag{2.36}$$

$$\mathbf{J_s} = \frac{\mathbf{q}}{T} \tag{2.37}$$

It can be observed that from the constitutive equations obtained (2.34)- (2.35), which satisfy the second principle of thermodynamics,one obtains easily the MCV equation, in fact replacing them in the system (2.26)-(2.27) and using the relation

$e = c_v T$ you get

$$\rho\, c_v \frac{\partial T}{\partial t} + \operatorname{div} \mathbf{q} = 0$$
$$\tau \frac{\partial \mathbf{q}}{\partial t} + \mathbf{q} = -\lambda \nabla T$$

Observation 3. *The following expression for temperature can be obtained*

$$\frac{\partial s}{\partial e} = \frac{\partial s_{eq}}{\partial e} + \frac{\tau c_v^2}{\rho \lambda e^3} |\mathbf{q}|^2 \quad \Leftrightarrow \quad \frac{1}{T} = \frac{1}{T_{eq}} + \frac{\tau c_v^2}{\rho \lambda e^3} |\mathbf{q}|^2$$

which can be interpreted as non-equilibrium temperature, T, is composed by two contributions, the first term related to the equilibrium temperature, T_{eq}, the second addend represents a non-equilibrium term related to dissipative fluxes through the heat flux module $|\mathbf{q}|^2 = \mathbf{q} \cdot \mathbf{q}$. Let us observe that the latter term is different from zero when you are far from equilibrium ($\mathbf{q} \neq \mathbf{0}$), while it is null at equilibrium ($\mathbf{q} = \mathbf{0}$). In this case, the temperature is defined as

$$\frac{1}{T} = \frac{\partial s_{eq}}{\partial e} \equiv \frac{1}{T_{eq}}.$$

This observation allows the concept of temperature to be extended, which needs generalization, i.e. the introduction of the concept of temperature of non-equilibrium. Similarly from relation (2.36) the expression of non equilibrium entropy is obtained

$$s(e, \mathbf{q}) = s_{eq}(e) - \frac{\tau}{2\rho\lambda T^2} \mathbf{q} \cdot \mathbf{q} = s_{eq}(e) - \frac{\tau c_v^2}{2\rho\lambda e^2} |\mathbf{q}|^2.$$

The term of non-equilibrium is always positive, according to the principle of equilibrium ($\mathbf{q} = \mathbf{0}$).

2.4 Extended Irreversible Thermodynamics (EIT)

The **Extended Irreversible Thermodynamics** was born in Spain by Casas-Vasquez, Jou and Lebon [58, 59, 84], with the aim of proposing a theory that goes beyond the classical formulation of irreversible thermodynamics (CIT). This theory is achieved by expanding the state space by introducing in addition to the classical variables, new non-equilibrium variables such as dissipative fluxes appearing in the mass, momentum and energy balance equations. However, the next step is to determine the evolution equations for these additional variables. Whereas the evolution equations of classical variables are provided by balance laws, there are no general criteria for the evolution equations of fluxes except for the restrictions imposed on them by the second law of thermodynamics.

The independent character of dissipative fluxes is evident in high frequency phenomena. In general, they are fast variables that decay to their local equilibrium values after a short time of relaxation. Many authors have studied the elimination of these fast variables, we describe phenomena at frequencies comparable to the inverse of flow relaxation times, including these variables. Therefore, at such time scales, it is natural to include the fast (dissipative flows) in the set of basic independent variables. A simple way to obtain the evolution equations for flows from a macroscopic point of view is to generalize the classical theories presented in the previous sections. Many authors have studied the elimination of these fast variables,

being that we want to describe phenomena at frequencies comparable to the inverse of the relaxation times of the fluxes, therefore, in such time scales, it is natural to include these variables (dissipating fluxes) in the set of basic independent variables. A simple way to obtain the equations of flux evolution from a macroscopic point of view is to generalize the classical theories presented in the previous sections.

In particular, it is assumed the existence of a generalized entropy function which depends on the dissipative fluxes and on the classical variables as well. A physical interpretation of the different contributions to the generalized entropy is propose. Once this expression is known, it is an easy matter to derive generalized constitutive relations.

In this dissertation, we focus on the problem of heat transport in a rigid isotropic body when only the heat flux is introduced as an additional variable.

2.4.1 Guidelines of EIT

As in CIT, the entropy and the Gibbs equation play a central role in EIT. The fundamental idea of EIT is to extend the concepts of entropy, the Gibbs equation, the entropy flux and temperature of the non-equilibrium, adding terms that depend on dissipative fluxes. Here, it is assumed that the entropy will not depend only on classical variables, such as specific internal energy e, but in addition on the heat flux $\mathbf{q}$ and the flux of heat flux $\mathbf{Q}$ (a tensor of rank two),

$$s = s(e, \mathbf{q}, \mathbf{Q}) \tag{2.38}$$

The following properties will be attributed to generalized entropy properties:

- It is an additive quantity
- It is a concave function of the set of variables
- Its production rate is locally positive.

The hypothesis of a generalized macroscopic entropy dependent on dissipative fluxes was advanced in 1953 by Machlup and Onsager indirectly. During the 1960s a more direct formulation applied to fluids was developed by Nettleton (1959) and Muller (1967). In 1970s, new formulations were proposed independently by several authors and have inspired many researches including Gyarmati, Jou, Garcia-Colin et al.

The differential form of the generalized entropy is written as follows:

$$ds = \frac{\partial s}{\partial e} de + \frac{\partial s}{\partial \mathbf{q}} \cdot d\mathbf{q} + \frac{\partial s}{\partial \mathbf{Q}} : d\mathbf{Q}$$

In analogy with the classical theory, we define the non-equilibrium temperature θ by

$$\frac{1}{\theta} = \frac{\partial s}{\partial e}\Big|_{\mathbf{q},\mathbf{Q}} \tag{2.39}$$

not to be confused with the local-equilibrium temperature

$$\frac{1}{T} = \frac{\partial s}{\partial e}\Big|_{\mathbf{q}=\mathbf{0},\mathbf{Q}=\mathbf{0}}$$

We note that in the CIT, one assumes the local-equilibrium hypothesis, where it is assumed that, despite the fact that the system is globally out of equilibrium, it remains locally in equilibrium. In other words, it is assumed that it may be decomposed in

subsystems small enough to be almost homogeneous at the macroscopic scale, and large enough, on the microscopic scale, to have many particles in such a way that macroscopic quantities keep a well-defined meaning.

Within this framework, the problem of a generalization of temperature does not even arise: it is assumed that the entropy and all the derived equations of state keep locally the same meaning as in equilibrium, and that temperature coincides with that indicated by a sufficiently small and fast thermometer. The problem of the meaning of entropy and temperature arises when one goes beyond the local equilibrium, as in this case, because genuinely non-equilibrium contributions must be taken into account in the entropy and, consequently, in temperature.

This explains the motivation that we need to extend the concept of entropy, Gibbs relation, temperature of non-equilibrium and entropy flux [85–87].

The inverse of non-equilibrium temperature can be expanded around the inverse of the local-equilibrium temperature and written as

$$\theta^{-1} = T^{-1} + \alpha(e)\mathbf{q}\cdot\mathbf{q} + \beta(e)\mathbf{Q}:\mathbf{Q}$$

where the coefficients $\alpha(e)$ and $\beta(e)$ depend generally on e.

The remaining partial derivatives are

$$\frac{\partial s}{\partial \mathbf{q}} = -\boldsymbol{\alpha_1}(e,\mathbf{q},\mathbf{Q}),$$
$$\frac{\partial s}{\partial \mathbf{Q}} = -\boldsymbol{\alpha_2}(e,\mathbf{q},\mathbf{Q}),$$

in particular without losing generality it is assumed

$$\boldsymbol{\alpha_1}(e,\mathbf{q},\mathbf{Q}) = m(e)\mathbf{q},$$
$$\boldsymbol{\alpha_2}(e,\mathbf{q},\mathbf{Q}) = M(e)\mathbf{Q},$$

from which we obtain the generalized Gibbs equation

$$ds = \frac{1}{\theta}de - m(e)\mathbf{q}\cdot d\mathbf{q} - M(e)\mathbf{Q}\cdot d\mathbf{Q}$$

Furthermore, we postulate the entropy flux $\mathbf{J_s}$ as

$$\mathbf{J_s} = \frac{\mathbf{q}}{\theta} + \mathbf{K} \tag{2.40}$$

where the classical term $\mathbf{q}/T$ is replaced with $\mathbf{q}/\theta$ and an additional contribution is present, for example in terms of $\mathbf{Q}\cdot\mathbf{q}$. Then we compute the entropy production $\Sigma_s = \rho\dot{s} + \nabla\cdot\mathbf{J_s}$ and requiring it to be is non-negative, we get the shape of the evolution equations for the dissipative fluxes $\mathbf{q}, \mathbf{Q}$.

In the following we present the thermodynamic compatibility of MCV and GK evolution equations.

2.4.2 Cattaneo equation compatibility

In order to obtain the Cattaneo evolution equation for the heat flux $\mathbf{q}$, we assume that the state space is spanned by variables $(e, \mathbf{q})$,

$$\mathbb{Z} = < e, \mathbf{q} >$$

the idea is to consider the heat flux $\mathbf{q}$ as a state variable, for which is necessary to determine an evolution equation of the form

$$\dot{\mathbf{q}} = \mathbf{f}(e, \mathbf{q}) \tag{2.41}$$

and to close the system (2.1)-(2.41), we need a costitutive relations for the function $\mathbf{f}$, the entropy flux and specific entropy as

$$\begin{aligned} \mathbf{f} &= \mathbf{f}(e, \mathbf{q}) \\ \mathbf{J_s} &= \mathbf{J_s}(e, \mathbf{q}) \\ s &= s(e, \mathbf{q}) \end{aligned}$$

In EIT we assume the following extended form for the specific entropy

$$s(e, \mathbf{q}) = s_{eq}(e) - \frac{m(e)}{2}\, \mathbf{q} \cdot \mathbf{q}, \tag{2.42}$$

where s_{eq} is the classical specific entropy representing equilibrium entropy and $m(e)$ is a positive function, this guarantees that entropy is a concave function and maximum at the equilibrium (i.e. $\mathbf{q} = \mathbf{0}$).

The resulting generalized Gibbs relation is expressed by

$$ds = \frac{\partial s}{\partial e} de + \frac{\partial s}{\partial \mathbf{q}} \cdot d\mathbf{q} \quad \Longleftrightarrow \quad ds = \theta^{-1} de - m(e)\, \mathbf{q} \cdot d\mathbf{q}$$

where the derivative of specific entropy w.t.r the internal energy and heat flux are, respectively

$$\frac{ds}{de}(e, \mathbf{q}) = \frac{1}{T} - \frac{1}{2}\frac{dm(e)}{de}\mathbf{q} \cdot \mathbf{q} \equiv \frac{1}{\theta} \tag{2.43a}$$

$$\frac{ds}{d\mathbf{q}}(e, \mathbf{q}) = -m(e)\, \mathbf{q} \tag{2.43b}$$

We compute the entropy production

$$\begin{aligned} \Sigma_s = \rho \dot{s} + \nabla \cdot \mathbf{J_s} &= \rho \frac{\partial s}{\partial e} \dot{e} + \rho \frac{\partial s}{\partial \mathbf{q}} \cdot \dot{\mathbf{q}} + \nabla \cdot \mathbf{J_s} \\ &= -\frac{\partial s}{\partial e} \nabla \cdot \mathbf{q} + \rho \frac{\partial s}{\partial \mathbf{q}} \cdot \mathbf{f}(e, \mathbf{q}) + \nabla \cdot \mathbf{J_s} \\ &= -\frac{1}{\theta} \nabla \cdot \mathbf{q} - \rho\, m(e)\, \mathbf{q} \cdot \mathbf{f}(e, \mathbf{q}) + \nabla \cdot \mathbf{J_s} \\ &= -\rho\, m(e)\, \mathbf{q} \cdot \mathbf{f}(e, \mathbf{q}) - \nabla \cdot \left(\frac{\mathbf{q}}{\theta}\right) + \nabla \left(\frac{1}{\theta}\right) \cdot \mathbf{q} + \nabla \cdot \mathbf{J_s} \\ &= -\rho\, m(e)\, \mathbf{q} \cdot \mathbf{f}(e, \mathbf{q}) + \nabla \cdot \left(J_s - \frac{\mathbf{q}}{\theta}\right) + \nabla \left(\frac{1}{\theta}\right) \cdot \mathbf{q} \end{aligned}$$

Now we assume the classical form for the entropy flux, but we replace the equilibrium temperature T with the non-equilibrium temperature θ

$$\mathbf{J_s} = \frac{\partial s}{\partial e}\mathbf{q} = \frac{\mathbf{q}}{\theta}$$

this implies that the entropy flux contains an extra non-equilibrium term from the definition of the non-equilibrium temperature (2.43a), i.e.

$$\mathbf{J_s} = \frac{\mathbf{q}}{T} - \left(\frac{1}{2}\frac{dm(e)}{de}\mathbf{q}\cdot\mathbf{q}\right)\mathbf{q}$$

and one has

$$\Sigma_s = \left[\nabla\left(\frac{1}{\theta}\right) - \rho\, m(e)\,\mathbf{f}(e,\mathbf{q})\right]\cdot\mathbf{q} \tag{2.44}$$

The simplest solution of this inequality is linear, in fact using the Onsager procedure, we identify the generalized fluxes and forces as in Table 2.2.

	Thermal
Forces	$\mathbf{q}$
Fluxes	$\nabla\left(\frac{1}{\theta}\right) - \rho\, m(e)\,\mathbf{f}(e,\mathbf{q})$

TABLE 2.2: Thermodynamic 'forces' and 'fluxes'.

Then the relation (2.44) is the product between a generalized forces and fluxes, for the theorem 1 and the Curie principle 1 (for the isotropic material), the generalized fluxes are expressed as a linear function of the generalized forces (Onsager-Casimir relation [9]), as follow

$$\nabla\left(\frac{1}{\theta}\right) - \rho\, m(e)\,\mathbf{f}(e,\mathbf{q}) = l\,\mathbf{q}$$

where $l = l(e,\mathbf{q})$ is the phenomenological coefficient, with $l \geq 0$. After some manipulation is possible to determine

$$\mathbf{f}(e,\mathbf{q}) = -\frac{l(e,\mathbf{q})}{\rho\, m(e,\mathbf{q})}\,\mathbf{q} + \frac{1}{\rho\, m(e,\mathbf{q})}\nabla\left(\frac{1}{\theta}\right)$$

substituting into the evolution equation of the heat flux (2.41) we obtain

$$\frac{\rho\, m(e,\mathbf{q})}{l(e,\mathbf{q})}\,\dot{\mathbf{q}} + \mathbf{q} = l(e,\mathbf{q})\,\nabla\left(\frac{1}{\theta}\right),$$

from which

$$\frac{\rho\, m(e,\mathbf{q})}{l(e,\mathbf{q})}\,\dot{\mathbf{q}} + \mathbf{q} = -\frac{l(e,\mathbf{q})}{\theta^2}\,\nabla\theta.$$

Identifying with

$$\tau = \frac{\rho\, m(e,\mathbf{q})}{l(e,\mathbf{q})}, \qquad \tilde{\lambda} = \frac{l(e,\mathbf{q})}{\theta^2}$$

the relaxation time and the generalized thermal conductivity, respectively, the *Maxwell-Cattaneo-Vernotte* evolution equation for the heat flux

$$\tau\partial_t\mathbf{q} + \mathbf{q} = -\tilde{\lambda}\nabla\theta \tag{2.45}$$

is obtained. Here, we observe the temperature that appears in (2.45) is the non-equilibrium temperature and if we expand the gradient of this temperature

$$\nabla\left(\frac{1}{\theta}\right) = \nabla\left(\frac{1}{T}\right) - \frac{1}{2}\nabla\left(\frac{dm(e)}{de}\,\mathbf{q}\cdot\mathbf{q}\right) - \frac{dm(e)}{de}\,\nabla\mathbf{q}\cdot\mathbf{q}$$

from which

$$-\frac{1}{\theta^2}\nabla\theta = -\frac{1}{T^2}\nabla T - \frac{1}{2}\nabla\left(\frac{dm(e)}{de}\,\mathbf{q}\cdot\mathbf{q}\right) - \frac{dm(e)}{de}\nabla\mathbf{q}\cdot\mathbf{q}$$

moreover substituting in (2.45) the Cattaneo equation with additional terms, but in which the local equilibrium temperature T appears

$$\tau\partial_t\mathbf{q} + \mathbf{q} = -\lambda\nabla T - \frac{l(e,\mathbf{q})}{2}\nabla\left(\frac{dm(e)}{de}\,\mathbf{q}\cdot\mathbf{q}\right) - l(e,\mathbf{q})\,\frac{dm(e)}{de}\nabla\mathbf{q}\cdot\mathbf{q}. \tag{2.46}$$

where

$$\tau = \frac{\rho\, m(e,\mathbf{q})}{l(e,\mathbf{q})}, \qquad \lambda = \frac{l(e,\mathbf{q})}{T^2}$$

are the relaxation time and the thermal conductivity, respectively.

Remark 2. *For small heat flux values, the contribution of order $\mathbf{q}\cdot\mathbf{q}$ in the absolute temperature (non-equilibrium temperature) can be neglected, so that θ coincides with the local-equilibrium temperature T. Then, one gets*

$$\tau\partial_t\mathbf{q} + \mathbf{q} = -\lambda\nabla T. \tag{2.47}$$

Remark 3. *If the function $m(e,\mathbf{q})$ is constant, i.e. $m(e,\mathbf{q}) = m$ achieves*

$$\tau\partial_t\mathbf{q} + \mathbf{q} = -\lambda\nabla T \tag{2.48}$$

where

$$\tau = \frac{\rho\, m}{l(e,\mathbf{q})}, \qquad \lambda = \frac{l(e,\mathbf{q})}{T^2}$$

and the non-equilibrium temperature θ coincides with the local-equilibrium temperature T and the entropy flux is in the classical form, i.e.

$$\frac{1}{\theta} \equiv \frac{1}{T}, \qquad \mathbf{J_s} = \frac{\mathbf{q}}{T}.$$

Alternative method

An alternative method to obtain the Cattaneo evolution equation is to extend the state space by adding the heat flux $\mathbf{q}$, extend the entropy but leave the entropy flux in the classical form of Colemann-Noll $\mathbf{J_s} = \mathbf{q}/T$.

Specifically assuming the state space is spanned by variables $(e,\mathbf{q})$, [29, 30, 42],

$$\mathbb{Z} =< e, \mathbf{q} >$$

it is necessary to determine an evolution equation of the form (2.41). Let us introduce the extended specific entropy as (2.42)

$$s(e,\mathbf{q}) = s_{eq}(e) - \frac{m(e)}{2}\,\mathbf{q}\cdot\mathbf{q},$$

Taking into account the Gibbs relation

$$ds = \left(\frac{1}{T} - \frac{1}{2}\frac{dm(e)}{de}\,\mathbf{q}\cdot\mathbf{q}\right)de - m(e)\,\mathbf{q}\cdot d\mathbf{q},$$

the energy balance equation (2.1) and the expression for the entropy flux

$$\mathbf{J}_s = \mathbf{q}/T$$

after some rearrangements the entropy production reads

$$\Sigma_s = \left[\nabla\left(\frac{1}{T}\right) - \rho\, m(e,\mathbf{q})\, \mathbf{f}(e,\mathbf{q}) - \left(\frac{1}{2}\frac{dm(e)}{de}\nabla\cdot\mathbf{q}\right)\mathbf{q}\right]\cdot\mathbf{q}.$$

Limiting the case to $\partial_e m(e) = 0$, hence $m(e) = m$ is a positive constant, one obtains

$$\sigma_s = \left[-\rho\, m\, \partial_t\mathbf{q} + \nabla\left(\frac{1}{T}\right)\right]\cdot\mathbf{q} \geq 0.$$

Following Onsager's procedure [9], a relation between the thermodynamic fluxes and forces is provided

$$-\rho\, m\, \frac{\partial\mathbf{q}}{\partial t} + \nabla\left(\frac{1}{T}\right) = l\mathbf{q},$$

where the phenomenological coefficients m and l are positive functions. The following identifications

$$\tau = \frac{\rho\, m}{l}, \qquad \lambda = \frac{1}{lT^2} \tag{2.49}$$

lead to the nonlinear MCV heat equation

$$\tau(T)\frac{\partial\mathbf{q}}{\partial t} + \mathbf{q} = -\lambda(T)\,\nabla T.$$

Now suppose that thermal conductivity is expressed by (2.11) and the relaxation time is also linearly related to the temperature, as follows

$$\tau(T) = \tau_0 + b(T - T_0) \tag{2.50}$$

wherein τ_0 is the relaxation time at the initial or reference temperature, b is the coefficient that assumes positive or negative values in relation to the increase or decrease of the relaxation time caused by the temperature change. A non-zero value of the parameter b generates the non-linearity of the relaxation time. After taking into account the identifications (2.49), in order to get these linear expressions for λ and τ, (2.11) and (2.50), the following constraints arise, [29, 30]:

$$l(T) = \frac{1}{[\lambda_0 + a(T - T_0)]\, T^2}, \quad \rho m = \frac{\tau_0 + b(T - T_0)}{[\lambda_0 + a(T - T_0)]\, T^2}.$$

Since m is a constant, it is necessary to consider a temperature-dependent mass density, $\rho = \rho(T)$, that refers to the presence of mechanical effects. Therefore, while it would contradict our basic assumption of dealing with rigid material, we still find it necessary to study that particular subsystem without mechanics but with the inclusion of the nonlinear term, $\rho = \rho(T)$.

When $\frac{dm(e)}{de} \neq 0$, i.e we consider the case in which the quantity m is a function depending on the internal energy (i.e. on the temperature) and the following constitutive relation is obtained

$$-\rho m(e)\,\partial_t\mathbf{q} - \frac{1}{2}\frac{dm(e)}{de}(\nabla\cdot\mathbf{q})\mathbf{q} - \nabla\left(\frac{1}{T}\right) = l\mathbf{q} \tag{2.51}$$

under the previous identification, one has

$$\tau(T)\partial_t \mathbf{q} + \left(\mathbf{I} + \frac{1}{2c_v l}\frac{dm(T)}{dT}\nabla\cdot\mathbf{q}\right)\mathbf{q} = -\lambda(T)\nabla T \tag{2.52}$$

where $\mathbf{I}$ stands for the identity tensor and $c_v = \frac{de}{dT}$.

2.4.3 Guyer-Krumhansl equation compatibility

In the case of rigid conductor the following system yields

$$\rho\partial_t e + \nabla\cdot\mathbf{q} = 0$$
$$\partial_t \mathbf{q} + \nabla\cdot\mathbf{Q} = \mathbf{r_q}$$

where $\mathbf{Q}$ represents the flux of the heat flux and $\mathbf{r_q}$ is the source term. To close this system we must assign the constitutive relations for the last flux and for all productions, let us consider the non-local state

$$\mathbb{Z} =< e, \mathbf{q}, \nabla e, \nabla\mathbf{q} > .$$

The constitutive relations to be determined are:

$$\mathbf{Q} = \mathbf{Q}(e, \mathbf{q}, \nabla e, \nabla\mathbf{q})$$
$$\mathbf{r_q} = \mathbf{r_q}(e, \mathbf{q}, \nabla e, \nabla\mathbf{q})$$
$$s = s(e, \mathbf{q}, \nabla e, \nabla\mathbf{q})$$
$$\mathbf{J_s} = \mathbf{J_s}(e, \mathbf{q}, \nabla e, \nabla\mathbf{q})$$

In particular, we assume that the heat flux is written

$$\mathbf{J_s} = \frac{\mathbf{q}}{\theta} + \mathbf{K}$$

moreover let us observe that without involving the extra-flux of entropy $\mathbf{K}$, as we will see it will not be possible to reproduce GK heat equation. Now let's calculate the entropy production

$$\begin{aligned}
\Sigma_s &= \rho\dot{s} + \nabla\cdot\mathbf{J_s} = \rho\dot{s} + \nabla\cdot\left(\frac{\mathbf{q}}{\theta} + \mathbf{K}\right)\\
&= \rho\frac{\partial s}{\partial e}\dot{e} + \rho\frac{\partial s}{\partial \mathbf{q}}\cdot\dot{\mathbf{q}} + \rho\frac{\partial s}{\partial\nabla e}\cdot\dot{\nabla}e + \rho\frac{\partial s}{\partial\nabla\mathbf{q}} : \dot{\nabla}\mathbf{q} + \frac{1}{\theta}\nabla\cdot\mathbf{q} - \frac{1}{\theta^2}\mathbf{q}\cdot\nabla\theta + \nabla\cdot\mathbf{K}\\
&= \rho\left(\frac{\partial s}{\partial e} - \frac{1}{\theta}\right)\dot{e} + \frac{\partial s}{\partial\nabla e}\cdot\dot{\nabla}e + \frac{\partial s}{\partial\nabla\mathbf{q}} : \dot{\nabla}\mathbf{q} - \left(\frac{\partial\mathbf{K}}{\partial e} - \rho\frac{\partial s}{\partial\mathbf{q}}\cdot\frac{\partial\mathbf{Q}}{\partial e} - \frac{1}{\rho c_v\theta^2}\mathbf{q}\right)\cdot\nabla e\\
&\quad + \left(\frac{\partial\mathbf{K}}{\partial\mathbf{q}} - \rho\frac{\partial s}{\partial\mathbf{q}}\cdot\frac{\partial\mathbf{Q}}{\partial\mathbf{q}}\right) : \nabla\mathbf{q} + \left(\frac{\partial\mathbf{K}}{\partial\nabla e} - \rho\frac{\partial s}{\partial\mathbf{q}}\cdot\frac{\partial\mathbf{Q}}{\partial\nabla e}\right) : \nabla^2 e\\
&\quad \left(\frac{\partial\mathbf{K}}{\partial\nabla\mathbf{q}} - \rho\frac{\partial s}{\partial\mathbf{q}}\cdot\frac{\partial\mathbf{Q}}{\partial\nabla\mathbf{q}}\right) : \nabla^2\mathbf{q} + \frac{\partial s}{\partial\mathbf{q}}\cdot\mathbf{r_q}
\end{aligned}$$

The entropy production in components assumes the following form

$$\Sigma_s = \rho\left(\frac{\partial s}{\partial e}-\frac{1}{\theta}\right)\dot{e}+\frac{\partial s}{e_{,j}}\dot{e}_{,j}+\frac{\partial s}{\partial q_{i,j}}\dot{q}_{i,j}-\left(\frac{\partial K_j}{\partial e}-\rho\frac{\partial s}{\partial q_i}\frac{\partial Q_{ij}}{\partial e}-\frac{1}{\rho c_v\theta^2}q_j\right)e_{,j}+$$
$$+\left(\frac{\partial K_j}{\partial q_m}-\rho\frac{\partial s}{\partial q_i}\frac{\partial Q_{ij}}{\partial q_m}\right)q_{m,l}+\left(\frac{\partial K_j}{\partial e_{,m}}-\rho\frac{\partial s}{\partial q_i}\frac{\partial Q_{ij}}{\partial e_{,m}}\right)e_{,ml}$$
$$+\left(\frac{\partial K_j}{\partial q_{m,l}}-\rho\frac{\partial s}{\partial q_i}\frac{\partial Q_{ij}}{\partial q_{m,l}}\right)q_{l,mj}+\frac{\partial s}{\partial q_{i,j}}(\mathbf{r_q})_j$$

where the comma $_{,j}$ indicated the partial spatial derivative respect to x_j. Then the constrains imposed from the second law are

$$\dot{e}\notin\mathbb{Z}\Rightarrow\frac{\partial s}{\partial e}=\frac{1}{\theta} \tag{2.54}$$
$$\dot{e}_{,j}\notin\mathbb{Z}\Rightarrow\frac{\partial s}{\partial e_{,j}}=0_j \tag{2.55}$$
$$\dot{q}_{i,j}\notin\mathbb{Z}\Rightarrow\frac{\partial s}{\partial q_{i,j}}=0_{ij} \tag{2.56}$$
$$e_{,mj}\notin\mathbb{Z}\Rightarrow\frac{\partial K_{(j}}{\partial e_{,m)}}-\rho\frac{\partial s}{\partial q_i}\frac{\partial Q_{i(j}}{\partial e_{,m)}}=0_{(jm)} \tag{2.57}$$
$$q_{l,mj}\notin\mathbb{Z}\Rightarrow\frac{\partial K_(j}{\partial q_{m),l}}-\rho\frac{\partial s}{\partial q_i}\frac{\partial Q_{i(j}}{\partial q_{m),l}} \tag{2.58}$$
$$e_{,j},q_{m,j},(\mathbf{r_q})_j\in\mathbb{Z}\Rightarrow\left(\frac{\partial K_j}{\partial e}-\rho\frac{\partial s}{\partial q_i}\frac{\partial Q_{ij}}{\partial e}-\frac{1}{\rho c_v\theta^2}q_j\right)e_{,j}+\left(\frac{\partial K_j}{\partial q_m}-\rho\frac{\partial s}{\partial q_i}\frac{\partial Q_{ij}}{\partial q_m}\right)q_{m,l}$$
$$+\frac{\partial s}{\partial q_{i,j}}(\mathbf{r_q})_j\geq 0 \tag{2.59}$$

From the relations (2.55)-(2.56) follows $s=s(e,q_j)$. Moreover from (2.57)-(2.58) it obtains

$$K_j=\rho\frac{\partial s}{\partial q_i}Q_{ij}+\varphi_j(e,q_k)$$
$$\varphi_j=\varphi_j(e,q_k)$$

A solution compatible with (2.59) is

$$Q_{ij}=-l^2\left[\frac{1}{2}(q_{i,j}+q_{j,i})+2q_{k,k}\delta_{i,j}\right]$$
$$(\mathbf{r_q})_j=-\frac{q_j}{\tau}-\frac{\lambda}{\tau}\theta_{,j}$$

see for details [86, 87]. In conclusion, we choose $\phi_j = 0$ and in compact form we have

$$\mathbf{Q} = -l^2 \left[(\nabla \mathbf{q})^{sym} + 2\nabla \cdot \mathbf{q} \mathbb{I} \right] \tag{2.60}$$

$$\mathbf{r_q} = -\frac{1}{\tau}\mathbf{q} - \frac{\lambda}{\tau}\nabla\theta \tag{2.61}$$

$$s(e, \mathbf{q}) = s_{eq}(e) - \frac{\tau}{2\lambda\theta^2}\mathbf{q}\cdot\mathbf{q} = s_{eq}(e) - \frac{\tau\rho^2 c_v^2}{\lambda e^2}|\mathbf{q}|^2 \tag{2.62}$$

$$\mathbf{J_s} = \frac{\mathbf{q}}{\theta} - \frac{\tau}{2\lambda\theta^2}\mathbf{q}\cdot\mathbf{Q} \tag{2.63}$$

Substituting the relations (2.60) and (2.61) in the balance law for the heat flux, we get

$$\tau\partial_t\mathbf{q} + \mathbf{q} = -\lambda\nabla\theta + l^2\left[\Delta\mathbf{q} + 2\nabla(\nabla\cdot\mathbf{q})\right]$$

We note that the non-equilibrium temperature θ consists of two contributions :

$$\frac{1}{\theta} = \frac{\partial s}{\partial e} = \frac{ds_{eq}(e)}{de} - \frac{\tau\rho^2 c_v^2}{\lambda e^3}|\mathbf{q}|^2 = \frac{1}{T} - \frac{\tau\rho^2 c_v^2}{\lambda e^3}|\mathbf{q}|^2$$

one is related to the equilibrium temperature, the other one is related to the heat flux $|\mathbf{q}|^2 = \mathbf{q}\cdot\mathbf{q}$ and represents the contribution of the non-equilibrium. However, if this contribution is neglected, the classical definition of temperature is achieved $1/\theta = 1/T$ and we obtain

$$\tau\partial_t\mathbf{q} + \mathbf{q} = -\lambda\nabla T + l_p^2\left[\Delta\mathbf{q} + 2\nabla(\nabla\cdot\mathbf{q})\right] \tag{2.64}$$

where l_p^2 is the the phonon mean-free path.

Starting from the linearized Boltzmann equation in the Callaway approximation, Guyer and Krumhansl obtain the following evolution equation [4–6]

$$\tau_R\partial_t\mathbf{q} + \mathbf{q} = -\frac{1}{3}\tau_R\rho c_v c_0^2\nabla T + \frac{1}{5}c_0^2\tau_N\left[\Delta\mathbf{q} + 2\nabla(\nabla\cdot\mathbf{q})\right] \tag{2.65}$$

Clearly, the expression (2.64) obtained above is the same as relation (2.65) obtained by Guyer and Krumhansln [4–6] with the following identifications

$$\tau = \tau_R, \qquad \lambda = \frac{1}{3}\tau_R\rho c_v c_0^2, \qquad l_p^2 = \frac{1}{5}c_0^2\tau_N$$

where the relaxation time of the heat flux is then identified as the relaxation time of the resistive phonon collisions and the coefficient l_p^2, associated to non-locality, is related to the relaxation time of the normal phonon collisions, emphasizing the interdependency of normal collisions and non-locality.

Note that the Guyer-Krumhansl equation is often used to study heat transport in non-metallic solids. However, it should be noted, that, like the Fourier law, the Guyer-Krumhansl equation predicts that signals propagate at infinite velocity because the corresponding temperature equation (T-representation) obtained by removing the heat flux in the energy balance law is parabolic, as we will see in Chapter 5. In literature are present generalized Guyer-Krumhansel equations.

2.4.4 Thermodynamical compatibility of hyperbolic generalization of Guyer-Krumhansl

Our objective is first, to generalize the Guyer–Krumhansl's equation by introducing the second-order tensor $\mathbf{Q}$ as a indipendent variable; secondly, circumvent the problem of infinite velocity of propagation.

In the following, the state space is formed by

$$\mathbb{Z} = \{e, \mathbf{q}, \mathbf{Q}\} = \{e, \mathbf{q}, \overset{\mathbf{0}}{\mathbf{Q}}, Q\}$$

where the second order tensor $\mathbf{Q}$ (assumed to be symmetric) is splitted into its deviatoric $\overset{\mathbf{0}}{\mathbf{Q}}$ and bulk part Q (the trace of $\mathbf{Q}$), i.e. $\mathbf{Q} = Q\mathbb{I} + \overset{\mathbf{0}}{\mathbf{Q}}$. The evolution equations are

$$\begin{aligned}
&\rho\partial_t e + \nabla\cdot\mathbf{q} = 0\\
&\partial_t\mathbf{q} + \nabla\cdot\mathbf{Q} = \mathbf{r_q}\\
&\partial_t\mathbf{Q} + \nabla\cdot\mathbf{\Phi} = \mathbf{r_Q}
\end{aligned}$$

and it is possible to prove that the evolution equations for Q and $\overset{\mathbf{0}}{\mathbf{Q}}$, compatible with the second law, can be written as follows

$$\begin{aligned}
&\rho\partial_t e + \nabla\cdot\mathbf{q} = 0\\
&\partial_t\mathbf{q} + \nabla\cdot\mathbf{Q} = \mathbf{r_q}\\
&\tau_1\partial_t Q + Q = \gamma_1\nabla\cdot\mathbf{q}\\
&\tau_1\partial_t\overset{\mathbf{0}}{\mathbf{Q}} + \overset{\mathbf{0}}{\mathbf{Q}} = \gamma_2(\nabla\mathbf{q})^0_{sym}
\end{aligned}$$

where $(\nabla\mathbf{q})^0_{sym}$ denotes the symmetric and traceless part of $\nabla\mathbf{q}$, for further details see [58, 59, 84, 87, 88].

We observe that assuming the relaxation times τ_1 and τ_2 negligible we get the Guyer-Krumhansel model (2.64)

$$\tau\partial_t\mathbf{q} + \mathbf{q} = -\lambda\nabla T + \gamma_1\Delta\mathbf{q} + \left(\gamma_0 + \frac{1}{3}\gamma_2\right)\nabla(\nabla\cdot\mathbf{q})$$

Clearly, this expression is the same as (2.64) with the following identifications

$$\tau = \tau_R, \qquad \gamma_1 = \frac{5}{3}l_p^2 \qquad \gamma_2 = l_p^2$$

However in this case it is easily derived by introducing extended constitutive equations for the specific entropy and the entropy flux of the form, respectively

$$\begin{aligned}
&s(e, \mathbf{q}, \overset{\mathbf{0}}{\mathbf{Q}}, Q) = s_{eq}(e) - \frac{\tau}{2\lambda\theta^2}\mathbf{q}\cdot\mathbf{q} - \frac{\tau_1}{4\lambda\theta^2\gamma_1}Q^2 - \frac{\tau_2}{4\lambda\theta^2\gamma_2}\overset{\mathbf{0}}{\mathbf{Q}} : \overset{\mathbf{0}}{\mathbf{Q}}\\
&\mathbf{J_s} = \frac{\mathbf{q}}{T} - \frac{\tau}{2\lambda\theta^2}\,Q\,\mathbf{q} - \frac{\tau}{2\lambda\theta^2}\mathbf{q}\cdot\overset{\mathbf{0}}{\mathbf{Q}}
\end{aligned}$$

the symbol : denotes the complete contraction of the corresponding tensors which gives a scalar as result, and the symbol $\mathbf{q}\cdot\overset{\mathbf{0}}{\mathbf{Q}}$ denotes the contraction of the last index

of $\mathbf{Q}$, giving a vector as result.

The reciprocal of absolute temperature is given by the derivative of entropy w.r.t. internal energy (keeping constant the values of the other extensive variables) and it is obtained

$$\begin{aligned}\frac{1}{\theta} = \frac{\partial s}{\partial e} &= \frac{ds_{eq}(e)}{de} - \frac{d}{de}\left(\frac{\tau}{2\lambda\theta^2}\right)\mathbf{q}\cdot\mathbf{q} - \frac{d}{de}\left(\frac{\tau_1}{4\lambda\theta^2\gamma_1}\right)Q^2 - \frac{d}{de}\left(\frac{\tau_2}{4\lambda\theta^2\gamma_2}\right)\overset{\mathbf{0}}{\mathbf{Q}}:\overset{\mathbf{0}}{\mathbf{Q}} \\ &= \frac{1}{T} - \frac{d}{de}\left(\frac{\tau}{2\lambda\theta^2}\right)\mathbf{q}\cdot\mathbf{q} - \frac{d}{de}\left(\frac{\tau_1}{4\lambda\theta^2\gamma_1}\right)Q^2 - \frac{d}{de}\left(\frac{\tau_2}{4\lambda\theta^2\gamma_2}\right)\overset{\mathbf{0}}{\mathbf{Q}}:\overset{\mathbf{0}}{\mathbf{Q}}\end{aligned}$$

this is in agreement with the experimental evidence that the local-equilibrium temperature loses its validity in situations where the deviation from equilibrium is not negligible, such as heat propagation in nanosystems.

Remark 4. *If we disregard the two relaxation times for the second order tensor* $\mathbf{Q}$*, i.e.* $\tau_1, \tau_2 \to 0$ *we get the Guyer-Krumhansl model* (2.64).

2.5 Non-Equilibrium Thermodynamic with Internal Variables (NET-IV)

The classical theory of irreversible processes (CIT or TIP), as already mentioned in Section 2.1, is not sufficient for such a description of phenomena far from equilibrium, since the basic hypothesis on which it is based is the local thermodynamic equilibrium. According to the classical formulation, thermodynamic quantities and equations of state are valid in local equilibrium, even if the total system is not in equilibrium. Therefore, the principle of local equilibrium suggests a localization.

The introduction of additional fields, the **internal variables** [65, 89–94], can be considered as a universal tool for modelling macroscopic theories since they allow a quantitative characterization of the deviation from the local equilibrium, and can express: microstructural effects, heterogeneity of the material, delay in heat conduction and so on.

These variables are based on a minimum number of assumptions, in particular no hypothesis is made in advance about the physical mechanism of the modelled phenomenon and thus it can be developed in a universal form; furthermore, the evolution equations for internal variables are not governed by a balance law but are determined by thermodynamic constraints (macroscopic principles). This means that the internal variables must be such that entropy is a concave function, and that it increases in any isolated part of the material.

Among the various versions of non-equilibrium thermodynamics, the **thermodynamic with internal variables (NET-IV)** [65, 89, 90, 92, 94] represents the direct extension of the CIT or TIP theory beyond the local equilibrium.

2.5.1 Guidelines of NET-IV

The starting point of NET-IV is the introduction of an additional field variable with arbitrary tensor order. The tensor order of the internal variable can usually be deduced from the properties of the phenomenon to be analyzed. The use of an internal variable suggests that the influence of an internal structure on the dynamic behaviour of a material will be taken into account, in our case it concerns thermal dissipative effects.

The main question is: how to construct or derive the evolution equation for an internal variable? What should this internal variable satisfy? There are two answers to these questions [65], namely two basic methods for constructing or deriving the evolution equations of internal variables. Both methods are based on fundamental principles.

The first method generates evolution equations by exploiting entropy inequality. This approach uses only thermodynamic laws and the corresponding variables are called internal state variables. This approach has the advantage of working with familiar thermodynamic concepts such as thermodynamic forces and entropy, but does not consider inertial effects. Internal state variables are generally introduced in the case of dissipative processes and must satisfy only the second law of thermodynamics and not necessarily have a balance law. Internal variables add extra dimensions to the space of thermodynamic states.

The second method constructs the evolution equations from a variational Hamiltonian principle and therefore inertial effects are inevitable. In this mechanical approach the corresponding variables are called internal degree of freedom and the dissipation is then taken into account by means of potentials. This theoretical framework has the advantage of working with familiar mechanical concepts such as force and energy.

Here we will use an example to present the first approach in brief lines.

Constructive example

Let us consider a heat conducting rigid material with the description of its microstructure by means of a scalar internal variable, ξ. The thermodynamic state of material points is characterized by the internal energy density e and an internal variable ξ. The balance of internal energy in this simple case without internal heat sources reads

$$\rho \dot{e} + \nabla \cdot \mathbf{q} = 0$$

The entropy s depends on the thermodynamic state, i.e., on internal energy and an internal variable, $s = s(e, \xi)$. Its balance can be represented in the following form:

$$\Sigma_s = \rho \dot{s} + \nabla \cdot \mathbf{J_s} \geq 0$$

The Gibbs relation reads

$$de = T ds - A \, d\xi$$

from which in agreement with classical thermodynamic rules, the partial derivative of the entropy w.r.t. internal energy is the reciprocal of temperature

$$\frac{\partial s}{\partial e} = \frac{1}{T}$$

In addition, the term A represents the $\xi-$*affinity* and for it we choose the following expression

$$A = -T \frac{\partial s}{\partial \xi}$$

On the other hand, the second law requires a non-negative entropy production and in order to compute the entropy production is necessary to define entropy flux. Here assuming the classical form for the entropy flux

$$\mathbf{J_s} = \frac{\mathbf{q}}{T} \tag{2.68}$$

we arrive at the following entropy production

$$\begin{aligned}\Sigma_s &= \rho\dot{s} + \nabla\cdot\mathbf{J_s}\\ &= \rho\frac{\partial s}{\partial e}\dot{e} + \rho\frac{\partial s}{\partial \xi}\dot{\xi} + \nabla\cdot\left(\frac{\mathbf{q}}{T}\right)\\ &= -\frac{1}{T}\nabla\cdot\mathbf{q} - \frac{\rho}{T}A\,\dot{\xi} + \frac{1}{T}\nabla\cdot\mathbf{q} + \mathbf{q}\cdot\nabla\left(\frac{1}{T}\right)\\ &= -\frac{\rho}{T}A\,\dot{\xi} + \mathbf{q}\cdot\nabla\left(\frac{1}{T}\right)\end{aligned}$$

where undetermined functions are the heat flux and the evolution equation for the internal variable.

Since the internal variable is a scalar quantity and the heat flux is a vectorial one, both terms of Σ_s should be independently non-negative in isotropic materials. Therefore, the Fourier law of heat conduction

$$\mathbf{q} = l_{11}\nabla\left(\frac{1}{T}\right) = -\frac{l_{11}}{T^2}\nabla T$$

and the evolution equation for the internal variable

$$\dot{\xi} = -l_{22}\,\frac{\rho}{T}A$$

are obtained. The phenomenological coefficients l_{11} and l_{22} must be non-negative due to the second law. Finally, since the entropy must be a concave function, it is assumed that it has the following form

$$s(e,\xi) = s_{eq}(e) - \frac{m}{2}\xi^2$$

with $m \geq 0$. Then quantity $A/T = -m\xi$ and the evolution equation for the internal variable reads as

$$\dot{\xi} = l_{22}m\,\xi$$

We will use this approach to derive the equation of Fourier, Cattaneo and Guyer-Krumhansl and other generalizations, by introducing an internal vector variable and determining for it an evolution equation which allows us to eliminate the internal variable and obtain a general equation for the heat flux that under certain assumptions on phenomenological coefficients reproduces the Guyer-Krumhansl equation, the Cattaneo equation and of course Fourier's law.

2.5.2 Entropy production and thermodynamic compatibility

Let the state space be spanned by variables $(e,\boldsymbol{\xi})$, where $\boldsymbol{\xi}$ represents an vectorial internal variable [42, 63]. Thus the following form it is postulated for the specific entropy

$$s(e,\boldsymbol{\xi}) = s_{eq}(e) - \frac{m(e)}{2}\boldsymbol{\xi}\cdot\boldsymbol{\xi},$$

where s_{eq} is the classical specific entropy describing the equilibrium entropy and $m(e)$ a positive function, this ensures that the entropy is maximum at equilibrium

(i.e. the internal variable vanishes, $\boldsymbol{\xi} = \mathbf{0}$). Taking into account the Gibbs relation

$$ds = \frac{\partial s}{\partial e} de + \frac{\partial s}{\partial \boldsymbol{\xi}} \cdot d\boldsymbol{\xi} \quad \Longleftrightarrow \quad de = Tds + mT\boldsymbol{\xi} \cdot d\boldsymbol{\xi},$$

the energy balance equation (2.1) and the expression for the entropy flux $\mathbf{J}_s = \mathbf{B} \cdot \mathbf{q}$, where $\mathbf{B}$ is the Nyiri current multiplier [42], after some rearrangements, according to the hypothesis $\partial_e m(e) = 0$, i.e $m(e) = m$ with m positive constant, the entropy production, becomes in components

$$\Sigma_s = \partial_i \left(B_{ij}\right) q_j + \partial_i q_j \left(B_{ij} - \frac{1}{T}\delta_{ij}\right) - \rho m\, \xi_i \dot{\xi}_i \geq 0.$$

where ∂_i is the compact form of the partial derivative with respect to the i-th space variable, x_i. Following Onsager's procedure [9] the following relations between the thermodynamic fluxes and forces are obtained for an isotropic continuum

$$\begin{aligned} q_j &= l_{11}\partial_i \left(B_{ij}\right) - l_{12}\, \xi_j, \\ \rho m\, \dot{\xi}_j &= l_{21}\partial_i \left(B_{ij}\right) - l_{22}\, \xi_j, \\ B_{ij} - \frac{1}{T}\delta_{ij} &= k_1 \partial_i q_j + k_2 \partial_j q_i + k_3 \partial_k q_k \delta_{ij}, \end{aligned} \tag{2.69}$$

wherein $l_{11}, l_{12}, l_{21}, l_{22}, k_1, k_2, k_3$ are the scalar phenomenological coefficients, and δ_{ij} is the Kronecker symbol. Furthermore, the non-negative entropy production requires the following constrains

$$l_{11} \geq 0,\ l_{12} \geq 0,\ l_{21} \geq 0,\ l_{22} \geq 0,\ k_1 \geq 0,\ k_2 \geq 0,\ k_3 \geq 0,\ l_{11}l_{22} - \frac{1}{4}\left(l_{12}l_{21}\right)^2. \tag{2.70}$$

Let us rewrite the relations (2.69) in one spatial dimension and one gets

$$\begin{aligned} q &= l_{11}\frac{\partial B}{\partial x} - l_{12}\, \xi, \\ \rho m\, \dot{\xi} &= l_{21}\frac{\partial B}{\partial x} - l_{22}\, \xi, \\ B - \frac{1}{T} &= (k_1 + k_2 + k_3)\frac{\partial q}{\partial x}, \end{aligned} \tag{2.71}$$

After some calculations it is achieved

$$\frac{\rho m}{l_{22}}\frac{\partial q}{\partial t} + q = \frac{\rho m}{l_{22}}\frac{\partial}{\partial t}\left(l_{11}\frac{\partial B}{\partial x}\right) + \left(l_{11}l_{22} - l_{12}l_{12}\right)\frac{\partial B}{\partial x}$$

Guyer-Krumhansl equation

The GK equation is obtained by setting $l_{11} = 0, l_{22} = l_2, l_{21} = 1, k_1 + k_2 + k_3 = l_1$ and using the constrains (2.70) the relation $\left(l_{12} + l_{21}\right)^2 \leq 0$ is satisfied if and only if $l_{12} = -l_{21}$. By removing the current multiplier B and after some calculations one gets

$$\frac{\rho m}{l_2}\frac{\partial q}{\partial t} + q = \frac{1}{l_2}\frac{\partial}{\partial x}\left(\frac{1}{T} + l_1\frac{\partial q}{\partial x}\right) \tag{2.72}$$

Here, it is possible to consider two different cases. Let's discuss these cases separately:

Case I : l_1 is constant

In this case the equation (2.72) becomes

$$\frac{\rho m}{l_2}\frac{\partial q}{\partial t} + q = -\frac{1}{l_2 T^2}\frac{\partial T}{\partial x} + \frac{l_1}{l_2}\frac{\partial^2 q}{\partial x^2}$$

and with the following identifications

$$\tau = \frac{\rho m}{l_2}, \qquad \lambda = \frac{1}{l_2 T^2}, \qquad \eta^2 = \frac{l_1}{l_2} \tag{2.73}$$

the GK equation

$$\tau(T)\frac{\partial q}{\partial t} + q = -\lambda(T)\frac{\partial T}{\partial x} + \eta^2\frac{\partial^2 q}{\partial x^2} \tag{2.74}$$

is obtained.

Let us suppose that the thermal conductivity and the relaxation time are expressed by relations (2.11) and (2.50). Taking into account the identifications (2.73), to obtain the linear expressions for λ and τ, (2.11) and (2.50) respectively, the following constraints arise

$$l_2(T) = \frac{1}{\left[\lambda_0 + a(T - T_0)\right] T^2}, \tag{2.75a}$$

$$\rho m = \frac{\tau_0 + b(T - T_0)}{\left[\lambda_0 + a(T - T_0)\right] T^2}, \tag{2.75b}$$

$$\eta^2(T) = l_1 \left[\lambda_0 + a(T - T_0)\right] T^2. \tag{2.75c}$$

Let us observe that the relations (2.75a) and (2.75b) are the same restrictions obtained for the MCV equation, and since m is a constant, it is necessary to consider a temperature-dependent mass density, $\rho = \rho(T)$, which refers to the presence of mechanical effects. Therefore, being in contradict with our basic assumption of treating a rigid material, we still find it necessary to study a particular subsystem without mechanical contribution but with the inclusion of the nonlinear term, $\rho = \rho(T)$.

Case II : $l_1 = l_1(T)$ is a function of temperature (see [53])

In this situation the equation (2.72) becomes

$$\frac{\rho m}{l_2}\frac{\partial q}{\partial t} + q = \left[-\frac{1}{l_2 T^2} + \frac{1}{l_2}\frac{dl_1(T)}{dT}\frac{\partial q}{\partial x}\right]\frac{\partial T}{\partial x} + \frac{l_1(T)}{l_2}\frac{\partial^2 q}{\partial x^2}$$

and using the identifications (2.73) the GK equation with the presence of the new term is recovered [51]

$$\tau(T)\frac{\partial q}{\partial t} + q = \left[-\lambda(T) + \frac{1}{l_2(T)}\frac{dl_1(T)}{dT}\frac{\partial q}{\partial x}\right]\frac{\partial T}{\partial x} + l^2(T)\frac{\partial^2 q}{\partial x^2} \tag{2.76}$$

Let us suppose that the thermal conductivity and relaxation time are expressed by (2.11) and (2.50), and that also the mean-free path $l^2(T)$ is a linear function of temperature

$$\eta^2(T) = \eta_0 + c(T - T_0) \tag{2.77}$$

where η_0 denotes the mean-free path at the initial or reference temperature, and c is a suitable coefficient depending on the material to be examined. After

taking into account the identifications (2.73), to obtain these linear expressions for λ, τ and l^2, (2.11), (2.50) and (5.12), the following constraints arise, [51]

$$\begin{aligned} l_2(T) &= \frac{1}{[\lambda_0 + a(T - T_0)]\, T^2}, \\ \rho m &= \frac{\tau_0 + b(T - T_0)}{[\lambda_0 + a(T - T_0)]\, T^2}, \\ l_1(T) &= \frac{\eta_0 + c(T - T_0)}{[\lambda_0 + a(T - T_0)]\, T^2}. \end{aligned} \tag{2.78}$$

The first and second relations identify the same restrictions as the MCV model, and since being m a constant, it is necessary to consider a temperature-dependent mass density, $\rho = \rho(T)$, which relates to the presence of mechanical effects. Again, in order not to contradict our assumption of rigid body, it is necessary to study a subsystem without mechanics but with the involvement of nonlinear relation terms of the type, $\rho = \rho(T)$.

Maxwell-Cattaneo-Vernotte equation

The MCV equation is obtained setting $l_{11} = 0, l_{22} = l_2, l_{21} = 1, k_1 + k_2 + k_3 = l_1 = 0$ and using the constrains (2.70) the relation $(l_{12} + l_{21})^2 \leq 0$ is satisfied if and only if $l_{12} = -l_{21}$. By eliminating the current multiplier B and after some calculations we obtain

$$\frac{\rho m}{l_2}\frac{\partial q}{\partial t} + q = \frac{1}{l_2}\frac{\partial}{\partial x}\left(\frac{1}{T}\right)$$

where the phenomenological coefficients m and $l = l_2$ are positive functions. The following identifications

$$\tau = \frac{\rho m}{l}, \qquad \lambda = \frac{1}{lT^2}$$

lead to the nonlinear MCV heat equation and the internal variable is identified by heat flux $\xi = -q$. After calculation similar to EIT case, it is possible to extend this derivation in three dimension and obtain

$$\tau(T)\frac{\partial \mathbf{q}}{\partial t} + \mathbf{q} = -\lambda(T)\nabla T$$

see Section 2.4.2.

Fourier equation

The Fourier's law is obtained setting $l_{11} = 0, l_{22} = l_2, l_{21} = 1, k_1 + k_2 + k_3 = l_1 = 0$ and $m = 0$. By eliminating the current multiplier B and after some calculations we obtain

$$q = \frac{1}{l_2}\frac{\partial}{\partial x}\left(\frac{1}{T}\right) = -\frac{1}{l_2 T^2}\frac{\partial T}{\partial x}$$

where the phenomenological coefficients $l = l_2$ is positive function. The following identifications

$$\lambda = \frac{1}{lT^2}$$

lead to the nonlinear Fourier's law. After some computations is possible to extend this derivation in three dimension and obtain

$$\mathbf{q} = -\lambda(T)\nabla T.$$

Chapter 3

Fourier heat conduction

In this chapter we will present the classic constitutive relation for heat flux, i.e. the Fourier's law. By highlighting how the latter leads to an infinite speed of propagation, we focus on the causality problem.

In addition, numerical results of the heat pulse application in which the thermal conductivity is considered to be linearly dependent on temperature, will be presented.

3.1 Brief historical background

The well known model for heat conduction in isotropic rigid solids is Fourier's law, which linearly relates the temperature gradient ∇T to the heat flux $\mathbf{q}$ according to

$$\mathbf{q} = -\lambda(T)\nabla T \tag{3.1}$$

where $\lambda(T)$ is the thermal conductivity, generally depending on temperature. In CIT, see Section 2.1, the thermodynamic compatibility of the Fourier law is proof and we obtain $\lambda = l/T^2$, with $l > 0$ phenomenological coefficient. The coefficient l is scalar for isotropic media and became a second order tensor for anisotropic media.

By substituting (3.1) in the energy balance equation (2.1), one obtains a parabolic differential equation for the temperature (T-representation) given by

$$\rho c\, \partial_t T + \nabla \cdot (\lambda(T)\nabla T) = S \tag{3.2}$$

where $c = \frac{de}{dT}$ represents the isochoric specific heat capacity and $S = \rho\, r$ is the volumetric heat source. Dividing for $\rho\, c$, the equation (3.2) can be rewrite as

$$\partial_t T - \nu\, \nabla T \cdot \nabla T - \alpha \Delta T = \frac{1}{\rho\, c} S \tag{3.3}$$

where α is the thermal diffusivity and the term ν representing a non constant value of thermal conductivity, expressed as the following ratios

$$\alpha = \frac{\lambda(T)}{\rho\, c}, \qquad \nu = \frac{\lambda'(T)}{\rho\, c}$$

whit $\lambda'(T)$ indicates the first derivative of the function $\lambda(T)$ with respect to temperature.

The equation (3.3) is called **heat equation**. In the case of constant thermal conductivity, i.e. $\lambda(T) \equiv \lambda_0$ and zero heat source (i.e. $S = 0$), one gets

$$\partial_t T - \alpha \Delta T = 0.$$

Note that it is possible to write the same equation in the q-representation, as

$$\partial_t \mathbf{q} + \frac{\nu}{\lambda(T)}(\nabla \cdot \mathbf{q})\,\mathbf{q} + \alpha \nabla(\nabla \cdot \mathbf{q}) = 0,$$

when λ is constant one has

$$\partial_t \mathbf{q} + \alpha \nabla(\nabla \cdot \mathbf{q}) = 0$$

and note that the temperature boundary conditions are completely excluded. Both forms represent the same system

$$\begin{aligned} &\text{T - representation} && \partial_t T - \alpha \Delta T - \nu\, \nabla T \cdot \nabla T = \frac{1}{\rho\, c} S \\ &\text{q - representation} && \partial_t \mathbf{q} + \frac{\nu}{\lambda(T)}(\nabla \cdot \mathbf{q})\,\mathbf{q} + \alpha \nabla(\nabla \cdot \mathbf{q}) = -\frac{\nu}{\lambda(T)} S\,\mathbf{q} - \alpha \nabla S \end{aligned}$$

or for constant thermal conductivity and zero heat source

$$\begin{aligned} &\text{T - representation} && \partial_t T - \alpha \Delta T = 0 \\ &\text{q - representation} && \partial_t \mathbf{q} + \alpha \nabla(\nabla \cdot \mathbf{q}) = 0. \end{aligned}$$

The most convenient form should be chosen according to the situation, for example when it is time-dependent boundary heat flux, the q-representation may be more convenient for the analytical solutions, the temperature evolution can be reconstructed using the balance law of energy.

Therefore, if we consider the T-representation with λ constant and $S = 0$, and if we assign the following initial condition

$$T(\mathbf{x}, 0) = T_0(\mathbf{x})$$

it is possible to prove that the solution is expressed by the relation

$$T(\mathbf{x}, t) = \frac{1}{(4\pi\alpha t)^{3/2}} \int_{\mathbb{R}^3} T_0(\mathbf{y}) \cdot \exp\left(-\frac{(\mathbf{x}-\mathbf{y})^2}{4\alpha t}\right) d\mathbf{y} \tag{3.4}$$

As we can observe the temperature $T(\mathbf{x}, t)$ is different from zero in any spatial position $\mathbf{x} \in \mathbb{R}^3$ and for a very short time instant $t > 0$. This means that if initially a temperature perturbation $T_0(\mathbf{x})$ is different from zero in the compact set $\Omega \subset \mathbb{R}^3$, i.e. it is localized, at any time instant $(\forall, t > 0)$ this perturbation is perceived to be very distant, i.e it propagates instantaneously throughout space. It is possible to understand that the physical phenomenon propagates at a speed higher than the speed of light. This has led to different interpretations, such as that of Fichera who argued: not being able to have a zero-precision temperature measuring instrument available, it is true that the latter is different from the initial temperature at very long distances, but this variation is zero as it cannot be measured experimentally.

In particular, Onsager in 1931 noted that Fourier's model contradicts the principle of microscopic reversibility, but this contradiction

'. . . is removed when we recognize that [Fourier's law] is only an approximate description of the process of conduction, neglecting the time needed for acceleration of the heat flow'.

In other words, Fourier's law has the unphysical property that it lacks inertial effects: if a sudden temperature perturbation is applied at one point in the solid, it will be instantly and anywhere in distant locations. Moreover, Fourier's model is

not adequate for describing heat transport at very high frequencies and short wavelengths. Such situations are met when the phenomena are very fast or very steep (as ultrasound propagation, light scattering in gases, neutron scattering in liquids, heat propagation at low temperatures, shock waves, etc.) or when the relaxation times of the fluxes are very long (as in polymer solutions, suspensions, superfluids or superconductors). Historically, Cattaneo was the first to introduce inertia effects in heat equation. To eliminate the anomalia of infinite speed propagation, he proposed in 1948, [1], a damped version of Fourier's law by introducing a heat–flux relaxation term, as as discussed in detail in the Chapter 4.

However, the Fourier's law shows a good concordance with experiments for more practical eingenering problems.

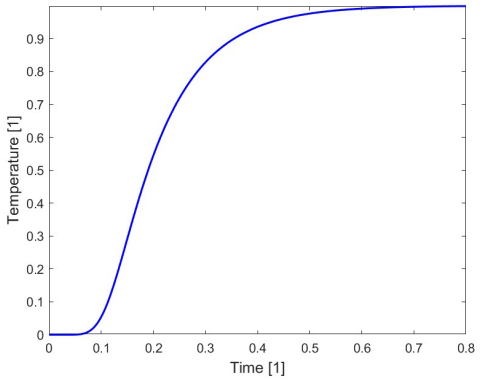

FIGURE 3.1: A typical solution for Fourier equation

3.1.1 Causality problem

The questions that many researchers been asking themselves over the years are: *What do we do with Fourier's law, which leads to a parabolic equation? What do we do with the Navier-Stokes equations, which are parabolic? Should we exclude these systems, which are classical equations still used today in various applications?*

One approach is to incorporate these systems of parabolic nature by reformulating the weak causality principle. Although parabolic theories do not respect the strong causality principle, one can demand that they satisfy a more refined (weak) causality principle which does not require hyperbolicity but focuses instead on the estimates of solutions.

The parabolic theories, in the context of RET, are paradoxical because, according to the **cause and effect principle**, cause and effect cannot occur simultaneously. For example, if we consider the classical heat diffusion equation (3.3), in which the heat flux is assigned according to Fourier's law, we observe that this equation is parabolic. This means that if we initially heat only a compact set D, since the heat propagates at an infinite speed $v = +\infty$, all the points outside of D are immediately heated in an infinitesimally small time. This shows that the effect occurs simultaneously with the cause that generated it, rather than later. This is, in simple terms, the absurdity referred to by I. Müller in RET.

Some researchers such as I. Müller and T. Ruggeri [54–56, 80] dealth with the concept of causality, coming to the conclusion that systems leading to a finite propagation speed of solutions are hyperbolic, whose prototype is the d'Alembert wave

equation (for electromagnetic waves in a vacuum):

$$\partial_{tt} u = c^2 \, \Delta u$$

where c corresponds to the speed of light in a vacuum. In this case, the propagation speed is finite, and to calculate it, we consider the characteristic equation associated with the PDE, which is obtained simply by setting

$$\partial_{tt} u = \lambda^2 \, \Delta u = 1$$

from which

$$\lambda^2 = c^2 \quad \Leftrightarrow \quad \lambda = \pm c$$

Based on this, the idea is that since this equation is the typical one which allows wave propagation at a finite speed, it should require that all phenomenological systems have the same nature, i.e., hyperbolic. This explains why, the **strong causality principle** is required in RET. This means that the constitutive equations must be assigned in such a way that the system is symmetric. A symmetric system implies that it is also hyperbolic, which ensures that solutions propagate at finite speeds.

Therefore, there must necessarily be a way to reconcile these theories with the principles of thermodynamics. Indeed, the way to do this could be to formulate a new causality principle, the **weak causality principle**. The formulation of this last principle is reached after showing some illustrative examples of what will be the mathematical formalization of the principle.

Is the Fourier heory of heat conduction paradoxical?

Fichera raised the question of the paradox of Fourier's theory of heat conduction. He gave a negative answer after dealing with the problem mathematically, considering something that no one had considered before. In particular, it is true that the temperature, which he denoted by T, is different from 0 even at infinite distances. But to consider a temperature different from zero, it means that it can be measured, and therefore, one must consider that Fourier's law is derived under the assumption that $\exists, \varepsilon \in (0,1)$ such that the components of ∇T are of order ε, and quantities of order ε^2 or higher are negligible.

He considered the following Cauchy problem:

$$\begin{aligned} &\partial_t T = \alpha \Delta T \quad \forall \, (x,y,z) \in \mathbb{R}^3 \, \forall \, t > 0 \\ &T(x,y,z,0) = \begin{cases} f(x,y,z) \text{ if } (x,y,z) \in R_0 \subset \mathbb{R}^3 \\ 0 \text{ if } (x,y,z) \notin R_0 \end{cases} \end{aligned}$$

Since the heat equation holds throughout the entire space, i.e., in $\mathbb{R}^3$, boundary conditions need not to be specified. Furthermore, it is assumed that the initial conditions have compact support, meaning that at the initial time, the temperature is non-zero only in a compact region R_0 and is zero outside it.

The solution to this equation is well-known and is given by (3.4), i.e.

$$T(x,y,z,t) = \frac{1}{(4\pi\alpha)^{\frac{3}{2}}} \int_{R_0} f(\xi,\eta,\gamma) e^{-\frac{(x-\xi)^2+(y-\eta)^2+(z-\gamma)^2}{4\alpha t}}$$

and one can observe that the temperature is always non-zero.

$$T(x,y,z,t) > 0 \quad \forall (x,y,z) \in \mathbb{R}^3 \quad \forall t > 0$$

Thus, for every arbitrarily small time t, the temperature T is different from zero even at points (x,y,z) which are an infinite distance from R_0. This means that in an infinitesimally small time, the heat, which was initially confined to R_0, has propagated to an infinite distance from R_0, i.e., throughout the entire space $\mathbb{R}^3$. Therefore, the heat has traveled an infinite distance in an arbitrarily small time, and the only way this can happen is if the speed at which the heat propagates is infinite. However, this contradicts the theory of relativity and the strong causality principle. Moreover Fichera proved that:
$\exists\, C_0$, *a compact set with* $C_0 \supseteq R_0$, *where the solution* T *is of order* ε, *and outside of this, in* $\mathbb{R}^3 \setminus C_0$, *it is of order* ε^2.

Thus, in the experimental approximation where quantities of order ε^2 or higher are negligible ($\nabla T^2, \nabla T^3, \nabla T^4, \dots$), stating that the temperature is of order ε within a compact set C_0 containing the initial compact set R_0, and outside of it, in $\mathbb{R}^3 \setminus C_0$, is of order ε^2 and therefore negligible, it means saying that the temperature is different from zero only in a compact set. Therefore, with this idea, the heat equation is no longer paradoxical, since the solution is experimentally non-zero only within the compact set C_0, and thus propagates at a finite speed.

In order to formalize this, let us consider the previous Cauchy problem in one spatial dimension, in [95] states

$$\partial_t T = \alpha\, \partial_{xx} T \quad x \in \mathbb{R}^+ \tag{3.5}$$

$$T(x,0) = \begin{cases} 1 \text{ if } x = 0 \\ 0 \text{ if } x \neq 0 \end{cases} \tag{3.6}$$

where the initial condition that the only initially heated point is $x = 0$, and is at a temperature of 1. In this case, the compact set R_0 reduces to a single point. The solution to this Cauchy problem is the following:

$$T(x,t) = \frac{1}{2\sqrt{\pi \alpha t}} \exp\left(-\frac{x^2}{4\alpha t}\right)$$

and let us note that:

$$T(x,t) > 0 \quad \forall t > 0 \quad \forall x \in \mathbb{R}^+$$

thus, if we consider a point $\tilde{x} \in \mathbb{R}^+$ sufficiently far from $x = 0$, one has:

$$T(\tilde{x},t) > 0 \quad \forall t > 0$$

this means that the heat propagated from point $x = 0$ to point $x = \tilde{x}$ in an arbitrarily small time interval, which means that the heat propagated at an infinite speed, $v = +\infty$. Having a propagation speed of ∞ leads to two problems:

- **Theoretical problem**: The solution does not align with the principle of cause and effect, as in this case, the cause and the effect occur simultaneously.
- **Experimental problem**: The solution does not correspond to real-world experience. For instance, if we imagine holding one end of an aluminum rod with one hand while heating the other end with a lighter, we would expect to feel the heat on our fingers immediately if the heat propagation speed was infinite.

In reality, however, we do not feel anything initially; only after a certain time you notice an increase in temperature with our fingers.

Therefore, the idea is to choose, from a physical point of view, a precision level ε for x, t, and T, which means to fix a precision ε for all measurable quantities. If these quantities are of order ε^2, ε^3, etc., these are considered negligible because our measuring instruments cannot detect them, as they are below the sensitivity threshold of the instrument.

Thus

Saying that the temperature $T(x,t)$ is $\neq 0$ at every point x and at every time instant t, means that one must be able to measure it, i.e.

$$T(x,t) = \frac{1}{\sqrt{4\pi\alpha t}} \exp\left(\frac{x^2}{4\alpha t}\right) \geq \varepsilon$$

Let's perform an estimate

$$\frac{1}{\sqrt{4\pi\alpha t}} \exp\left(\frac{x^2}{4\alpha t}\right) \geq \varepsilon \quad \Leftrightarrow \quad \exp\left(\frac{x^2}{4\alpha t}\right) \geq 2\varepsilon\sqrt{\pi\alpha t} \quad \Leftrightarrow \quad \exp\left(\frac{x^2}{4\alpha t}\right) \geq \sqrt{4\pi\alpha t\varepsilon^2}$$

taking the logarithm of both sides, we obtain

$$-\frac{x^2}{4\alpha t} \geq \ln\left(\sqrt{4\pi\alpha t\varepsilon^2}\right) \quad \Leftrightarrow \quad x^2 \leq -4\alpha t \ln\left(\sqrt{4\pi\alpha t\varepsilon^2}\right)$$

but $x \in \mathbb{R}^+$ thus $x \geq 0$ and we have

$$0 \leq x^2 \leq -4\alpha t \ln\left(\sqrt{4\pi\alpha t\epsilon^2}\right) \quad \Leftrightarrow \quad 0 \leq -4\alpha t \ln\left(\sqrt{4\pi\alpha t\epsilon^2}\right)$$

from which

$$\ln\left(\sqrt{4\pi\alpha t\varepsilon^2}\right) \leq 0 \quad \Leftrightarrow \quad \sqrt{4\pi\alpha t\varepsilon^2} \leq 1 \quad \Leftrightarrow \quad t \leq \frac{1}{4\pi\alpha\varepsilon^2}$$

Then taking into account the inequality $x^2 \leq -4\alpha t \ln\left(\sqrt{4\pi\alpha t\varepsilon^2}\right)$ substituting what has been obtained, one has:

$$x^2 \leq -\frac{4\alpha}{4\pi\alpha\varepsilon^2} \ln\left(\sqrt{4\pi\alpha t\varepsilon^2}\right) \quad \Leftrightarrow \quad x^2 \leq -\frac{1}{\pi\varepsilon^2} \ln\left(\sqrt{4\pi\alpha t\varepsilon^2}\right)$$

If δ is the distance from point $x = 0$ to $x = \tilde{x}$ where the temperature is not heated for a time interval $t < \varepsilon$, we have

$$\delta^2 \leq -\frac{1}{\pi\epsilon^2} \ln\left(\sqrt{4\pi\alpha t\varepsilon^2}\right)$$

and if $\delta \geq \varepsilon$, it means that the points at a distance δ from the origin ($x = 0$), which is non-negligible, i.e., $\delta \geq \varepsilon$, are reached instantly by heat. In other words, this implies an infinite propagation speed

$$\varepsilon^2 \leq \delta^2 \leq -\frac{1}{\pi\epsilon^2} \ln\left(\sqrt{4\pi D t\varepsilon^2}\right) \quad \Leftrightarrow \quad \varepsilon^2 \leq -\frac{1}{\pi\varepsilon^2} \ln\left(\sqrt{4\pi\alpha t\varepsilon^2}\right)$$

from which

$$-2\pi\varepsilon^4 \geq \ln\left(\sqrt{4\pi\alpha\varepsilon^3}\right) \quad \Leftrightarrow \quad \exp\left(-2\pi\varepsilon^4\right) \geq 4\pi\alpha\varepsilon^3 \quad \Leftrightarrow \quad 4\pi\alpha \leq \frac{1}{\varepsilon^3}\exp\left(-2\pi\varepsilon^4\right)$$

Thus, the necessary and sufficient condition for having an infinite propagation speed is

$$4\pi\alpha \leq \frac{1}{\varepsilon^3}\exp\left(-2\pi\varepsilon^4\right) \tag{3.7}$$

This condition depends on the thermal diffusivity of the material α and therefore on the thermal conductivity of the material λ; it also depends on the precision degree ε. However, let us observe that the smaller precision degree ε (i.e., the larger $1/\varepsilon^3$), the more likely it is that the condition (3.7) will be satisfied, thus making it more likely that Fourier's theory will lose validity as $\varepsilon \to 0$.

However, for $\varepsilon = 0$, the right-hand side of (3.7) becomes $+\infty$, so from this relation, we have $4\pi\alpha \leq +\infty$, which is always satisfied. This states that if the error is zero, we would have an infinite heat propagation speed. But, as Fichera rightly observed, this is a physically unattainable case, since $\varepsilon = 0$ corresponds to measurements without errors.

Hence, we have seen that the propagation speed value depends on two factors:

- The order of magnitude of the physical parameters involved in the system, i.e. $\alpha = \frac{\lambda}{\rho c}$,
- The degree of accuracy of the measurements, i.e. ε.

In conclusion, it is true that the heat equation, which is a parabolic equation, implies an infinite propagation speed. However, its measured value would be finite whenever the experimental precision (accuracy) is sufficiently low, so that the temperature is non-zero only within a limited (compact) interval.

For example, consider a crystal of NaF (sodium fluoride) at the critical temperature of $T = 15.6, K$, which is the temperature at which heat propagation occurs in a wave-like manner (the second sound). In this case, $4\pi\alpha = 2.5 \cdot 10^5$.

Then

- If $\varepsilon = 0.01$, the propagation speed is infinite, as the condition (3.7) is satisfied.
- If $\varepsilon = 0.05$, the condition (3.7) is not satisfied, yielding a finite propagation speed, even with Fourier's law.

This simple example illustrates that we cannot label parabolic theories as paradoxical. Depending on the approximation order ε used to measure observable quantities, one may not have an infinite propagation speed.

Based on what we have seen, we aim to formalize the new principle of causality, the weak causality principle, which will replace the very restrictive strong causality principle.

To this end, consider a thermomechanical system described by:

$$\rho\,\dot{\mathbf{w}} + \operatorname{div}\boldsymbol{\Phi}(\mathbf{z}) = \rho\mathbf{z} \tag{3.8}$$

where $\mathbf{w} \in W \subseteq E^k$ represent the set of field variables and $\mathbf{z} \in Z \subseteq E^m$ all the thermomechanical variables, with $W \subseteq Z$ and $k \leq m$. Here, Z is the state space, W is the solution space, and E^k and E^m are Euclidean spaces.

In the context of extended thermodynamics, constitutive relations for fluxes and productions must be assigned in the form

$$\mathbf{\Phi}(\mathbf{z}) = \tilde{\mathbf{\Phi}}(\mathbf{z})$$
$$\sigma(\mathbf{z}) = \tilde{\sigma}(\mathbf{z})$$

and if the system (3.8) is:

- **hyperbolic**, the components of $\mathbf{w}$ propagate through space with finite speeds,
- **parabolic**, the components of $\mathbf{w}$ propagate through space with infinite speeds.

Definition 1. *A system (3.8) is said to be **kinematically admissible** if the propagation speeds of the components of $\mathbf{w}$ are all contained within the set C_I. Here, C_I is the **admissible speed set**:*

$$C_I = \{\textit{space of admissible velocity}\} = \begin{cases} \mathbb{R}^+ & \textit{Galileian Relativity} \\ [0, c] & \textit{Einstein Relativity} \end{cases}$$

The system (3.8), once built, cannot ignore the structure of spacetime, which is why we say that it must be kinematically admissible. Obviously, such kinematic admissibility must depend on the structure of spacetime.

Once the experimental error ε_i on each component w_i of $\mathbf{w}$ is known, it is possible to determine the vector $\boldsymbol{\varepsilon} \in W$, whose components represent the minimum detectable value of w_i with the measurement instruments available to us.

Definition 2. *Let us consider the Cauchy problem*

$$\rho\, \dot{\mathbf{w}} + \operatorname{div} \mathbf{\Phi}(\mathbf{z}) = \rho \mathbf{z} \; su \; E^3 \tag{3.9a}$$
$$\mathbf{w}(\mathbf{x}, 0) = \mathbf{w_0}(\mathbf{x}) \; con \; \mathbf{x} \in X_0 \tag{3.9b}$$

where X_0 is a compact subset of E^3, so $\mathbf{w_0}(\mathbf{x})$ is a function with compact support, meaning it is non-zero only within a compact set (X_0) and zero outside.

*We say that the solution of the Cauchy problem (3.9) $\mathbf{w} : E^3 \times [0, t_{max}] \to W$ is **non-negligible up to the experimental error $\boldsymbol{\varepsilon}$** if*

$$\exists X \subseteq E^3, X \neq \emptyset, \quad \exists U \subseteq [0, t_{max}], U \neq \emptyset, \quad t.c. \quad |w_i(\mathbf{x}, t)| \geq \varepsilon_i \quad \forall i = 1...k$$

i.e., each component w_i of $\mathbf{w}$ satisfies the relation $|w_i(\mathbf{x}, t)| \geq \varepsilon_i$.

Definition 3. *A solution of the Cauchy problem (3.9) is said to be **causally admissible up to the experimental error $\boldsymbol{\varepsilon}$** if X is compact, with $X_0 \subseteq X$, meaning $\mathbf{w} \neq \mathbf{0}$ in a compact set X, but not throughout the entire space E^3.*

This definition states that if the solution $\mathbf{w}$ is initially different from zero in a compact X_0, it immediately propagates, but is still different from $\mathbf{0}$ in a compact X containing the initial compact, $X \supseteq X_0$. Then the random admissibility corresponds to require that the propagation rates are finite in a suitable approximation, since X is compact and does not coincide with all space $E3$, therefore the set where the solution is nothing is not all space.

Now, we can finally state the **weak casuality principle**.

Principle 2 (Weak casuality principle)**.** *The constitutive equation*

$$\begin{aligned}\mathbf{\Phi}(\mathbf{z}) &= \tilde{\mathbf{\Phi}}(\mathbf{z})\\ \sigma(\mathbf{z}) &= \tilde{\sigma}(\mathbf{z})\end{aligned}$$

must be assigned in such a way that

- *the solutions of the Cauchy problem* (3.9) *are* ***kinematically admissible****,*
- *if a solution of the Cauchy problem* (3.9) *is* ***non-negligible up to the experimental error*** $\boldsymbol{\varepsilon}$*, then it must also be* ***causally admissible*** *up to that experimental error* $\boldsymbol{\varepsilon}$*.*

Then this makes it concluded that a solution $\mathbf{w}$ of (3.9) can be $\neq \mathbf{0}$ in the whole space $E3$, but experimentally is $\neq \mathbf{0}$ only in a compact, not in the all whole space. While the **strong causality principle** was:

Principle 3 (Strong causality principle)**.** *The constituent equations:*

$$\begin{aligned}\mathbf{\Phi}(\mathbf{z}) &= \tilde{\mathbf{\Phi}}(\mathbf{z})\\ B\sigma(\mathbf{z}) &= \tilde{\sigma}(\mathbf{z})\end{aligned}$$

must be assigned so that the (3.8) *is symmetric* $\Rightarrow$ *hyperbolic.*

3.1.2 Existence, uniqueness and maximum principle

When considering a problem of physical nature one of the first properties that you need to verify is the number of solutions that its admits once the initial and boundary conditions are assigned. In the case of Fourier heat conduction, the solution to the following problem is unique, as can be see in the 3 theorem.

$$\partial_t T - \alpha \Delta T = \frac{1}{\rho\, c} S, \quad \forall \mathbf{x} \in \Omega\, \forall t > 0 \tag{3.10a}$$

$$T(\mathbf{x}, 0) = T_0(\mathbf{x}), \qquad \forall \mathbf{x} \in \Omega \tag{3.10b}$$

with

$$\text{Dirichlet} \qquad T(\mathbf{x}, t) = f(\mathbf{x}), \qquad \forall \mathbf{x} \in \partial\Omega \tag{3.11a}$$

$$\text{Neumann} \qquad \partial_{\hat{\mathbf{n}}} T(\mathbf{x}, t) = g(\mathbf{x}), \qquad \forall \mathbf{x} \in \partial\Omega \tag{3.11b}$$

$$\begin{aligned}\text{Mixed} \qquad T(\mathbf{x}, t) &= f(\mathbf{x}) && \forall \mathbf{x} \in \partial\Omega_D\\ \partial_{\hat{\mathbf{n}}} T(\mathbf{x}, t) &= g(\mathbf{x}), && \forall \mathbf{x} \in \partial\Omega_N\end{aligned} \tag{3.11c}$$

wherein $\partial\Omega_D \cup \partial\Omega_N = \partial\Omega$ and $\partial\Omega_D \cap \partial\Omega_N = \emptyset$.

Often determining the analytical solution of the problem under consideration turns out is extremely complicated, therefore it becomes necessary to extract information concerning the solution from the analysis of the differential equation to the partial derivatives and the conditions (initial and edge) which must be met. Among these, a very important property concerns the principle of maximum and minimum, that is the values which the solution can assume and in which region of the domain it can take.

In the case of constant material parameters there are several methods to obtain exact solutions, and according to each problem one can choose which resolution method is the most efficient, including: the Laplace transform, the similarity variables, the separation of variables, Duhamel's method. However we are interested in

solving non-linear heat propagation problems where the thermal conductivity is a function of temperature, where numerical methods will be used, including the one we will focus on is the numerical method of shifted fields (will be presented in detail in the chapter 4)

Theorem 2. *The problem* (3.10) *with Dirichlet, Neumann or mixed boundary conditions,* (3.11)*, admit a unique solution.*

Proof. It is assumed, absurdly, that there are u, v two different solutions of (3.10)-(3.11), i.e. $u(\mathbf{x},t) \neq v(\mathbf{x},t)$, then the function $w := u - v$ is solution of the following problem

$$\begin{aligned} &\partial_t w - \alpha \Delta w = 0, && \forall \mathbf{x} \in \Omega \, \forall t > 0 \\ &w(\mathbf{x},0) = 0, && \forall \mathbf{x} \in \Omega \\ &w(\mathbf{x},t) = 0 && \forall \mathbf{x} \in \partial\Omega \, \forall t > 0 \end{aligned}$$

here the Dirichlet boundary conditions are choosen, but without losing generality it is possible to proceed similarly in the other two cases.

Now we consider the following function

$$E(t) := \frac{1}{2} \int_\Omega w(\mathbf{x},t)^2 \, \mathrm{d}\mathbf{x}$$

and computing the time derivative

$$\begin{aligned} \dot{E}(t) &= \frac{d}{dt}\left(\frac{1}{2}\int_\Omega w(\mathbf{x},t)^2 \, \mathrm{d}\mathbf{x}\right) = \frac{1}{2}\frac{d}{dt}\left(\int_\Omega w(\mathbf{x},t)^2 \, \mathrm{d}\mathbf{x}\right) = \frac{1}{2}\int_\Omega 2\, w(\mathbf{x},t)\, \partial_t w(\mathbf{x},t) \, \mathrm{d}\mathbf{x} \\ &= \alpha \int_\Omega w(\mathbf{x},t)\, \Delta w(\mathbf{x},t) \, \mathrm{d}\mathbf{x} = \alpha \int_\Omega w \, \nabla \cdot \nabla w \, \mathrm{d}\mathbf{x} = \alpha \int_\Omega w \, \partial_{x_i}(\partial_{x_i} w) \, \mathrm{d}\mathbf{x} \\ &= \alpha \int_\Omega \left[\partial_{x_i}(w\, \partial_{x_i} w) - (\partial_{x_i} w)^2\right] \, \mathrm{d}\mathbf{x} = \alpha \int_\Omega \partial_{x_i}(w\, \partial_{x_i} w) \, \mathrm{d}\mathbf{x} - \alpha \int_\Omega (\partial_{x_i} w)^2 \, \mathrm{d}\mathbf{x} \\ &= \alpha \int_{\partial\Omega} w\, \partial_{x_i} w \hat{n}_i \, \mathrm{d}\mathbf{x} - \alpha \int_\Omega \partial_{x_i} w\, \partial_{x_i} w \, \mathrm{d}\mathbf{x} = \alpha \int_{\partial\Omega} w\, \partial_{\hat{\mathbf{n}}} w \, \mathrm{d}\mathbf{x} - \alpha \int_\Omega \nabla w \cdot \nabla w \, \mathrm{d}\mathbf{x} \\ &= \alpha \int_{\partial\Omega} w\, \partial_{\hat{\mathbf{n}}} w \, \mathrm{d}\mathbf{x} - \alpha \int_\Omega ||\nabla w||^2 \, \mathrm{d}\mathbf{x} \end{aligned}$$

the first integral is zero from the Dirichlet boundary conditions (but is zero also for the Neumann or mixed boundary conditions), then

$$\dot{E}(t) = -\alpha \int_\Omega ||\nabla w||^2 \, \mathrm{d}\mathbf{x}.$$

Therefore the function $E(t)$ is always positive by definition, but initially is zero and has a negative derivative (it is decreasing),

$$\dot{E}(t) = -\alpha \int_\Omega ||\nabla w||^2 \, \mathrm{d}\mathbf{x} \leq 0 \qquad E(0) = \frac{1}{2}\int_\Omega w(\mathbf{x},0) \, \mathrm{d}\mathbf{x} = 0$$

and it must necessarily be zero

$$E(t) = 0 \quad \Leftrightarrow w(\mathbf{x},t) = 0 \quad \forall \mathbf{x} \in \Omega \, \forall t > 0$$

from which

$$u(\mathbf{x},t) = v(\mathbf{x},t) \quad \forall \mathbf{x} \in \Omega \, \forall t > 0$$

this is absurd for the hypothesis, then implies the solution is unique. □

Theorem 3. *Let $u(\mathbf{x}, t)$ a solution of the following problem*

$$\begin{aligned} &\partial_t T - \alpha \Delta T = \frac{1}{\rho\, c} S, && \forall \mathbf{x} \in \Omega\, \forall t > 0 \\ &T(\mathbf{x}, 0) = T_0(\mathbf{x}), && \forall \mathbf{x} \in \Omega \end{aligned}$$

then $u(\mathbf{x}, t)$ assumes its maximum and minimum values always on $\partial\Omega$ or for $t = 0$.

Proof. See [96]. □

3.2 L-F and NL-F in 1D

Let us consider the nonlinear Fourier's equation

$$\mathbf{q} = -\lambda(T)\nabla T$$

from the thermodynamic compatibility, see Section 2.1.1-2.2.1, we have the following identification

$$\lambda(T) = \frac{l}{T^2} \tag{3.12}$$

where l is the phenomenological coefficient. It is easy to see that the expression of thermal conductivity (2.11) is compatible with the linear constrain of the second law if the following relation

$$l = (\lambda_0 + a(T - T_0)))T^3$$

holds. Finally, the following system forms the NL-F heat equation

$$\rho\, c\, \partial_t T + \nabla \cdot \mathbf{q} = 0, \tag{3.13a}$$

$$\mathbf{q} = -\lambda(T)\, \nabla T. \tag{3.13b}$$

3.2.1 Numerical framework

The equations (3.13) contain coefficients with different orders of magnitude. Being from numerical point of view, it is pronouncedly unfavorable. Thus some dimensionless parameters are introduced

$$\hat{x} = \frac{x}{L}, \quad \hat{t} = \frac{\alpha_0 t}{L^2}, \quad \alpha_0 = \frac{\lambda(T_0)}{\rho c}, \quad \lambda(T_0) = \lambda_0 + aT_0, \quad \hat{T} = \frac{T - T_0}{T_{\text{end}} - T_0},$$

where L is the length of the rigid and isotropic conductor, ρ_0 is the value of the mass density corresponding to the temperature T_0, T_0 and T_{end} represent the initial and the equilibrium temperature corresponding to adiabatic boundaries, respectively, i.e.

$$T_{\text{end}} = T_0 + \frac{1}{\rho c L}\int_{t_0}^{t_p} q_0(t)\, \mathrm{d}t, \quad \bar{q}_0 = \frac{1}{t_p}\int_{t_0}^{t_p} q_0(t)\, \mathrm{d}t, \quad \hat{q} = \frac{q}{\bar{q}_0},$$

where t_p is the length of the pulse that acts on the boundary as a heat pulse. This setting corresponds to the so-called flash or heat pulse experiment [43, 97]. It is a common and widely used methodology for measuring the thermal material parameters in low or room temperature situations and observing its non-Fourier type behavior. Moreover, t_0 is the initial time instant which is considered to be 0 and $\tilde{q}_0$

is the integral average of the heat pulse $q_0(t)$. In order to simplify the notations, the hat is omitted in the following and only dimensionless parameters are used.

Now, in 1D, the dimensionless system of equations reads

$$\tau_{p_1}\partial_t T + \partial_x q = 0, \tag{3.14a}$$
$$q = -(\tau_{p_1} + \tau_{p_2} T)\partial_x T, \tag{3.14b}$$

with

$$\tau_{p_1} = \frac{\alpha_0 t_p}{L^2}, \quad \tau_{p_2} = \frac{a(T_{\text{end}} - T_0)t_p}{\rho c L^2}.$$

Let us remark that when $a = 0$ ($\tau_{p_2} = 0$), the non-linearity disappears and the following

$$\tau_{p_1}\partial_t T + \partial_x q = 0, \tag{3.15a}$$
$$q = -\tau_{p_1}\partial_x T, \tag{3.15b}$$

is obtained.

Difference equations and stability analysis

Here we present a numerical method developed for the nonlinear one-dimension model (3.14). Let us discretize the spatial domain $\Omega = [0, 1]$ with spatial steps Δx and the time interval $[0, t_{max}]$ with step Δt, the following discrete space and time values are obtained

$$x_j = x_0 + j\Delta x \quad j = 0, 1, 2, ..., N$$
$$t^n = n\Delta t \quad n = 0, 1, 2, ..., J.$$

We use the staggered field FDM and define the heat flux is on both boundaries and the temperature is shifted by half space step $\Delta x/2$ (i.e. it is computed in the internal nodes [29, 98])

$$T(x_{j+1/2}, t^n) \approx T^n_{j+1/2}$$
$$q(x_j, t^n) \approx q^n_j.$$

Therefore the difference equations are

$$\tau_{p_1}\frac{T^{n+1}_{j+1/2} - T^n_{j+1/2}}{\Delta t} + \frac{q^n_{j+1} - q^n_j}{\Delta x} = 0, \tag{3.16a}$$
$$q^n_j = -(\tau_{p_1} + \tau_{p_2} T^n_j) \cdot \frac{T^n_{j+1/2} - T^n_{j-1/2}}{\Delta x}. \tag{3.16b}$$

where an explicit forward finite difference approximation are used for the time and spatial derivatives

$$\frac{\partial T}{\partial t} \approx \frac{T^{n+1}_{i+1/2,j+1/2} - T^n_{i+1/2,j+1/2}}{\Delta t},$$
$$\frac{\partial q}{\partial x} \approx \frac{q^n_{j+1} - q^n_j}{\Delta x},$$
$$\frac{\partial T}{\partial x} \approx \frac{T^n_{j+1/2} - T^n_{j-1/2}}{\Delta x}.$$

where n denotes the time steps and j stands for the spatial steps.

Since a finite difference scheme can lead to instability, a stability analysis is recommended in order to investigate the region of the appropriate values of Δx and Δt for the given scheme.

It is important to emphasize that the conventional analysis using the von Neumann method is not directly applicable since the stability conditions depend on temperature, at least in the case under consideration. Weickert et al. [99] proposes a stability analysis method for nonlinear diffusion equations, and illustrates particular examples of image processing [100, 101]. In order to use this approach, the difference equations must be reformulated in order to obtain a mapping between the temperature values at two different times: $T^n \rightarrow T^{n+1}$. That mapping is represented by a tridiagonal matrix $\mathbf{Q}$ with elements Q_{ij}, and must satisfies the following criteria:

- continuity in the T-dependence,
- symmetry, $Q_{ij} = Q_{ji}$,
- unit row sum, $\sum_i Q_{ij} = 1$,
- non-negativity, $Q_{ij} > 0$,
- positive diagonal elements, $Q_{ii} > 0$,
- irreducibility, i.e., for any $T \geq 0$, $\lambda(T) > 0$.

The corresponding tridiagonal matrix has the elements $[\beta; 1 - 2\beta; \beta]$ in a row with

$$\beta = \Delta t \Delta x^2 (\tau_{p_1} + \tau_{p_2} T_j^n) / \tau_{p_1} > 0,$$

any other element is zero. Hence the non-negativity and positive diagonality requirements are equivalent and reads as

$$1 > 2 \max_j \beta,$$

that is, the maximum value of the temperature field shall be estimated. In the simulation of a heat pulse experiments using Fourier's law, it is simple as the equilibrium dimensionless temperature is 1 and cannot be higher. It restricts the maximum time step:

$$\Delta t < \frac{\Delta x^2 \tau_{p_1}}{2(\tau_{p_1} + \tau_{p_2})}.$$

Alternatively, one could assume or estimate apriori the maximum temperature, $Z = \max_{(j,n)} T_j^n = 1$, and applying a linear stability analysis following von Neumann's method [102] and Jury conditions [103]. In short, it starts with assuming a solution in a plane wave form

$$T_j^n = u_0 \, \xi^n e^{i k j \Delta x} \tag{3.17}$$

with i the imaginary unit, k the wave number, and ξ the growth factor representing the amplitude wave and must be bounded from above for stability. The stability condition is $|\xi| \leq 1$ i.e., the amplitude of the wave remains bounded.

$$p(\xi) = a_2 \xi^2 + a_1 \xi + a_0 = 0, \tag{3.18}$$

where the coefficients are

$$a_2 = 1 \tag{3.19a}$$

$$a_1 = \frac{4\Delta t(\tau_{p_1} + \tau_{p_2} Z)}{(\Delta x)^2 \tau_{p_1}} - 1, \tag{3.19b}$$

$$a_0 = 0. \tag{3.19c}$$

$$\tag{3.19d}$$

Theorem 4. *The numerical scheme is stable if the following condition is satisfied*

$$\Delta t \leq \frac{(\Delta x)^2 \tau_{p_1}}{2(\tau_{p_1} + \tau_{p_2} Z)}$$

Proof. Applying the Jury criterion restrict the roots of $p(\xi)$ and keep them inside the unit circle on the complex plane, we obtain

C1: $p(\xi = 1) \geq 0 \quad \Leftrightarrow \quad a_2 + a_1 + a_0 \geq 0$ i.e.

$$\frac{4\Delta t(\tau_{p_1} + \tau_{p_2} Z)}{(\Delta x)^2 \tau_{p_1}} \geq 0$$

which is trivially satisfied.

C2: $p(\xi = -1) \geq 0 \quad \Leftrightarrow \quad a_2 - a_1 + a_0 \geq 0$ i.e.

$$2 - \frac{4\Delta t(\tau_{p_1} + \tau_{p_2} Z)}{(\Delta x)^2 \tau_{p_1}} \geq 0$$

that is satisfied if

$$\Delta t \leq \frac{(\Delta x)^2 \tau_{p_1}}{2(\tau_{p_1} + \tau_{p_2} Z)}$$

is true.

C3: $|a_0| \leq 1$ which is trivially satisfied.

Then under the following condition the roots of the characteristic polynimial are in modulus less that 1,

$$\Delta t < \frac{(\Delta x)^2 \tau_{p_1}}{2(\tau_{p_1} + \tau_{p_2} Z)}. \tag{3.20}$$

□

This allows the linear stability analysis to be applied if the upper temperature bound can be estimates. Since it is not proved for other non-linearities such as thermal radiation, it is safe to state that it is true only if the nonlinearity occurs due to the temperature dependence in the thermal conductivity. In the case of $Z = 1$ we have

$$\Delta t < \frac{(\Delta x)^2 \tau_{p_1}}{2(\tau_{p_1} + \tau_{p_2})}. \tag{3.21}$$

Let us remark that in linear case, i.e. for $\tau_{p_2} = 0$, the inequality (3.20) reduces to the condition

$$\Delta t < \frac{(\Delta x)^2}{2} \tag{3.22}$$

that is the classical stability condition.

Furthermore, when we consider the extension of the Fourier law, as we will see later in Chapter 4, the correction related to the relaxation time also appears in the stability condition. We note here that this is the consequence of the temperature dependence of mass density.

3.2.2 Numerical results

In this section, the solutions of NL-F heat equation are introduced and the effects of non-linear terms are investigated. Here, only the rear side ($\hat{x} = 1$) temperature histories are presented because, in the heat pulse experiments, this is measured and used for evaluation.

Regarding the NL-F equation, see Figure 3.3, the parameter τ_{p_2} influences the slope at the point where temperature begins to increase. It is worth observing that the point corresponding to $\hat{T} = 0.5$ is significantly shifted to the left to increase τ_{p_2}. It is important because the conventional evaluation formula for the Fourier heat equation, which offers the thermal diffusivity as an outcome of the measurement, uses the time instant related to $\hat{T} = 0.5$. Here we emphasize that negative coefficient for the temperature dependence is also physically admissible and possible in several practical cases. However, care should be taken that the thermal conductivity must remain positive, restricted by the second law. Thus we are also test solutions for negative τ_{p_2}, see Fig. 3.3. It affects the slope oppositely.

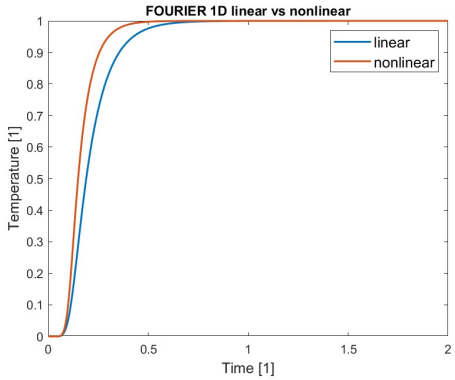

FIGURE 3.2: Comparison the rear side temperature history in linear and nonlinear case, using $\tau_{p_1} = 0.1$ and $\tau_{p_2} = \{0, 0.05\}$.

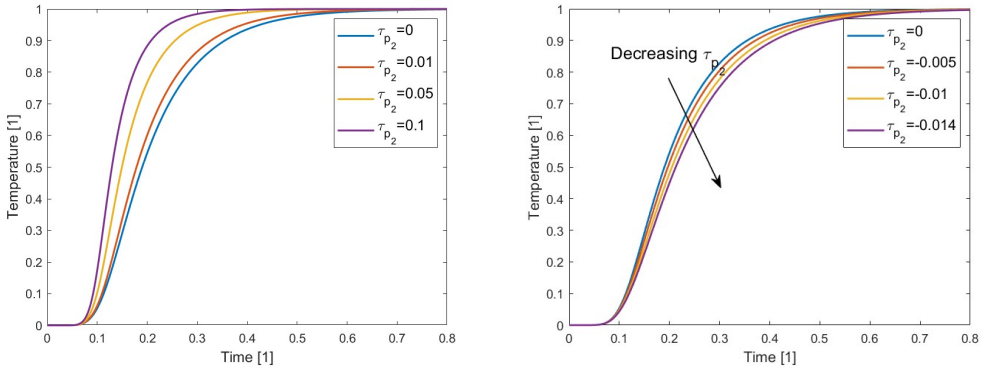

(a) (b)

FIGURE 3.3: The rear side temperature history when: increasing the nonlinear parameter $\tau_{p_2} \in \{0, 0.01, 0.05, 0.1\}$ in (a) and decreasing $\tau_{p_2} \in \{0, -0.005, -0.01, -0.014\}$ in (b). The other parameter is $\tau_{p_1} = 0.1$.

Chapter 4

Maxwell-Cattaneo-Vernotte heat conduction

In this chapter, we present the solutions to the hyperbolic Cattaneo model, focusing on the phenomenon of second sound heat conduction, where both the relaxation time and thermal conductivity exhibit non-linear behavior. Our principal aim is to investigate how these non-linearities influence the time evolution of temperature, particularly during a heat pulse experiment. This analysis will be conducted in both one-dimensional and two-dimensional spatial domains, allowing for a comprehensive understanding of the dynamics in various settings.

By examining these models, we seek to uncover the extent to which non-linear effects alter the thermal behavior predicted by classical linear theories, and to what degree these corrections are necessary for accurately describing real-world phenomena. The results of this investigation will not only provide insights into the fundamental aspects of heat conduction but also offer potential applications in fields where precise thermal management is crucial, such as in microelectronics, materials science, and high-temperature processes.

Finally we compare the non-linear Maxwell-Cattaneo-Vernotte model with another possible formulation.

4.1 Brief historical background

In 1948, the Italian mathematician Carlo Cattaneo solved the problem of infinite heat propagation velocity proposing a new equation [1]. He introduced the concept of characteristic thermal relaxation time τ, which he defined as "the time needed for a volume element to establish steady heat conduction when a temperature gradient is applied", in other words it represents the time required to achieve thermodynamic stability.

The equation proposed by Cattaneo is now widely known in literature as the Maxwell-Cattaneo-Vernotte (MCV) equation. In honor of the French mathematician Pierre Vernotte, who derived the same equation almost simultaneously with Cattaneo [2] and the British physicist Maxwell who had derived a similar law within the kinetic theory of gas [3]. This equation is

$$\mathbf{q} + \tau\, \partial_t \mathbf{q} = -\lambda \nabla T \tag{4.1}$$

where the additional term introduced by Cattaneo, i.e. $\tau\, \partial_t \mathbf{q}$, is referred to as thermal inertia and accounts for memory effects in the system. This term captures the idea that heat flux does not instantaneously respond to changes in the temperature gradient, but instead requires a finite relaxation time τ, which depends, of course, on the material properties. Its value has been determined experimentally for a wide

range of materials. For most metals, τ, is estremely small, typically on the order of picoseconds ($ps = 10^{-12}s$). However, in other materials, as biological tissues, τ can be much larger, reaching up to 100 seconds.

However, by incorporating the energy balance laws from (2.1), the resulting system of equations, comprising (2.1) and (4.1), is known as the Maxwell-Cattaneo-Vernotte (MCV) system

$$\rho c\, \partial_t T + \nabla \cdot \mathbf{q} = \rho r \tag{4.2a}$$
$$\tau\, \partial_t \mathbf{q} + \mathbf{q} = -\lambda \nabla T. \tag{4.2b}$$

This system addresses the shortcomings of classical Fourier's law, particularly the issue of infinite heat propagation, by introducing finite propagation speeds for thermal signals through the relaxation time τ.

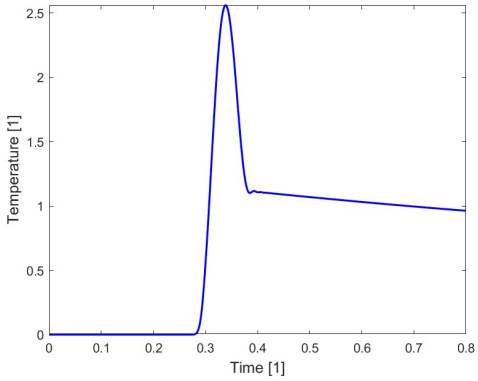

FIGURE 4.1: A typical solution for Cattaneo equation

Remark 5. *Let us observe that Cattaneo, taking an idea of Vernotte, hypothesized that the thermal flux depended not only on the value of the temperature gradient but also on the gradient of the time derivative of temperature, i.e.*

$$\mathbf{q} = -\lambda \nabla T + \tau\, \lambda \nabla (\partial_t T) = -\lambda \nabla T + \tau\, \lambda \nabla \dot{T}. \tag{4.3}$$

This relation can be rewritten as

$$\mathbf{q} = -\lambda \left(1 + \tau \frac{\partial}{\partial t}\right) \nabla T \tag{4.4}$$

and for "small" values of τ it is possible to show that the inverse operator turns out to be

$$\left(1 + \tau \frac{\partial}{\partial t}\right)^{-1} \simeq 1 + \tau \frac{\partial}{\partial t}$$

and then you get

$$\left(1 + \tau \frac{\partial}{\partial t}\right) \mathbf{q} = -\lambda \nabla T \tag{4.5}$$

which is obviously equivalent to the equation (4.1).

4.1.1 Characteristic velocity

As mentioned before, the Cattaneo equation for heat flux leads to a hyperbolic system, which implies that heat propagates with a finite velocity. In this section, we will demonstrate that the system (4.2) is indeed hyperbolic, and we will determine the corresponding propagation velocity.

To find the characteristic velocity of the system (4.2) in three dimensions, let us consider a general system of the following form:

$$\partial_t \mathbf{F}^0(\mathbf{U}) + \partial_{x_i} \mathbf{F}^i(\mathbf{U}) = \mathbf{F}(\mathbf{U}). \tag{4.6}$$

The most compact form of the system is to use the relativistic notation: $x_0 = t$ and $\partial_\alpha = \partial/\partial_{x_\alpha}$ with $\alpha = 0, 1, 2, 3$ from which we have

$$\partial_\alpha \mathbf{F}^\alpha(\mathbf{U}) = \mathbf{F}(\mathbf{U}). \tag{4.7}$$

In our case, for the system (4.2) we have

$$\begin{gathered}
\mathbf{F}^0 = \begin{bmatrix} \rho c T \\ \tau q_x \\ \tau q_y \\ \tau q_z \end{bmatrix}, \quad \mathbf{F}^1 = \begin{bmatrix} q_x \\ \lambda T \\ 0 \\ 0 \end{bmatrix}, \quad \mathbf{F}^2 = \begin{bmatrix} q_y \\ 0 \\ \lambda T \\ 0 \end{bmatrix}, \quad \mathbf{F}^3 = \begin{bmatrix} q_z \\ 0 \\ 0 \\ \lambda T \end{bmatrix}, \\
\mathbf{U} = \begin{bmatrix} T \\ q_x \\ q_y \\ q_z \end{bmatrix}, \quad \mathbf{F} = \begin{bmatrix} \rho r \\ -q_x \\ -q_y \\ -q_z \end{bmatrix}
\end{gathered} \tag{4.8}$$

The system (4.7) is a particular case of the following quasi-linear system

$$A_0(\mathbf{U})\partial_t \mathbf{U} + A_i(\mathbf{U})\partial_{x_i}\mathbf{U} = \mathbf{F}(\mathbf{U}) \quad \Leftrightarrow \quad A_\alpha(\mathbf{U})\partial_\alpha \mathbf{U} = \mathbf{F}(\mathbf{U}). \tag{4.9}$$

With the positions

$$\begin{gathered}
A_0(\mathbf{U}) = \begin{bmatrix} \rho c & 0 & 0 & 0 \\ 0 & \tau(T) & 0 & 0 \\ 0 & 0 & \tau(T) & 0 \\ 0 & 0 & 0 & \tau(T) \end{bmatrix}, \quad A_1(\mathbf{U}) = \begin{bmatrix} 0 & 1 & 0 & 0 \\ \lambda(T) & 0 & 0 & 0 \\ 0 & 0 & 0 & 0 \\ 0 & 0 & 0 & 0 \end{bmatrix}, \\
A_2(\mathbf{U}) = \begin{bmatrix} 0 & 0 & 1 & 0 \\ 0 & 0 & 0 & 0 \\ \lambda(T) & 0 & 0 & 0 \\ 0 & 0 & 0 & 0 \end{bmatrix}, \quad A_4(\mathbf{U}) = \begin{bmatrix} 0 & 0 & 1 & 0 \\ 0 & 0 & 0 & 0 \\ 0 & 0 & 0 & 0 \\ \lambda(T) & 0 & 0 & 0 \end{bmatrix},
\end{gathered} \tag{4.10}$$

In the linear case one gets

$$\begin{gathered}
A_0(\mathbf{U}) = \begin{bmatrix} \rho c & 0 & 0 & 0 \\ 0 & \tau_0 & 0 & 0 \\ 0 & 0 & \tau_0 & 0 \\ 0 & 0 & 0 & \tau_0 \end{bmatrix}, \quad A_1(\mathbf{U}) = \begin{bmatrix} 0 & 1 & 0 & 0 \\ \lambda_0 & 0 & 0 & 0 \\ 0 & 0 & 0 & 0 \\ 0 & 0 & 0 & 0 \end{bmatrix}, \\
A_2(\mathbf{U}) = \begin{bmatrix} 0 & 0 & 1 & 0 \\ 0 & 0 & 0 & 0 \\ \lambda_0 & 0 & 0 & 0 \\ 0 & 0 & 0 & 0 \end{bmatrix}, \quad A_4(\mathbf{U}) = \begin{bmatrix} 0 & 0 & 1 & 0 \\ 0 & 0 & 0 & 0 \\ 0 & 0 & 0 & 0 \\ \lambda_0 & 0 & 0 & 0 \end{bmatrix},
\end{gathered} \tag{4.11}$$

Recalling the following definition of hyperbolic system we will determine the characteristic velocity.

Definition 4. *A system in the form (4.9) is **hyperbolic (in t-direction)** if the following conditions are satisfied*

H1: $\det(A_0) \neq 0$

H2: *The eigenvalues of the matrix* $A_0^{-1}(A_1 n_1 + A_2 n_2 + A_3 n_3) = A_0^{-1}(A_i n_i)$ *are reals, for all unit vectors* $\hat{\mathbf{n}} = (n_1, n_2, n_3)$.

In our case the condition **H1** is easily satisfied since

$$\det(A_0) = \rho c \tau(T)^3 \neq 0 \tag{4.12}$$

being $\rho > 0, c > 0$ and $\lambda(T)$, $\tau(T) > 0$, $\forall\, T > 0$. To verify the condition **H2** it is necessary to determine the eigenvalues of matrix $A_0^{-1}(A_i n_i)$, thus considering the following eigenvalues problem $\det(A_0^{-1}(A_i n_i) - vI) = 0$, after using Binet rule, it is equivalent to

$$\det(A_i n_i - v A_0) = 0 \qquad \forall\, \hat{\mathbf{n}} = (n_i) \text{ with } |\hat{\mathbf{n}}| = 1 \tag{4.13}$$

from which

$$\begin{vmatrix} -\rho c v & n_1 & n_2 & n_3 \\ \lambda(T)\, n_1 & -\tau(T)\, v & 0 & 0 \\ \lambda(T)\, n_2 & 0 & -\tau(T)\, v & 0 \\ \lambda(T)\, n_3 & 0 & 0 & -\tau(T)\, v \end{vmatrix}; \tag{4.14}$$

the characteristic polynomial is

$$v^2 \left[\rho c \tau(T) v^2 - \lambda(T)\right] = 0 \tag{4.15}$$

and the eigenvalues are easily obtained

$$v_{1,2} = 0 \tag{4.16a}$$

$$v(T)_{3,4} = \pm \sqrt{\frac{\lambda(T)}{\rho c \tau(T)}}. \tag{4.16b}$$

The coefficients $\rho > 0, c > 0$ and $\lambda(T)$, $\tau(T) > 0$, $\forall\, T > 0$ are real, then it remains shown that the system is hyperbolic and the characteristic velocity is given by the relation (4.16b).

As can be seen below the relation (4.16b) has the dimensions of a velocity

$$[v] = \left[\sqrt{\frac{\lambda}{\rho c \tau}}\right] = \frac{[\lambda]}{[\rho][c][\tau]} = \sqrt{\frac{\frac{W}{mK}}{\frac{Kg}{m^3} \cdot \frac{J}{KgK} \cdot s}} = \frac{m}{s} \tag{4.17}$$

Then, we can conclude that $v(T)$ represents the propagation velocity of the thermal waves in a medium, commonly referred to as the **velocity of second sound**. As seen from its expression, this velocity is finite. It is called "second sound" because it is distinct from the ordinary speed of sound in the medium. Experimental results, for example for liquid helium II, have shown that the rate of heat propagation is typically an order of magnitude lower than the speed of sound in the same medium [12–15].

It is also important to note that as $\tau \to 0$ the propagation velocity tends towards infinity, i.e. $v \to +\infty$. In this case, the Cattaneo equation (4.1) reduces to the classical Fourier equation (3.1), which implies instantaneous heat propagation. This demonstrates that the model proposed by Cattaneo is consistent, as it naturally recovers the Fourier law in the appropriate limit.

Remark 6. *Similarly in the linear case, using the matrices* (4.11)*, the system is still hyperbolic with the following expressions of the characteristic speeds*

$$v_{3,4} = \pm\sqrt{\frac{\lambda_0}{\rho c \tau_0}}. \tag{4.18}$$

4.1.2 Particular case: constant material parameters

In the case where the material parameters are assumed to be constant, it is possible to derive a single equation for the temperature T, known as the T-representation. Specifically, by taking the divergence of equation (4.2b) and differentiating equation (4.2a) with respect to time, we can, after some calculations, arrive at the following result

$$\tau\, \partial_{tt} T + \partial_t T - \alpha \Delta T = \frac{1}{\rho c}\left(S + \tau\, \partial_t S\right) \tag{4.19}$$

where $\alpha = \lambda/(\rho c)$ is the thermal diffusivity and $S = \rho r$.

Note that by dividing by τ and assuming the source term is zero ($r \equiv 0$,) we get the equation known as **telegraph equation** which describes the wave damped propagation

$$\partial_{tt} T + \frac{1}{\tau}\partial_t T - v^2 \Delta T = 0 \tag{4.20}$$

where we identify

$$v = \sqrt{\frac{\alpha}{\tau}} = \sqrt{\frac{\lambda}{\rho c \tau}}.$$

It is possible to obtain the same equation for the heat flux $\mathbf{q}$ by eliminating the temperature T, which is called q-representation. In fact, by calculating the gradient of equation (4.2a) and the time derivative of the equation (4.2b), after some algebraic manipulation, we obtain

$$\partial_{tt}\mathbf{q} + \frac{1}{\tau}\partial_t \mathbf{q} - v^2 \Delta \mathbf{q} = -v^2 \nabla S, \tag{4.21}$$

This approach transforms the original system into a representation that depends solely on the heat flux, removing the explicit dependence on temperature. The temperature distribution can be recovered using the internal energy balance law (2.1) through time integration. Therefore, the two possible representations are:

- T-representation : where the system is expressed in terms of temperature, and the heat flux is derived from it.

$$\text{T - representation} \qquad \partial_{tt} T + \frac{1}{\tau}\partial_t T - v^2 \Delta T = \frac{1}{\rho c}\left(S + \tau\, \partial_t S\right).$$

- q-representation: where the system is expressed in terms of the heat flux, and the temperature distribution is recovered later from the energy balance law.

$$\text{q - representation} \qquad \partial_{tt}\mathbf{q} + \frac{1}{\tau}\partial_t\mathbf{q} - v^2\Delta\mathbf{q} = -v^2\nabla S.$$

We observe the source terms in this T- and q-representations appera differently; their time derivative do not directly contribute to the evolution when comparing equation (4.21) with (4.19). However, it is possible to see that T and $\mathbf{q}$ must satisfy the same partial differential equation (PDE), when $S = 0$, which is the telegraph equation. This implies that, in the absence of a source term, both temperature and heat flux evolve according to the same governing equation

$$\begin{aligned}\text{T - representation} \qquad & \partial_{tt}T + \frac{1}{\tau}\partial_t T - v^2\Delta T = 0\\ \text{q - representation} \qquad & \partial_{tt}\mathbf{q} + \frac{1}{\tau}\partial_t\mathbf{q} - v^2\Delta\mathbf{q} = \mathbf{0}.\end{aligned}$$

Firstly note that when $\lambda = \lambda(T)$ and $\tau = \tau(T)$, it is impossible to obtain the T-representation and one must solve as system (4.2) without eliminating any of the field variables. For short time $t << \tau$, the term ∂_t is negligible and thus (with $S = 0$)

$$\partial_{tt}T - v^2\Delta T = 0$$

the wave equation is a valid equation; while for long times $t >> \tau$ the term ∂_{tt} becomes negligible and thus (with $S = 0$)

$$\partial_t T - v^2\Delta T = 0$$

holds.

Note also that in this model (4.19), an initial condition must be introduced on the time derivative of temperature, i.e. $T_t(\mathbf{x}, 0)$ (called *initial thermal velocity*). This condition is completely absent in the Fourier model, but it becomes necessary here in order to solve the model analytically or numerically. This presents a practical difficulty, which lies in the way of making, arbitrary distributions of $\partial_t u(x, 0)$ in a laboratory setting.

If we consider the one-dimension case and the following change of variables

$$\bar{t} = \frac{1}{2\tau}t \qquad \bar{x} = \sqrt{\frac{\rho c}{4\tau\lambda}}x$$

the equation (4.19) is written in the following form

$$\partial_{\bar{t}\bar{t}}T + 2\partial_{\bar{t}}T - \partial_{\bar{x}\bar{x}}T = 0$$

and the following initial conditions are assigned

$$\begin{aligned}T(\bar{x}, \bar{t} = 0) &= f(\bar{x})\\ \partial_{\bar{t}}T(\bar{x}, \bar{t} = 0) &= g(\bar{x})\end{aligned}$$

where f and g are two arbitrary functions defined on the space interval $[0, a]$. Then the solution is

$$T(\bar{x}, \bar{t}) = \frac{e^{-\tau}}{2}\left[f(\bar{x}+\bar{\tau}) + f(\bar{x}-\bar{t}) + \int_{\bar{x}-\bar{t}}^{\bar{x}+\bar{t}} F(\xi, \bar{x}, \bar{t})\,\mathrm{d}\xi\right] \tag{4.22}$$

where

$$F(\xi, \bar{x}, \bar{t}) = [g(\xi) + f(\xi)]\psi((\xi-\bar{x})^2 - \bar{t}^2) + 2\bar{t}f(\xi)\psi'((\xi-\bar{x})^2 - \bar{t}^2)$$

with $\psi(2w) = J_0(\sqrt{2w})$ being J_0 the Bessel function of 0-order.

This solution (4.22) expresses the simultaneous existence, along the $\bar{x}$ axis, of two waves whose fronts initially coincide with the extremes of the interval $[0, a]$ and proceed in opposite direction at a velocity equal to 1 (in the original variables this correspond to a velocity $v = \sqrt{\lambda/(\rho c\tau)}$). However, these waves are without a rear front, after the wave front passes, the phenomenon loses its wave-like nature and becomes into a diffusive behavior. Therefore, heat propagation exhibits two characteristic: one diffusive and the other wave-like. This behavior is different from the classical case only in an initial phase, which corresponds to the short period during which the wave front passes, after which the heat propagation becomes similar to that described by the classical wave equation.

This behavior can be observed more clearly by comparing the asymptotic aspects of the Cattaneo solution (4.22) with the Fourier solution (3.4). For a fixed value of $\bar{x} \geq a$ and a sufficiently large value of $\bar{t}$ (specifically $\bar{t} > \bar{x}$), in the expression (4.22) both $f(\bar{x}+\bar{t})$ and $f(\bar{x}-\bar{t})$ vanish, and the limits of the integral, i.e. $\bar{x}-\bar{t}$ and $\bar{x}+\bar{t}$, can be replaced by 0 and a, respectively. Thus, it results in

$$T(\bar{x}, \bar{t}) \approx \frac{e^{-\tau}}{2}\int_0^a F(\xi, \bar{x}, \bar{t})\,\mathrm{d}\xi$$

For $\bar{t} \to +\infty$ the quantity $(\xi-\bar{x})^2$ is negligible compared to $\bar{t}^2$, so

$$\psi((\xi-\bar{x})^2 - \bar{t}^2) \approx \psi(-\bar{t}^2) = J_0(i\bar{t}) \approx \frac{e^{\bar{t}}}{\sqrt{2\pi\bar{t}}}$$
$$\psi'((\xi-\bar{x})^2 - \bar{t}^2) \approx \psi'(-\bar{t}^2) = \frac{\mathrm{d}J_0(i\bar{t})}{\mathrm{d}(-\bar{t}^2)} \approx \frac{-e^{\bar{t}}}{2\sqrt{2\pi}\bar{t}^{3/2}}$$

where we used the asymptotic expression of $J_0(i\bar{t})$. Therefore, The function F becomes

$$\begin{aligned} F(\xi, \bar{x}, \bar{t}) &\approx [g(\xi) + f(\xi)] \cdot \frac{e^{\bar{t}}}{\sqrt{2\pi\bar{t}}} - 2\bar{t}f(\xi) \cdot \frac{e^{\bar{t}}}{2\sqrt{2\pi}\bar{t}^{3/2}} \\ &= [g(\xi) + 2f(\xi)] \cdot \frac{e^{\bar{t}}}{\sqrt{2\pi\bar{t}}} \end{aligned}$$

The asymptotic expression of the solution $T(\bar{x}, \bar{t})$ is written in the form

$$T(\bar{x}, \bar{t}) \approx \frac{1}{2\sqrt{2\pi\bar{t}}}\int_0^a [g(\xi) + 2f(\xi)]\,\mathrm{d}\xi. \tag{4.23}$$

If a similar asymptotic analysis of the classical solution is performed (3.4) (rewrite in

one dimension), remembering in mind that $\frac{(x-\xi)^2}{4\alpha t} \to 0$ for $t \to +\infty$, and expressing it in variables $\bar{x}$, $\bar{t}$, we get

$$T(\bar{x},\bar{t}) \approx \frac{1}{\sqrt{2\pi\bar{t}}} \int_0^a f(\xi)\, \mathrm{d}\xi. \tag{4.24}$$

Thus, comparing the asymptotic expressions of the two solutions, (4.23) and (4.24), it can be seen that they do not differ, except by the coefficient of the function $1/\bar{t}$.

Remark 7. *If we indicated with* $\mathbf{q_F}$ *and* $\mathbf{q_{MCV}}$ *the Fourier and the Maxwell-Cattaneo-Vernotte heat flux, respectively, we have that the expression of* $\mathbf{q_F}$ *is given by* (3.1)*, i.e.*

$$\mathbf{q_F} = -\lambda \nabla T \tag{4.25}$$

while the expression of $\mathbf{q_{MCV}}$ *must be calculated after solving the hyperbolic equation for* T*, i.e.* (4.20)*. Assuming that the initial heat flux is* $\mathbf{q}_0$*, we get*

$$\tau_0\, \partial_t \mathbf{q_{MCV}} + \mathbf{q_{MCV}} = -\lambda \nabla T \tag{4.26a}$$

$$\mathbf{q_{MCV}}(\mathbf{x}, 0) = \mathbf{q_{MCV}}(0) = \mathbf{q}_0 \tag{4.26b}$$

from which it is noted that the temperature expression $T(\mathbf{x}, t)$ *represents a system of ordinary differential equations that has as solution*

$$\mathbf{q_{MCV}} = \mathbf{q}_0\, e^{-t/\tau} - \frac{\lambda}{\tau} \int_0^t e^{-\frac{t-s}{\tau}} \nabla T(\mathbf{x}, s) ds. \tag{4.27}$$

Assuming the initial heat flux is zero, i.e. $\mathbf{q}_0 = \mathbf{0}$*, the following expression arises*

$$\mathbf{q_{MCV}} = -\frac{\lambda}{\tau} \int_0^t e^{-\frac{t-s}{\tau}} \nabla T(\mathbf{x}, s) ds \tag{4.28}$$

from this equation, it is evident that the Cattaneo heat flux $\mathbf{q_{MCV}}$ *depends on the whole time history (complete history) of the temperature gradient up to the current time instant. This contrasts with the Fourier heat flux* (4.25) *where no such memory effect exists, the heat flux depends only on the value of the temperature gradient at the time instant considered. However, if the temperature remains constant, in the case of Fourier the flux becomes zer, since the temperature gradient is zero*

$$\mathbf{q_F} = \mathbf{0};$$

while for Cattaneo's equation, it necessary a certain time (related to τ*) for the heat flux to diminish to negligible levels, i.e. zero. In this case, the heat flux decays according to*

$$\mathbf{q_{MCV}} = \mathbf{q}_0\, e^{-t/\tau}, \tag{4.29}$$

(See Figure 4.2, where the heat flux is shown for different values of the relaxation time, in the latter case).

This highlights the fact that, unlike in Fourier's law, Cattaneo's model retains a "memory" of the initial conditions for a finite period before the flux becomes negligible.

4.1.3 MCV equation is frame-invariant?

An important question concerns the invariance of the Cattaneo equation with respect to changes in the reference frame. Galilean covariance implies that both the balance laws and constitutive relations should be independent of the reference frame.

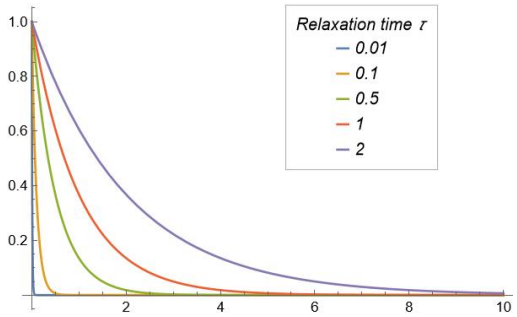

FIGURE 4.2: Heat flux (4.29) at the variation of relaxation time.

This raises the question: is the Cattaneo model, which well overcames the problem of the infinite propagation speed inherent in the Fourier equation, invariant under changes in the reference frame?

To answer this question, a further proposed model by Christov will be presented in brief lines [104, 105], without going to far in details, as this topic lies beyond the scope of this thesis.

Consider a heat transfer problem in a moving medium. In this context Christov [104] demonstrated that the model proposed by Cattaneo is not invariant under the Galilean transformations, i.e. the from of the equations and their solutions change with the variation of reference frame. Therefore, a more comprehensive formulation is required to ensure frame-invariant behavior.

The first modification introduced by Christov is the substitution, in the energy balance law, of the partial time derivative with the material derivative obtaining

$$\rho c \ (\partial_t T + \boldsymbol{v} \cdot \nabla T) + \nabla \cdot \mathbf{q} = S. \tag{4.30}$$

The second concerns the substitution, in the relation proposed by Cattaneo, of the partial time derivative of the heat flux, with the *upper convected time derivative* $\mathfrak{d}_t \mathbf{q}$, obtaining

$$\tau \ (\partial_t \mathbf{q} + \boldsymbol{v} \cdot \nabla \mathbf{q} - \mathbf{q} \cdot \nabla \boldsymbol{v} + (\nabla \cdot \boldsymbol{v})\mathbf{q}) + \mathbf{q} = -\lambda \nabla T. \tag{4.31}$$

The system of equations (4.30)- (4.31) is called Christov-Cattaneo model

$$\rho c \ (\partial_t T + \boldsymbol{v} \cdot \nabla T) + \nabla \cdot \mathbf{q} = S \tag{4.32a}$$
$$\tau \ (\partial_t \mathbf{q} + \boldsymbol{v} \cdot \nabla \mathbf{q} - \mathbf{q} \cdot \nabla \boldsymbol{v} + (\nabla \cdot \boldsymbol{v})\mathbf{q}) + \mathbf{q} = -\lambda \nabla T \tag{4.32b}$$

namely

$$\rho c \, D_t T + \nabla \cdot \mathbf{q} = S \tag{4.33a}$$
$$\tau \, \mathfrak{d}_t \mathbf{q}_t + \mathbf{q} = -\lambda \nabla T \tag{4.33b}$$

For simplicity, one-dimensional case without any source term is considered (similar results can be demonstrated in three dimensions and with a source term), obtaining

$$\rho c \ (\partial_t T + v \partial_x T) + \partial_x q = S \tag{4.34a}$$
$$\tau \ (\partial_t q + v \partial_x q) + q = -\lambda \partial_x T \tag{4.34b}$$

from which it is possible, as usual, to derive a single equation for the temperature (T-representation), achieving

$$\tau\partial_{tt}T + (1+\tau\partial_x v)\partial_t T + \tau v^2\partial_{xx}T + [v+\tau(\partial_t v + 2v\partial_x v)]\partial_x T + 2\tau v\partial_{tx}T = \alpha\partial_{xx}T \tag{4.35}$$

called *Cattaneo-Christov equation*. Now we introduce the following change of variables, which corresponds to a reference frame in motion at velocity V:

$$\begin{aligned} x' &= x - Vt, \\ t' &= t, \\ v' &= v - V \end{aligned} \tag{4.36}$$

from $\vartheta(x',t') = T(x,t)$ and using $\partial_t = \partial_{t'} - V\partial_{x'}, \partial_x = \partial_{x'}$ we get

$$\begin{aligned} &\partial_t T = \partial_{t'}\vartheta - V\partial_{x'}\vartheta, \\ &\partial_{tt}T = \partial_{t't'}\vartheta - 2V\partial_{t'x'}\vartheta + V^2\partial_{x'x'}\vartheta, \\ &v' = v - V \\ &\partial_x T = \partial_{x'}\vartheta \\ &\partial_{xx}T = \partial_{x'x'}\vartheta \\ &\partial_{tx}T = \partial_{t'x'}\vartheta - V\partial_{x'x'}\vartheta \\ &\partial_t v = \partial_{t'}v' - V\partial_{x'}v', \\ &\partial_x v = \partial_{x'}v' \end{aligned} \tag{4.37}$$

After substitution we obtain the same equation but in new variables

$$\tau\partial_{t't'}\vartheta + (1+\tau\partial_{x'}v')\partial_{t'}\vartheta + \tau(v')^2\partial_{x'x'}\vartheta + [v'+\tau(\partial_{t'}v' + 2v'\partial_{x'}v')]\partial_{x'}\vartheta + 2\tau v'\partial_{t'x'}\vartheta = \alpha\partial_{x'x'}\vartheta. \tag{4.38}$$

This leads to the conclusion that the Christov's equation is invariant before Galilean transformations. However, in this dissertation, we will assume that the medium is not in motion, i.e. $v = 0$, and in this case the Christov's equation reduces to the form of the Cattaneo equation.

A more general objective time derivative is proposed by Morro [106]

$$\tau\left(\partial_t\mathbf{q} + \boldsymbol{\nu}\cdot\nabla\mathbf{q} - \frac{\mu-1}{2}(\nabla\boldsymbol{\nu} - \nabla\boldsymbol{\nu}^T)\mathbf{q} + \gamma(\nabla\cdot\boldsymbol{\nu})\mathbf{q}\right) + \mathbf{q} = -\lambda\nabla T. \tag{4.39}$$

in which μ and γ are two parameters, with this generalization not exist the T-representation but the model remain hyperbolic.

The following definitions are useful

Definition 5. *(Material derivative)*
The material or total derivative of the function $f(\mathbf{x},t)$, assuming that the medium moves with a certain velocity $\boldsymbol{\nu}(\mathbf{x},t)$ is defined as follows

$$D_t f = \partial_t f + \boldsymbol{\nu}\cdot\nabla f \tag{4.40}$$

This material derivative represents the change of a given quantity $f(\mathbf{x},t)$ in a given point $\mathbf{x_0}$ which is due to two processes: the first is the change of this point, represented by the partial derivative with respect to time; the second one is due to

the transport that this point undergoes, described by the second term in which the velocity of the medium appears.

Definition 6. *(Upper convected time derivative)*
The upper convected time derivative of the vector density function $\mathbf{A}(\mathbf{x}, t)$*, assuming that the medium moves with a certain velocity* $\boldsymbol{\nu}(\mathbf{x}, t)$ *is defined as follows*

$$\mathfrak{d}_t \mathbf{A} = \partial_t \mathbf{A} + \boldsymbol{\nu} \cdot \nabla \mathbf{A} - \mathbf{A} \cdot \nabla \boldsymbol{\nu} + (\nabla \cdot \boldsymbol{\nu}) \mathbf{A} \tag{4.41}$$

Definition 7. *(Vector density)*
A mechanical quantity $\mathbf{A}$*, which is measured in two reference frames* $\mathbf{x}$ *and* $\mathbf{x}\prime$ *is a vector density, if it satisfies*

$$\int_D \mathbf{A} d\mathbf{x} = \int_{D'} \mathbf{A} d\mathbf{x}' \tag{4.42}$$

It can be verified that the heat flux $\mathbf{q}$ is a vector density, but this is obvious since the heat flux through a surface is invariant with respect to the chosen parametrization of the latter.

4.2 L-MCV and NL-MCV in 1D

We now focus on the study of effects induced by non-linearity. To explore this, let us revisit the thermodynamic derivation of the Cattaneo equation presented in Section 2.4.2. Notably, under the following identifications

$$\tau = \frac{\rho\, m}{l}, \qquad \lambda = \frac{1}{l T^2}$$

the nonlinear MCV heat equation (NL-MCV) is obtained

$$\tau(T)\, \partial_t \mathbf{q} + \mathbf{q} = -\lambda(T)\, \nabla T. \tag{4.43}$$

Now, suppose that thermal conductivity and the relaxation time are temperature-dependent. This scenario is relevant, for example, in modelling of second sound in superfluid helium [107, 108] where the temperature dependence of thermal conductivity plays a significant role in low-temperature regime (from near $0\,K$ to $2.2\,K$). This leads to a non constant propagation speed of second sound, as illustrated in Figure 4.3

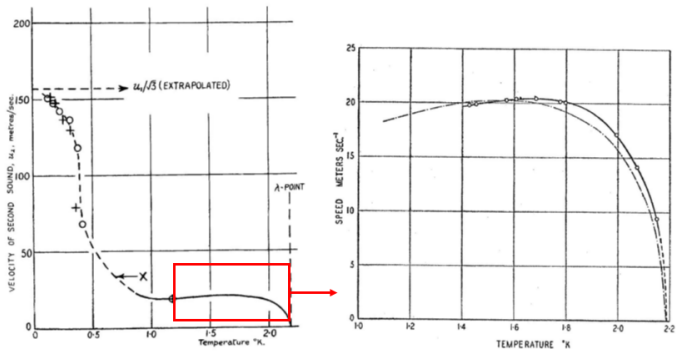

FIGURE 4.3: The temperature dependence of the propagation speed of second sound in He II, [13, 109]

This could also serve as an additional constraint on what temperature dependencies are physically admissible and how connect $\lambda(T)$ and $\tau(T)$. Moreover, Figure 4.4

provides further examples with various NaF crystals, illustrating how sensitive thermal conductivity and second sound are to sample purity [33].

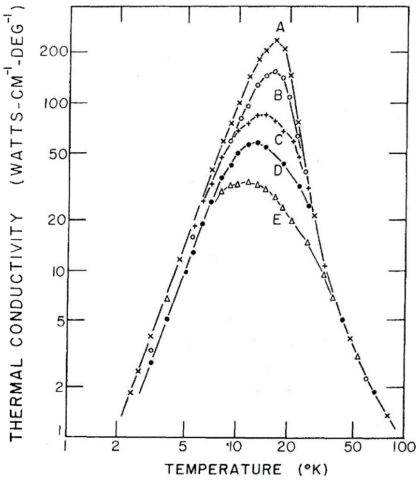

FIGURE 4.4: The thermal conductivity of NaF crystal.Temperature and purity dependence of the NaF crystals. The purity is decreasing from A to E, [21]

We assume here that the thermal conductivity and the relaxation time are expressed by (2.11) and (2.50) respectively, i.e.

$$\lambda(T) = \lambda_0 + a(T - T_0)$$
$$\tau(T) = \tau_0 + b(T - T_0)$$

wherein λ_0 and τ_0 are the thermal conductivity and the relaxation time at the initial or reference temperature, a and b are the coefficients that can take positive or negative values depending on whether the thermal conductivity and relaxation time increase or decrease due to changes in temperature. Non-zero values of these parameters, i.e. a and b, introduce nonlinearity into the thermal conductivity and relaxation time. By considering the identifications made in (2.49), the following constraints emerge to obtain these linear expressions for λ and τ, (2.11) and (2.50), the following constraints arise, [29, 30]:

$$l(T) = \frac{1}{[\lambda_0 + a(T - T_0)]\, T^2}, \quad \rho m = \frac{\tau_0 + b(T - T_0)}{[\lambda_0 + a(T - T_0)]\, T^2}.$$

Since $m(e) \equiv m$ is a constant, it is necessary to consider a temperature-dependent mass density, $\rho = \rho(T)$, which accounts for the presence of mechanical effects. While this contradicts our basic assumption of dealing with a rigid material, it remains necessary to study the subsystem without mechanical effects but with the inclusion of the nonlinear term, $\rho = \rho(T)$. Alternatively, one could consider $\frac{dm(e)}{de} \neq 0$ which would introduce a new term into the Cattaneo equation, as seen in equation (2.52) in Section 2.4.2. We will leave out of investigation equation (2.52). However, we have fixed our attention on the fact that it is not trivial to implement nonlinear terms in constitutive equations and how these may have influenced other parameters. In particular, we want to focus on the characteristics of temperature evolution and the properties of the solution method with respect to its stability and dispersion error.

Then the nonlinear model to be implemented in one and two spatial dimensions is given by the following system:

$$\rho c_v \partial_t T + \nabla \cdot \mathbf{q} = 0 \tag{4.44a}$$
$$[\tau_0 + b(T - T_0)]\partial_t \mathbf{q} + \mathbf{q} = -[\lambda_0 + a(T - T_0)]\,\nabla T. \tag{4.44b}$$

Application to heat pulse experiment

In the heat pulse experiment, at initial time, the temperature distribution is uniform and the sample is in thermal equilibrium with the external environment. A thin black coating is applied to the front side of the sample to guarantee uniform boundary conditions and to eliminate the transparency of the sample [42]. On the rear side, a silver coating is applied, and a thermocouple attached to this side measures the effective temperature. Regarding the boundary conditions, in agreement with the experimental setup, is applied to the left side of the sample, while the opposite side of the domain is treated as adiabatic. The sketch of the experiment is illustrated in Figure 4.5

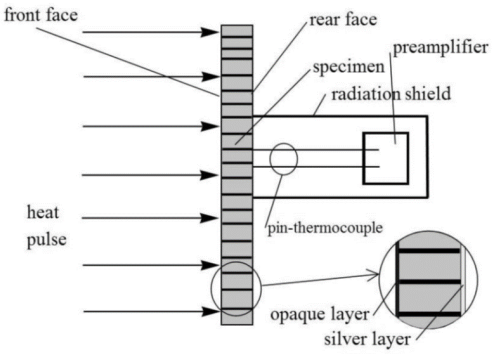

FIGURE 4.5: Sketch of the heat-pulse experiment. The front face of the specimen is excited by a heat pulse and rear-side temperature is measured with a termocouple.

In the first approximation, we consider the sample as one-dimensional, because if the heat pulse applied to the left side is uniform or homogeneous in space, we can simplify the problem by considering only the direction of heat pulse propagation (see figure 4.6). Under this assumption, the equations (4.44) reduce to the following form

$$\rho c_v \partial_t T + \partial_x q = 0 \tag{4.45a}$$
$$[\tau_0 + b(T - T_0)]\partial_t q + q = -[\lambda_0 + a(T - T_0)]\,\partial_x T. \tag{4.45b}$$

Next, we will extend this analysis to a more realistic scenario by considering two dimensions. In this case, we will observe that when a homogeneous heat pulse (in space) is applied, the results match those obtained in the one-dimensional case. However, we will also study the effect of a non-uniform (spatially non-homogeneous) heat pulse, as discussed in Section 4.3.

For this reason, first we consider the one-dimension case and assign the following initial

$$T(x, t_0) = T_0, \qquad q(x, t_0) = 0,$$

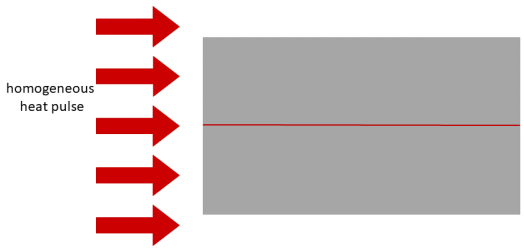

FIGURE 4.6:]
Setup of the heat-pulse experiment where we put in evidence that the front face of the specimen is excited by a homogeneous heat pulse.

and boundary conditions (which apply only to the heat flux)

$$q(0,t) = q_0(t) = \begin{cases} \dfrac{q_{max}}{2}\left[1 - \cos\left(\dfrac{2\pi t}{t_p}\right)\right] & \text{if } 0 < t \leq t_p, \\ 0 & \text{if } t > t_p. \end{cases}$$
$$q(L,t) = 0,$$

wherein t_0 is the initial time, q_{max} represents the pulse amplitude and t_p denotes the duration of the pulse, which should be much shorter than the characteristic time scale of the experiment.

This setup corresponds to the laser flash or heat pulse experiment [43, 97], which is a common and widely applied method for measuring the thermal diffusivity of a material and observing its non-Fourier heat conduction behavior.

4.2.1 Numerical framework

The equations (4.45) contain coefficients of several orders of magnitude. From a numerical point of view, this is highly unfavorable, then is convenient to introduce some dimensionless variables, as follow

$$\hat{x} = \frac{x}{L}, \quad \hat{t} = \frac{\alpha_0 t}{L^2}, \quad \hat{T} = \frac{T - T_0}{T_{\text{end}} - T_0}, \quad \hat{q} = \frac{q}{\tilde{q}_0} \quad \alpha_0 = \frac{\lambda(T_0)}{\rho c},$$

where L is the length of the rigid and isotropic conductor, T_0 and T_{end} are the initial and the equilibrium temperature corresponding to adiabatic boundaries, i.e.,

$$T_{end} = T_0 + \frac{1}{\rho c L}\int_{t_0}^{t_p} q_0(t)\,\mathrm{d}t, \quad \tilde{q}_0 = \frac{1}{t_p}\int_{t_0}^{t_p} q_0(t)\,\mathrm{d}t = \frac{q_{max}}{2},$$

where t_p is the length of the pulse that acts on the boundary as a heat pulse. Moreover, t_0 is the initial time instant which is considered to be 0 and $\tilde{q}_0$ is the integral average of the heat pulse $q_0(t)$.

Now, the dimensionless form of the system of equations (4.45) reads

$$\tau_{p_1}\partial_{\hat{t}}\hat{T} + \partial_{\hat{x}}\hat{q} = 0, \tag{4.46a}$$
$$(\tau_{q_1} + \tau_{q_2}\hat{T})\partial_{\hat{t}}\hat{q} + \hat{q} = -(\tau_{p_1} + \tau_{p_2}\hat{T})\partial_{\hat{x}}\hat{T}, \tag{4.46b}$$

where the dimensionless parameters are

$$\tau_{p_1} = \frac{\alpha_0 t_p}{L^2}, \quad \tau_{p_2} = \frac{a(T_{\text{end}} - T_0)t_p}{\rho c L^2}, \quad \tau_{q_1} = \frac{\alpha_0(\tau_0 + b\, T_0)}{L^2}, \quad \tau_{q_2} = \frac{\alpha_0 b(T_{\text{end}} - T_0)}{L^2}. \tag{4.47}$$

The dimensionless form of the boundary conditions namely, heat pulse, becomes

$$\begin{aligned} &\hat{q}(0,\hat{t}) = \hat{q}_0(\hat{t}) = \begin{cases} 1 - \cos\left(\dfrac{2\pi\hat{t}}{\tau_d}\right) & \text{if } 0 < \hat{t} \leq \tau_d, \\ 0 & \text{if } \hat{t} > \tau_d. \end{cases}, \\ &\hat{q}(1,\hat{t}) = 0. \end{aligned} \tag{4.48}$$

In order to simplify the notations the hat is omitted in the following.

Characteristic velocity

The characteristic velocity, from the relation (4.16), can be expressed as follows

$$v(T) = \sqrt{\frac{\lambda(T)}{\rho c \tau(T)}} = \sqrt{\frac{\lambda_0 + a(T - T_0)}{\rho c\,[\tau_0 + b(T - T_0)]}} \tag{4.49}$$

introducing the dimensionless quantities (i.e $\hat{v} = v/v_0$) and using the positions (4.47) the expression (4.49) rewrites

$$\begin{aligned} \hat{v}(\hat{T}) &= \frac{1}{v_0} \cdot \sqrt{\frac{\lambda(\hat{T})}{\rho c \tau(\hat{T})}} = \frac{1}{v_0} \cdot \sqrt{\frac{\lambda_0 + a(T_{end} - T_0)\hat{T}}{\rho c\left[\tau_0 + b(T_{end} - T_0)\hat{T}\right]}} = \frac{1}{v_0} \cdot \sqrt{\frac{\lambda_0 + \frac{\rho c L^2}{t_p}\tau_{p_2}\hat{T}}{\rho c\left(\tau_0 + \frac{L^2}{\alpha_0}\tau_{q_2}\hat{T}\right)}} \\ &= \frac{1}{v_0} \cdot \sqrt{\frac{\tau_{p_1} + \tau_{p_2}\hat{T}}{\tau_{q_1} + \tau_{q_2}\hat{T}} \cdot \frac{\alpha_0}{t_p}} = \sqrt{\frac{\tau_{p_1} + \tau_{p_2}\hat{T}}{\tau_{q_1} + \tau_{q_2}\hat{T}}} \end{aligned}$$

where is possible to identify

$$v_0 = \sqrt{\frac{\alpha_0}{t_p}}. \tag{4.50}$$

Furthermore the expression of characteristic velocity in a dimensionless form becomes

$$\hat{v}(\hat{T}) = \sqrt{\frac{\tau_{p_1} + \tau_{p_2}\hat{T}}{\tau_{q_1} + \tau_{q_2}\hat{T}}}. \tag{4.51}$$

Remark 8. *Similarly in the linear case, the relation (4.51), can be expressed as follow*

$$\hat{v} = \sqrt{\frac{\tau_{p_1}}{\tau_{q_1}}}$$

it is trivial to find this expression by (4.51) when $\tau_{p_2} = \tau_{q_2} = 0$.

Difference equations

Here we present a numerical method developed for the nonlinear one-dimension model (4.46). Let us discretize the spatial domain $\Omega = [0, 1]$ with spatial steps Δx and the time interval $[0, t_{max}]$ with step Δt, the following discrete space and time

values are obtained

$$x_j = x_0 + j\Delta x \quad j = 0, 1, 2, ..., N$$
$$t^n = n\Delta t \quad n = 0, 1, 2, ..., J.$$

This method has been developed for linear heat equations and validated using an analytical solution for the Guyer-Krumhansl equation in [49]. The basic principle remains the same: a staggered spatial field is used to distinguish 'surface' and 'volume average' quantities. In heat pulse experiments when the heat flux is defined on both boundaries, the temperature is shifted by half space step $\Delta x/2$ (i.e. it is computed in the internal nodes [29, 98])

$$T(x_{j+1/2}, t^n) \approx T^n_{j+1/2}$$
$$q(x_j, t^n) \approx q^n_j.$$

as shown in Fig. 4.7. As a consequence, there is no need to define boundaries for the temperature field. In time, only an explicit forward differencing scheme is used.

Therefore the difference equations are

$$\frac{\tau_{p_1}(\tau_{q_1} + \tau_{q_2} T^n_{j+1/2})}{\tau_{q_1}} \cdot \frac{T^{n+1}_{j+1/2} - T^n_{j+1/2}}{\Delta t} + \frac{q^n_{j+1} - q^n_j}{\Delta x} = 0, \tag{4.52a}$$

$$(\tau_{q_1} + \tau_{q_2} T^n_j) \cdot \frac{q^{n+1}_j - q^n_j}{\Delta t} + q^n_j + (\tau_{p_1} + \tau_{p_2} T^n_j) \cdot \frac{T^n_{j+1/2} - T^n_{j-1/2}}{\Delta x} = 0. \tag{4.52b}$$

where a explicit forward finite difference approximation are used for the time and spatial derivatives

$$\frac{\partial T}{\partial t} \approx \frac{T^{n+1}_{i+1/2,j+1/2} - T^n_{i+1/2,j+1/2}}{\Delta t},$$
$$\frac{\partial q}{\partial t} \approx \frac{q^{n+1}_{i+1/2,j} - q^n_{i+1/2,j}}{\Delta t},$$
$$\frac{\partial q}{\partial x} \approx \frac{q^n_{j+1} - q^n_j}{\Delta x},$$
$$\frac{\partial T}{\partial x} \approx \frac{T^n_{j+1/2} - T^n_{j-1/2}}{\Delta x}.$$

where n denotes the time steps and j stands for the spatial steps.

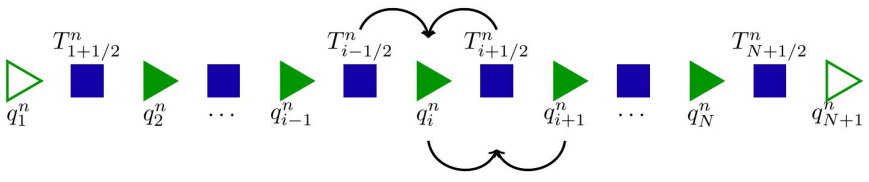

FIGURE 4.7: Concept of the spatial discretization [98]). The filled squares represent the temperature, and the filled triangles, which are oriented differently, are vector components. Empty symbols denote boundary conditions.

By virtue of the evolution equation of the heat flux component q, (4.52b), the quantity T_j^n in the non linear terms is replaced by the following average:

$$T_j^n \longmapsto \frac{T_{j-1/2}^n + T_{j+1/2}^n}{2},$$

as shown in Fig. 4.7.

4.2.2 Stability analysis, Dissipation and Dispersion Errors

Since finite difference schemes can lead to instability, it is essential to perform a stability analysis to determine the appropriate ranges for Δx and Δt in a given numerical scheme.

In this particular case, the challenge arises from the fact that the heat flux cannot be easily eliminated, as the relaxation time depends on temperature, leading to a complicate partial differential equation (PDE) that would be impractical to discretize. Additionally, the correct treatment of boundary conditions requires both the temperature and the heat flux to be retained. Therefore, eliminating any variables is not an appropriate approach.

Before proceeding with the stability analysis presented above in the Chapter 3, we can directly estimate the stability criterion for the NL-MCV equation. In the case of Fourier heat equation, we have seen that the correction factor $\tau_{p_1}/(\tau_{p_1} + \tau_{p_2})$ appears in the stability condition, which reduces the maximum permissible time step in the numerical algorithm (see Section 3.2.1). Similarly, due to the non-linearity in the relaxation time in addition to the thermal conductivity, we expect a comparable correction factor, $\tau_{q_1}/(\tau_{q_1} + \tau_{q_2})$, to emerge in the stability condition of the NL-MCV equation.

Using the results of the linear case [98], which is

$$\Delta t < \frac{\Delta x^2}{4},$$

we expect that

$$\Delta t < \frac{\Delta x^2}{4} \frac{\tau_{p_1}}{\tau_{p_1} + \tau_{p_2} \max_{(j,n)} T_j^n} \tag{4.53}$$

will appear without the relaxation time as it does not appear even in the linear case. However, with the estimation for temperature $\max_{(j,n)} T_j^n = 1$, it could be too optimistic as the MCV model is a damped wave equation. It is safe to say that the $\max_{(j,n)} T_j^n \approx 3$ for real parameters which could occur in experiments. This approximation means that the maximum temperature in the simulation is three times higher compared to the equilibrium. Note that this maximum depends strongly on τ_{q_1} and higher temperature values may occur.

Since we do not intend to use only a single variable (T or q), the stability analysis present above regard is not applicable as far as mapping is concerned. Instead, let us assume again that the estimation about the $\max_{(j,n)} T_j^n = 3$ can be made as a first step. Then, to study the stability of the numerical scheme (4.52) the Von-Neumann procedure is used. Let us suppose that the solutions of the difference equations are in the following form [102]:

$$u_j^n = u_0 \, \xi^n e^{i k j \Delta x} \tag{4.54}$$

with $u \in \{T, q\}$, i is the imaginary unit, k the wave number, and ξ is the growth factor representing the amplitude wave and must be bounded from above for stability.

By substituting equation (4.54) into the finite difference equations in (4.52), a system of linear algebraic equations is achieved

$$\mathbf{M} \cdot \begin{pmatrix} T_0 \\ q_0 \end{pmatrix}$$

wherein the coefficient matrix is:

$$\mathbf{M} = \begin{pmatrix} \dfrac{\tau_{p_1}}{\Delta t}\left(1 + \dfrac{\tau_{q_2}}{\tau_{q_1}} Z\right)(\xi - 1) & \dfrac{1}{\Delta x}\left(e^{i\,k\Delta x} - 1\right) \\ \dfrac{\tau_{p_1} + \tau_{p_2} Z}{\Delta x}\left(1 - e^{-i\,k\Delta x}\right) & 1 + \dfrac{\tau_{q_1} + \tau_{q_2} Z}{\Delta t}(\xi - 1) \end{pmatrix},$$

with $Z = \max_{j,n} T_j^n$.

The characteristic equation for ξ ($\det \mathbf{M} = 0$) can be expressed as

$$p(\xi) = a_2 \xi^2 + a_1 \xi + a_0 = 0, \tag{4.55}$$

where the coefficients are

$$a_2 = \frac{\tau_{p_1}(\tau_{q_1} + \tau_{q_2} Z)^2}{\tau_{q_1}(\Delta t)^2}, \tag{4.56a}$$

$$a_1 = -2\frac{\tau_{p_1}(\tau_{q_1} + \tau_{q_2} Z)^2}{\tau_{q_1}(\Delta t)^2} + \frac{\tau_{p_1}(\tau_{q_1} + \tau_{q_2} Z)}{\Delta t}, \tag{4.56b}$$

$$\begin{aligned} a_0 &= \frac{\tau_{p_1}(\tau_{q_1} + \tau_{q_2} Z)^2}{\tau_{q_1}(\Delta t)^2} - \frac{\tau_{p_1}(\tau_{q_1} + \tau_{q_2} Z)}{\Delta t} - \frac{2(\tau_{p_1} + \tau_{p_2} Z)}{(\Delta x)^2}\left[\cos(k\Delta_x) - 1\right] \\ &= \frac{\tau_{p_1}(\tau_{q_1} + \tau_{q_2} Z)^2}{\tau_{q_1}(\Delta t)^2} - \frac{\tau_{p_1}(\tau_{q_1} + \tau_{q_2} Z)}{\Delta t} + \frac{4(\tau_{p_1} + \tau_{p_2} Z)}{(\Delta x)^2} S^2. \end{aligned} \tag{4.56c}$$

with $S = \sin(k\Delta x/2)$.

Theorem 5. *The numerical scheme is stable if the following conditions are satisfied*

1. $\Delta t < 2(\tau_{q_1} + \tau_{q_2} Z)$,

2. $\Delta t < \dfrac{(\Delta x)^2}{4} \cdot \dfrac{\tau_{q_1} + \tau_{q_2} Z}{\tau_{q_1}} \cdot \dfrac{\tau_{p_1}}{\tau_{p_1} + \tau_{p_2} Z}$.

Proof. Applying the Jury criteria we have the following three conditions

C1 $p(\xi = 1) \geq 0 \quad \Leftrightarrow \quad a_2 + a_1 + a_0 \geq 0$ i.e.

$$\frac{4(\tau_{p_1} + \tau_{p_2} Z)}{(\Delta x)^2} S^2 \geq 0$$

which is trivially satisfied.

C2 $p(\xi = -1) \geq 0 \quad \Leftrightarrow \quad a_2 - a_1 + a_0 \geq 0$ i.e.

$$4\frac{\tau_{p_1}(\tau_{q_1} + \tau_{q_2} Z)^2}{\tau_{q_1}(\Delta t)^2} - 2\frac{\tau_{p_1}(\tau_{q_1} + \tau_{q_2} Z)}{\Delta t} + 4\frac{(\tau_{p_1} + \tau_{p_2} Z)}{(\Delta x)^2} S^2$$

that is satisfied if $\Delta t \leq 2(\tau_{q_1} + \tau_{q_2} Z)$ is true.

C3 $|a_0| \leq a_2$ which is satisfied if

$$\Delta t < \frac{(\Delta x)^2}{4} \cdot \frac{\tau_{q_1} + \tau_{q_2} Z}{\tau_{q_1}} \cdot \frac{\tau_{p_1}}{\tau_{p_1} + \tau_{p_2} Z}$$

where the last criterion is the strongest. It consists in the temperature-dependent thermal conductivity correction as expected. However, it may be higher than the real upper bound, that is, it is proposed to use also the other correction for the relaxation time:

$$\Delta t < \frac{\Delta x^2}{4} \frac{\tau_{p_1}}{\cdot} \tau_{p_1} + \tau_{p_2} \max_{j,n} T_j^n \cdot \frac{\tau_{q_1}}{\tau_{q_1} + \tau_{q_2} \max_{j,n} T_j^n}. \tag{4.57}$$

For further information, see [29]. □

Let us remark that in linear case (i.e. when $\tau_{q_2} = 0$, τ_{p_2}), the inequality (4.57) reduces to the condition (4.53). Additionally, a correction factor related to the relaxation time appears in the stability condition, which results from temperature dependence of the mass density.

Remark 9. *It is important to note that the numerical method described above was originally developed for linear heat equations. However, since a nonlinearity appears in the right hand side of the resulting finite difference equations (4.52), one could assume a priori the maximum temperature and apply a linear stability analysis by following von Neumann's method [102] and Jury's criterion [103]. Let us admit that is strongly based on the initial assumption of maximum temperature. To partially overcoming this difficult, a practical first step could be to perform a linear simulation and observe the maximum value reached in the resulting temperature field. This value can be use as a reasonable estimate, as the practically relevant nonlinearities do not significantly increase the temperature but rather distort the time history more notably.*

In this way, the method allows for an estimate of stability while accounting for nonlinear effects in the system.

4.2.3 Numerical results

In this section, we present the solutions of nonlinear MCV heat equation and investigate the effects of non-linear terms. We focus solely on the temperature histories at rear side ($\hat{x} = 1$) of the sample, as these are the value measured and used for evaluation in heat pulse experiment, as previously explained.

Investigating the effects of the parameter τ_{p_2} in solutions of the MCV equation, it is observed that: this parameter influences the slope at the point when the temperature starts to increase. It is worth observing that the point corresponding to $\hat{T} = 0.5$ is significantly shifted to the left for increasing of τ_{p_2}. Using $\tau_{p_1} = 0.1$ and $\tau_{q_1} = 0.08$ the wave signal dominates the solution and is further shifted to the left, affecting only the slope of the wave front. However, as can be seen, the MCV solution becomes more dispersive for larger τ_{p_2}. This dispersive behavior also occur when τ_{q_2} is increased (see Fig. 4.9). Apparently, these parameters act against each other, τ_{q_2} shifts the wave signal to the right. In both situations, the solution remains stable, and the dispersive error can be minimized by increasing the resolution of the numerical discretization. Despite the simplicity of the scheme, it is able to solve the non-linear heat equation of MCV. Dispersive errors are present only when one of the

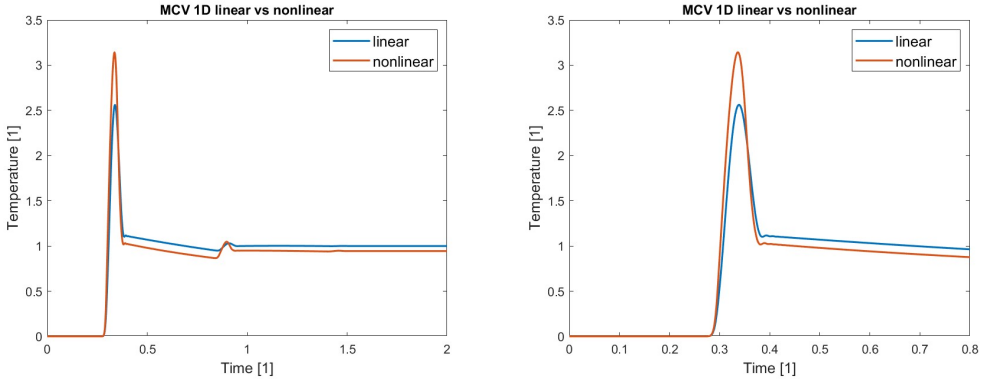

(a) (b)

FIGURE 4.8: Comparison the rear side temperature history in linear and nonlinear case, using $\tau_{p_1} = 0.1$, $\tau_{q_1} = 0.08$, $\tau_{p_2} = \{0, 0.03\}$ and $\tau_{q_2} = \{0, 0.01\}$.

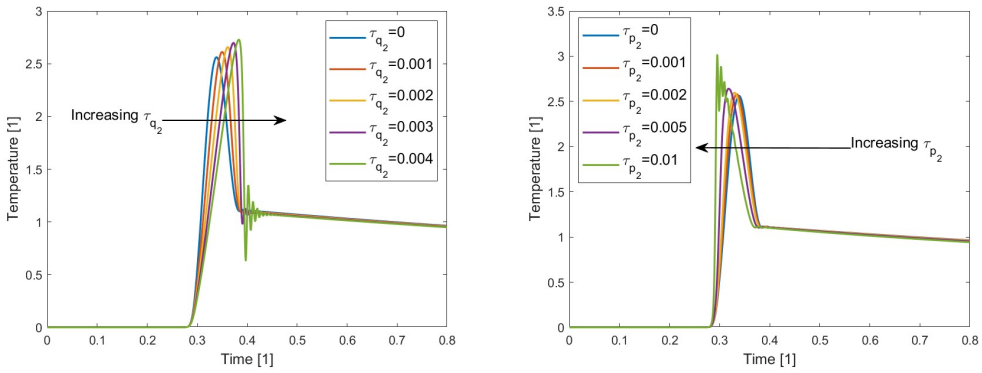

(a) (b)

FIGURE 4.9: The rear side temperature history when increasing the nonlinear parameter : $\tau_{q_2} \in \{0, 0.001, 0.002, 0.003, 0.004\}$ with $\tau_{p_2} = 0$ in (a) and $\tau_{p_2} \in \{0, 0.001, 0.002, 0.005, 0.01\}$ with $\tau_{q_2} = 0$ in (b). The other parameters are: $\tau_{p_1} = 0.1$, $\tau_{q_1} = 0.08$.

temperature dependent begins to dominate. Note that Figure 4.9 shows a different case where both parameters, τ_{p_2} and τ_{q_2} are much larger than before and the numerical solutions become free of artificial oscillations, even using the same discretization. It is because these parameters influence the solution in opposite ways.

However, in Figure 4.11 it is possible to observe better the propagation of the heat pulse, initially generated at $\hat{x} = 0$. The pulse moves in the direction $\hat{x}$, gradually damping until it reaches the opposing wall $\hat{x} = 1$, where it is then reflected. This process of reflection continues until the thermal pulse is completely damped out.

4.3 L-MCV and NL-MCV in 2D

Let us now move on to the more realistic situation, considering two spatial dimensions. According to this hypotesis, in a rectangular domain $\Omega = [0, L_1] \times [0, L_2]$ with

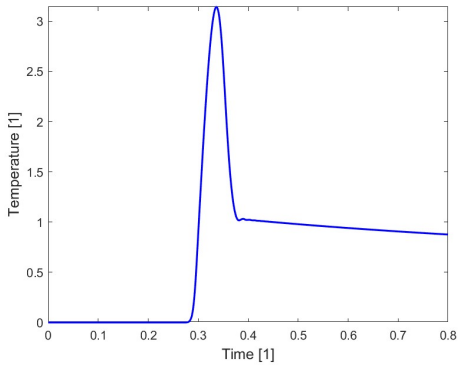

FIGURE 4.10: The rear side temperature history, using the MCV heat equation, using $\tau_{p_1} = 0.1$, $\tau_{p_2} = 0.03$, $\tau_{q_1} = 0.08$ and $\tau_{q_2} = 0.01$.

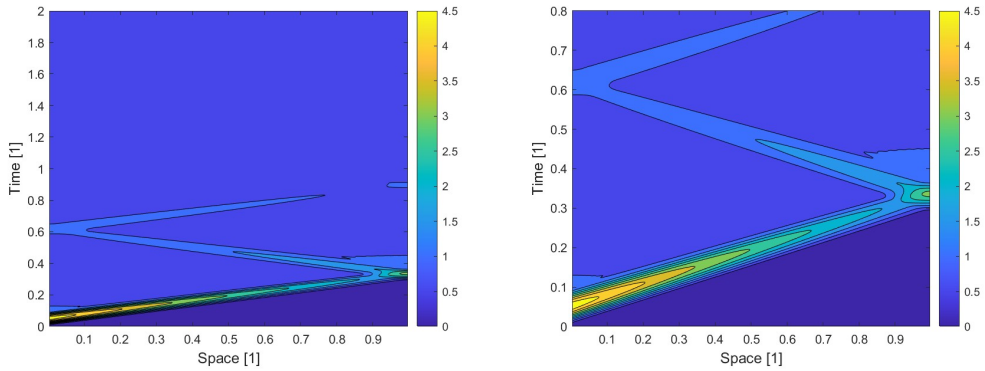

(a) (b)

FIGURE 4.11: The contour plot of the temperature distribution, in (b) the zoom in the time interval $[0, 0.8]$.

lengths of L_1 and L_2, the equations (4.44) become

$$\rho c\, \partial_t T + \partial_x q_x + \partial_y q_y = 0, \tag{4.58a}$$
$$\tau(T)\partial_t q_x + q_x = -\lambda(T)\partial_x T, \tag{4.58b}$$
$$\tau(T)\partial_t q_y + q_y = -\lambda(T)\partial_y T, \tag{4.58c}$$

where c is the specific heat, $e = c\,T$, and q_x, q_y are the components of the heat flux $\mathbf{q} = (q_x, q_y)$. The material parameters, density ρ, and specific heat capacity c, are assumed to be constant.

Initially, in a heat pulse experiment, it is required that the temperature distribution be homogeneous and that the sample be in thermal equilibrium with its environment. So, both heat flux fields are zero at the initial time instant. For boundary conditions, the heat pulse excites the lower side of the sample in the y-axis direction, the other sides of the domain are considered adiabatic. Let us show that if we consider a heat pulse uniform in space (homogeneous) we get the solutions obtained in 1D, however we investigate the case where the heat pulse is not homogeneous, as shown in Figure 4.12.

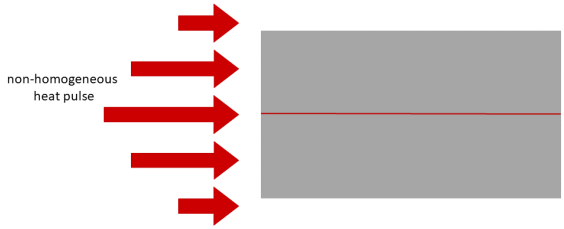

FIGURE 4.12: Setup of the heat-pulse experiment where we put in evidence that the front face of the specimen is excited by a non-homogeneous heat pulse.

Hence, we assign the following initial conditions

$$\begin{aligned} T(x,y,0) &= T_0, \\ q_x(x,y,0) &= 0, \\ q_y(x,y,0) &= 0. \end{aligned}$$

Then, on three of its edges the heat flux is identical to zero

$$\begin{aligned} q_x(0,y,t) &= 0, \\ q_x(L_1,y,t) &= 0, \\ q_y(x,L_2,t) &= 0 \end{aligned}$$

on the other side, a homogeneous heat flux is applied

$$q_y(x,0,t) = q_y^0(t) = \begin{cases} \dfrac{q_{max}}{2}\left[1-\cos\left(\dfrac{2\pi t}{t_p}\right)\right] & \text{if } 0 < t \leq t_p, \\ 0 & \text{if } t > t_p. \end{cases}$$

or not homogeneous in space

$$q_y(x,0,t) = q_y^0(t) = \begin{cases} \dfrac{q_{max}}{4}\left[1-\cos\left(\dfrac{2\pi t}{t_p}\right)\right]\cdot\left[1-\cos\left(\dfrac{2\pi x}{w_x}\right)\right] & \text{if } 0 < t \leq t_p, \\ & \text{and} \\ & \frac{L_1-w_x}{2} \leq x \leq \frac{L_1+w_x}{2} \\ 0 & \text{if } t > t_p, \end{cases}$$

where t_p is the duration of the pulse, q_{max} is its amplitude, w_x is its spatial width. On the other hand, the heat flux is identically zero.

Dimensionless form

The system (4.58) may contain coefficients with several orders of magnitude difference, this is unfavorable from a numerical point of view. Thus it is convenient to introduce dimensionless variables (as in the one dimensional case)

$$\hat{x} = \frac{x}{L_1}, \quad \hat{y} = \frac{y}{L_2}, \quad \hat{t} = \frac{\alpha_0 t}{L_1 L_2}, \quad \hat{q}_x = \frac{q_x}{\tilde{q}_0}, \quad \hat{q}_y = \frac{q_y}{\tilde{q}_0}, \quad \hat{T} = \frac{T - T_0}{T_{end} - T_0},$$

where

$$\alpha_0 = \frac{\lambda(T_0)}{\rho_0 c_v}, \qquad T_{end} = T_0 + \frac{t_p \tilde{q}_0}{\rho c_v L_2}$$

with

$$\tilde{q}_0 = \frac{q_{max}}{2t_p} \qquad \text{for spatially homogeneous boundary heat flux,} \qquad \text{or}$$
$$\tilde{q}_0 = \frac{q_{max}}{4t_p} \qquad \text{for spatially hon-homogeneous boundary heat flux.}$$

and thus, the dimensionless parameters are

$$\tau_{p_1}^{q_x} = \frac{\alpha_0 t_p}{L_1 L_2} = \tau_{p_1}, \quad \tau_{p_1}^{q_y} = \frac{\alpha_0 t_p}{(L_2)^2}, \quad \tau_{p_2}^{q_x} = \frac{a(T_{end} - T_0) t_p}{\rho_0 c_v L_1 L_2},$$
$$\tau_{p_2}^{q_y} = \frac{a(T_{end} - T_0) t_p}{\rho_0 c_v (L_2)^2}, \quad \tau_{q_1} = \frac{\alpha_0 \tau_0}{L_1 L_2}, \quad \tau_{q_2} = \frac{\alpha_0\, b(T_{end} - T_0)}{L_1 L_2}, \quad \tau_{p_1} = \frac{\alpha_0 t_p}{L_1 L_2}.$$

Under these assumptions, the two-dimensional version of the dimensionless system of equations becomes:

$$\tau_d \left(1 + \frac{\tau_{q_2}}{\tau_{q_1}} \hat{T}\right) \partial_{\hat{t}} \hat{T} + \frac{L_2}{L_1} \partial_{\hat{x}} \hat{q}_x + \partial_{\hat{y}} \hat{q}_y = 0, \tag{4.59a}$$
$$(\tau_{q_1} + \tau_{q_2} \hat{T})\, \partial_{\hat{t}} \hat{q}_x = -\hat{q}_x - \left(\tau_{p_1}^{q_x} + \tau_{p_2}^{q_x} \hat{T}\right) \partial_{\hat{x}} \hat{T}, \tag{4.59b}$$
$$(\tau_{q_1} + \tau_{q_2} \hat{T})\, \partial_{\hat{t}} \hat{q}_y = -\hat{q}_y - \left(\tau_{p_1}^{q_y} + \tau_{p_2}^{q_y} \hat{T}\right) \partial_{\hat{y}} \hat{T}, \tag{4.59c}$$

Furthermore, the dimensionless initial data are given:

$$\hat{T}(\hat{x}, \hat{y}, 0) = 0, \tag{4.60a}$$
$$\hat{q}_x(\hat{x}, \hat{y}, 0) = 0, \tag{4.60b}$$
$$\hat{q}_y(\hat{x}, \hat{y}, 0) = 0, \tag{4.60c}$$

and the dimensionless form of boundary conditions for heat flux with the heat pulse with t_p duration read:

$$\hat{q}_x(0, \hat{y}, \hat{t}) = 0, \tag{4.61a}$$
$$\hat{q}_x(1, \hat{y}, \hat{t}) = 0, \tag{4.61b}$$
$$\hat{q}_y(\hat{x}, 1, \hat{t}) = 0. \tag{4.61c}$$

Additionally, the heat pulse in the homogeneous case is

$$\hat{q}_y(\hat{x}, 0, \hat{t}) = \begin{cases} 1 - \cos\left(\dfrac{2\pi \hat{t}}{\tau_d}\right) & \text{if } 0 < \hat{t} \le \tau_d, \\ 0 & \text{if } \hat{t} > \tau_d. \end{cases}, \tag{4.62}$$

and in the non-homogeneous situation it reads

$$\hat{q}_y(x, 0, t) = \begin{cases} \left[1 - \cos\left(\dfrac{2\pi \hat{t}}{\tau_d}\right)\right] \cdot [1 - \cos(2\pi \hat{x})] & \text{if } 0 < \hat{t} \le \tau_d, \text{ and } 0 \le \hat{x} \le 1 \\ 0 & \text{if } \hat{t} > \tau_d. \end{cases} \tag{4.63}$$

Remark 10. *If we choose* $\tau_{q_2} = \tau_{p_2}^{q_x} = \tau_{p_2}^{q_y} = 0$, *it yields the linear case:*

$$\tau_{p_1}\partial_{\hat{t}}\hat{T} + \frac{L_2}{L_1}\partial_{\hat{x}}\hat{q}_x + \partial_{\hat{y}}\hat{q}_y = 0, \tag{4.64a}$$

$$\tau_{q_1}\partial_{\hat{t}}\hat{q}_x = -\hat{q}_x - \tau_{p_1}^{q_x}\partial_{\hat{x}}\hat{T}, \tag{4.64b}$$

$$\tau_{q_1}\partial_{\hat{t}}\hat{q}_y = -\hat{q}_y - \tau_{p_1}^{q_y}\partial_{\hat{y}}\hat{T}. \tag{4.64c}$$

From now on, the 'hat' is omitted in order to simplify the notation.

As in [110, 111], we apply a numerical scheme to solve the system (4.59) with a staggered field discretization for spatial derivatives in which the specific extensive quantities are calculated at the center of the cells. At the same time, the boundary-related fluxes are computed on the cell boundary, as we can see in the next section.

As a result, the spatial positions of the temperature values are shifted by a half space step from the positions of the **q** values (see Fig.4.13).

4.3.1 Numerical framework

Here we present a numerical method developed for the nonlinear two-dimensions model (4.59). In this case, it is not possible to obtain the T-representation, and the numerical study is more difficult compared to the linear case, i.e. where τ and λ are constant. Therefore, the MCV system (4.59) must be solved by simultaneously solving both the energy balance law and the evolution equation for the heat flux. For this purpose, using a staggered field discretization is much more advantageous, and its schematic is possible to see in Figure 4.13.

Let us discretize the spatial domain $\Omega = [0, L_1] \times [0, L_2]$ with spatial steps $\Delta x, \Delta y$ and the time interval $[0, t_{max}]$ with time step Δt, the following discrete space and time values are obtained

$$x_j = x_0 + j\Delta x \quad j = 0, 1, 2, ..., N \tag{4.65a}$$

$$y_i = y_0 + i\Delta y \quad i = 0, 1, 2, ..., M \tag{4.65b}$$

$$t^n = n\Delta t \quad n = 0, 1, 2, ..., J. \tag{4.65c}$$

An explicit forward finite difference method is used for the time derivatives

$$\frac{\partial T}{\partial t} \approx \frac{T_{i+1/2,j+1/2}^{n+1} - T_{i+1/2,j+1/2}^{n}}{\Delta t},$$

$$\frac{\partial q_x}{\partial t} \approx \frac{(q_x)_{i+1/2,j}^{n+1} - (q_x)_{i+1/2,j}^{n}}{\Delta t},$$

$$\frac{\partial q_y}{\partial t} \approx \frac{(q_y)_{i,j+1/2}^{n+1} - (q_y)_{i,j+1/2}}{\Delta t},$$

and for the spatial derivatives

$$\begin{aligned}
\frac{\partial q_x}{\partial x} &\approx \frac{(q_x)^n_{i+1/2,j+1} - (q_x)^n_{i+1/2,j}}{\Delta x} = \mathcal{D}_x(q_x),\\
\frac{\partial q_y}{\partial y} &\approx \frac{(q_y)^n_{i+1,j+1/2} - (q_y)^n_{i,j+1/2}}{\Delta y} = \mathcal{D}_y(q_y),\\
\frac{\partial T}{\partial x} &\approx \frac{T^n_{i+1/2,j+1/2} - T^n_{i+1/2,j-1/2}}{\Delta x} = \mathcal{D}_x(T),\\
\frac{\partial T}{\partial y} &\approx \frac{T^n_{i+1/2,j+1/2} - T^n_{i-\frac{1}{2},j+1/2}}{\Delta y} = \mathcal{D}_y(T).
\end{aligned}$$

In addition, for nonlinear terms, the following identifications are given

$$\begin{aligned}
\left(\tau_{q_1} + \tau_{q_2} T\right) &\approx \left(\tau_{q_1} + \tau_{q_2} T^n_{i+1/2,j+1/2}\right) = \mathcal{A}^n_{i+1/2,j+1/2}\\
\left(\tau^{q_x}_{p_1} + \tau^{q_x}_{p_2} T\right) &\approx \left(\tau^{q_x}_{p_1} + \tau^{q_x}_{p_2} T^n_{i+1/2,j}\right) = (\mathcal{B}_x)^n_{i+1/2,j}\\
\left(\tau^{q_y}_{p_1} + \tau^{q_y}_{p_2} T\right) &\approx \left(\tau^{q_y}_{p_1} + \tau^{q_y}_{p_2} T^n_{i,j+1/2}\right) = (\mathcal{B}_y)^n_{i,j+1/2}
\end{aligned}$$

As a result, the difference equations consist of an explicit forward differencing scheme

$$\mathcal{A}^n_{i+1/2,j+1/2} \cdot \frac{\tau_{p_1}}{\tau_{q_1}} \frac{T^{n+1}_{i+1/2,j+1/2} - T^n_{i+1/2,j+1/2}}{\Delta t} + \frac{L_2}{L_1}\mathcal{D}_x(q_x) + \mathcal{D}_y = 0, \tag{4.66a}$$

$$\mathcal{A}^n_{i+1/2,j} \cdot \frac{(q_x)^{n+1}_{i+1/2,j} - (q_x)^n_{i+1/2,j}}{\Delta t} = -(q_x)^n_{i+1/2,j} - (\mathcal{B}_x)^n_{i+1/2,j} \cdot \mathcal{D}_x(T), \tag{4.66b}$$

$$\mathcal{A}^n_{i,j+1/2} \cdot \frac{(q_y)^{n+1}_{i,j+1/2} - (q_y)_{i,j+1/2}}{\Delta t} = -(q_y)^n_{i,j+1/2} - (\mathcal{B}_x)^n_{i,j+1/2} \cdot \mathcal{D}_y(T), \tag{4.66c}$$

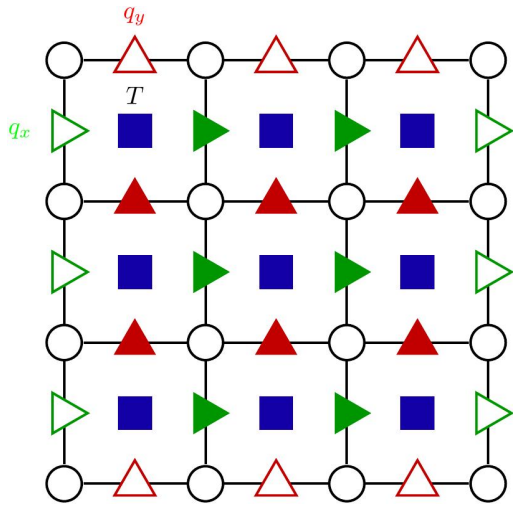

FIGURE 4.13: Representation of the finite difference numerical scheme. The filled squares represent the temperature, and the filled triangles, which are oriented differently, are vector components. Empty symbols denote boundary conditions.

Accordingly, the discrete values of temperature are shifted in x and y directions

$$T(x_{j+1/2},\, y_{i+1/2},\, t^n) \approx T^n_{i+1/2,j+1/2}$$

and the heat flux components are only shifted in the direction corresponding to their Cartesian index, i.e. q_y in the x direction while q_x in the y direction (see Fig. 4.13):

$$q_x(x_{j+1/2},\, y_i,\, t^n) \approx (q_x)^n_{i,j+1/2}$$
$$q_y(x_j,\, y_{i+1/2},\, t^n) \approx (q_y)^n_{i+1/2,j}$$

Hence, the temperature is computed at the internal nodes [29, 98]. The two components of heat flux, q_x and q_y, are shifted by half space step $\Delta x/2$ and $\Delta y/2$, respectively, as it is shown in Figure 4.13. Furthermore, no boundary conditions will be prescribed as may be expressed explicitly stated, as a function of the above quantities.

By virtue of the evolution equation of the heat flux component q_x, (4.66b), the term $T^n_{i+1/2,j+1/2}$ is replaced by the following average

$$T^n_{i+1/2,j} \longmapsto \frac{T^n_{i+1/2,j-1/2} + T^n_{i+1/2,j+1/2}}{2},$$

as shown in Fig. 4.14(a).
By equation (4.66c), the term $T^n_{i+1/2,j+1/2}$ is replaced by the following average

$$T^n_{i,j+1/2} \longmapsto \frac{T^n_{i-1/2,j+1/2} + T^n_{i+1/2,j+1/2}}{2},$$

as shown in Fig. 4.14(b).

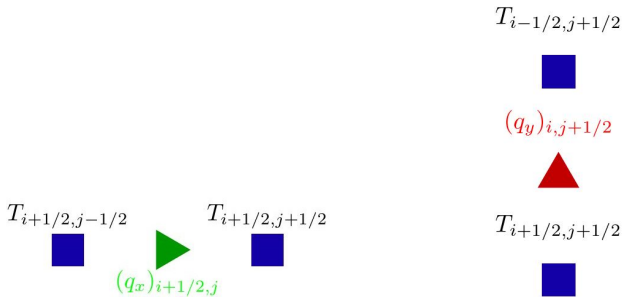

FIGURE 4.14: Concept of the discretization for the first component of heat flux, q_x, in (a), and for the second one, q_y, in (b).

4.3.2 Stability analysis, Dissipation and Dispersion Errors

Since a finite difference scheme can lead to instability, a stability analysis is recommended to investigate the region of the appropriate values of Δx, Δy and Δt for the given scheme. In order to study the stability of the assigned numerical scheme (4.66) the Von-Neumann procedure is used, then let us suppose that the solutions of the

difference equations are in the following form [102]:

$$u_{l,j}^{n} = u_0\, \xi^n e^{i\, k_x\, j\Delta x} e^{i\, k_y\, l\Delta y} \tag{4.67}$$

with $u \in \{T, q_x, q_y\}$, i is the imaginary unit, k_x and k_y the wave numbers, and ξ is the growth factor representing the amplitude wave and must be bounded from above for stability. Substituting the equation (4.67) into the difference equations, the system of linear algebraic equations is achieved:

$$\mathbf{M} \cdot \begin{pmatrix} T_0 \\ q_{x(0)} \\ q_{y(0)} \end{pmatrix} = 0$$

wherein the coefficient matrix is

$$\mathbf{M} = \begin{pmatrix} \dfrac{\tau_d}{\Delta t}\left(1 + \dfrac{\tau_{q_2}}{\tau_{q_1}} Z\right)(\xi - 1) & \dfrac{1}{\hat{L}\Delta x}\left(e^{i\, k_x \Delta x} - 1\right) & \dfrac{1}{\Delta y}\left(e^{i\, k_y \Delta y} - 1\right) \\ \dfrac{\tau_{p_1}^{q_x} + \tau_{p_2}^{q_x} Z}{\Delta x}\left(1 - e^{-i\, k_x \Delta x}\right) & 1 + \dfrac{\tau_{q_1} + \tau_{q_2} Z}{\Delta t}(\xi - 1) & 0 \\ \dfrac{\tau_{p_1}^{q_y} + \tau_{p2}^{q_y} Z}{\Delta y}\left(1 - e^{-i\, k_y \Delta y}\right) & 0 & 1 + \dfrac{\tau_{q_1} + \tau_{q_2} Z}{\Delta t}(\xi - 1) \end{pmatrix},$$

with $Z = \max\limits_{i,j,n} T_{ij}^{n}$ and $\hat{L} = \dfrac{L_2}{L_1}$. The characteristic equation for ξ ($\det \mathbf{M} = 0$) can be expressed as

$$p(\xi) = a_3 \xi^3 + a_2 \xi^2 + a_1 \xi + a_0 = 0, \tag{4.68}$$

in which the coefficients are

$$a_3 = \frac{\tau_d (\tau_{q_1} + \tau_{q_2} Z)^3}{\tau_{q_1} (\Delta t)^3}, \tag{4.69a}$$

$$a_2 = -3\frac{\tau_d (\tau_{q_1} + \tau_{q_2} Z)^3}{\tau_{q_1} (\Delta t)^3} + 2\frac{\tau_d (\tau_{q_1} + \tau_{q_2} Z)^2}{\tau_{q_1} (\Delta t)^2}, \tag{4.69b}$$

$$a_1 = 3\frac{\tau_d (\tau_{q_1} + \tau_{q_2} Z)^3}{\tau_{q_1} (\Delta t)^3} - 4\frac{\tau_d (\tau_{q_1} + \tau_{q_2} Z)^2}{\tau_{q_1} (\Delta t)^2} + \frac{\tau_{q_1} + \tau_{q_2} Z}{\Delta t}\left(\frac{\tau_d}{\tau_{q_1}} - \Gamma\right), \tag{4.69c}$$

$$a_0 = -\frac{\tau_d (\tau_{q_1} + \tau_{q_2} Z)^3}{\tau_{q_1} (\Delta t)^3} + 2\frac{\tau_d (\tau_{q_1} + \tau_{q_2} Z)^2}{\tau_{q_1} (\Delta t)^2} - \frac{\tau_{q_1} + \tau_{q_2} Z}{\Delta t}\left(\frac{\tau_d}{\tau_{q_1}} - \Gamma\right) - \Gamma, \tag{4.69d}$$

$$\begin{aligned} \Gamma &= \frac{\tau_{p_1}^{q_y} + \tau_{p_2}^{q_y} Z}{(\Delta y)^2}\left[\cos(k_y \Delta_y) - 1\right] + \frac{\tau_{p_1}^{q_x} + \tau_{p_2}^{q_x} Z}{\hat{L}(\Delta x)^2}\left[\cos(k_x \Delta_x) - 1\right] \\ &= -2S_2^2 \frac{\tau_{p_1}^{q_y} + \tau_{p_2}^{q_y} Z}{(\Delta y)^2} - 2S_1^2 \frac{\tau_{p_1}^{q_x} + \tau_{p_2}^{q_x} Z}{\hat{L}(\Delta x)^2} \leq 0, \end{aligned} \tag{4.69e}$$

with $S_1 = \sin(k_x \Delta x/2), S_2 = \sin(k_y \Delta y/2)$.

Theorem 6. *The numerical scheme (4.66) is stable if the following conditions are satisfied*

1. *if* $\Gamma \leq -\dfrac{\tau_d}{4\tau_{q_1}}$ *then* $0 < \Delta t < -\dfrac{\tau_d (\tau_{q_1} + \tau_{q_2} Z)}{2\tau_{q_1} \Gamma}$,

2. *if* $-\dfrac{\tau_d}{4\tau_{q_1}} < \Gamma < 0$ *then* $0 < \Delta t < 2(\tau_{q_1} + \tau_{q_2} Z)$.

Proof. In order to prove this result, we apply the Jury criterion [103]. In fact, we have that the roots of the characteristic equation (4.68) are in module all less than 1 (this guarantees that the numerical scheme is stable) if the following four conditions are satisfied

C1 $p(1) \geq 0$, which is trivially verified since $\Gamma \leq 0$;

C2 $(-1)^3 p(-1) > 0 \Leftrightarrow p(-1) < 0$, if the restriction

$$\tau_{q_1}\Gamma(\Delta t)^3 + 2(\tau_{q_1} + \tau_{q_2} Z)(\tau_d - \tau_{q_1}\Gamma)(\Delta t)^2 - 8\tau_d(\tau_{q_1} + \tau_{q_2} Z)^2 \Delta t + 8\tau_d(\tau_{q_1} + \tau_{q_2} Z)^3 > 0$$

holds;

C3 $|a_3| > |a_0|$, which is satisfied if the inequality

$$0 < \tilde{a}_0 < 2a_3,$$

with

$$\tilde{a}_0 = 2\frac{\tau_d(\tau_{q_1} + \tau_{q_2} Z)^2}{\tau_{q_1}(\Delta t)^2} - \frac{\tau_{q_1} + \tau_{q_2} Z}{\Delta t}\left(\frac{\tau_d}{\tau_{q_1}} - \Gamma\right) - \Gamma$$

is guaranteed;

$|b_2| < |b_0|$, wherein:

$$b_2 = \begin{vmatrix} a_0 & a_1 \\ a_3 & a_2 \end{vmatrix}, \quad b_0 = \begin{vmatrix} a_0 & a_3 \\ a_3 & a_0 \end{vmatrix}.$$

This inequality can be rearranged into the form

$$|a_0 a_2 - a_1 a_3| < |a_0^2 - a_3^2|$$

which is fulfilled if the condition $-a_0^2 - a_3^2 < a_0 a_2 - a_1 a_3 < a_0^2 + a_3^2$ holds.

s After some calculations, the constraints 1. and 2. are obtained from the above restrictions. □

In order to perform numerical solutions, since the first condition of the theorem includes the term Γ, without losing its generality, after introducing its minimum value, $\min(\Gamma)$, obtained with positions $S_1 = S_2 = 1$,

$$\min(\Gamma) = -2\left(\frac{\tau_{p_1}^{q_y} + \tau_{p_2}^{q_y} Z}{(\Delta y)^2} + \frac{\tau_{p_1}^{q_x} + \tau_{p_2}^{q_x} Z}{\hat{L}(\Delta x)^2}\right), \tag{4.70}$$

we impose the following strongest constraint for the time step Δt

$$\Delta t < -\frac{\tau_d(\tau_{q_1} + \tau_{q_2} Z)}{2\tau_{q_1}\min(\Gamma)} \leq -\frac{\tau_d(\tau_{q_1} + \tau_{q_2} Z)}{2\tau_{q_1}\Gamma} \tag{4.71}$$

To proceed further, after substituting the value of $\min(\Gamma)$, expressed by (4.70), in the relation (4.71), after simple calculations the final form of the previous inequality reads

$$\Delta t < \frac{\tau_d}{4} \cdot \frac{\tau_{q_1} + \tau_{q_2} Z}{\tau_{q_1}} \cdot \frac{\hat{L}(\Delta x)^2 (\Delta y)^2}{\hat{L}(\Delta x)^2 \left(\tau_{p_1}^{q_y} + \tau_{p_2}^{q_y} Z\right) + (\Delta y)^2 \left(\tau_{p_1}^{q_x} + \tau_{p_2}^{q_x} Z\right)} \tag{4.72}$$

Remark 11. *It can be easily recognized that if*

$$\tau_{p_1}^{q_y} = \tau_{p_1}^{q_y} = 0, \qquad \tau_{p_1}^{q_x} = \tau_{p_1}, \qquad \tau_{p_2}^{q_x} = \tau_{p_2}, \qquad \hat{L} = 1, \qquad \Delta x = \Delta y;$$

then

$$\Delta t < \frac{(\Delta x)^2}{4} \cdot \frac{\tau_{q_1} + \tau_{q_2} Z}{\tau_{q_1}} \cdot \frac{\tau_d}{\tau_{p_1} + \tau_{p_2} Z}. \tag{4.73}$$

and the one-dimensional constrain (4.57) for the stability of the NL-MCV scheme is recovered, [29].

Remark 12. *It is important to note that the numerical method described above is initially developed for linear heat equations. Since a nonlinearity appears in the right hand side of the resulting finite difference equations (4.66), requires a different approach. An a priori assumption of the maximum temperature can be made, allowing for a linear stability analysis using von Neumann's method [102] and Jury criterion [103]. In the A, we also explore the stability of this scheme in a one-dimensional context. Admit that is based largely on the initial assumption of the maximum temperature. To overcome this difficult, an initial estimate can be obtained through a linear simulation, which provides an approximate maximum temperature. This estimate is useful because, in practice, the relevant nonlinearities do not significantly increase the temperature but rather distort its temporal evolution.*

4.3.3 Numerical Results

In this Section, we present some numerical solutions of the nonlinear CV heat equation and discuss the effects of nonlinear terms. Consider a domain with $L_1 = L_2 = 7.9 \cdot 10^{-3}$ m. In detail, let us choose the current set of material parameters, such as the mass density $\rho = 2866$ kg/m^3, the specific heat capacity $c = 1.81$ J/(kg K), the thermal conductivity $\lambda_T = 150001$ W/(m K), and the relaxation time $\tau = 3.8 \cdot 10^{-6}$ s. From these parameters, the following dimensionless quantities are obtained:

$$\begin{aligned} &\tau_d = 0.4659, \quad \tau_{q_1} = 0.1770, \quad \tau_{q_2} = 0.01, \quad \tau_{p_1}^{q_x} = 0.4659, \\ &\tau_{p_1}^{q_y} = 0.4659, \quad \tau_{p_2}^{q_x} = 0.03; \quad \tau_{p_2}^{q_y} = 0.02, \quad \hat{L} = 1. \end{aligned}$$

Numerical integrations are carried out using the scheme (4.66) with spatial spatial and time steps $\Delta x = \Delta y = 0.02$ and $\Delta t = 10^{-5}$ respectively, where the complete time interval is $t_{max} = 2.6\,s$. The initial conditions are give by (4.60) with the initial temperature $T_0 = 13$ K. As regards the boundary conditions these are chosen in such a way that only one side of the square domain is non-adiabatic. In addition, these conditions are expressed by relations (4.61)-(4.62) in the case of spatially homogeneous heat pulse or by (4.61)-(4.63) in the spatially non-homogeneous case. In both cases, numerical results are obtained using the pulse duration is $t_p = 1.0 \cdot 10^{-5}$ s and the maximum heat flux $q_{max} = 1.0 \cdot 10^4$ W/m^2.
The temperature distribution values were represented by a color scale ranging from yellow (maximum value) to blue (minimum value).

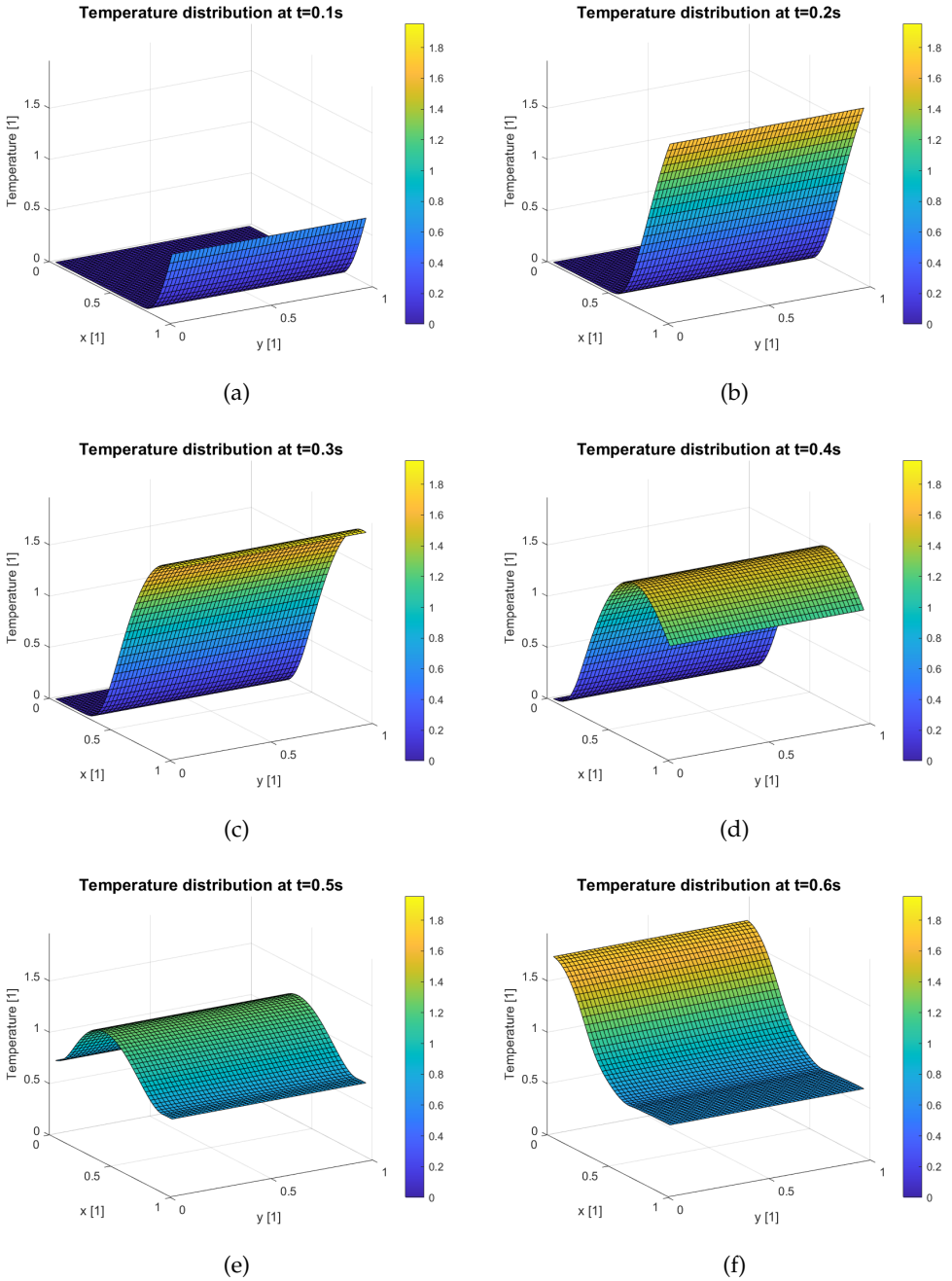

FIGURE 4.15: Temperature distribution of the sample, for different time instants, using the boundary conditions homogeneous in space.

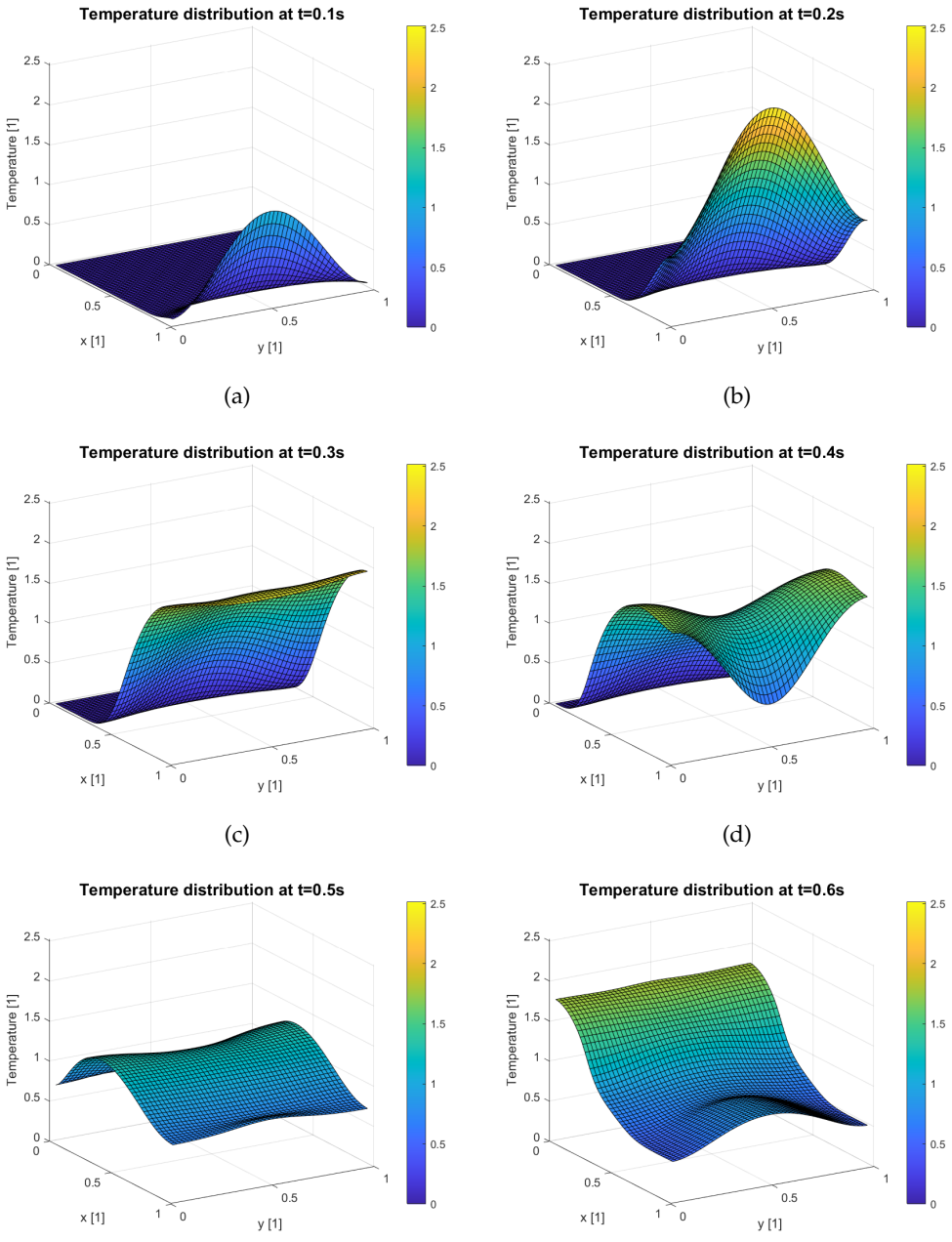

(a) (b)

(c) (d)

(e) (f)

FIGURE 4.16: Temperature distribution of the specimen, for different time instants, using the boundary conditions non-homogeneous in space.

Figures 4.15 and 4.16 illustrate the temperature distribution at various points within the domain at different time instants.

It can be observed that the heat pulse applied to the edge leads to the same value at each point along the non-adiabatic edge. If it has a higher intensity at the center, it shows a gradual decrease towards the boundary propagating in the y direction. A damping follows this until it reaches the opposite side, which, being adiabatic, provides a reflection of the thermal pulse. This decrease continues until the pulse reaches the opposite, adiabatic side, where it is reflected. These reflections persist until the thermal disturbance is fully damped and the system reaches equilibrium, which, in the dimensionless case, equals to 1 (see Figures 4.17(a) and 4.17(b)).

Comparing the linear problem (4.64) with the nonlinear one (4.59), it can be deduced that the presence of nonlinearities in thermal conductivity and relaxation time, i.e. (2.11) and (2.50), introduces a delay in the propagation of the thermal signal.

The effects of nonlinear terms have been examined in greater detail. Specifically, the parameters τ_{q_2} and $\tau_{p_2}^{q_y}$, appear to influence the signal in opposing ways. In particular, their increase affects the slope when the temperature increases, implying a signal significantly shifted to the right or left. In fact, it is observed that increasing the value of the parameter τ_{q_2}, the wave signal is shifted to the right, this occurs independently of the type of boundary conditions assigned (either in the homogeneous case (see Fig.4.18(a)) or in the non-homogeneous case (see Fig. 4.18(b)). An opposite behavior is observed if the value of the parameter $\tau_{p_2}^{q_y}$ is increased, as it is emphasized in the Figures 4.19(a) and 4.19(b). It is worth pointing out the absence of variations in the signal that changes another nonlinear parameter, $\tau_{p_2}^{q_x}$, (see Figures 4.20(a) and 4.20(b)). However, in both situations, the solution remains stable, and the dispersive error can be reduced by increasing the resolution of the discretization.

Numerical stability, dissipative and dispersive errors are analyzed in detail in the A.

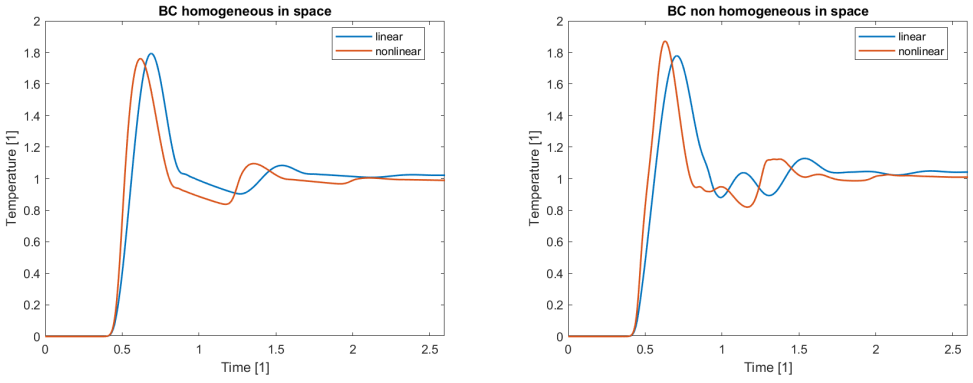

(a) (b)

FIGURE 4.17: Comparison between linear and nonlinear solution, with (a) boundary conditions homogeneous in space, (b) boundary conditions non-homogeneous in space.

In this study, we investigated both linear and nonlinear versions of the two-dimensional MCV equation. We examined the linear temperature dependence of thermal conductivity and relaxation time, simplifying the problem by neglecting mechanical effects at this stage of research. We employed a staggered numerical scheme for discretization, demonstrating its stability and convergence properties. Although

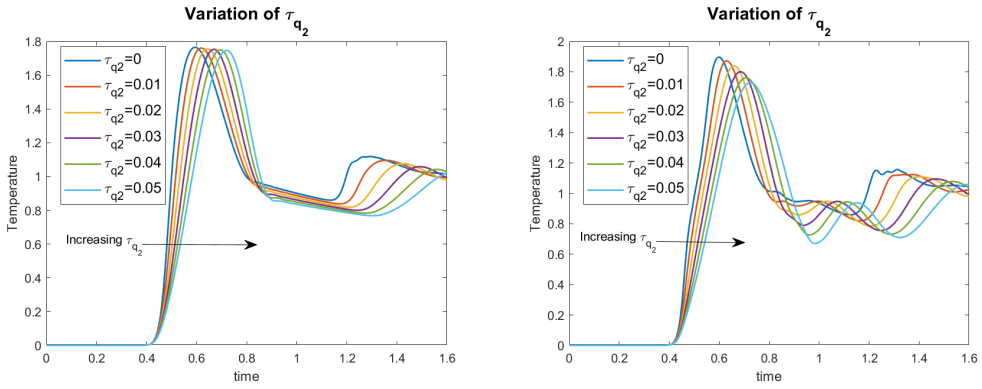

(a) (b)

FIGURE 4.18: The temperature history when increasing the nonlinear parameter $\tau_{q_2} \in \{0, 0.01, 0.02, 0.03, 0.04, 0.05\}$ in (a) homogeneous boundary conditions and (b) non-homogeneous boundary conditions). Other parameters are: $\tau_d = 0.4659$, $\tau_{q_1} = 0.1770$, $\tau_{p_1}^{q_x} = 0.4659$, $\tau_{p_2}^{q_x} = 0.3$, $\tau_{p_1}^{q_y} = 0.4659$, $\tau_{p_2}^{q_y} = 0.2$ and $\hat{L} = 1$.

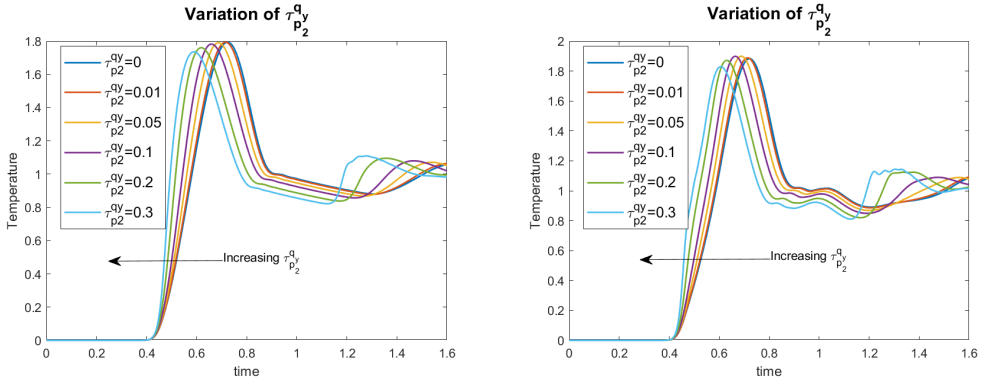

(a) (b)

FIGURE 4.19: The temperature history for increasing the nonlinear parameter $\tau_{p_2}^{q_y} \in \{0, 0.01, 0.05, 0.1, 0.2, 0.3\}$ in (a) homogeneous boundary conditions and (b) non-homogeneous boundary conditions). Other parameters are: $\tau_d = 0.4659$, $\tau_{q_1} = 0.1770$, $\tau_{q_2} = 0.01$, $\tau_{p_1}^{q_x} = 0.4659$, $\tau_{p_2}^{q_x} = 0.3$, $\tau_{p_1}^{q_y} = 0.4659$ and $\hat{L} = 1$.

the approach of estimating the stability limit by reducing the nonlinear problem to a linear one lacks mathematical rigor for providing a precise a priori estimate of the maximum temperature value, it proved useful for running efficient simulations.

Our analysis of temperature histories, which could be measured in heat pulse experiments, revealed that varying temperature-dependent material parameters can significantly alter the measurable temperature history. These parameters influence the steepness of the wave-front, which can serve as an immediate indicator of nonlinearity from an experimental perspective. However, their effects can be contradictory, complicating the task of uniquely determining the exact non-linearity from measurements.

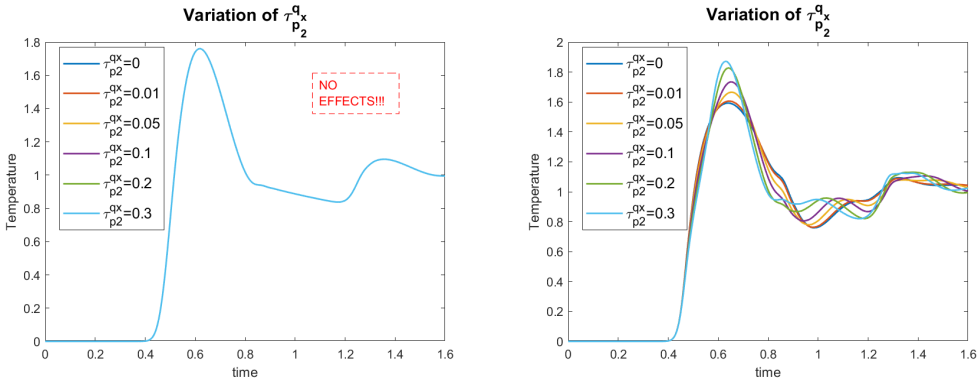

(a) (b)

FIGURE 4.20: The temperature history when increasing the nonlinear parameter $\tau^{qx}_{p_2} \in \{0, 0.01, 0.05, 0.1, 0.2, 0.3\}$ in (a) homogeneous boundary conditions and (b) non-homogeneous boundary conditions). Other parameters are: $\tau_d = 0.4659$, $\tau_{q_1} = 0.1770$, $\tau_{q_2} = 0.01$, $\tau^{qx}_{p_1} = 0.4659$, $\tau^{qy}_{p_1} = 0.4659$, $\tau^{qy}_{p_2} = 0.2$ and $\hat{L} = 1$.

Interestingly, in two-dimensional scenarios with spatially non-homogeneous boundary conditions, we observed a notable delay in the second rear-side reflection compared to the linear case, accompanied by more pronounced oscillations. These oscillations are genuine and not artifacts, as confirmed by analyzing the dispersion properties of the scheme. Such characteristics may be valuable for future experimental investigations.

On the other hand, since the real heat transfer situations are associated with complex geometries, in future researches the analysis of nonlinear heat conduction, could be extended to situations with irregular domains. More complex geometries can also be solved by other numerical methods such as the finite element or finite volume method [112].

4.4 NL-CE-MCV in 1D

In the previous sections (4.2 and 4.3), we explored the impact of nonlinear terms arising from the temperature-dependence of thermal conductivity and relaxation time. These terms are particularly relevant when studying systems subjected to short thermal pulses with significant temperature perturbations.

In this section, we introduce an alternative nonlinear formulation of the Cattaneo equation for thermal transport, termed the *Nonlinear Conjugate Extension of the Maxwell-Cattaneo-Vernotte equation (NL-CE-MCV)*. We compare the effects of this formulation with those of the traditional nonlinear Cattaneo-type equations on thermal pulse propagation. Notable differences in the velocities and magnitudes of perturbation peaks between these formulations could be experimentally discerned.

The usual form of the NL-MCV equation (4.43) has been discussed in Section 4.2, with references to works such as [53, 64, 113–119]. Another formulation is to consider as independent variable the thermodynamic conjugate of the heat flux [120, 121]. This leads to the following equation:

$$\lambda(T)\, T^2\, \partial_t \left(\frac{\tau(T)}{\lambda(T)\, T^2} \mathbf{q} \right) + \mathbf{q} = -\lambda(T) \nabla T, \tag{4.74}$$

presented in detail below. This nonlinear generalization of the MCV equation (4.74) is derived using a conservation-dissipation framework within the extended thermodynamics. As discussed in [120], in the high-frequency limit, this equation approximates a nonlinear wave equation for the heat flux, analogous to the equations for electromagnetic waves in nonlinear optics.

We will employ the same mathematical methods previously used to explore and compare the implications of both equations, (4.43) and (4.74). Our goal is to propose experimental strategies to determine which of these generalizations aligns better with observational data. Theoretical considerations support both formulations, making experimental validation crucial for deciding which approach is preferable.

4.4.1 One-dimensional formulation of nonlinear conjugate extension of the Cattaneo

Here, as in [29, 30], we neglect the small deformations arising from thermal expansion effects and consider the specimens as rigid conductors without lateral heat losses to the environment. In future research such simplifications should be avoided in terms of a more detailed comparison with experiments. The system composed by the balance law of the internal energy (2.1) for the rigid body and the new evolution equation for the heat flux proposed in [120, 121] is

$$\rho c\, \partial_t T + \nabla \cdot \mathbf{q} = 0 \tag{4.75a}$$

$$\partial_t \left(\frac{\tau(T)}{\lambda(T)\, T^2} \mathbf{q} \right) + \frac{1}{\lambda(T)\, T^2} \mathbf{q} = -\frac{1}{T^2} \nabla T. \tag{4.75b}$$

Note that when $\tau(T)/\lambda(T)T^2$ is constant, equation (4.74) reduces to (4.43). Refer the reader to [120, 121] for the theoretical bases of (4.74), since our aim is the mathematical analysis of the consequences of (4.74) rather than the theoretical reflection on its foundations.

As we did in [29, 30], it is assumed which the specific heat capacity c is constant (a simplification valid for many materials at room temperature but which should be removed in future analyses of lower temperature situations, and which we take here to compare with the results obtained in [30] with respect to the nonlinear equation (4.1)), while the functions $\lambda(T)$, $\tau(T)$ are expressed by the relations (2.11) and (2.50).

In fact, we are using this linear approximation as an illustration to explore the effects that may follow from temperature-dependent thermal conductivity and relaxation time. A detailed quantitative analysis would depend on the material and temperature interval to be considered. In fact, the approximations (2.11) and (2.50) should be valid for relatively narrow intervals of temperature, let us say between two given reference temperatures T_1 and T_0, with a being $a = (\lambda_1 - \lambda_0)/(T_1 - T_0)$ and $b = (\tau_1 - \tau_0)/(T_1 - T_0)$, with τ_1 and λ_1 the values of τ and λ at T_1 respectively. At room temperature or higher, if $T_1 > T_0$ is usually $\lambda_1 < \lambda_0$. We stress that the resulting thermal conductivity and relaxation time must remain positive at the end; hence their values are limited in this sense.

Let us remark that here it is assumed that the parameters λ and τ depend only on T; however, since in the Maxwell-Cattaneo models $\mathbf{q}$ is also an independent variable, the independent variables are actually T and $\mathbf{q}$, and situations could be imagined were λ and τ both depend on T and on $\mathbf{q}$ [59]. Indeed, using maximum-entropy arguments it may be seen that λ and τ also depend in $\mathbf{q}$, but in a less sensitive way than on T [59].

The system (4.75) in one-dimensional domain $\Omega = [0, L]$ with length L becomes

$$\rho c\, \partial_t T + \partial_x q = 0, \tag{4.76a}$$

$$\partial_t \left(\frac{\tau(T)}{\lambda(T)\, T^2} q \right) + \frac{1}{\lambda(T)\, T^2} q = -\frac{1}{T^2} \partial_x T. \tag{4.76b}$$

Let us suppose to apply this model in the heat pulse experiment as in Section 4.2, then at initial time, a homogeneous temperature distribution is considered and the sample is in thermal equilibrium with the external environment,

$$T(x, 0) = T_0, \qquad q(x, 0) = 0.$$

and boundary conditions (these latter only for heat flux),

$$q(0, t) = q_0(t) = \begin{cases} \dfrac{q_{max}}{2} \left[1 - \cos\left(\dfrac{2\pi t}{t_p} \right) \right] & \text{if } t_0 < t \leq t_p, \\ 0 & \text{if } t > t_p. \end{cases}$$

$$q(L, t) = 0,$$

wherein $t_0 = 0$ is the initial time, q_{max} represents the pulse amplitude and t_p its duration, which must be much shorter than the characteristic time scale of the experiment.

Remark 13. *We observe, that is possible to rewrite the system (4.76) as*

$$\rho c\, \partial_t T + \partial_x q = 0, \tag{4.77a}$$

$$\partial_t w + \frac{1}{\lambda(T)\, T^2} q = -\frac{1}{T^2} \partial_x T, \tag{4.77b}$$

$$q = \frac{\lambda(T)\, T^2}{\tau(T)} w. \tag{4.77c}$$

Remark 14. *Let us observe that according to the single relaxation approximation of the Boltzmann transport equation, [122], the relaxation time and the thermal conductivity satisfy*

$$\lambda(T) = \frac{1}{3} \rho\, c\, v_g^2 \tau(T)$$

where v_g is the group velocity of the heat carriers. Then, in the case of ρc and v_g independent of T, a and b should fulfill the following equality,

$$\frac{a}{b} = \frac{\lambda_0}{\tau_0} = \frac{1}{3} \rho\, v_g^2$$

this provides that the ratio $\dfrac{\lambda(T)}{\tau(T)} = \dfrac{\lambda_0}{\tau_0}$ is constant.

The system (4.77) may contain coefficients with several orders of magnitude. Thus, let us introduce the following dimensionless variables,

$$\hat{x} = \frac{x}{L}, \quad \hat{t} = \frac{\alpha_0 t}{L^2}, \quad \hat{q} = \frac{q}{\tilde{q_0}}, \quad \hat{T} = \frac{T - T_0}{T_{end} - T_0}, \quad \hat{w} = \frac{L T_0}{\tau_0} w,$$

where

$$\alpha_0 = \frac{\lambda(T_0)}{\rho c}, \quad T_{end} = T_0 + \frac{t_p \tilde{q}_0}{\rho_0 c_v L}, \quad \tilde{q}_0 = \frac{q_{max}}{2},$$

the dimensionless parameters related to material properties of the system read

$$\begin{aligned} \tau_{p_1} &= \frac{\alpha_0 t_p}{L^2} = \tau_d, \quad \tau_{p_2} = \frac{a(T_{end} - T_0)t_p}{\rho c L^2} = \frac{a\tilde{q}_0 t_p^2}{\rho^2 c^2 L^2}, \quad a_0 = \frac{\rho c L T_0}{\tilde{q}_0 t_p}, \\ \tau_{q_1} &= \frac{\alpha_0 \tau_0}{L^2}, \quad \tau_{q_2} = \frac{\alpha_0\, b(T_{end} - T_0)}{L^2} = \frac{\alpha_0\, b\, \tilde{q}_0\, t_p\, \lambda(0)}{L^2}, \end{aligned} \tag{4.78}$$

Under these assumptions, the dimensionless version of the one-dimensional system of equations (4.77) is the following

$$\tau_{p_1} \partial_{\hat{t}} \hat{T} + \partial_{\hat{x}} \hat{q} = 0, \tag{4.79a}$$

$$\tau_{q_1} \partial_{\hat{t}} \hat{w} + \frac{\tau_{q_1}}{\tau_{q_1} + \tau_{q_2} \hat{T}} \cdot \hat{w} + \frac{1}{a_0 + 2\hat{T} + \frac{1}{a_0}\hat{T}^2} \cdot \partial_{\hat{x}} \hat{T} = 0, \tag{4.79b}$$

$$\hat{q} - \tau_{q_1} \left(a_0 + 2\hat{T} + \frac{1}{a_0}\hat{T}^2 \right) \cdot \frac{\tau_d + \tau_{p_2} \hat{T}}{\tau_{q_1} + \tau_{q_2} \hat{T}} \cdot \hat{w} = 0. \tag{4.79c}$$

Furthermore, the dimensionless initial data are given:

$$\hat{T}(\hat{x}, 0) = 0, \qquad \hat{q}(\hat{x}, 0) = 0,$$

and the dimensionless form of the boundary conditions namely, heat pulse, becomes

$$\begin{aligned} \hat{q}(0, \hat{t}) = \hat{q}_0(\hat{t}) &= \begin{cases} 1 - \cos\left(\dfrac{2\pi \hat{t}}{\tau_d}\right) & \text{if } 0 < \hat{t} \leq \tau_d, \\ 0 & \text{if } \hat{t} > \tau_d. \end{cases}, \\ \hat{q}(1, \hat{t}) &= 0. \end{aligned}$$

Characteristic velocity

In order to determine the characteristic velocity, we rewrite the system (4.76) in the quasi-linear compact form (4.9), i.e.

$$A_0(\mathbf{U})\partial_t \mathbf{U} + A_i(\mathbf{U})\partial_{x_i} \mathbf{U} = \mathbf{F}(\mathbf{U}) \quad \Leftrightarrow \quad A_\alpha(\mathbf{U})\partial_\alpha \mathbf{U} = \mathbf{F}(\mathbf{U}).$$

with

$$\begin{aligned} A_0(\mathbf{U}) &= \begin{bmatrix} \rho c & 0 \\ 0 & \beta(T) \end{bmatrix}, \quad A_1(\mathbf{U}) = \begin{bmatrix} 0 & 1 \\ \dfrac{1}{T^2} & 0 \end{bmatrix}, \\ \mathbf{F}(\mathbf{U}) &= \begin{bmatrix} 0 \\ -\left(\dfrac{1}{\lambda(T)T^2} + \dfrac{d\beta(T)}{dt} \right) q \end{bmatrix}, \quad \mathbf{U} = \begin{bmatrix} T \\ q \end{bmatrix}, \end{aligned}$$

where $\beta(T) = \dfrac{\tau(T)}{\lambda(T)T^2}$. In the linear case one gets

$$A_0(\mathbf{U}) = \begin{bmatrix} \rho c & 0 \\ 0 & \tau_0 \end{bmatrix}, \quad A_1(\mathbf{U}) = \begin{bmatrix} 0 & 1 \\ \lambda_0 & 0 \end{bmatrix}, \quad \mathbf{F}(\mathbf{U}) = \begin{bmatrix} 0 \\ -q \end{bmatrix}. \tag{4.80}$$

From the definition of hyperbolic system 4, we observe that the condition **H1** is trivially satisfied

$$\det(A_0) = \frac{\rho c \tau(T)}{\lambda(T) T^2} \neq 0, \tag{4.81}$$

being $\rho > 0, c > 0$ and $\lambda(T), \tau(T) > 0, \ \forall\, T > 0$. To verify the condition **H2** you need to determine the eigenvalues of the matrix $A_0^{-1}A_1$, thus considering the following eigenvalues problem $\det(A_0^{-1}A_1 - vI) = 0$. The eigenvalues can be obtained straightforwardly from this equation

$$v(T)_{1,2} = \pm\sqrt{\frac{\lambda(T)}{\rho c \tau(T)}}. \tag{4.82}$$

The coefficients $\rho > 0, c > 0$ and $\lambda(T), \tau(T) > 0, \ \forall\, T > 0$ are real, then it remains shown that the system is hyperbolic and the characteristic velocity is given by the relation (4.82).

Similarly in the linear case, the system is still hyperbolic with the following expressions of the characteristic speeds

$$v_{1,2} = \pm\sqrt{\frac{\lambda_0}{\rho c \tau_0}}. \tag{4.83}$$

The characteristic velocity, from the relation (4.82), can be expressed as follows

$$v(T) = \sqrt{\frac{\lambda(T)}{\rho c \tau(T)}} = \sqrt{\frac{\lambda_0 + a(T - T_0)}{\rho c \left[\tau_0 + b(T - T_0)\right]}}, \tag{4.84}$$

introducing the dimensionless quantities (i.e $\hat{v} = v/v_0$) and using the positions (4.78) the expression (4.84) beomes

$$\begin{aligned}
\hat{v}(\hat{T}) &= \frac{1}{v_0} \cdot \sqrt{\frac{\lambda(\hat{T})}{\rho c \tau(\hat{T})}} = \frac{1}{v_0} \cdot \sqrt{\frac{\lambda_0 + a(T_{end} - T_0)\hat{T}}{\rho c \left[\tau_0 + b(T_{end} - T_0)\hat{T}\right]}} \\
&= \frac{1}{v_0} \cdot \sqrt{\frac{\lambda_0 + \frac{\rho c L^2}{t_p}\tau_{p_2}\hat{T}}{\rho c \left(\tau_0 + \frac{L^2}{\alpha_0}\tau_{q_2}\hat{T}\right)}} = \frac{1}{v_0} \cdot \sqrt{\frac{\tau_d + \tau_{p_2}\hat{T}}{\tau_{q_1} + \tau_{q_2}\hat{T}} \cdot \frac{\alpha_0}{t_p}} \\
&= \sqrt{\frac{\tau_d + \tau_{p_2}\hat{T}}{\tau_{q_1} + \tau_{q_2}\hat{T}}},
\end{aligned}$$

where it is identified

$$v_0 = \sqrt{\frac{\alpha_0}{t_p}}. \tag{4.85}$$

Furthermore the expression of characteristic velocity in a dimensionless form is given as

$$\hat{v}(\hat{T}) = \sqrt{\frac{\tau_d + \tau_{p_2}\hat{T}}{\tau_{q_1} + \tau_{q_2}\hat{T}}}. \tag{4.86}$$

and in the linear case assume the following form

$$\hat{v} = \sqrt{\frac{\tau_d}{\tau_{q_1}}}, \tag{4.87}$$

which can be found from the (4.86) by putting $\tau_{p_2} = \tau_{q_2} = 0$.

4.4.2 Numerical framework

Here we present a numerical method (explicit finite difference method (FDM) developed for the nonlinear one-dimension model (4.46).

Let us discretize the spatial domain $\Omega = [0, 1]$ with space steps Δx and the time interval $[0, t_{max}]$ with step Δt, the following discrete values of space e time are obtained

$$\begin{aligned} x_j &= x_0 + j\Delta x \quad j = 0, 1, 2, ..., N \\ t^n &= n\Delta t \quad n = 0, 1, 2, ..., J. \end{aligned}$$

Using the same method described in Sections 4.2.1 results the solution is approximated as

$$\begin{aligned} T(x_{j+1/2},\, t^n) &\approx T^n_{j+1/2} \\ q(x_j,\, t^n) &\approx q^n_j \\ w(x_j,\, t^n) &\approx w^n_j. \end{aligned}$$

as shown in Figure 4.21. As a consequence, it is not necessary to define boundaries for the temperature field. Over time, only an explicit forward differencing scheme is used.

Therefore the difference equations are

$$\tau_d \frac{T^{n+1}_{i+1/2} - T^n_{i+1/2}}{\Delta t} + \frac{q^n_{i+1} - q^n_i}{\Delta x} = 0, \tag{4.88a}$$

$$\tau_{q_1} \frac{w^{n+1}_i - w^n_i}{\Delta t} + \frac{\tau_{q_1}}{\tau_{q_1} + \tau_{q_2} T^n_i} \cdot w^n_i + \frac{1}{a_0 + 2\,T^n_i + \frac{1}{a_0}\left(T^n_i\right)^2} \cdot \frac{T^n_{i+1/2} - T^n_{i-1/2}}{\Delta x} = 0, \tag{4.88b}$$

$$q^{n+1}_i - \tau_{q_1}\left(a_0 + 2\,T^n_i + \frac{1}{a_0}\left(T^n_i\right)^2\right) \cdot \frac{\tau_d + \tau_{p_2} T^n_i}{\tau_{q_1} + \tau_{q_2} T^n_i} \cdot w^n_i = 0, \tag{4.88c}$$

where a explicit forward finite difference approximations are used for the time and spatial derivatives of the field variables

$$\begin{aligned} \left(\frac{\partial T}{\partial t}\right)^{n+1}_{i+1/2} &\approx \frac{T^{n+1}_{i+1/2} - T^n_{i+1/2}}{\Delta t}, \\ \left(\frac{\partial w}{\partial t}\right)^{n+1}_{i} &\approx \frac{w^{n+1}_i - w^n_i}{\Delta t}, \\ \left(\frac{\partial q}{\partial x}\right)^{n}_{i} &\approx \frac{q^n_{i+1} - q^n_i}{\Delta x} = \mathcal{D}_x(q), \\ \left(\frac{\partial T}{\partial x}\right)^{n}_{i+1/2} &\approx \frac{T^n_{i+1/2} - T^n_{i-1/2}}{\Delta x} = \mathcal{D}_x(T), \end{aligned}$$

let us observe, that we have used a forward finite difference for the time derivatives and the spatial derivatives of the heat flux, while a backward finite difference for the spatial derivatives of the temperature is considered.

Now, for simplicity of notation we omitted the symbol "ˆ" and after some rearrangement, we have

$$T_{i+1/2}^{n+1} = T_{i+1/2}^{n} - \mathcal{C}_0 \left(q_{i+1}^{n} - q_i^{n} \right), \tag{4.89a}$$

$$w_i^{n+1} = (1 - \mathcal{C}_1)\, w_i^{n} - \mathcal{C}_2 \left(T_{i+1/2}^{n} - T_{i-1/2}^{n} \right), \tag{4.89b}$$

$$q_i^{n+1} = \mathcal{C}_3\, w_i^{n+1}, \tag{4.89c}$$

wherein

$$\mathcal{C}_0 = \frac{\Delta t}{\tau_d \cdot \Delta x}, \qquad \mathcal{A}(T_i^n) = \frac{\tau_q}{\tau_{q_1} + \tau_{q_2} T_i^n},$$

$$\mathcal{C}_1 = \frac{\mathcal{A}(T_i^n) \cdot \Delta t}{\tau_{q_1}}, \qquad \mathcal{B}(T_i^n) = a_0 + 2\, T_i^n + \frac{1}{a_0} \left(T_i^n \right)^2,$$

$$\mathcal{C}_2 = \frac{\Delta t}{\tau_{q_1} \cdot \mathcal{B}(T_i^n) \cdot \Delta x}, \qquad \mathcal{C}(T_i^n) = \frac{\tau_d + \tau_{p_2} T_i^n}{\tau_{q_1} + \tau_{q_2} T_i^n},$$

$$\mathcal{C}_3 = \tau_d \cdot \mathcal{B}(T_i^n) \cdot \mathcal{C}(T_i^n),$$

in this approximations the term T_i^n, which appears in the non-linear terms of the evolution equation of the heat flux component q and the new field variable w, (4.89b) and (4.89c), is replaced by the following average

$$T_i^n \longmapsto \frac{T_{i-1/2}^n + T_{i+1/2}^n}{2}, \tag{4.90}$$

as shown in the Fig. 4.21.

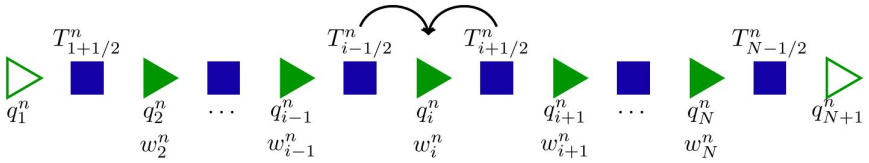

FIGURE 4.21: Concept of the spatial discretization [98]. The filled squares represent the temperature T, and the filled triangles represents the heat flux q and the new field variable w. Empty symbols denote boundary conditions.

4.4.3 Numerical results

In this Section the results of propagation and reflection of heat pulses according to the nonlinear generalization (4.74) of the MCV equation (4.74) obtained in [59] are treated. We have plotted them in Figure 4.22 and these are compared with the corresponding results of the linear MCV equation and its nonlinear formulation (4.1).

Figure 4.22 shows the evolution of T at the rear surface of the system, i.e. at $x = L$, after the pulse has been sent from $x = 0$ at $t = 0$, but for two different ranges of the interval of time, from 0 to 0.8 and from 0 to 2, respectively. Thus, Figure 4.22(a) is focused on comparison of the behaviour predicted by the models (4.1) and (4.74) at the first peak, while Figure 4.22(b) also shows the second peak, produced at a time after the first peak.

The two main features which deserve to be commented on are:

a) In the nonlinear generalization (4.74) the peak of the pulse signals arrives before than the peaks described the MCV equation and by its nonlinear formulation (4.1), which are found to arrive approximately at the same time (note that the time position of the peaks of L-MCV and of NL-MCV (4.1) is practically the same, whereas that of the peak described by NL-CE-MCV (4.74) comes slightly earlier). The latter peak reaches $t = 0.3$ whereas the other two peaks arrive at $t = 0.35$; thus, the relative difference in arrival time is of the order of $0.05/0.35 \equiv 14\%$, which should be observable. In contrast, the linear decay of the signal after the peaks decayed is approximately the same in three equations.

b) The height of the peak in NL-CE-MCV (4.74) is higher than the corresponding to the MCV equation but lower than the peak in the NL-MCV (4.1) equation. More or less, the height of the peaks is 2.5618 in MCV, 2.9105 in NL-CE-MCV (4.74) and 3.1432 in NL-MCV (4.1). Thus, in principle the difference of heights in peaks is non-negligible and should be observable in a sufficiently detailed experiment.

c) Figure 4.22(b) represents the same as in Figure 4.22(a) but in a longer interval on time, in such a way that one sees a second peak is seen corresponding to the arrival of the reflected signal. Whereas the arrival time of this second peak is the same for MCV and NL-MC V(4.1), it arrives before for NL-CE-MCV (4.74), consistently with the anticipation already noted in the first peak. Thus, a salient feature if that the peak in NL-CE-MCV (4.74) goes faster.

d) For our results some particular values were assigned to the dimensionless parameters, namely $\tau_d = 0.1$, $\tau_{q_1} = 0.08$, $\tau_{p_2} = 0.01$, $\tau_{q_2} = 0.02$, $a_0 = 60$. Other vàlues could be used, depending on the situation that is being explored. For instance, by $\tau_d = \dfrac{a_0 t_p}{L^2}$ (see (4.47)) in the case where the material considered was silicon at room temperature we have $a_0 = 0.8cm^2/s$, so that the value $t_d = 0.1$ could correspond, for instance, to $\tau_p = 1s$ and $L = 2,83cm$. Analogously, since $\tau_{q_1} = \dfrac{a_0 \tau_0}{L^2}$, the value $\tau_{q_1} = 0.08$ could correspond to $\tau_0 = 0.08s$. Also, since $a_0 = \dfrac{\rho c L T_0}{q_0 t_p}$, and since for Si at room temperature ρc is $1,65 \times 10^6\, J/m^3K$, the value $a_0 = 60$ for $T_0 = 300K$, $L = 2,83cm$ and $t_p = 1s$, would correspond to $q_0 = 2.31 \times 10^5 W/m^2$. Thus, the dimensionless values used in the calculations are closely related to the physical parameters used in the experiment, concerning the duration of the pulse tp, the length of the system L, and the physical proerties of the material.

Model	Peak temperature	Velocity
MCV	2.5618	1.1180
NL-MCV(4.1)	3.1432	1.0933
NL-MCV(4.74)	2.9105	1.0950

TABLE 4.1: Height of the peaks in Fig 4.22 for linear MCV and nonlinear NL-MCV (4.1) and NL-CE-MCV (4.74) models and their corresponding propagation velocities.

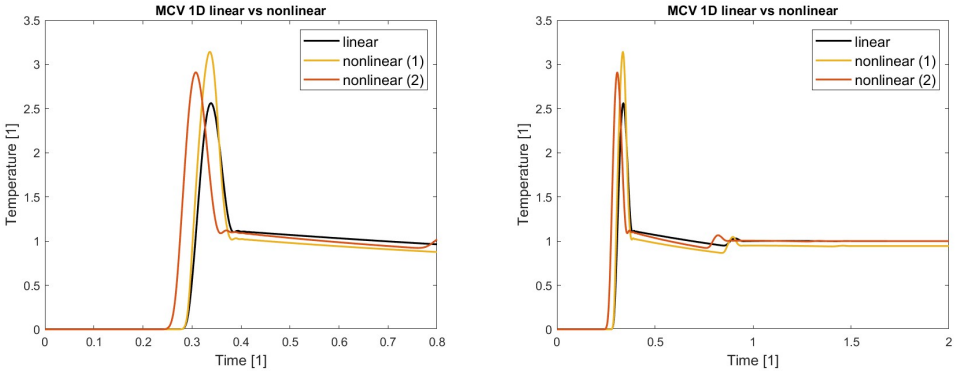

(a) (b)

FIGURE 4.22: Comparison from NL-MCV (4.1) and NL-CE-MCV (4.74), with $\tau_d = 0.1$, $\tau_{q_1} = 0.08$, $a_0 = 60$, $\tau_{p_2} = 0.001$, $\tau_{q_2} = 0.002$, defined in expressions (4.47), for two different ranges of the time interval, from 0 to 0.8 in (a) and from 0 to 2 in (b). The longer time interval considered in (b) allows one to see a second peak of temperature, corresponding to the arrival of the perturbation reflected at the border.

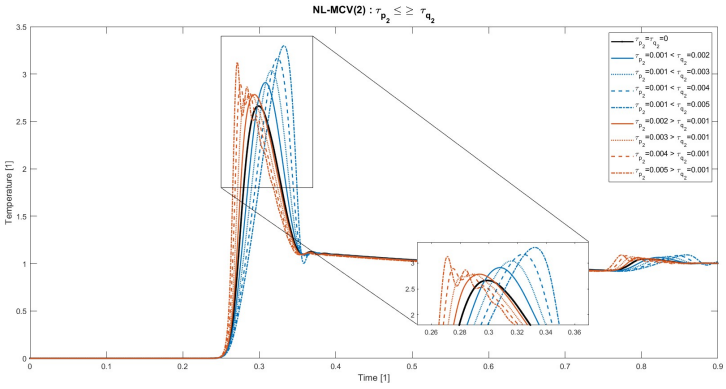

(a)

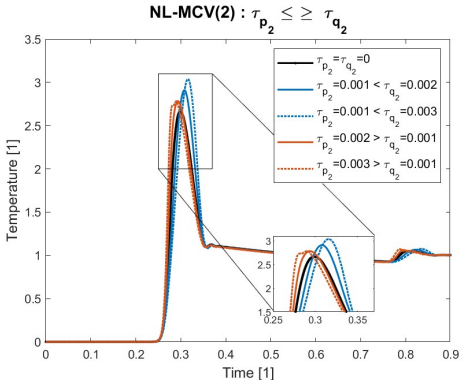

(b)

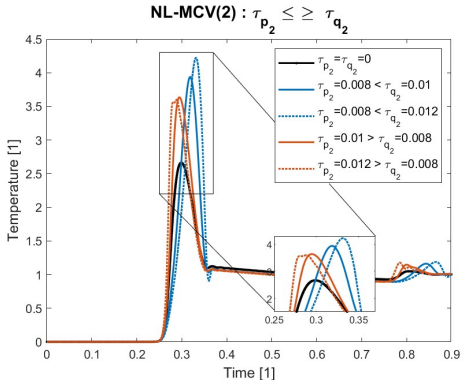

(c)

FIGURE 4.23: Comparison of the form of the temperature peak for different values of τ_{p_2} and τ_{q_2}, for NL-CE-MCV (4.74), defined in expressions (4.47). The blue and orange curve family corresponds to the $\tau_{p_2} < \tau_{q_2}$ and $\tau_{p_2} > \tau_{q_2}$, respectively, while the black curve represents the linear case. The other values of the parameters are: $\tau_d = 0.1$, $\tau_{q_1} = 0.08$, $a_0 = 60$.

The next research in this field should be a wider analysis of different physical situations for concrete materials and values of L and t_p, with the aim to a detailed comparison with experimental results ([53, 64]). Up to now, these results have been interpreted by the linear version of the MCV equation. One should try to interpret them in terms of the nonlinear versions MCV(4.1) and MCV(4.74) to see which one describes better the results.

Another interesting topic would be to compare MCV(4.1) and MCV(4.74) in connection to soliton propagation of thermal pulses along wires and nanowires. In [123], these were made by keeping the linear form of MCV but taking nonlinear terms for the heat exchange between wire and the environment. It might be interesting to combine these terms with a non-linear version of MVC. Indeed, as noted in [123], the propagation of thermal solitons would allow to transmit bits of information, so that the speed and duration of the solitons would be relevant in the connection between thermal energy and information transmission and processing.

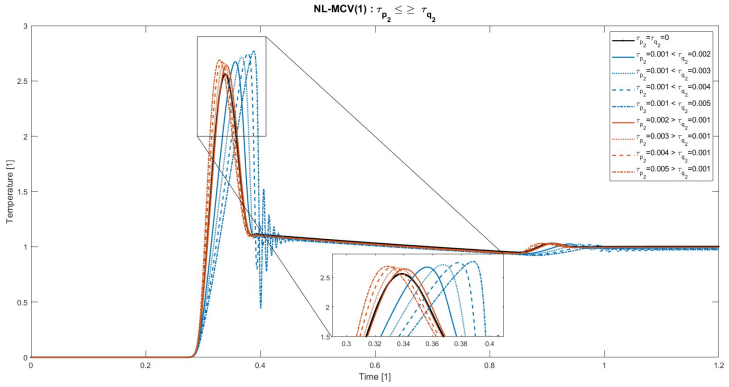

(a)

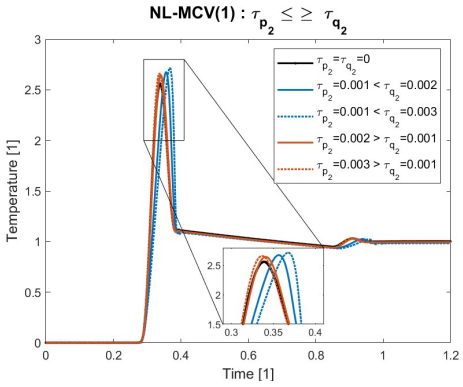

(b)

FIGURE 4.24: Comparison of the form of the temperature peak for different values of τ_{p_2} and τ_{q_2}, for NL-MCV(4.1), defined in expressions (4.47). The blue and orange curve family corresponds to the $\tau_{p_2} < \tau_{q_2}$ and $\tau_{p_2} > \tau_{q_2}$, respectively, while the black curve represents the linear case. The other values of the parameters are: $\tau_d = 0.1$, $\tau_{q_1} = 0.08$.

Chapter 5

Guyer-Krumansl heat conduction

In this chapter, we first explore the effects of nonlinear thermal conductivity and relaxation time by solving the one-dimensional Guyer-Krumhansl equation. Next we focus on the consequences of the existence of the whirling heat current density by solving the two-dimensional Guyer-Krumhansl equation with a space and time-dependent heat pulse boundary conditions, using a staggered scheme.

We place the emphasis on the transient evolution that highlights particular temperature decrease effects occurring locally due to the heat current vorticity in agreement with the results of [124]. This phenomenon is evident only during the transient phase, the time evolution of the heat current vorticity causes a local temperature decrease compared to the initial state. Such observations remain hidden in the paper of Beardo et al. [125], as their study applied the GK equation to a stationary problem. Numerical resolution, poses further challenges to the boundary condition for which we propose a particular extrapolation method. Furthermore, using the Helmholtz decomposition, we show an analogy with the linearized acoustics of Newtonian fluids, which reveals how the heat flux density plays the role of the velocity field. The solutions obtained also reveal an unexpected temperature evolution influenced by the whirling heat flux density, namely, the temperature can locally be decreased for a short time when the curl of the heat flux density dominates the heat conduction process. Additionally, longitudinal and transversal modes are also discussed, highlighting the role of the rotational part of the heat flux field and providing further insights into the structure of the Guyer-Krumhansl equation.

Furthermore, this chapter delves into the impact of boundary conditions on heat flux behavior in thin nanowires and sets the stage for a deeper exploration of these topics. Particularly focusing on how boundary conditions affect heat flux in nanowires and the role of non-local effects in the heat conduction process. This analysis is conducted using a theoretical model that emphasizes non-local effects, i.e. the GK model. We also assess these results in the context of the second law of thermodynamics.

5.1 Brief historical background

In 1966, Guyer and Krumnhansl published an article [4, 5], in which the solution of the linearized Boltzmann equation for phonons is determined. The authors discovered that the heat flux does not follow the Cattaneo equation but instead adheres to what is now referred to as its non-local generalization. This finding highlighted that the traditional models, which assume a purely local relationship between heat flux and temperature gradients, are inadequate for capturing heat transport behaviors in certain regimes, especially at micro and nanoscales. The Guyer-Krumhansl equation introduces additional terms that account for spatial non-locality, reflecting how

phonon scattering and other microstructural effects influence the heat conduction process.

$$\tau \partial_t \mathbf{q} + \mathbf{q} = -\lambda \nabla T + l^2 \left[\Delta \mathbf{q} + 2 \nabla (\nabla \cdot \mathbf{q}) \right] \tag{5.1}$$

where l represents the mean free path of phonon. As noted in 2.4.3-2.5.2 to prove thermodynamic compatibility for such heat flux evolution equation, we need non-local constitutive equations. This is suggested by the presence of the additional term in comparison to MCV equation, i.e. $l^2 \left[\Delta \mathbf{q} + 2 \nabla (\nabla \cdot \mathbf{q}) \right]$. This term introduces non-locality, as it depends not only on the value of the heat flux $\mathbf{q}$ at a given point but also on the values of the heat flux in the surrounding neighborhood, owing to the spatial derivatives ($\Delta \mathbf{q}$ and $\nabla (\nabla \cdot \mathbf{q})$) present. However, it is important to note that the GK equation (5.1), combined with the energy balance law (2.1), forms a parabolic system, so the hyperbolic properties of the MCV system is lost. This involves the violation of the strong causality principle, and it goes out of the guidelines of the RET.

Several heat conduction models and approaches have been developed and tested over the past decades, such as the Cattaneo [1], Guyer-Krumhansl (GK) [4, 5], two-temperature [126–128], and Jeffreys equations [7]. From an engineering perspective, however, the GK and Jeffreys equations are often considered promising alternatives to the classical Fourier law [24]. The GK equation is particularly noteworthy, as it not only includes Fourier's law as a special case but also models the phenomenon of second sound (similar to the Cattaneo equation) and provides an effective description for heterogeneous materials [24], using a continuous approach. Therefore, the continuum background of the GK equation has high potential for increasingly advanced practical applications, which includes foam-based heat exchangers and thermal storage technologies [129–131]. So the Guyer-Krumhansl equation has a special role. In addition to its various applications in the fiekd of nanotechnology, cryotechnology and also in the case of heterogeneous materials modelling, it poses further mathematical challenges compared to the Fourier or Cattaneo equations. This gives the GK equation a special role in modern heat conduction models.

Beyond its applications in nanotechnology, cryotechnology, and heterogeneous material modeling, the GK equation poses additional mathematical challenges compared to the simpler Fourier and Cattaneo equations. Notably, the GK equation is the first heat conduction model to account for the curl of the heat flux density within its evolution equation, as will be discussed in Section 5.3. This makes the GK equation (5.1) significantly more complicate, particularly in two or three spatial dimensions.

Originating from the phonon hydrodynamics [6, 55, 57], the GK model behaves as a special type of fluid model, which allows for the inclusion of heat flux curl. This is especially relevant for phenomena such as second sound in superfluids [132–134], but it also shows how similar effects can manifest in the temperature history of solids.

However, in the last years, its continuum background offers more flexibility but keeps the structure of the GK equation (kinetic or phononic). While the classical GK equation is derived from phonon hydrodynamics, the continuum approach allows greater flexibility, as the model is no longer constrained by the specifics of phonon behavior. In this context, the only restrictions on the parameters stem from the second law of thermodynamics. As a result, the GK equation can effectively describe heterogeneous materials [24] while still accommodating coefficients derived from phonon hydrodynamics.

Regarding the hydrodynamic properties of phonon, we can refer to the recent work by Shang et al. [135] in which they also conduct a similar survey to ours,

but slightly modify the GK equation based on particular phonon hydrodynamic assumptions which are characteristic at nanoscale for two-dimensional materials. Because the phonon hydrodynamics strictly restrict the applicable parameters, the effects of the whirling heat current density remain hidden, however, the flexibility given by the current continuum approach allows for further insights.

The most flexible Guyer–Krumhansl equation, in continuum background, presented in Sections 2.4.3-2.5.2, is

$$\tau \partial_t \mathbf{q} + \mathbf{q} = -\lambda \nabla T + \eta_1 \Delta \mathbf{q} + \eta_2 \nabla (\nabla \cdot \mathbf{q}) \tag{5.2}$$

where η_1 and η_2 are the phenomenological coefficients. Let us observe when η_1, η_2 goes to zero, the GK equation (5.1) returns to the MCV form (4.1). The balance of internal energy 2.1, the Guyer–Krumhansl equation together with the (thermostatic caloric) equation of state

$$e = cT,$$

forming a closed system of equations,

$$\rho c\, \partial_t T + \nabla \cdot \mathbf{q} = \rho r \tag{5.3a}$$

$$\tau\, \partial_t \mathbf{q} + \mathbf{q} = -\lambda \nabla T + \eta_1 \Delta \mathbf{q} + \eta_2 \nabla (\nabla \cdot \mathbf{q})\,. \tag{5.3b}$$

which, with appropriate initial and boundary conditions, can be solved.

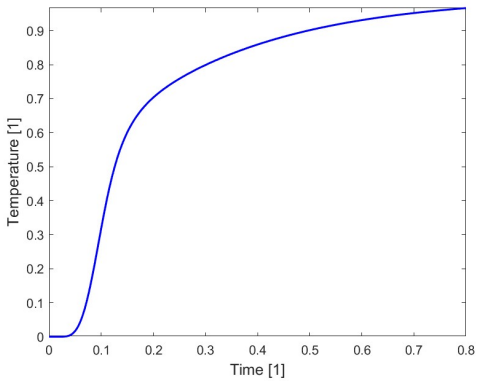

FIGURE 5.1: A typical solution for Guyer-Krumhansl equation

The coefficients η_1 and η_2 are linearly independent and are restricted by the second law of thermodynamics. Therefore, these are positive semidefinite and free from the restrictions given by the phonon hydrodynamic background, i.e. η_1 is not identical to the square of the mean free path, and the ratio of η_2 over η_1 is not necessarily equal to 2 either. The current continuum context provides a notably more flexible adjustment for the coefficients, either by means of an experiment such as [24] or inheriting the phonon hydrodynamic approach [55, 57]. Furthermore, we also wish to draw attention to the coefficients whose functional relations become apparent. It is clear that if $\lambda = \lambda(T)$ holds (i.e. a linear or exponential one), then $l_{11} = l_{11}(T)$ can be immediately given and that T-dependence is inherited in all the other coefficients. The different parameters can optionally adjust the necessary T-dependence. Additionally, if such nonlinearities are required, must be the starting point in order to take into account the further contributions correctly, as we seen in Section 2.5.2.

5.1.1 Longitudinal and transversal heat propagation

Via the vector Laplacian identity

$$\Delta \mathbf{q} = \nabla (\nabla \cdot \mathbf{q}) - \nabla \times \nabla \times \mathbf{q}$$

we can express the second-order spatial derivative of the heat flux vector $\mathbf{q}$ in the Guyer-Krumhansl equation (5.2) can be given as

$$\tau \partial_t \mathbf{q} + \mathbf{q} = -\lambda \nabla T + (\eta_1 + \eta_2) \nabla (\nabla \cdot \mathbf{q}) - \eta_1 \nabla \times \nabla \times \mathbf{q}, \tag{5.4}$$

therefore, theoretically, in a GK-type heat conductor transversal heat propagation can also be observed. This shows that the heat flux evolution is influenced by both the divergence (representing compressive effects) and the curl (representing rotational effects) of the heat flux. These non-local terms reflect how heat flow at one point depends on the behavior of the heat flux in the surrounding region, which is a key feature of the Guyer-Krumhansl model.

Via the Helmholtz decomposition, the heat current density can be uniquely – up to a space-independent but arbitrary time-dependent vector function – given as a sum of irrotational (i.e. curl-free, $\mathbf{q}^*$) and solenoidal (i.e. divergence-free, $\mathbf{q}^\circ$) vector fields, i.e.

$$\mathbf{q} = \mathbf{q}^* + \mathbf{q}^\circ$$

with

$$\nabla \cdot \mathbf{q} = \nabla \cdot \mathbf{q}^*$$
$$\nabla \times \mathbf{q} = \nabla \times \mathbf{q}^\circ.$$

Curl-free and divergence-free components of the vector field are usually referred to as longitudinal and transversal components, respectively. Since ∇T is curl-free, the governing equations of a GK-type heat conductor can be reformulated as

$$\rho c \partial_t T = -\nabla \cdot \mathbf{q}^*, \tag{5.5a}$$
$$\tau \partial_t \mathbf{q}^* + \mathbf{q}^* = -\lambda \nabla T + (\eta_1 + \eta_2) \Delta \mathbf{q}^*, \tag{5.5b}$$
$$\tau \partial_t \mathbf{q}^\circ + \mathbf{q}^\circ = \eta_1 \Delta \mathbf{q}^\circ, \tag{5.5c}$$

which decomposition reveals the time evolutions of the longitudinal and transversal components of heat current density. Here, the evolution of $\mathbf{q}^\circ$ is decoupled from evolutions of $\mathbf{q}^*$ and T, thus $\mathbf{q}^\circ$ can only be introduced through a spatially-dependent boundary condition or by a particular initial condition. An inhomogeneous temperature field alone cannot induce non-zero $\mathbf{q}^\circ$. Since the boundary conditions on heat current density define same $\mathbf{q}$ itself, it is inevitable to introduce disturbances in both parts of $\mathbf{q}$, but the single separation of these ar the boundary can be complicated.

Later on, $\eta_1 + \eta_2$ is referred to as the longitudinal GK coefficient and on η_1 as the transversal GK coefficient. Based on our previous one dimensional studies of the GK equation [23], the longitudinal GK coefficient (denoted usually in one spatial dimension with κ^2) has to be positive semi-definite, hence the seemingly indefinite η_2 parameter is constraint by

$$\eta_2 \geq -\eta_1.$$

Remark 15. *Let us refer here on the governing equations of linearized acoustics of Newtonian fluids, which reads – via applying Helmholtz decomposition on the velocity field* $\mathbf{v}$

$$\partial_r \rho = -\bar{\rho} \nabla \cdot \mathbf{v}^*, \tag{5.6a}$$

$$\bar{\rho} \partial_t \mathbf{v}^* = -\bar{a}_s^2 \nabla \rho + \left(\bar{\eta}_{\text{Vol}} + \frac{4}{3} \bar{\eta}_{\text{Sh}} \right) \Delta \mathbf{v}^*, \tag{5.6b}$$

$$\bar{\rho} \partial_t \mathbf{v}^\circ = \bar{\eta}_{\text{Sh}} \Delta \mathbf{v}^\circ \tag{5.6c}$$

with density difference ρ measured from density $\bar{\rho}$ of the unperturbed state, isentropic speed of sound $\bar{a}_s$, volume and shear viscosities $\bar{\eta}_{\text{Vol}}$ and $\bar{\eta}_{\text{Sh}}$, respectively (cf. equations (3.100) and (3.109) in [136]). Via the curl of velocity, the vorticity $\boldsymbol{\omega} = \nabla \times \mathbf{v} = \nabla \times \mathbf{v}^\circ$ is defined, hence the relation 5.6c can also be written as $\boldsymbol{\omega}$ instead of $\mathbf{v}^\circ$. Therefore, Helmholtz decomposition highlights that in the linear approximation of acoustics the evolution of $\boldsymbol{\omega}$ is decoupled by ρ and $\mathbf{v}^*$, hence resulting that the sound is a transversal wave [cf. 5.6a and 5.6b] and vorticity cannot be introduced through the acoustic fields ρ and $\mathbf{v}^*$ (nor through the pressure field). We are dealing with something very similar in the case of GK equations 5.5a, 5.5b and 5.5c.

An additional interesting property is related to the **Fourier resonance condition**, i.e. the temperature history given by the GK equation is identical with the Fourier's one. Namely, replacing the gradient of 5.5a into the partial time derivative of 5.5b and taking advantage of the commutation of ∇ and ∂_t, one gets

$$\tau \, \partial_t \left(\partial_t \mathbf{q}^* - \frac{\eta_1 + \eta_2}{\tau} \Delta \mathbf{q}^* \right) + \left(\partial_t \mathbf{q}^* - \alpha \Delta \mathbf{q}^* \right) = \mathbf{0},$$

which is the sum of a Fourier heat conduction equation and the partial time derivative of a slight modification of the Fourier heat conduction equation. If the additional time scale becomes to that identical given by the thermal diffusivity, i.e.

$$\frac{\eta_1 + \eta_2}{\tau} = \alpha \equiv \frac{\lambda}{\rho c}, \tag{5.7}$$

Fourier resonance occurs. The resonance condition 5.7 is the same as obtained in the one-dimensional case [23], where is possible to write the T-representation of the GK equation. In the general three dimensional case the T-representation of the GK model is

$$\tau \, \partial_t \left(\partial_t T + \frac{\eta_1 + \eta_2}{\tau} \Delta T \right) + \left(\partial_t T + \alpha \Delta T \right) = \frac{1}{\rho \, c} \left(\tau \partial_t S - (\eta_1 + \eta_2) \Delta S \right) \tag{5.8}$$

in which is possible to see various contributions of the heat source S appear. Considering $S = 0$ one get

$$\tau \, \partial_t \left(\partial_t T + \frac{\eta_1 + \eta_2}{\tau} \Delta T \right) + \left(\partial_t T + \alpha \Delta T \right) = 0 \tag{5.9}$$

in which a kind of time derivative of the Fourier equation and the Fourier equation itself. So the *Fourier resonance condition* is

$$\alpha = \frac{\eta_1 + \eta_2}{\tau}$$

under this condition the solution of GK equation is qualitatively equal to that of Fourier. However, in the three-dimensional setting, Fourier resonance appears only

in the longitudinal direction, the transversal contribution may distort this behaviour. In addition

- $\frac{(\eta_1+\eta_2)/\tau}{\lambda/(\rho c)} < 1$, Fourier resonance condition;
- $\frac{(\eta_1+\eta_2)/\tau}{\lambda/(\rho c)} < 1$, over-diffusive solutions are obtained;
- $\frac{(\eta_1+\eta_2)/\tau}{\lambda/(\rho c)} < 1$, attenuated wave-like propagation of the temperature field is observable.

From an engineering perspective, Fourier resonance is a natural and desirable requirement, as the GK equation includes the Fourier equation as a special case. This characteristic is highly advantageous in practical applications because it allows the GK equation to replicate the simpler Fourier solution under specific conditions, achieved through the appropriate alignment of its coefficients. Crucially, this can be done without any modifications to the underlying model, making it both versatile and efficient for situations where classical Fourier heat conduction is sufficient, while still being capable of handling more complex scenarios when necessary.

When we consider the constant coefficient (and only in this case) is possible to eliminate the heat flux $\mathbf{q}$ or the temperature from the equation (5.3), and we obtain

$$\text{T - representation} \quad \tau\,\partial_t\left(\partial_t T + \frac{\eta_1+\eta_2}{\tau}\Delta T\right) + (\partial_t T + \alpha\Delta T) = \frac{1}{\rho\, c}\left(\tau\partial_t S - (\eta_1+\eta_2)\Delta S\right)$$
$$\text{q - representation} \quad \tau\,\partial_t\left(\partial_t \mathbf{q} - \frac{\eta_1+\eta_2}{\tau}\Delta \mathbf{q}\right) + (\partial_t \mathbf{q} - \alpha\Delta \mathbf{q}) = -\alpha\Delta S,$$

We observe the source terms in this T-(q-)representation apperas differently, however when $S = 0$ we obtain

$$\text{T - representation} \quad \tau\,\partial_t\left(\partial_t T + \frac{\eta_1+\eta_2}{\tau}\Delta T\right) + (\partial_t T + \alpha\Delta T) = 0$$
$$\text{q - representation} \quad \tau\,\partial_t\left(\partial_t \mathbf{q} - \frac{\eta_1+\eta_2}{\tau}\Delta \mathbf{q}\right) + (\partial_t \mathbf{q} - \alpha\Delta \mathbf{q}) = \mathbf{0}.$$

5.2 L-GK and NL-GK in 1D

The Guyer-Krumhansl model is promising and could be the standard model for future engineering practice. However, its practical application depends on a thorough investigation and deep understanding of its mathematical properties, particularly the study of nonlinear effects arising from non-constant material parameters. For this reason, we investigate the effects of non-constant material parameters, such as thermal conductivity and relaxation time. Given the practical importance of accounting for these nonlinearities, understanding their impact is essential for addressing real-world heat transfer problems effectively. This deeper insight will enable more accurate modeling of complex scenarios where material properties are not constant, ensuring the GK model's successful implementation in engineering solutions.

In the Section 2.5.2 we obtain, after some calculations, the following evolution equation for the heat flux in one dimension

$$\frac{\rho m}{l_{22}}\frac{\partial q}{\partial t}+q=\frac{\rho m}{l_{22}}\frac{\partial}{\partial t}\left(l_{11}\frac{\partial B}{\partial x}\right)+\left(l_{11}l_{22}-l_{12}l_{12}\right)\frac{\partial B}{\partial x}$$

The GK equation is obtained setting $l_{11}=0, l_{22}=l_2, l_{21}=1, k_1+k_2+k_3=l_1$ and using the constrains (2.75) the relation $\left(l_{12}+l_{21}\right)^2\leq 0$ is satisfied if and only if $l_{12}=-l_{21}$. By eliminating the current multiplier B and after some computation the equation (2.72)

$$\frac{\rho m}{l_2}\frac{\partial q}{\partial t}+q=\frac{1}{l_2}\frac{\partial}{\partial x}\left(\frac{1}{T}+l_1\frac{\partial q}{\partial x}\right)$$

is obtained. Here, it is possible to consider two different cases, as it has been see in Section 2.5.2. Here we summarize the following cases:

Case I : l_1 is constant

$$\tau(T)\partial_t q+q=-\lambda(T)\partial_x T+\eta^2\partial_{xx}q \tag{5.10}$$

with the following identifications

$$\tau=\frac{\rho m}{l_2},\qquad \lambda=\frac{1}{l_2T^2},\qquad \eta^2=\frac{l_1}{l_2}.$$

if thermal conductivity and relaxation time are assumed to be expressed as functions of temperature, i.e. (2.11) and (2.50), the following constraints arise

$$\begin{aligned}
l_2(T)&=\frac{1}{\left[\lambda_0+a(T-T_0)\right]T^2},\\
\rho m&=\frac{\tau_0+b(T-T_0)}{\left[\lambda_0+a(T-T_0)\right]T^2},\\
\eta^2(T)&=l_1\left[\lambda_0+a(T-T_0)\right]T^2.
\end{aligned}$$

Case II : $l_1=l_1(T)$ is a function of temperature (see [53])

In this situation the evolution equation for the heat flux is

$$\tau\,\partial_t q+q=\left[-\lambda(T)+\frac{1}{l_2(T)}\frac{dl_1(T)}{dT}\partial_x q\right]\partial_x T+\eta^2(T)\partial_{xx}q \tag{5.11}$$

which contains the GK equation but appear the presence of a new term, as in [51].

Assuming thermal conductivity and relaxation time are expressed as a functions of temperature, i.e. (2.11) and (2.50), and also the coefficient $\eta^2(T)$ is assumed to be a linear function of temperature

$$\eta^2(T)=\eta_0+\tilde{c}(T-T_0) \tag{5.12}$$

wherein η_0 denotes this coefficient at the initial time, and $\tilde{c}$ is a suitable coefficient depending on the material under examination; the following constraints

arise,

$$
\begin{aligned}
l_2(T) &= \frac{1}{[\lambda_0 + a(T - T_0)]\, T^2}, \\
\rho m &= \frac{\tau_0 + b(T - T_0)}{[\lambda_0 + a(T - T_0)]\, T^2}, \\
l_1(T) &= \frac{\eta_0 + \tilde{c}(T - T_0)}{[\lambda_0 + a(T - T_0)]\, T^2}.
\end{aligned}
\tag{5.13}
$$

5.2.1 Formulation of nonlinear GK model : heat pulse application

Let us consider the set of equations (2.1) and (2.76) in the one-dimensional domain $\Omega = [0, L]$ with length L. The one dimensional case, in the heat pulse experiment, is a good approximation when the thickness of the samples is smaller and the front face is heated homogeneously by the heat pulse. In addition, the small deformation is neglected here and the samples are assumed to be rigid conductors. Under these assumptions, the balance law of the internal energy and the evolution equation for the heat flux read in the form

$$\rho c\, \partial_t T + \partial_x q = 0, \tag{5.14a}$$

$$\tau(T)\, \partial_t q + q = \left[-\lambda(T) + \frac{1}{l_2(T)} \frac{dl_1(T)}{dT} \partial_x q \right] \partial_x T + \eta^2(T)\, \partial_{xx} q, \tag{5.14b}$$

wherein η is the phenomenological coefficient (characteristic length) with $\eta^2 = \eta_1^2 + \eta_2^2$. The material parameters and specific heat capacity c are assumed to be constant, while the functions $\lambda(T), \tau(T)$ are expressed by the equations (2.11), (2.50).

Here we examine both the cases where the parameter η^2 is constant and it depends on temperature : as seen earlier in Section 2.5.2, assuming constant the phenomenological coefficient l_1. This induces a well-defined non-linearity on the parameter $\eta^2(T)$, which could be appropriately modified by introducing an suitable function for $l_1(T)$, but this as noted in [51] leads to the presence of an additional term in the GK equation.

The same I.C. and B.C. as in heat pulse experiments are used, explained in the Chapter 4.2

$$T(x, 0) = T_0, \qquad q(x, 0) = 0,$$

and

$$q(1, t) = 0,$$

$$q(0, t) = q_0(t) = \begin{cases} \dfrac{q_{max}}{2} \left[1 - \cos\left(\dfrac{2\pi t}{t_p} \right) \right] & \text{if } t_0 < t \leq t_p, \\ 0 & \text{if } t > t_p. \end{cases}$$

Approximation with constant coefficient $\eta^2(T)$

As is usual to proceed, since (5.14) may contain coefficients of different order of magnitude, dimensionless variables are introduced

$$\hat{x} = \frac{x}{L}, \quad \hat{t} = \frac{\alpha_0 t}{L^2}, \quad \hat{q} = \frac{q}{\tilde{q}_0}, \quad \hat{T} = \frac{T - T_0}{T_{end} - T_0}, \tag{5.15}$$

where

$$\alpha_0 = \frac{\lambda(T_0)}{\rho_0 c}, \quad T_{end} = T_0 + \frac{t_p \tilde{q}_0}{\rho_0 c L}, \quad \tilde{q}_0 = \frac{q_{max}}{2}.$$

The dimensionless version of (5.14) reads

$$\tau_{p_1}\left(1 + \frac{\tau_{q_2}}{\tau_{q_1}}\hat{T}\right)\partial_{\hat{t}}\hat{T} + \partial_{\hat{x}}\hat{q} = 0, \tag{5.16a}$$

$$(\tau_{q_1} + \tau_{q_2}\hat{T})\partial_{\hat{t}}\hat{q} + \hat{q} = -\left(\tau_{p_1} + \tau_{p_2}\hat{T}\right)\partial_{\hat{x}}\hat{T} + \tau_c \partial_{\hat{x}\hat{x}}\hat{q}, \tag{5.16b}$$

where the dimensionless parameters are

$$\begin{aligned} &\tau_{p_1} = \frac{\alpha_0 t_p}{L^2} = \tau_d, \quad \tau_{p_2} = \frac{a(T_{end} - T_0)t_p}{\rho_0 c L^2}, \quad \tau_c = \frac{\eta^2}{L^2} \\ &\tau_{q_1} = \frac{\alpha_0 \tau_0}{L^2}, \quad \tau_{q_2} = \frac{\alpha_0\, b(T_{end} - T_0)}{L^2}, \end{aligned} \tag{5.17}$$

Furthermore, the dimensionless initial and boundary conditions are, respectively

$$\hat{T}(\hat{x}, 0) = 0, \qquad \hat{q}(\hat{x}, 0) = 0, \tag{5.18}$$

and

$$\begin{aligned} &\hat{q}(1, \hat{t}) = 0, \\ &\hat{q}(0, \hat{t}) = \begin{cases} 1 - \cos\left(\dfrac{2\pi\hat{t}}{\tau_d}\right) & \text{if } 0 < \hat{t} \leq \tau_d, \\ 0 & \text{if } \hat{t} > \tau_d. \end{cases}, \end{aligned} \tag{5.19}$$

Remark 16. *If we choose $a = b = 0$ (i.e. $\tau_{q_2} = \tau_{p_2} = 0$), the linear case is recovered*

$$\begin{aligned} &\tau_{p_1}\frac{\partial \hat{T}}{\partial \hat{t}} + \frac{\partial \hat{q}}{\partial \hat{x}} = 0, \\ &\tau_{q_1}\frac{\partial \hat{q}}{\partial \hat{t}} + \hat{q} = -\tau_d \frac{\partial \hat{T}}{\partial \hat{x}} + \tau_c \frac{\partial \hat{q}}{\partial \hat{x}^2}. \end{aligned}$$

Non-linearity induced by $\eta^2(T)$

Using the same set of dimensionless variables (5.15), if the non-linearity induced by $\eta^2(T)$ is recognized, from the system (5.14) the following one-dimensional model is achieved

$$\tau_{p_1}\left(1 + \frac{\tau_{q_2}}{\tau_{q_1}}\hat{T}\right)\partial_{\hat{t}}\hat{T} + \partial_{\hat{x}}\hat{q} = 0, \tag{5.20a}$$

$$(\tau_{q_1} + \tau_{q_2}\hat{T})\,\partial_{\hat{t}}\hat{q} + \hat{q} = -\left(\tau_{p_1} + \tau_{p_2}\hat{T}\right)\partial_{\hat{x}}\hat{T} + \left(\tau_{c_0} + 2\tau_{c_1}\hat{T} + \tau_{c_2}\hat{T}^2\right)\cdot\left(\tau_d + \tau_{p_2}\hat{T}\right)\partial_{\hat{x}\hat{x}}q, \tag{5.20b}$$

with the same dimensionless initial and boundary conditions, (5.18) and (5.19) respectively. Furthermore, the dimensionless parameters are the same as in (5.17) with additional identifications

$$\tau_{c_0} = \frac{\rho_0 c\, l_1 T_0}{t_p}, \quad \tau_{c_1} = \tau_{c_0}(T_{end} - T_0), \quad \tau_{c_2} = \tau_{c_0}(T_{end} - T_0)^2.$$

General non-linearity for $\eta^2(T)$

The study of the non-linearity of $\eta^2(T)$, is very important, for this reason it is necessary to study the case in which it is possible to assign for it a temperature-dependent function that is not induced by the assumption of $\lambda(T)$ and $\tau(T)$. For instance, here suppose that $\eta(T)^2$ is expressed by (5.12).

As seen in Section (2.5.2) this assumption implies the presence of a new term in the GK equation. Under the same set of dimensionless variables (5.15) from the system (5.14) where we now consider $\eta^2(T)$ as (5.12), we get the following dimensionless version

$$\tau_{p_1}\left(1+\frac{\tau_{q_2}}{\tau_{q_1}}\hat{T}\right)\partial_{\hat{t}}\hat{T}+\partial_{\hat{x}}\hat{q}=0, \tag{5.21a}$$

$$\begin{aligned}(\tau_{q_1}+\tau_{q_2}\hat{T})\,\partial_{\hat{t}}\hat{q}+\hat{q} = &-\left(\tau_d+\tau_{p_2}\hat{T}\right)\partial_{\hat{x}}\hat{T}+\left(\tau_{l_1}+\tau_{l_2}\hat{T}\right)\partial_{\hat{x}\hat{x}}\hat{q}+\\ &\left(\tau_{p_2}-2\frac{\tau_{l_1}+\tau_{l_2}\hat{T}}{\tau_{T_1}+\tau_{T_2}\hat{T}}-\tau_{p_2}\frac{\tau_{l_1}+\tau_{l_2}\hat{T}}{\tau_{p_1}+\tau_{p_2}\hat{T}}\right)\partial_{\hat{c}}\hat{q}\,\partial_{\hat{x}}\hat{T},\end{aligned} \tag{5.21b}$$

with the same dimensionless initial and boundary conditions, (5.18) and (5.19) respectively. The dimensionless parameters are similar to the previous cases, (5.17), with the addition of the following identifications

$$\tau_{l_1}=\frac{\eta_0}{L^2},\quad \tau_{l_2}=\frac{\tilde{c}(T_{end}-T_0)}{L^2},\quad \tau_{T_1}=\frac{\rho_0 cLT_0}{t_p\,q_0},\quad \tau_{T_2}=\frac{\rho_0 cL(T_{end}-T_0)}{t_p\,q_0}.$$

In the sequel the 'hat' is omitted in all cases to simplify the notation.

Now we present some numerical results in these three different scenarios, first a brief summary of the numerical method used to solve the nonlinear systems (5.16), (5.20) and (5.21) is discussed and then the results obtained are shown.

5.2.2 Numerical framework

Let us discretize the spatial domain $\Omega=[0,1]$ with spatial step Δx and the time interval $[0,t_{max}]$ with step Δt, the following discrete space and time values are obtained

$$\begin{aligned}x_j &= x_0+j\Delta x \quad j=0,1,2,...,N\\ t^n &= t_0+n\Delta t \quad n=0,1,2,...,J.\end{aligned}$$

The discrete values of temperature are shifted in x direction, then the temperature is computed in the internal nodes [29, 98], while the heat flux is computed in the nodes (see Fig. 5.2), as

$$\begin{aligned}T(x_{j+1/2},t^n)&\approx T^n_{j+1/2},\\ q(x_j,t^n)&\approx q^n_j,\end{aligned}$$

Furthermore, no boundary conditions for temperature will be prescribed as can be expressed explicitly, as a function of the above quantities.

An explicit forward finite difference method is used for the first order time and spatial derivatives, centered finite difference for second order spatial derivatives

$$\begin{aligned}
\frac{\partial T}{\partial t} &\approx \frac{T_{j+1/2}^{n+1} - T_{j+1/2}^{n}}{\Delta t}, \\
\frac{\partial q}{\partial t} &\approx \frac{q_{j}^{n+1} - q_{j}^{n}}{\Delta t}, \\
\frac{\partial q}{\partial x} &\simeq \frac{q_{j+1}^{n} - q_{j}^{n}}{\Delta x} = \mathcal{D}_x(q), \\
\frac{\partial^2 q}{\partial x^2} &\simeq \frac{q_{j+1}^{n} - 2\,q_{j}^{n} + q_{j-1}^{n}}{\Delta x^2} = \mathcal{D}_{xx}(q), \\
\frac{\partial T}{\partial x} &\simeq \frac{T_{j+1/2}^{n} - T_{j-1/2}^{n}}{\Delta x} = \mathcal{D}_x(T).
\end{aligned}$$

In addition, for nonlinear terms, the following identifications are given

$$\begin{aligned}
\left(\tau_{q_1} + \tau_{q_2} T\right) &\approx \left(\tau_{q_1} + \tau_{q_2} T_j^n\right) = \mathcal{A} \\
\left(\tau_{p_1} + \tau_{p_2} T\right) &\approx \left(\tau_{d} + \tau_{p_2} T_j^n\right) = \mathcal{B}, \\
\left(\tau_{c_0} + 2\tau_{c_1} T + \tau_{c_2} T^2\right) &\approx \left(\tau_{c_0} + 2\tau_{c_1} T_j^n + \tau_{c_2} (T_j^n)^2\right) = \mathcal{C}, \\
\left(\tau_{l_1} + \tau_{l_2} T\right) &\approx \left(\tau_{l_1} + \tau_{l_2} T_j^n\right) = \mathcal{L}, \\
\left(\tau_{T_1} + \tau_{T_2} T\right) &\approx \left(\tau_{T_1} + \tau_{T_2} T_j^n\right) = \mathcal{T}, \\
\left(\tau_{p_2} - 2\frac{\tau_{l_1} + \tau_{l_2}\hat{T}}{\tau_{T_1} + \tau_{T_2}\hat{T}} - \tau_{p_2}\frac{\tau_{l_1} + \tau_{l_2}\hat{T}}{\tau_{p_1} + \tau_{p_2}\hat{T}}\right) &\approx \left(\tau_{p_2} - 2\frac{\mathcal{L}}{\mathcal{T}} - \tau_{p_2}\frac{\mathcal{L}}{\mathcal{B}}\right) = \mathcal{M}.
\end{aligned} \tag{5.22}$$

in this approximations the term T_j^n is replaced by the following average

$$T_j^n \longmapsto \frac{T_{j-1/2}^n + T_{j+1/2}^n}{2},$$

as shown in the Fig. 5.2.

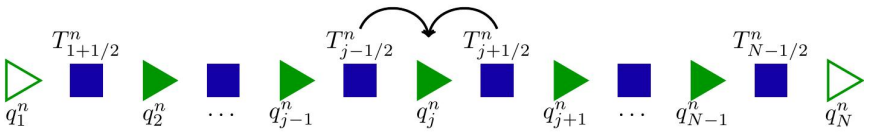

FIGURE 5.2: Concept of the spatial discretization : The filled squares represent the temperature T, and the filled triangles represents the heat flux q. Empty symbols denote boundary conditions.

As a result, the difference equations consist of an explicit forward differencing scheme

$$\mathcal{A}\frac{\tau_d}{\tau_{q_1}}\frac{T_{j+1/2}^{n+1}-T_{j+1/2}^{n}}{\Delta t}+\mathcal{D}_x(q)=0, \tag{5.23a}$$

$$\mathcal{A}\frac{q_j^{n+1}-q_j^n}{\Delta t}+q_j^n+\mathcal{B}\,\mathcal{D}_x(T)-\xi_1\cdot\mathcal{D}_{xx}(q)-\xi_2\cdot\mathcal{D}_x(q)\cdot\mathcal{D}_x(T)=0. \tag{5.23b}$$

wherein

$$\xi_1=\begin{cases}\tau_c \text{ for (5.16)}\\ \mathcal{C}\cdot\mathcal{B} \text{ for (5.20)}\\ \mathcal{T} \text{ for (5.21)}\end{cases}\qquad\text{and}\qquad \xi_2=\begin{cases}0 \text{ for (5.16)}\\ 0 \text{ for (5.20)}\\ \mathcal{M} \text{ for (5.21)}\end{cases}$$

5.2.3 Numerical results

As mentioned before, the GK equation represents a nonlocal generalization of the Cattaneo equation, therefore we are interested in investigating the contribution of the nonlocal term on the behavior of the thermal wave and especially what effects it implies when it is as temperature-dependent.

Approximation with constant coefficient $\eta^2(T)$

For this purpose we initially place, the coefficient of the nonlocal term ($\partial_{xx}q$) constant, i.e. η^2 constant (i.e. τ_c constant). It is observed that in the absence of this term, i.e $\tau_c=0$, there is a wave-like trend, typical of Cattaneo model, because the system is hyperbolic. For values of $\tau_c\in[0,\,0.03]$ the temperature behavior is similar to that obtained using by MCV relation ($\tau_c=0$), but increasing the value of τ_c, this wave effect tends to disappear, since the parabolic character of the system prevails, (see Figure 5.3).

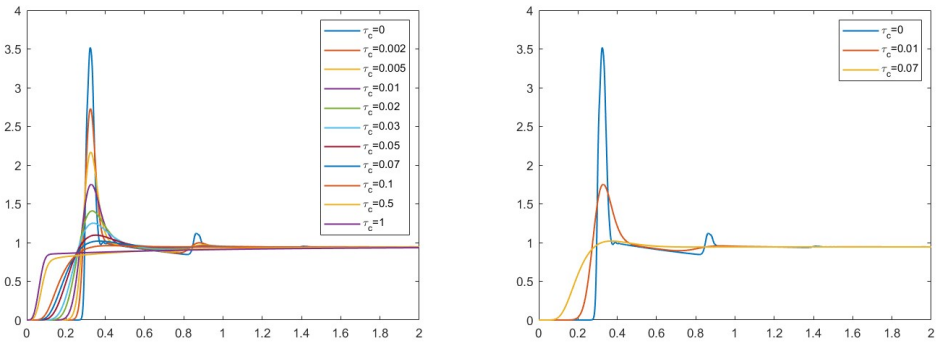

(a) (b)

FIGURE 5.3: The rear side temperature history, using the GK heat equation when we change value of the coefficient τ_c of the non-local term. The parameters used are: $\tau_d=0.1$, $\tau_{p_2}=0.03$, $\tau_{q_1}=0.08$, $\tau_{q_2}=0.01$.

In particular, it can be observed that as the value of τ_c increases, the thermal pulse generated at the input propagates forward and does not return to the point where it

was measured (see Figure 5.3, where the second blue wave tends to dampen more quickly as τ_c grows).

Once we understand that the effect of this parameter τ_c, contributes as a measure of how far the model deviates from the hyperbolic regime; we aim to investigate interested the consequences of assuming non-constant thermal conductivity and relaxation time. For this reason, in Figure (5.4) $\tau_{q_2} = 0$ to focus solely on the contribution of non-linearity in thermal conductivity. It is observed that as the non-linearity parameter, τ_{p_2}, increases, the temperature profile shifts to the left. A similar behavior was observed in the Cattaneo model in one spatial dimension, with almost analogous observations in the two-dimensional case, as seen in Chapter 4.2.

In other words, as the thermal conductivity increases, it is expected that the material conducts heat more efficiently, causing the heat propagation to advance and reach higher peaks. This study was conducted for different values of the parameter τ_c, as shown in Figure 5.4, for $\tau_c = 0$ the same behavior observed in [29] is recovered.

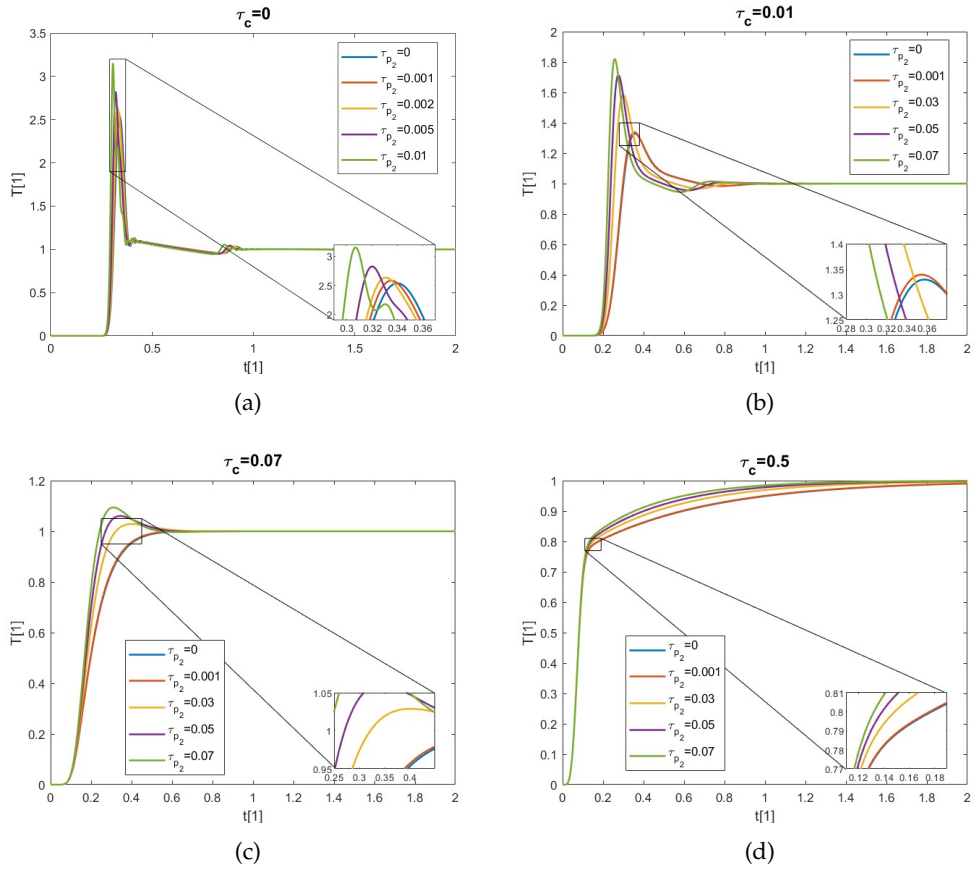

FIGURE 5.4: The rear side temperature history, using the equation (5.16b) when we increasing the non-linear term present in the thermal conductivity, τ_{p_2}: $0, 0.001, 0.03, 0.05, 0.07$ and we put to zero the other non linear term $\tau_{q_2} = 0$. The other parameters are $\tau_d = 0.1$, $\tau_{q_1} = 0.08$.

Similar considerations can be carried out regarding the effects caused by assuming a non-constant relaxation time. To fully understand the implications of treating the relaxation time as a function of temperature, in Figure 5.5 placing $\tau_{p_2} = 0$. It is observed that as the value of the parameter causing the non-linearity, τ_{q_2}, increases,

the temperature profile shifts to the right. This behavior highlights that as the relaxation time increases, the heat flux q responds to temperature changes with a greater delay, meaning the temperature gradient is not formed instantaneously. The results for $\tau_c = 0$ are again consistent with those presented in [29].

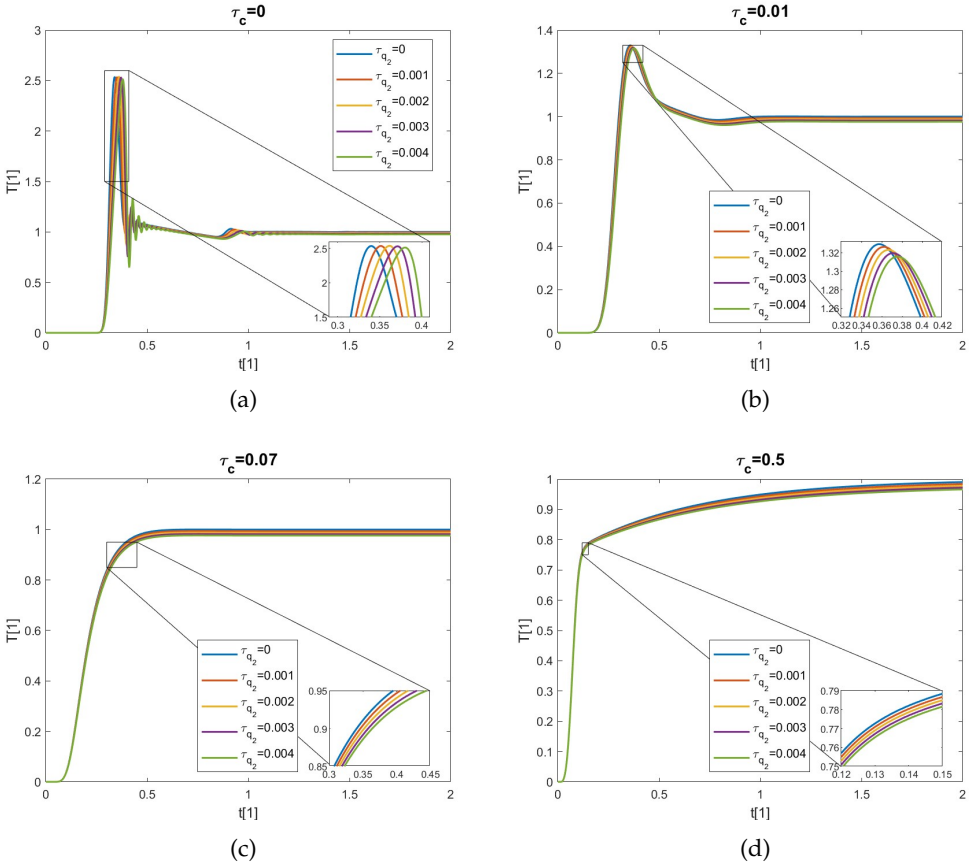

FIGURE 5.5: The rear side temperature history, using the equation (5.16b) when we increasing the non-linear term present in the relaxation time, τ_{q_2}: $0, 0.001, 0.002, 0.003, 0.004$ and we put to zero the other non linear term $\tau_{p_2} = 0$. The other parameters are $\tau_d = 0.1$, $\tau_{q_1} = 0.08$.

Non-linearity induced by $\eta^2(T)$

The second step in the study of the nonlocal term is to consider the non-linearity induced by thermal conductivity, (see Section 5.2.1). We observe that as this non-linearity increases, caused by the increase of the coefficient of the nonlocal term, i.e. $mean((\tau_c)_i^n)$, that corresponds to increase of the coefficients τ_{c_m} with $m \in \{0, 1, 2\}$, the temperature peak tends to decrease and the heat conduction occurs more slowly, in Figure 5.6 we note the transition of the temporal evolution of the temperature from blue to yellow.

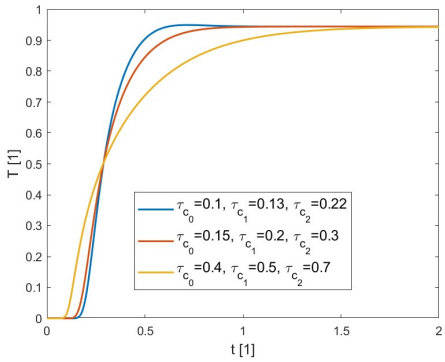

FIGURE 5.6: We choose the parameters τ_{c_m} with $m \in \{0,1,2\}$ such that the mean of the nonlinear term $\tau_c \equiv \left(\tau_{c_0} + 2\tau_{c_1}\hat{T} + \tau_{c_2}\hat{T}^2\right) \cdot \left(\tau_d + \tau_{p_2}\hat{T}\right)$ is: (a) $mean((\tau_c)_i^n) = 0.0718$, (b) $mean((\tau_c)_i^n) = 0.1045$ and (c) $mean((\tau_c)_i^n) = 0.2555$. In particular we choose in : (a) $\tau_{c_0} = 0.1, \tau_{c_1} = 0.13, \tau_{c_2} = 0.22$; (b) $\tau_{c_0} = 0.15, \tau_{c_1} = 0.2, \tau_{c_2} = 0.3$; and (c) $\tau_{c_0} = 0.4, \tau_{c_1} = 0.4, \tau_{c_2} = 0.7$.

In this case, attention is drawn to the consequences of non-constant thermal conductivity and relaxation time. It is observed that basically, their effect are almost similar to those observed in the previous case, (see figure 5.7-5.8).

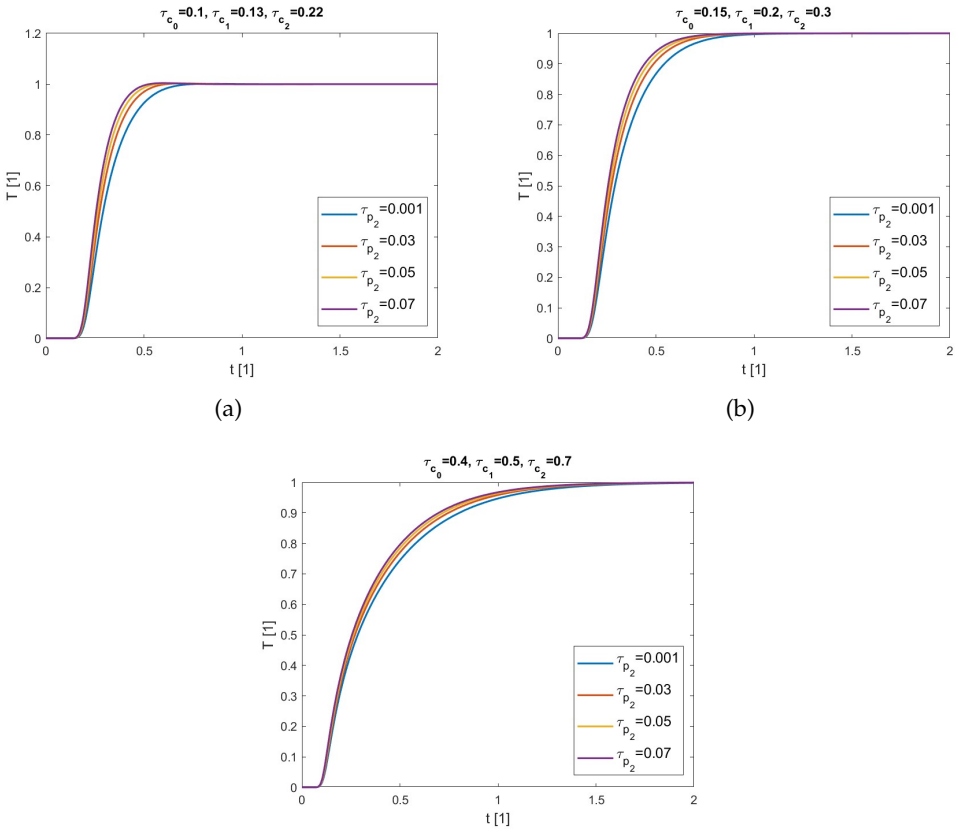

(a) (b)

(c)

FIGURE 5.7: The rear side temperature history, using the equation (5.20b) when we increasing the non-linear term present in the relaxation time, τ_{p_2}: 0.001, 0.03, 0.05, 0.07 and we put to zero the other non-linear term $\tau_{p_2} = 0$, this is because we want to study only the effect of the nonlinear term present in the relaxation time. The other parameters are $\tau_d = 0.1$, $\tau_{q_1} = 0.08$.
Furthermore, we choose the parameters τ_{c_m} with $m \in \{0, 1, 2\}$ such that the mean of the nonlinear term $\tau_c \equiv \left(\tau_{c_0} + 2\tau_{c_1}\hat{T} + \tau_{c_2}\hat{T}^2\right) \cdot \left(\tau_d + \tau_{p_2}\hat{T}\right)$ is: (a) $mean((\tau_c)_i^n) = 0.0718$, (b) $mean((\tau_c)_i^n) = 0.1045$ and (c) $mean((\tau_c)_i^n) = 0.2555$. In particular we assume in : (a) $\tau_{c_0} = 0.1, \tau_{c_1} = 0.13, \tau_{c_2} = 0.22$; (b) $\tau_{c_0} = 0.15, \tau_{c_1} = 0.2, \tau_{c_2} = 0.3$; and (c) $\tau_{c_0} = 0.4, \tau_{c_1} = 0.4, \tau_{c_2} = 0.7$.

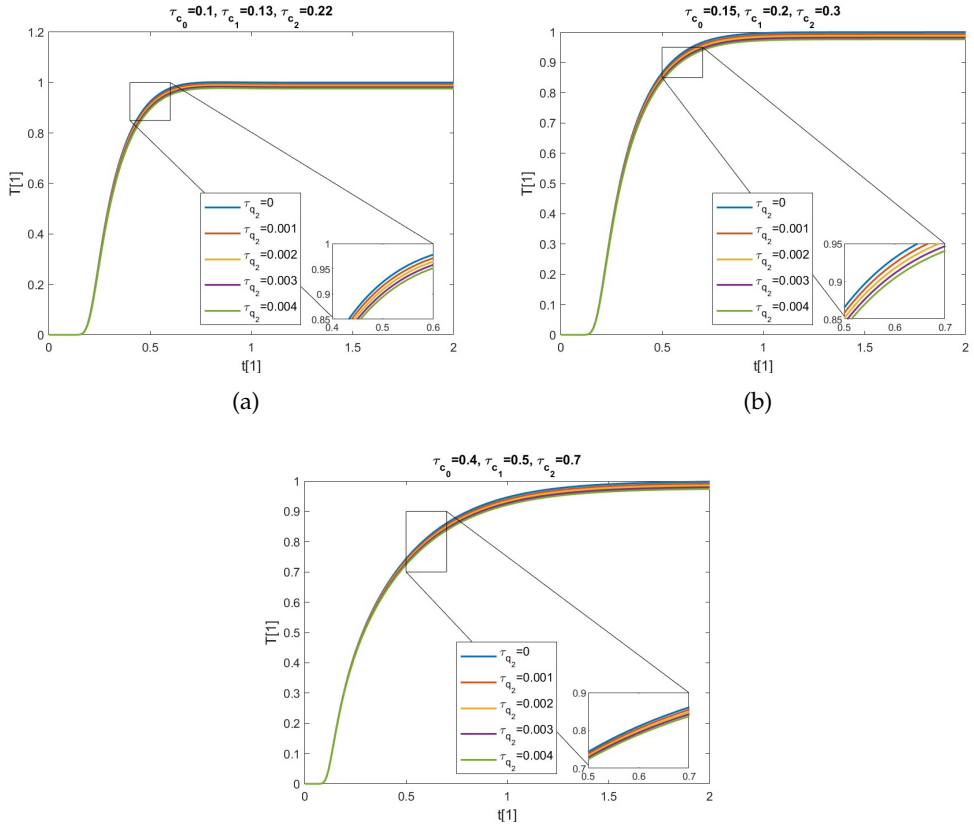

(a) (b)

(c)

FIGURE 5.8: The rear side temperature history, using the equation (5.20b) when we increasing the nonlinear term present in the thermal conductivity, τ_{q_2}: $0.001, 0.002, 0.003, 0.004$ and we put to zero the other nonlinear term $\tau_{q_2} = 0$, this is because we want to study only the effect of the nonlinear term present in thermal conductivity. The other parameters are $\tau_d = 0.1$, $\tau_{q_1} = 0.08$.
Furthermore, we choose the parameters τ_{c_m} with $m \in \{0, 1, 2\}$ such that the mean of the nonlinear term $\tau_c \equiv \left(\tau_{c_0} + 2\tau_{c_1}\hat{T} + \tau_{c_2}\hat{T}^2\right) \cdot \left(\tau_d + \tau_{p_2}\hat{T}\right)$ is: (a) $mean((\tau_c)_i^n) = 0.0718$, (b) $mean((\tau_c)_i^n) = 0.1045$ and (c) $mean((\tau_c)_i^n) = 0.2555$. In particular we assume in : (a) $\tau_{c_0} = 0.1, \tau_{c_1} = 0.13, \tau_{c_2} = 0.22$; (b) $\tau_{c_0} = 0.15, \tau_{c_1} = 0.2, \tau_{c_2} = 0.3$; and (c) $\tau_{c_0} = 0.4, \tau_{c_1} = 0.4, \tau_{c_2} = 0.7$.

General non-linearity for $\eta^2(T)$

Finally, the third scenario involves considering a non-linearity for the coefficient of the nonlocal term which does not fit into the previously treated cases. In this case, the parameter $\eta^2(T)$ is assumed to be a function of temperature. The effect of this type of non-linearity, represented by the parameters τ_{T_m} with $m \in 1,2$, leads to a delay in thermal propagation as these parameters increase. This behavior can be clearly observed in Figure 5.9.

Additionally, as the parameter regulating the non-linearity of the thermal conductivity, τ_{p_2}, increases, the initial results align with those observed in [29]. However, if the value of this parameter continues to increase, wave propagation reappears. This suggests that incorporating non-linear contributions in both the thermal conductivity and the coefficient of the nonlocal term introduces a hyperbolic nature to the model, as seen in Figure 5.10.

On the other hand, the analysis of the non-linearity effect in the relaxation time, or the increase in value of the parameter τ_{q_2} with $\tau_{p_2} = 0$, does not significantly differ from the results observed in the previous cases.

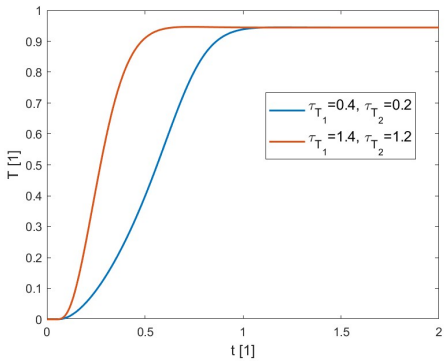

FIGURE 5.9: We choose the following parameters for τ_{T_m} with $m \in \{1,2\}$: $\tau_{T_1} = 1.4, \tau_{T_2} = 1.2$ for orange line and $\tau_{T_1} = 0.2, \tau_{T_2} = 0.1$ for blue line.

Finally, two non-linear cases of the GK equation are studied: the phenomenological coefficient l_1 is constant, a well defined non-linearity on the parameter $\eta^2(T)$ is induced; it is temperature dependent $l_1(T)$. The latter situation, observed by Kovács in [51] leads to the presence of an additional term in the GK equation. However, for both the heat equations of MCV and GK, it found that the introduction of the simpler non-linearity, which is a consequence of the linear dependence of relaxation time and thermal conductivity on the temperature, induces a temperature-dependent mass density, $\rho = \rho(T)$. Here, such mechanical effects induced by $\rho(T)$ have been neglected, but in the future these will be included as thermal expansion to describe a more realistic situation.

The analysis of the nonlocal term reveals that, whether in the constant case, with non-linearity induced by thermal conductivity, or in the presence of a more general non-linearity, the effects of varying relaxation time and thermal conductivity are comparable to those observed in the Maxwell-Cattaneo model in one or two spatial dimensions (see Chapters 4.2 and 4.3). Specifically, as thermal conductivity increases, heat propagation is advanced and achieves higher peaks. Conversely, an increase in relaxation time results in delayed thermal propagation.

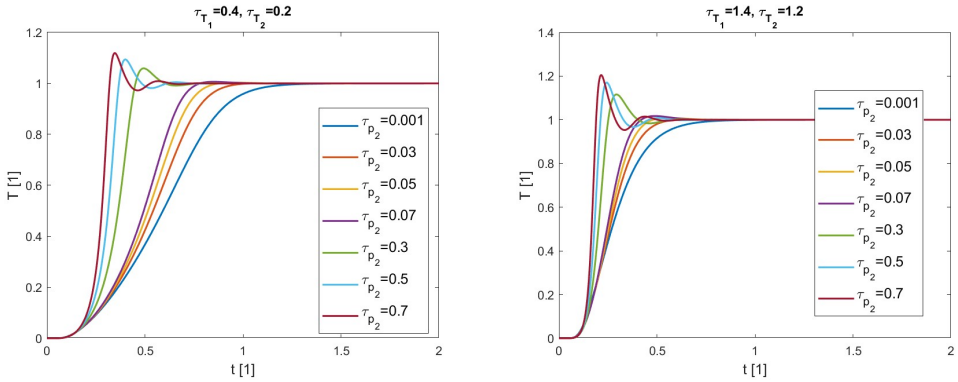

(a) (b)

FIGURE 5.10: The rear side temperature history, using the equation (5.21b) when we increasing the non-linear term present in the thermal conductivity, τ_{p_2}: $0.001, 0.03, 0.05, 0.07, 0.3, 0.5, 0.7$ and we put to zero the other non linear term $\tau_{q_2} = 0$, this is because we want to study only the effect of the nonlinear term present in thermal conductivity. The other parameters are $\tau_d = 0.1$, $\tau_{q_1} = 0.08$ and in (a) $\tau_{T_1} = 0.4, \tau_{T_2} = 0.2$ in (b) $\tau_{T_1} = 1.4, \tau_{T_2} = 1.2$.

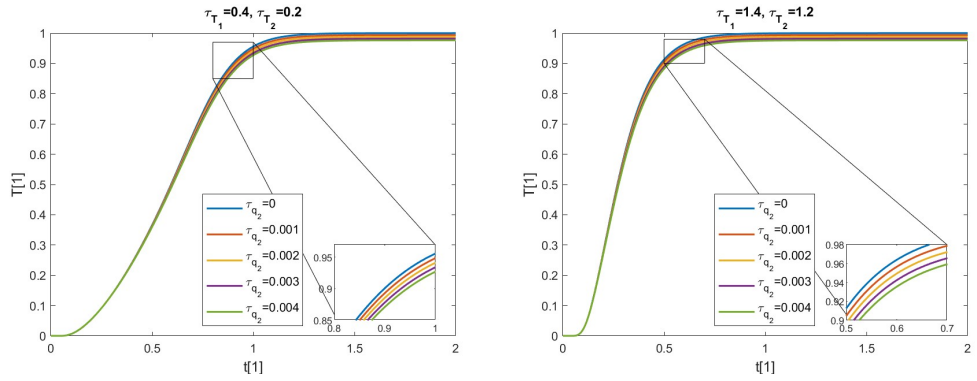

(a) (b)

FIGURE 5.11: The rear side temperature history, using the equation (5.21b) when we increasing the non-linear term present in the thermal conductivity, τ_{q_2}: $0.001, 0.002, 0.003, 0.004$ and we put to zero the other non linear term $\tau_{p_2} = 0$, this is because we want to study only the effect of the nonlinear term present in thermal conductivity. The other parameters are $\tau_d = 0.1$, $\tau_{q_1} = 0.08$ and in (a) $\tau_{T_1} = 0.4, \tau_{T_2} = 0.2$ in (b) $\tau_{T_1} = 1.4, \tau_{T_2} = 1.2$.

We can remarked that, in the constant case, the nonlocal term measures the deviation from the hyperbolic model. However, when considering non-linearity induced by thermal conductivity, it is noted that as thermal conductivity increases, the temperature peak tends to decrease and thermal conduction proceeds more slowly.

In the more general case, where the nonlocal term is defined by a generic temperature-dependent function, we observe that this type of non-linearity results in a delay in thermal propagation as the non-linearity increases. Moreover, if the value of this parameter that characterizes the non-linearity is further increased, wave propagation

can reappear. Thus, it appears that incorporating nonlinear contributions both in thermal conductivity and in the coefficient of the nonlocal term introduces a hyperbolic nature to the model.

In conclusion we show the comparison between the linear and nonlinear results of Fourier, MCV and GK models in Figure 5.12

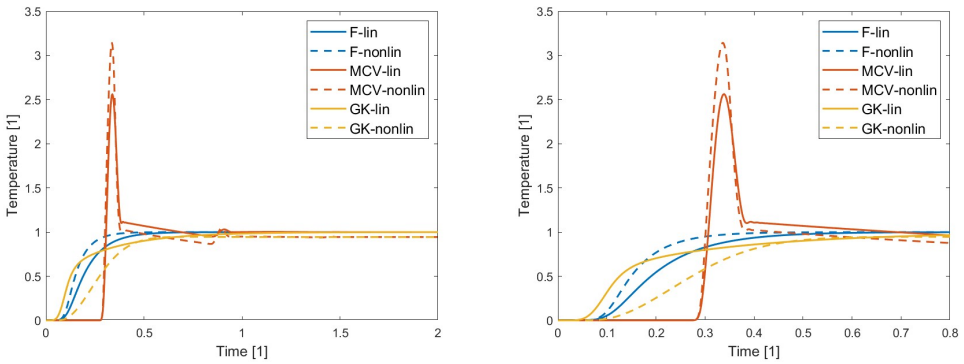

(a) (b)

FIGURE 5.12: The rear side temperature history, using the Fourier, MCV and GK model.

5.3 L-GK in 2D

Here, a staggered discretization approach we will apply to numerically solve a two-dimensional setting that include time and space varying boundary condition of heat flux. The discretization is facilitated by introducing a second-order tensory, $\mathbf{Q}$ as an auxiliary quantity, and $\mathbf{Q}$ is also useful in the proper realization of boundary conditions. The quantity $\mathbf{Q}$ is not independent of the given boundary condition for $\mathbf{q}$, however, not all components of $\mathbf{Q}$ can be found immediately. In order to avoid artificial and unnecessary assumptions, we will propose using a quadratic Lagrangian extrapolation based on the bulk points to update the unknown $\mathbf{Q}$ components on the boundary. This approach has successfully reproduced the solutions of the Fourier equation which apply the resonance condition ($\hat{\eta}_1 = 0$, i.e. with vanishing rotational term).

However, when rotational terms dominate the heat flux density evolution, we observe that the temperature can be significantly decreased, even falling below the initial temperature. It is important to emphasize that this phenomenon does not imply negative temperatures but occurs locally for a short period. This behavior is a characteristic result of the whirling heat current density.

5.3.1 A staggered grid finite difference method demonstrated on the heat pulse experiment in three spatial dimensions

Our aim to numerically model the heat pulse experiment in which a single short pulse thermally excites the sample. Let us consider both the spatial and time dependencies of the pulse. This setup provides an exceptional example for illustrating the role of boundary conditions, particularly due to the presence of in-plane derivatives.

In order to ease the discretization of the second-order derivative of $\mathbf{q}$, it is advantageous to introduce the gradient of heat current density as an auxiliary variable

$$\mathbf{Q} := \mathbf{q} \otimes \nabla,$$

hence, a system of first-order equations has to be solved. After this reformulation, it obtained

$$\tau\, \partial_t \mathbf{q} + \mathbf{q} = -\lambda \nabla T + \eta_1 \mathbf{Q} \cdot \nabla + \eta_2 \nabla \operatorname{Tr} \mathbf{Q} \tag{5.24}$$

for which it is crucial to properly discretize $\mathbf{Q}$ on the boundary.

You want to solve the GK equation in Cartesian coordinate system for a rectangular domain with the size of $X \times Y \times Z$. It is assumed that the heat pulse excites the entire Z direction uniformly, therefore we can reduce the problem to two-dimensional in X and Y. Furthermore, let us consider the symmetry at $y = 0$, so that $-\frac{Y}{2} \leq y \leq \frac{Y}{2}$, and thus we treat only the half of the rectangle. Consequently, the boundary conditions are

$$q_x(x = 0, y, t) = \begin{cases} \frac{Q_{\mathrm{P,Z}}}{\tau_{\mathrm{P}} Y_{\mathrm{P}}} \left[1 - \cos\left(2\pi \frac{t}{\tau_{\mathrm{P}}}\right)\right] \left[1 + \cos\left(2\pi \frac{y}{Y_{\mathrm{P}}}\right)\right] & \text{if } 0 \leq t \leq \tau_{\mathrm{P}} \\ & \text{and } 0 \leq y \leq \frac{Y_{\mathrm{P}}}{2} \leq \frac{Y}{2}\,, \\ 0 & \text{otherwise} \end{cases} \tag{5.25}$$

$$q_x(t, x = X, y) = 0, \tag{5.26}$$

$$q_y(t, x, y = 0) = 0, \tag{5.27}$$

$$q_y(t, x, y = +\frac{Y}{2}) = 0. \tag{5.28}$$

where $Q_{\mathrm{P,Z}}$ is the Z-length specific amount of heat introduced during the heat pulse, measured in $\frac{\mathrm{J}}{\mathrm{m}}$. The initial condition describes the equilibrium state with homogeneous temperature distribution

$$\begin{aligned} T(x, y, t = 0) &= T_0, \\ \mathbf{q}(x, y, t = 0) &= \mathbf{0}, \\ \mathbf{Q}(x, y, t = 0) &= \mathbf{0}. \end{aligned}$$

We want to transform the GK equation into a non-dimensional form, using the following characteristic scales. We choose X for the length scale and $\frac{X^2}{\alpha}$ for the time scale using the thermal diffusivity $\alpha := \frac{\lambda}{\rho c}$ (this leads to the usual Fourier number). Using these scales, the non-dimensional variables can be defined as follows

$$\hat{t} := \frac{t}{\frac{X^2}{\alpha}}, \qquad \hat{x} := \frac{x}{X}, \qquad \hat{y} := \frac{y}{X},$$

whose derivatives are give

$$\partial_{\hat{t}} = \frac{X^2}{\alpha}\, \partial_t, \qquad \partial_{\hat{x}} = X\, \partial_x, \qquad \partial_{\hat{y}} = X\, \partial_y.$$

The non-dimensional fields read

$$\hat{q}_i := \frac{q_i}{\frac{\alpha Q_{\mathrm{P,Z}}}{X^3 R_Y}}, \quad \hat{Q}_{ij} = \frac{Q_{ij}}{\frac{\alpha Q_{\mathrm{P,Z}}}{X^2 R_Y}}, \quad \hat{T} := \frac{T - T_0}{T_{\max} - T_0} = \frac{\rho c X^2 R_Y\, (T - T_0)}{Q_{\mathrm{P,Z}}}$$

in which $i,j = x,y$, $R_Y = \frac{Y}{X}$ and $T_{\max}$ is calculated by integration of 2.1 on the total volume of the sample over time from the initial homogeneous temperature state T_0 to the final homogeneous temperature state $T_{\max}$. Let us summarize the complete system of non-dimensional equations,

$$\partial_{\hat{t}}\hat{T} = -\left(\partial_{\hat{x}}\hat{q}_x + \partial_{\hat{y}}\hat{q}_y\right), \tag{5.29}$$

$$\hat{\tau}\partial_{\hat{t}}\hat{q}_x + \hat{q}_x = -\partial_{\hat{x}}\hat{T} + \left(\hat{\eta}_1 + \hat{\eta}_2\right)\partial_{\hat{x}}\hat{Q}_{xx} + \hat{\eta}_1\partial_{\hat{y}}\hat{Q}_{xy} + \hat{\eta}_2\partial_{\hat{x}}\hat{Q}_{yy}, \tag{5.30}$$

$$\hat{\tau}\partial_{\hat{t}}\hat{q}_y + \hat{q}_y = -\partial_{\hat{y}}\hat{T} + \left(\hat{\eta}_1 + \hat{\eta}_2\right)\partial_{\hat{y}}\hat{Q}_{yy} + \hat{\eta}_1\partial_{\hat{x}}\hat{Q}_{yx} + \hat{\eta}_2\partial_{\hat{y}}\hat{Q}_{xx}, \tag{5.31}$$

$$\hat{Q}_{xx} = \partial_{\hat{x}}\hat{q}_x, \tag{5.32}$$

$$\hat{Q}_{xy} = \partial_{\hat{y}}\hat{q}_x, \tag{5.33}$$

$$\hat{Q}_{yx} = \partial_{\hat{x}}\hat{q}_y, \tag{5.34}$$

$$\hat{Q}_{yy} = \partial_{\hat{y}}\hat{q}_y \tag{5.35}$$

wherein

$$\hat{\tau} = \frac{\tau}{\frac{X^2}{\alpha}}, \qquad \hat{\eta}_1 = \frac{\eta_1}{X^2}, \qquad \hat{\eta}_2 = \frac{\eta_2}{X^2}, \tag{5.36}$$

and the non-dimensional heat pulse boundary conditions reads

$$\hat{q}_x(\hat{x}=0,\hat{y},\hat{t}) = \begin{cases} \frac{R_Y}{\hat{\tau}_{\mathrm{P}} R_{Y,\mathrm{P}}}\left[1-\cos\left(2\pi\frac{\hat{t}}{\hat{\tau}_{\mathrm{P}}}\right)\right]\left[1+\cos\left(2\pi\frac{\hat{y}}{R_{Y,\mathrm{P}}}\right)\right] & \text{if } 0 \le \hat{t} \le \hat{\tau}_{\mathrm{P}} \\ & \text{and } 0 \le \hat{y} \le R_{Y,\mathrm{P}} \le R_Y \\ 0 & \text{otherwise} \end{cases}, \tag{5.37}$$

where $R_{Y,\mathrm{P}} = \frac{Y_{\mathrm{P}}}{X}$ stands.

Spatial discretization is achieved by a staggered scheme [110], which is depicted in Figure 5.13, and the structure of governing equations 5.29–5.35 restricts how each field can be represented on the discrete lattice with directional equidistant grid points with distance $\Delta\hat{x}$ and $\Delta\hat{y}$, hence $\hat{x}_m = m\Delta\hat{x}, 1, m = 1,\dots,M$, $\hat{y}_n = n\Delta\hat{y}$, $n = 1,\dots,N$, where $M = \frac{1}{\Delta\hat{x}}$ and $N = \frac{R_Y}{2\Delta\hat{y}}$. The investigated time interval is also discretized through equidistant time steps $\Delta\hat{t}$, i.e. $\hat{t}^j = j\Delta\hat{t}$, $j = 1,\dots,J$. Therefore, the approximated value of a function f in the discrete time and space coordinates $\left(\hat{t}^j,\hat{x}_m,\hat{y}_n\right)$ is denoted by $f^j_{m,n}$. The temperature, as a state variable characterizing homogeneously one discrete cell, is placed in the center of the cell, while heat current density characterizing fluxes through the boundaries of the cell, therefore, the corresponding normal components of the heat current density are placed on the boundaries of the cell in line with the discrete temperature values. Discretization of $\mathbf{Q}$ follows directly from the discrete values of heat current density and equations 5.32–5.35, consequently, its diagonal elements are in the middle of the cell, but its off-diagonal elements are placed in the corners of the cell. Since we apply $\mathbf{q}$-boundaries, only complete cells are used to discretize the entire spatial domain.

Furthermore, let us note that according to Figure 5.13, one needs to prescribe Q_{xy} and Q_{yx} on the boundaries, in accordance with the $\mathbf{q}$-boundaries. On each side, one of these off-diagonal quantities can be determined analytically and represented on the discrete lattice. For instance, for a given $q_x(x=0,y,t)$, Q_{xy} can be determined immediately, however, Q_{yx} must be extrapolated from the bulk nodes. This procedure holds for all four boundaries. For the extrapolation, the quadratic Lagrange polynomials is used to preserve the sign given by three bulk points next to

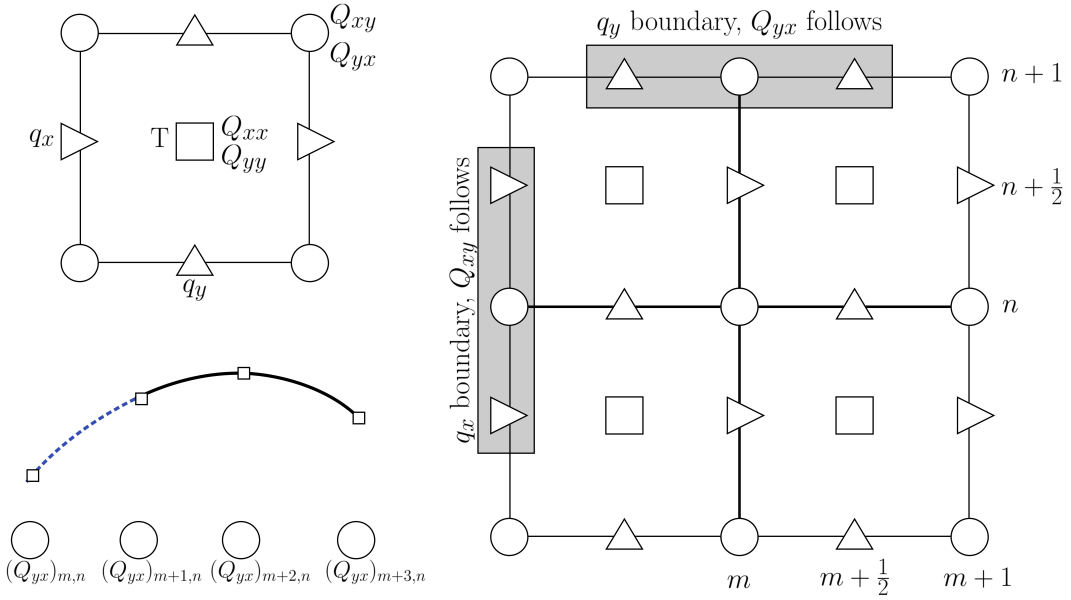

FIGURE 5.13: Discretization of the 2D GK equation, showing the staggered grid, and how **Q** points are allocated and extrapolated from the bulk. Additionally, the lower left figure demonstrated the extrapolation we use to determine the unknown off-diagonal elements.

each boundary. This extrapolation is schematically illustrated in Figure 5.13 for a setting in which the m^{th} value of Q_{yx} is calculated based on the bulk point of $m+1$, $m+2$, and $m+3$. It is worth to emphasizing that any direct definition of the **Q** on boundaries can significantly distort the physical content of the solution, and most probably, a different problem is solved than expected in that case. With our method using Lagrange polynomials, we can avoid the definition of any additional, unnecessary boundary conditions or the introduction of virtual nodes.

For the time derivatives, we choose the simplest forward time stepping method, the explicit Euler, which is eligible for our aim to investigate the solutions of the two-dimensional GK equation. Summarizing the numerical scheme built in accordance of Figure 5.13:

$$\hat{T}^{j+1}_{m+1/2,n+1/2} = \hat{T}^{j}_{m+1/2,n+1/2} + \Delta\hat{t}\left(\frac{(\hat{q}_x)^j_{m,n+1/2} - (\hat{q}_x)^j_{m+1,n+1/2}}{\Delta\hat{x}} + \right.$$
$$\left. + \frac{(\hat{q}_y)m+1/2,n^j - (\hat{q}_x)^j_{m+1/2,n+1}}{\Delta\hat{y}}\right), \tag{5.38a}$$

$$(\hat{q}_x)^{j+1}_{m,n+1/2} = \left(1 - \frac{\Delta\hat{t}}{\hat{\tau}}\right)(\hat{q}_x)^j_{m,n+1/2} + \frac{\Delta\hat{t}}{\hat{\tau}}\left(\frac{\hat{T}^j_{m-1/2,n+1/2} - \hat{T}^j_{m+1/2,n+1/2}}{\Delta\hat{x}} + \right.$$
$$+ (\hat{\eta}_1 + \hat{\eta}_2)\frac{(\hat{Q}_{xx})^j_{m+1/2,n+1/2} - (\hat{Q}_{xx})^j_{m-1/2,n+1/2}}{\Delta\hat{x}} +$$
$$+ \hat{\eta}_1\frac{(\hat{Q}_{xy})^j_{m,n+1} - (\hat{Q}_{xy})^j_{m,n}}{\Delta\hat{y}} +$$
$$\left. + \hat{\eta}_2\frac{(\hat{Q}_{yy})^j_{m+1/2,n+1/2} - (\hat{Q}_{yy})^j_{m-1/2,n+1/2}}{\Delta\hat{x}}\right), \tag{5.38b}$$

$$(\hat{q}_y)^{j+1}_{m+1/2,n} = \left(1 - \frac{\Delta\hat{t}}{\hat{\tau}}\right)(\hat{q}_y)^j_{m+1/2,n} + \frac{\Delta\hat{t}}{\hat{\tau}}\left(\frac{\hat{T}^j_{m+1/2,n-1/2} - \hat{T}^j_{m+1/2,n+1/2}}{\Delta\hat{x}} + \right.$$
$$+ (\hat{\eta}_1 + \hat{\eta}_2)\frac{(\hat{Q}_{yy})^j_{m+1/2,n+1/2} - (\hat{Q}_{yy})^j_{m+1/2,n-1/2}}{\Delta\hat{y}} +$$
$$\hat{\eta}_1\frac{(\hat{Q}_{xy})^j_{m+1,n} - (\hat{Q}_{xy})^j_{m,n}}{\Delta\hat{x}} +$$
$$\left. + \hat{\eta}_2\frac{(\hat{Q}_{xx})^j_{m+1/2,n+1/2} - (\hat{Q}_{xx})^j_{m+1/2,n-1/2}}{\Delta\hat{y}}\right), \tag{5.38c}$$

$$(\hat{Q}_{xx})^j_{m+1/2,n+1/2} = \frac{(\hat{q}_x)^j_{m+1,n+1/2} - (\hat{q}_x)^j_{m,n+1/2}}{\Delta\hat{x}}, \tag{5.38d}$$

$$(\hat{Q}_{xy})^j_{m,n} = \frac{(\hat{q}_x)^j_{m,n+1/2} - (\hat{q}_x)^j_{m,n-1/2}}{\Delta\hat{y}}, \tag{5.38e}$$

$$\hat{Q}_{yx})^j_{m,n} = \frac{(\hat{q}_y)^j_{m+1/2,n} - (\hat{q}_y)^j_{m-1/2,n}}{\Delta\hat{x}}, \tag{5.38f}$$

$$(\hat{Q}_{yy})^j_{m+1/2,n+1/2} = \frac{(\hat{q}_y)^j_{m+1/2,n+1} - (\hat{q}_y)^j_{m+1/2n}}{\Delta\hat{y}}. \tag{5.38g}$$

5.3.2 Numerical results

Here, let us start with the Fourier heat equation and present the plots that are used to display the temperature and heat flux density history in time and space. We want to point out that we have a different code for the Fourier equation in which we solve only the Fourier equation and not the simplification of the GK equation, hence there are no difficulties with the boundary conditions in this case, i.e **Q** is not used. Figure 5.14 represents the temperature histories at specified spatial points. The first column shows the front face, and each column increases the spatial step by 1/4, and the last one is related to the rear face of the sample. In addition, the first row indicates the

top side, and the last one presents the temperature history on the symmetry axis. We use the same plot concept for the GK equation as well.

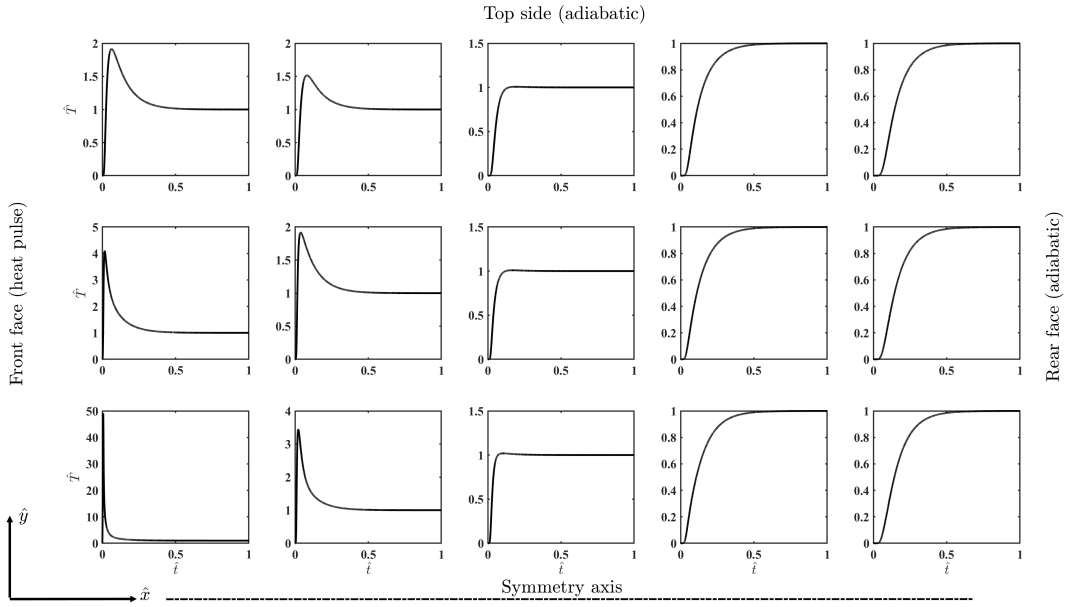

FIGURE 5.14: 2D Fourier solution in space and time, also indicating the corresponding boundary conditions.

Furthermore, it is insightful to check the vector plot for the heat flux field in which we can observe the effect of space-dependent excitation and compare it immediately with the corresponding temperature distribution, see Figure 5.15. Also, Figure 5.15 shows that it is straightforward to reproduce the well-known 1D solutions by applying a spatially homogeneous boundary condition. The curl of the heat flux field is identically zero. For all the subsequent calculations, we assign $R_{Y,\mathrm{P}} = 0.4$ with fixed spatial resolution ($\Delta\hat{x} = \Delta\hat{y} = 0.02$), and $\hat{\tau}_{\mathrm{P}} = 0.01$.

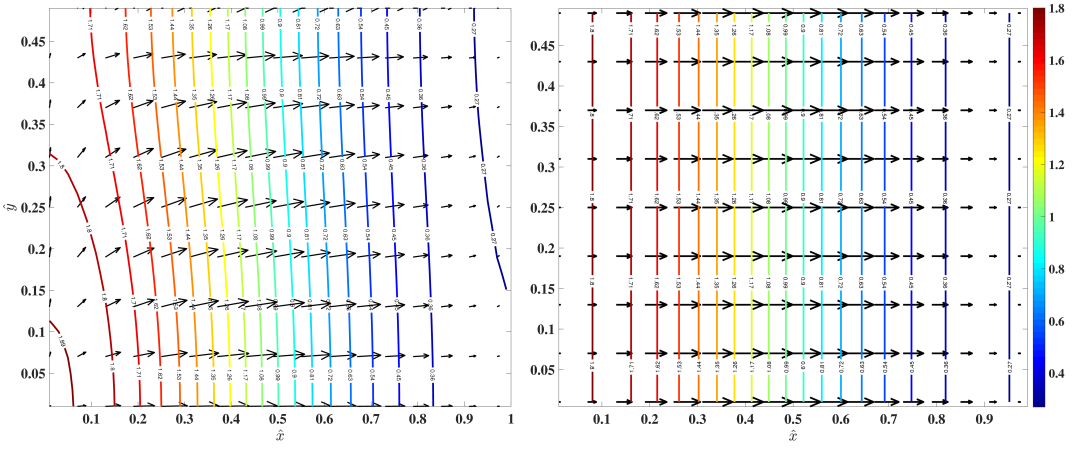

FIGURE 5.15: 2D vector plot of the heat flux field for the Fourier equation at $\hat{t} = 0.1$, using the same color bar for both figures. Left: spatially inhomogeneous heat pulse boundary condition. Right: spatially homogeneous heat pulse boundary condition.

Demonstration of Fourier resonance First, let us start by showing that the GK equation reproduces the Fourier solutions when $\hat{\eta}_1 = 0$, and $\hat{\eta}_2 = \hat{\tau} = 0.05$, Figure 5.16 indicate the difference between the two temperature fields (Fourier and GK). The observed errors are practically zero. This solution also supports our handling of **Q** on the boundary and extrapolation method as it reproduces the Fourier solution in a particular parameter setting. In this parameter setting, the $\nabla \times \nabla \times \mathbf{q}$ term vanishes in the Eq. (5.4), thus the Laplacian of **q** remains.

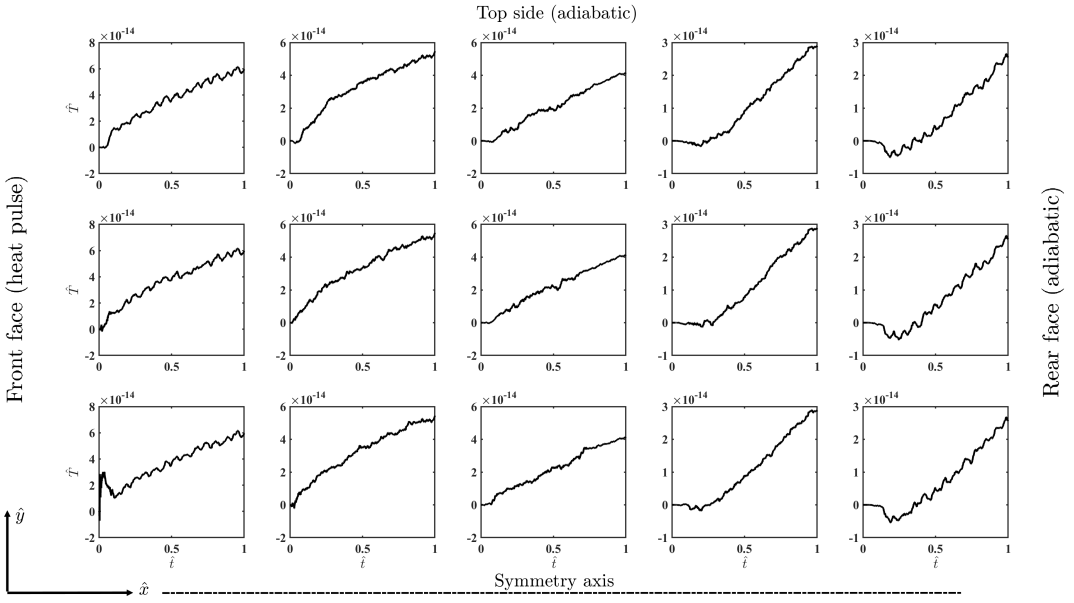

FIGURE 5.16: The difference between the Fourier and GK temperature histories when $\hat{\eta}_1 = 0$, and $\hat{\eta}_2 = \hat{\tau} = 0.05$.

Appreciable differences emerge when we keep $\hat{\tau} = 0.05$, but $\hat{\eta}_1 = \hat{\eta}_2 = 0.025$, i.e. despite that $\hat{\eta}_1 + \hat{\eta}_2 = \hat{\tau}$, the resonance condition is violated and the solution differs significantly from the Fourier equation, see Figure 5.17 for details.

Let us turn our attention to the most interesting and intriguing solutions when $\hat{\eta}_1 \neq 0$, and thus the curl of the heat flux field becomes meaningful.

Vorticity-free solution The solution is called over-diffusive if $\hat{\eta}_1 + \hat{\eta}_2 > \hat{\tau}$. Let us start with the case where we keep $\hat{\eta}_1 = 0$ to avoid the effects of the nonzero curl of the heat flux field. It is worth comparing the characteristics of the temperature history in the middle to the rear side. In the middle, the two distinct time scales are visible in the opposite direction to the rear side (see Figure 5.18). In a heat pulse experiment using heterogeneous materials, two distinct time scales are visible, and that numerical solution reflects the size dependence of the observation [23]. This effect may not be evident for thicker samples, and also depends on the material properties.

Figure 5.19 shows the 2D vector plot of the heat flux in which the over-diffusive behavior remains hidden; the temperature contours (isothermal lines) are slightly distorted compared to the Fourier case. Furthermore, since $\eta = 0$, the curl of the heat flux field should be zero, and this is reflected in Figure 5.19, too.

Solutions with strong vorticity Let us turn our attention to the reverse case in which we keep $\hat{\eta}_2 = 0$, and now let us investigate the effects of the parameter $\hat{\eta}_1$,

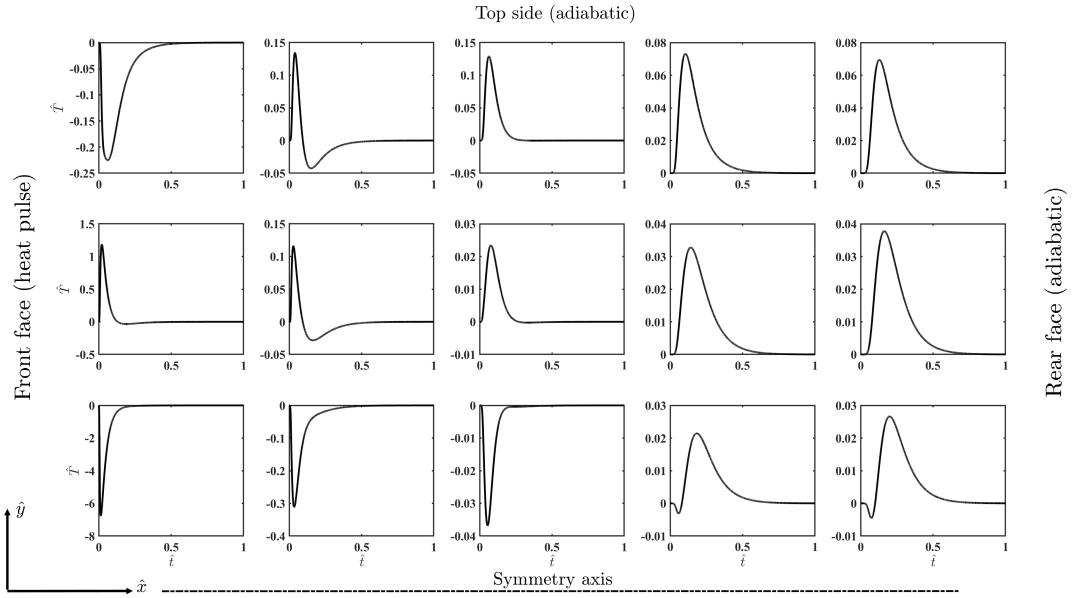

FIGURE 5.17: The difference between the Fourier and GK temperature histories when $\hat{\eta}_1 = \hat{\eta}_2 = 0.025$, and $\hat{\tau} = 0.05$.

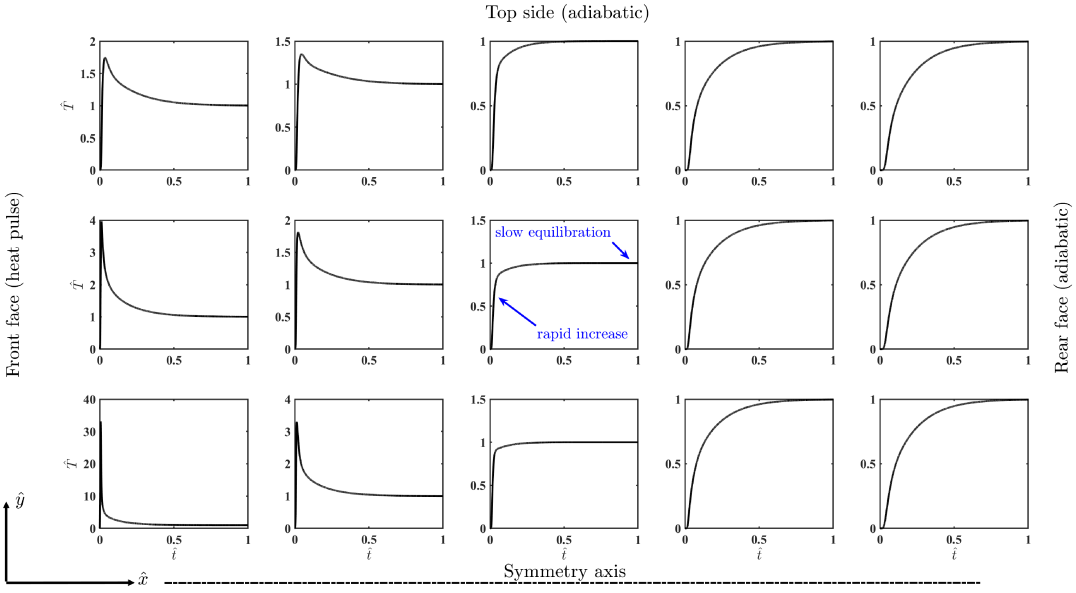

FIGURE 5.18: The GK temperature history when $\hat{\eta}_1 = 0$, $\hat{\eta}_2 = 0.1$, and $\hat{\tau} = 0.05$.

that is $\hat{\eta}_1 = 0.075$. Figure 5.20 illustrates the temperature history for the given spatial points. Comparing it with the previous case, we can observe a significantly different behavior. First, near the front face, the temperature decreases due to the significant curl effects. Let us stress that this is not identical to achievement of a negative absolute temperature. It should be noted that the apparent negative temperature is relative to the initial temperature on contrary to the observations of Zhukovsky [137]. However, the temperature field may exhibit unusual evolution in such a particular parameter setting since the GK equation is based on a hydrodynamic analogy, and the curl of the heat flux field may naturally appear. Here, we strengthened in particular this effect to make it easily observable. This is meaningful only in a two or three

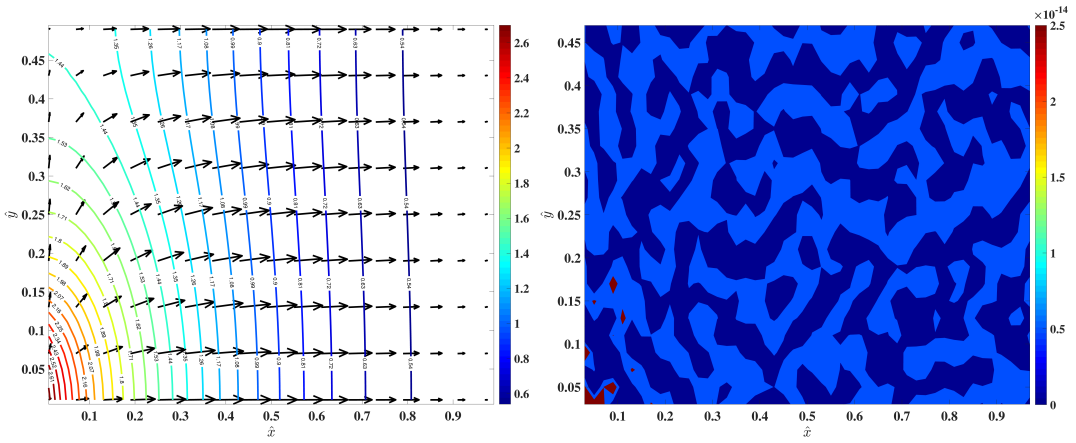

FIGURE 5.19: Left: 2D vector plot of the heat flux field when $\hat{\eta}_1 = 0$, $\hat{\eta}_2 = 0.1$, and $\hat{\tau} = 0.05$ at $\hat{t} = 0.1$. Right: the curl of the heat flux field is practically zero in accordance with the parameter settings.

dimensional setting. This temperature-decreasing effect disappears soon and is not observable for any other spatial domains. This is also depicted in Figure 5.21. Furthermore, contrary to the previous situations, the curl of the heat flux field becomes significantly larger (Figure 5.22).

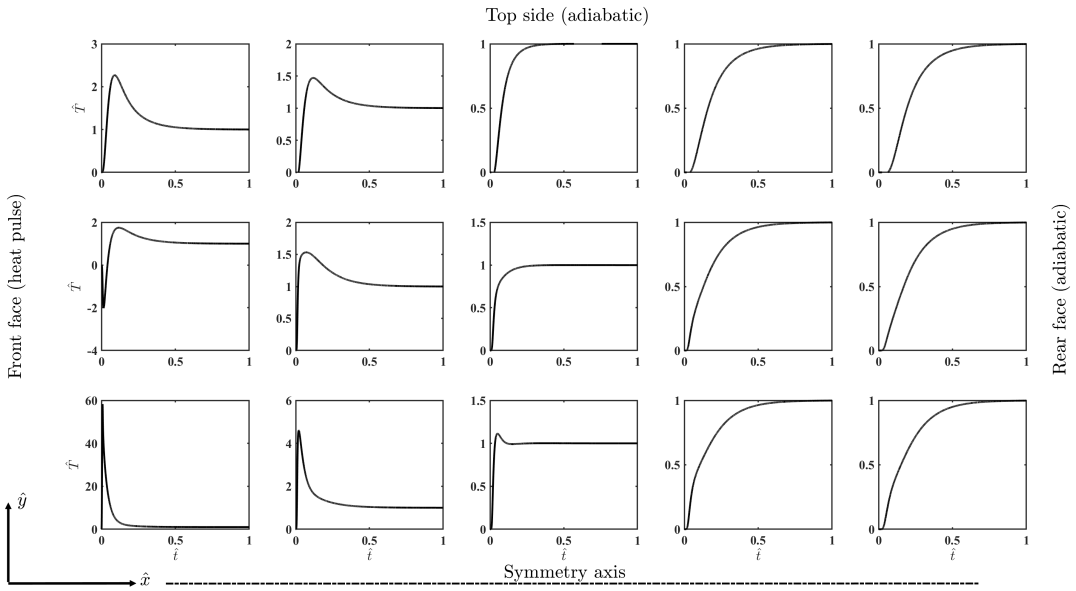

FIGURE 5.20: The GK temperature history when $\hat{\eta}_1 = 0.075$, $\hat{\eta}_2 = 0$, and $\hat{\tau} = 0.05$.

Deviation from the phonon hydrodynamic ratio Let us recall that the ratio $\hat{\eta}_2/\hat{\eta}_1 = 2$ is fixed in a phonon hydrodynamic approach, but this does not necessarily hold in a continuum framework. In order to make this difference evident, we provided solutions with respect to $\hat{\eta}_2/\hat{\eta}_1$. Figure 5.23 shows the rear side temperature history for three situations in which $\hat{\eta}_2/\hat{\eta}_1 = \{1.5, 2, 2.5\}$ with fixed $\hat{\eta}_1 = 0.05$. This does not highlight any remarkable property compared to the one-dimensional case, for which only the effect of $\hat{\eta}_1 + \hat{\eta}_2$ is observable, and the increase of the over-diffusion makes the temperature signal propagate faster.

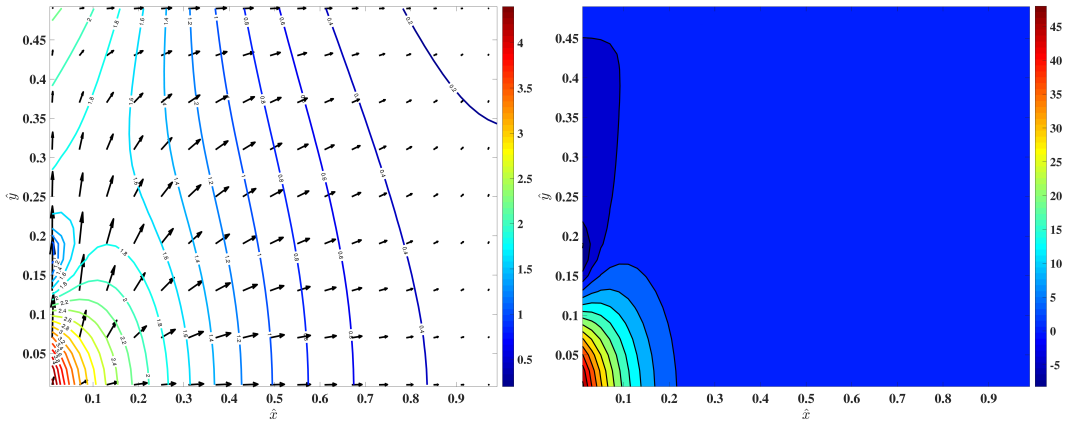

FIGURE 5.21: Left: 2D vector plot of the heat flux field when $\hat{\eta}_1 = 0.075$, $\hat{\eta}_2 = 0$, and $\hat{\tau} = 0.05$ at $\hat{t} = 0.1$. Right: the contour plot of the temperature field, highlighting the temperature-decrease effect next to the heat pulse at $\hat{t} = 0.01$.

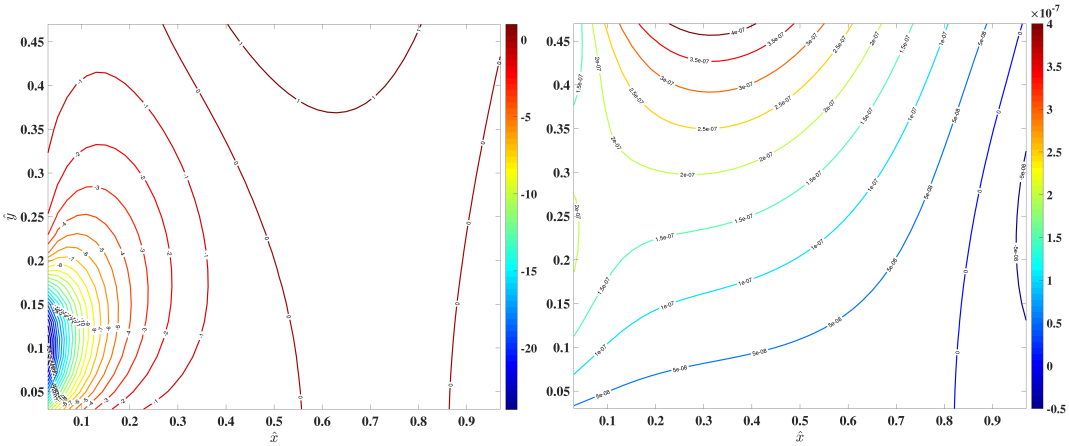

FIGURE 5.22: Left: the curl of the heat flux field when $\hat{\eta}_1 = 0.075$, $\hat{\eta}_2 = 0$, and $\hat{\tau} = 0.05$ right after the heat pulse at $\hat{t} = 0.01$. Right: the curl vanishes with time and becomes practically zero (at $\hat{t} = 1$).

However, if you consider the front-side temperature history in the middle (Figure 5.24), then it makes more visible how the ratio of $\hat{\eta}_2/\hat{\eta}_1$ modifies the solution. Decreasing $\hat{\eta}_2/\hat{\eta}_1$ amplifies the temperature-decrease effect near the heat pulse since $\hat{\eta}_1$ – the rotational part – becomes more dominant.

How does the curl of heat current density behave on the boundary? Previously, the auxiliary field $\mathbf{Q}$ was introduced to facilitate the discretization of the second-order spatial derivatives and make it easier to realize the boundary conditions properly. Since the diagonal elements of $\mathbf{Q}$ are inside the spatial domain, they are not directly related to the boundary conditions. However, the off-diagonals are not independent of the $\mathbf{q}$-boundary. An extrapolation from the bulk has been introduced to avoid defining of incompatible boundary data for the unknown off-diagonals, and thus avoiding introducing any artificial distortion. Now let us depict the difference between the Q_{xy} and Q_{yx} components in two cases. In fact, this difference is the only component of the curl of the in-plane heat current density. In the first case, $\hat{\eta}_1 = 0$ is considered, hence, the rotational term is zero ($\hat{\eta}_2 = \hat{\tau} = 0.05$). In the second case,

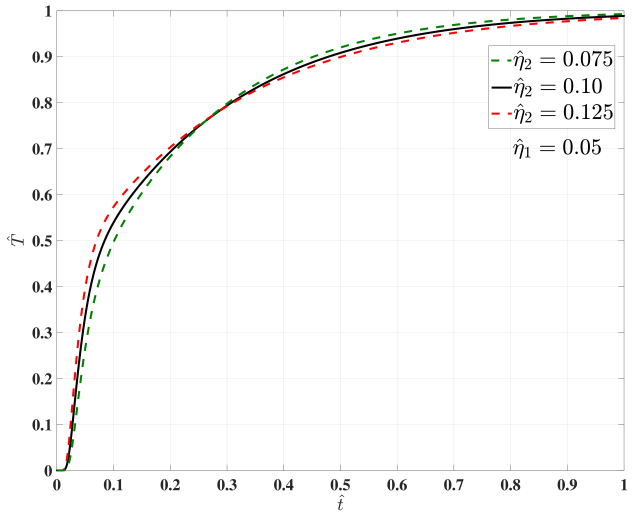

FIGURE 5.23: The GK temperature history on the rear side ($\hat{x} = 1$, $\hat{y} = 0.25$) when $\hat{\eta}_1 = 0.05$, $\hat{\tau} = 0.05$, and $\hat{\eta}_2 = \{0.075, 0.1, 0.125\}$, demonstrating the deviation from the phonon hydrodynamic ratio $\hat{\eta}_2/\hat{\eta}_1 = 2$.

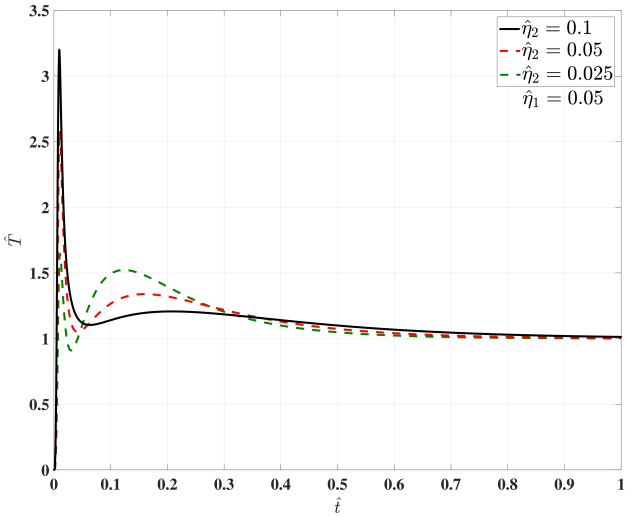

FIGURE 5.24: The GK temperature history on the front side ($\hat{x} = 0$, $\hat{y} = 0.25$) when $\hat{\eta}_1 = 0.05$, $\hat{\tau} = 0.05$, and $\hat{\eta}_2 = \{0.1, 0.05, 0.025\}$.

$\hat{\eta}_1 = \hat{\eta}_2 = 0.05$, and major differences are expected. Figure 5.25 presents their difference, highlighting that $\hat{\eta}_1$ indeed introduces significant changes in the evolution of off-diagonals of $\mathbf{Q}$, especially near the boundaries, but also particularly affecting the bulk behavior. Figure 5.26 illustates the time evolution in agreement with Eq. (5.5c), which presents an exponential decay in time.

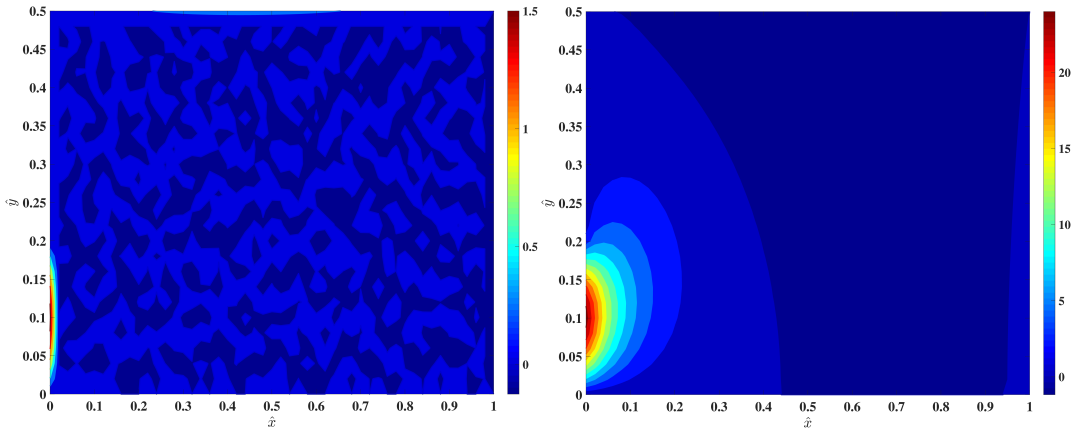

FIGURE 5.25: Left: $(\mathbf{q} \times \nabla)_z$ without the rotational term at $\hat{t} = 0.1$. Right: $-(\mathbf{q} \times \nabla)_z$ with the rotational term at $\hat{t} = 0.1$. The sign is changed in order to have colors correctly emphasizing the differences in magnitudes.

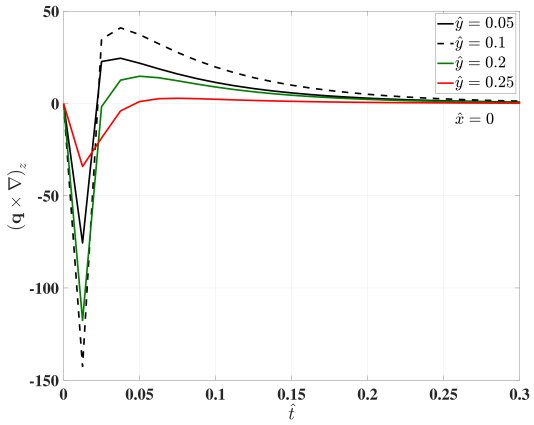

FIGURE 5.26: The time evolution of $(\mathbf{q} \times \nabla)_z$ including the rotational term on the front face, indicating that the vorticities are the strongest at the heat pulse, and quickly attenuate after $\hat{y} = 0.2$. Furthermore, shortly after the heat pulse, the exponential decay is apparent in agreement with Eq.(5.5c).

5.4 Heat transfer at nano-scale and boundary conditions: GK model

The heat transfer at nano-scale gives inspiration for several interesting research topics; what is the correct model to describe it in agreement with the experimental observations, or what is the best way of accounting for the interactions between the heat carriers and the lateral walls, for example, are two compelling questions that have been currently not satisfactorily answered. In this Section we principally deepen into the influence of the boundary conditions on the heat-flux behavior in the case of thin nano-wires. This analysis is performed here by employing a theoretical model which principally emphasizes the role played by the non-local effects. All the results carried out are analyzed in view of the second law of thermodynamics as well.

The last two decades have been the witnesses of an important surge in the searching of enhanced theoretical models beyond the classical Fourier law for the description of the heat conduction in out-of-equilibrium systems [53, 59, 138–143]. Among the several reasons which can be adduced to understand the above interest, the incessant rise of nano-technologies may be certainly considered as the principal one. Since nano-systems are usually employed in *highly* non-equilibrium situations, in fact, it is well-known that at nano-scale the classical approach of the macroscopic heat-transfer theory is no longer applicable, namely, it cannot be used to correctly describe and predict the thermo-mechanical behavior and properties of modern nano-devices [144–147]. Because of the very compact sizes involved and the high performances required, we note that at nano-scale there are very significant heat-transfer and heat-dissipation problems that have to be tackled and possibly solved in order to avoid the devices' burnout.

The nano-scale heat-transfer analysis can be addressed by different approaches [59, 148–151]; among them the macroscopic method based on the phonon hydrodynamics [122, 147, 152, 153] is worth of being considered since it easily allows to gain useful information about the physics of phonon motion [59]. Phonon hydrodynamics is interesting because it not only depicts, in a clear and intuitive way, the heat-conduction phenomenon, but also allows a refined mathematical analysis, especially if one is wondering what is the correct way to model the boundary conditions (BCs) [154]. For this purpose we note that the BCs, as well as the initial data (ID), have to be not only assigned in such a way that the corresponding initial boundary value problem (IBVP) is well posed, but they should also display clear physical meanings.

By looking at the phenomenon of nano-scale heat conduction as the final result of the regular motion of suitable *heat carriers* through the crystal lattice [152, 155], in several recent papers [154, 156, 157], for example) the authors proposed to assume a non-vanishing value for the tangential component $q_{\parallel} = \mathbf{q} \cdot \widehat{\mathbf{t}}$ of the local heat-flux vector $\mathbf{q}(\mathbf{X}, t)$ at the boundary $\partial\Omega$ of the medium, with $\widehat{\mathbf{t}}$ being the unit tangent vector to $\partial\Omega$. Up to a second-order approximation (in space), for example, the above assumption yields that a suitable way of assigning the BCs is

$$q_{\parallel} - C\ell\, \nabla q_{\parallel} \cdot \widehat{\mathbf{n}} + \alpha \ell^2\, \nabla \left(\nabla q_{\parallel} \cdot \widehat{\mathbf{n}} \right) \cdot \widehat{\mathbf{n}} = 0 \qquad \forall\, \mathbf{X} \in \partial\Omega,\, \forall\, t \geq 0 \tag{5.39}$$

wherein $\widehat{\mathbf{n}}$ stands for the outward unit normal vector to $\partial\Omega$.

Referring the readers to [152, 154, 156, 157] for comments about the physical standing of Eq. (5.39), here we only observe that therein ℓ stands for the mean-free path of the heat carriers; C and α, instead, are two (non-dimensional) parameters which are principally related to the scatterings of the heat carriers at the lateral walls. By means of the phonon-hydrodynamic approach it could be get idea from the Wu's slip model [158] of fluid-dynamics, for example, thus estimating those parameters as

$$C = \frac{2}{3} \left[\frac{3 - \nu\, p^3}{\nu} - \frac{3}{2} \left(\frac{1 - p^2}{\mathrm{Kn}} \right) \right] \tag{5.40a}$$

$$\alpha = \frac{1}{4} \left[p^4 + \frac{2}{\mathrm{Kn}^2} \left(1 - p^2 \right) \right], \quad p = \min\{\mathrm{Kn}^{-1}, 1\} \tag{5.40b}$$

wherein Kn is the so-called Knudsen number (i.e., the ratio between the mean-free path ℓ and the characteristic length of the system at hand) and the parameter $\nu \in (0, 1]$ is the momentum accommodation coefficient meant as the portion of total heat carriers that collide with the wall and that are reflected and spread by the lateral

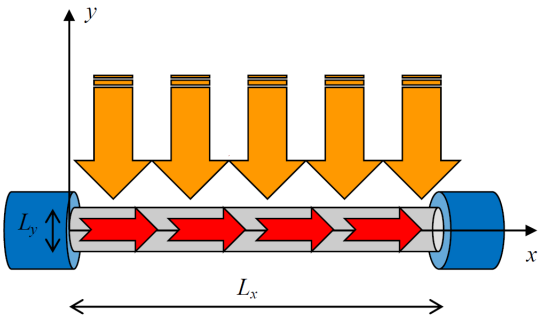

FIGURE 5.27: Thin nano-wire (i.e., the grey cylinder in figure) connected with two other nano-devices (i.e., the blu cylinders in figure) which are always kept at the same (constant) temperature. The thin nano-wire is initially perturbed by the application of an external heat flux perpendicular it (i.e., the vertical arrows – orange in figure) which generates a heat flux (i.e., the horizontal arrow – red in figure) longitudinally propagating throughout the nano-wire. The two Cartesian coordinates which characterizes the problem are x (spanning along the longitudinal direction) and y (spanning along the transversal direction). In figure the two characteristic sizes of the nano-wire L_x and L_y have been also indicated.

walls.

For the investigation of the effective role played by the above BCs on the heat transfer in a rigid nano-system Ω, in this thesis we merge the local balance of energy, i.e.,

$$c_v \partial_t \theta + \nabla \cdot \mathbf{q} = 0 \qquad \forall \mathbf{X} \in \Omega, \forall t \geq 0 \tag{5.41}$$

with a heat flux beyond the heat conduction beyond the classical Fourier law, i.e. GK. For the sake of clarity, in Eq. (5.41) $\theta = T - T_0$, wherein T_0 and T stand for the local-equilibrium (constant) and the non-equilibrium temperature values, respectively. However the temperature T is related to the internal energy (per unit volume) e by means of the relation $de = c_v dT$, with c_v being the specific heat at constant volume.

In order to reduce to a simpler level the aforementioned analysis, but focusing the attention on a situation that is worth to be considered at nano-scale, in this Section we suppose that a homogeneous thin nano-wire, connected with two other nano-cylindrical devices (both kept at the same constant temperature), is perturbed from its initial equilibrium by the application of an external heat flux perpendicular to it, as it is sketched in Fig. 5.27.

However, in the case of the system of Fig. 5.27, if the characteristic length of the transversal section, L_y is much smaller than the longitudinal characteristic size, L_x, we may investigate the particular situation in which the aforementioned external perturbation generates a heat flux only propagating in the longitudinal direction (which is characterized by the Cartesian coordinate x), namely, in the next we turn attention only to the situation in which the local heat flux reduces to

$$\mathbf{q} = [q(x,t), 0, 0] \tag{5.42}$$

Our aim is the determination of the unknown basic fields $\theta = \theta(x,t)$ and $q = q(x,t)$ in the one-dimensional domain $[0, L_x]$ (i.e., inside the nano-wire), provided that all the variations of those fields along the $y-$direction are vanishingly small.

5.4.1 L-GK in 1D with slip first/second order boundary conditions

A very usual starting point of the phonon-hydrodynamic approach is a consequence of the results obtained by Guyer and Krumhansl in 1966 [5, 6] wherein the authors formally solved the linearized Boltzmann equation for phonons [1] in terms of the eigenvectors of the normal-process collision operator. The solution they found was formally summarized therein by two macroscopic equations which relate the temperature variations θ with the heat flux $\mathbf{q}$. One of those equations (see Eq. (22b), or equivalently Eq. (58), in [5, 6] is the usual thermal-energy balance law, namely, it is practically Eq. (5.41) earlier introduced. The other one (see Eq. (57), or its particular form (59), in [5, 6]) is a generalized phonon-thermal-conductivity equation which reads as follows

$$\tau_r \partial_t \mathbf{q} + \mathbf{q} + \lambda \nabla\theta - \ell^2 \left(2\nabla\nabla\cdot\mathbf{q} + \nabla^2\mathbf{q}\right) = \mathbf{0} \qquad \forall\, \mathbf{X}\in\Omega,\, \forall\, t \geq 0 \tag{5.43}$$

where λ is the thermal conductivity corresponding to the Ziman limit, τ_r represents the relaxation time of resistive phonon scatterings (umklapp, mass-fluctuation, etc.) wherein the quasi-momentum (or the wave number) is not conserved, and ℓ is the mean-free path of phonons. The latter is related to the relaxation time of normal phonon scatterings, i.e., the part of phonon-phonon collisions in which the quasi-momentum (or the wave number) is conserved. The main focus of Eq. (5.43) is certainly the emphasis given to the non-local effects.

Equations (5.41) and (5.43) can be used to examine the second-sound propagation with damping, the Poiseuille flow in a phonon gas or other related problems [5, 6]. In particular here we consider the following IBVP

$$c_v \partial_t \theta + \partial_x q = 0 \qquad \forall\, x\in[0,L_x],\, \forall\, t\geq 0 \tag{5.44a}$$
$$\tau_r \partial_t q + q + \lambda \partial_x \theta - 3\ell^2 \partial_{xx} q = 0 \qquad \forall\, x\in[0,L_x],\, \forall\, t\geq 0 \tag{5.44b}$$
$$\theta(x,0) = 0 \qquad \forall\, x\in[0,L_x] \tag{5.44c}$$
$$q(x,0) = q^\bullet \sin\left(\pi\frac{x}{L_x}\right) \qquad \forall\, x\in[0,L_x] \tag{5.44d}$$
$$q(0,t) + C\ell\partial_x q(0,t) + \alpha\ell^2\partial_{xx} q(0,t) = 0 \qquad \forall\, t\geq 0 \tag{5.44e}$$
$$\theta(0,t) = \theta^\bullet \qquad \forall\, t\geq 0 \tag{5.44f}$$
$$q(L_x,t) - C\ell\partial_x q(L_x,t) + \alpha\ell^2\partial_{xx} q(L_x,t) = 0 \qquad \forall\, t\geq 0 \tag{5.44g}$$
$$\theta(L_x,t) = \theta^\bullet \qquad \forall\, t\geq 0 \tag{5.44h}$$

wherein the heat-flux amplitude $q^\bullet$ accounts for the amount of energy which is initially supplied to the nano-wire by the external heat flux, and $\theta^\bullet$ turns out information about the constant temperature value of the two nano-devices arranged at the two ends of the thin nano-wire.

Dimensionless problem

In order to obtain very general results (i.e. results which are independent both of the particular material, and of the thermodynamic conditions), it is convenient rewrite

[1] Phonons are elementary excitations which have a complete meaning only in the harmonic approximation.

Eqs. (5.44) in terms of non-dimensional quantities. Therefore, we introduce the following dimensionless quantities

$$\mathrm{x} = \frac{x}{L_x}, \qquad \mathrm{t} = \frac{t}{\tau_r}, \qquad \vartheta = \frac{\theta}{T_0}, \qquad h = \left(\frac{L_x}{\lambda T_0}\right) q \tag{5.45}$$

wherein, for the sake of simplicity, we also assume

$$\tau_r = \frac{\ell}{\mathrm{v}_p} \tag{5.46a}$$

$$\lambda = \frac{c_\mathrm{v}\,\tau_r\,\mathrm{v}_p^2}{3} \tag{5.46b}$$

with v_p being the average phonon-speed measured at T_0, [122]. We incidentally note that the identifications in Eqs. (5.46) imply that here the consequences of the non-linear effects related to the temperature dependence of the different material functions will be neglected.

Introducing Eqs. (5.45) and (5.46) into Eqs. (5.44) one may obtain

$$\partial_\mathrm{t}\vartheta + \frac{\mathrm{Kn}^2}{3}\partial_\mathrm{x} h = 0 \qquad \forall\,\mathrm{x}\in[0,1],\ \forall\,\mathrm{t}\in\mathbb{R}^+ \tag{5.47a}$$

$$\partial_\mathrm{t} h + h + \partial_\mathrm{x}\vartheta - 3\mathrm{Kn}^2\partial_{\mathrm{xx}} h = 0 \qquad \forall\,\mathrm{x}\in[0,1],\ \forall\,\mathrm{t}\in\mathbb{R}^+ \tag{5.47b}$$

$$\vartheta(\mathrm{x},0) = 0 \qquad \forall\,\mathrm{x}\in[0,1] \tag{5.47c}$$

$$h(\mathrm{x},0) = h^\bullet \sin(\pi\mathrm{x}) \qquad \forall\,\mathrm{x}\in[0,1] \tag{5.47d}$$

$$h(0,\mathrm{t}) + C\,\mathrm{Kn}\,\partial_\mathrm{x} h(0,\mathrm{t}) + \alpha\,\mathrm{Kn}^2\,\partial_{\mathrm{xx}} h(0,\mathrm{t}) = 0 \qquad \forall\,\mathrm{t}\in\mathbb{R}^+ \tag{5.47e}$$

$$\vartheta(0,\mathrm{t}) = \vartheta^\bullet \qquad \forall\,\mathrm{t}\in\mathbb{R}^+ \tag{5.47f}$$

$$h(1,\mathrm{t}) - C\,\mathrm{Kn}\,\partial_\mathrm{x} h(1,\mathrm{t}) + \alpha\,\mathrm{Kn}^2\,\partial_{\mathrm{xx}} h(1,\mathrm{t}) = 0 \qquad \forall\,\mathrm{t}\in\mathbb{R}^+ \tag{5.47g}$$

$$\vartheta(1,\mathrm{t}) = \vartheta^\bullet \qquad \forall\,\mathrm{t}\in\mathbb{R}^+ \tag{5.47h}$$

where $h^\bullet = \left(\frac{L_x}{\lambda T_0}\right) q^\bullet$ and $\vartheta^\bullet = \frac{\theta^\bullet}{T_0}$. Moreover, in Eqs. (5.47), as well as in the following, the Knudsen number is expressed by the ratio $\mathrm{Kn} = \frac{\ell}{L_x}$.

Numerical results: Behavior of the dimensionless heat flux

Here we highlight some comments about the behavior of the non-dimensional heat flux $h(\mathrm{x},\mathrm{t})$ arising from the IBVP in Eqs. (5.47) once the parameters C and α have been computed by means of the Wu's model [158], i.e., by employing Eqs. (5.40). We have solved this model with a staggered field FDM presented in Appendix B. We have also set $h^\bullet = 1$ and $\vartheta^\bullet = 0$, the latter values pointing out that both the left-hand cylindrical nano-device, and the right-hand one in Figure 5.27 act as thermal dissipators. However we note that those two values do not influence the qualitative results plotted below.

Since the above behavior is principally influenced by the Knudsen number Kn and the accommodation parameter ν, below we separately deepen into the role played by them.

- **The influence of the Knudsen number** Kn In Fig. 5.28 we plot the behavior of the non-dimensional heat flux h versus x (i.e., the longitudinal axis in sub-figures (a)–(d)) for different time instants t (i.e., t = 0.001 in (a), t = 0.01 in (b), t = 0.1 in (c) and t = 1 in (d)).

  For computational needs, in order to point out only the role played by the Knudsen number on the behavior of the heat flux, in obtaining the results plotted in Fig. 5.28 we set $\nu = 0.3$ in Eqs. (5.40), we assume that portion of phonons that is diffusively reflected by the walls is 30% of the phonons colliding at each boundaries.

  As it can be clearly seen from Fig. 5.28, in the case of the GK model the larger Kn, the faster h tends to its plateau value, i.e., the value attained by h at the boundary.

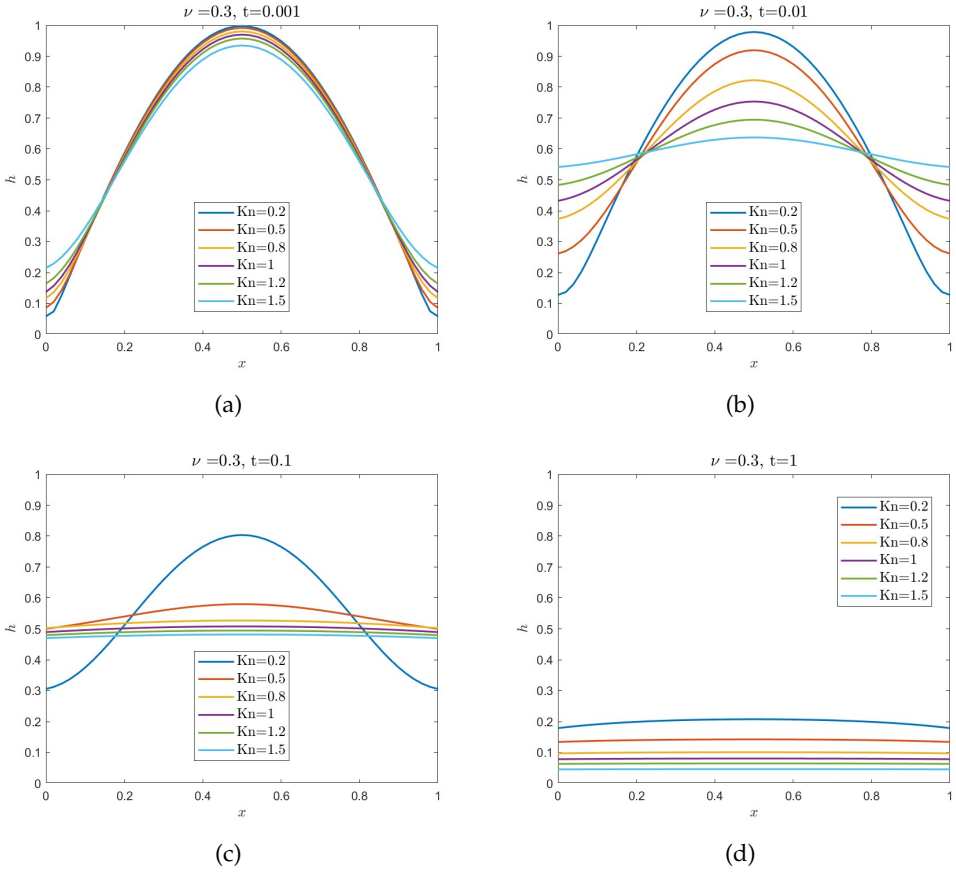

FIGURE 5.28: Behavior of the non-dimensional heat flux $h(x,t)$ for different values of the Knudsen numbers: theoretical results arising from the numerical solution of the IBVP in Eqs. (5.47) with: $h^\bullet = 1$, $\vartheta^\bullet = 0$, and $\nu = 0.3$. The two parameters C and α, instead, arise from Eqs. (5.40).

- **The influence of the accommodation parameter** ν In Fig. 5.29 we plot the behavior of the non-dimensional heat flux h versus x (i.e., the longitudinal axis in sub-figures (a)–(e)) for different time instants t (i.e., t = 0.001 in (a) and (d), t = 0.01 in (b) and (e), t = 0.1 in (c) and (f)).

For computational needs, in order to point out only the role played by the accommodation parameter on the behavior of the heat flux, in the results plotted in Fig. 5.29 we set both Kn $=$ 0.8, and Kn $=$ 1.5, namely, we investigate the regime of heat transfer both in the case of a moderate Kn, and in the case of a large Kn.

As it can be clearly seen from Fig. 5.29, the larger ν, the smaller the plateau value of h, both for a moderate value of Kn, and for a large value of it.

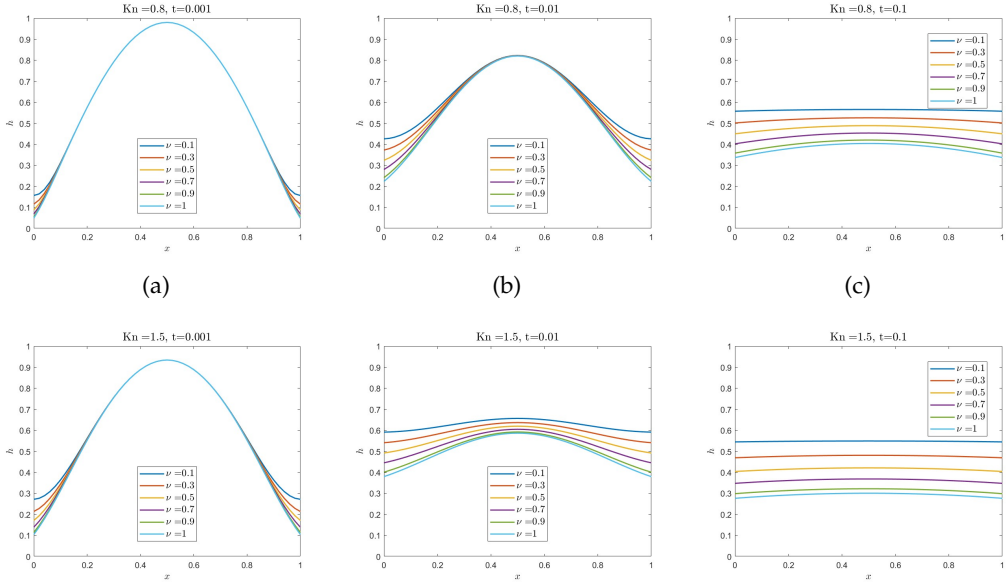

FIGURE 5.29: Behavior of the non-dimensional heat flux $h(x,t)$ for different values of the accommodation parameter: theoretical results arising from the numerical solution of the IBVP in Eqs. (5.47) with: $h^\bullet = 1$, $\vartheta^\bullet = 0$, Kn $= 0.8$ (sub-figures (a)–(c)), and Kn $= 1.5$ (sub-figures (d)–(e)). The two parameters C and α, instead, arise from Eqs. (5.40).

5.4.2 Thermodynamic considerations

Besides a good fit of the theoretical predictions with the experimental evidences, an important benchmark of a theoretical model is certainly its agreement with the second law of thermodynamics: if the model satisfies it, in fact, then one is sure that all the mathematical solutions of the field equations are in principle meaningful from the physical point of view [159].

The second law of thermodynamics states that the specific-entropy production σ_s has to be non-negative along any admissible thermodynamic process [53]. A theoretical model is compatible with the second law if, and only if, the basic fields predicted by it are such that the last term in left-hand side of the specific-entropy balance law, i.e.,

$$\partial_t s + \nabla \cdot \mathbf{J}_s - \sigma_s = 0 \qquad \forall\, \mathbf{X} \in \Omega,\ \forall\, t \geq 0 \tag{5.48}$$

where $\mathbf{J}_s$ is the flux and σ_s represents the production of the specific entropy s, that is never smaller than zero $\forall\, \mathbf{X} \in \Omega$ and $\forall\, t \geq 0$.

Therefore, here we analyze the results of Secs. 5.1 in view of the second law.

The GK model and the second law

The agreement between the GK model (based on Eqs. (5.41) and (5.43)) and the second law of thermodynamics can be proved by different approaches [53].

In [59], for example, it has been shown that in the framework of Extended Irreversible Thermodynamics the compatibility of those equations with the second law of thermodynamics, provided the following constitutive relations for the specific-entropy flux and entropy production, respectively

$$\mathbf{J}_s^{\mathrm{GK}} = \frac{\mathbf{q}}{T} - \frac{\ell^2}{\lambda T^2}\nabla\mathbf{q}\cdot\mathbf{q} \qquad \forall \mathbf{X}\in\Omega,\ \forall t\geq 0 \tag{5.49a}$$

$$\sigma_s^{\mathrm{GK}} = \frac{\mathbf{q}\cdot\mathbf{q}}{\lambda T^2} + \frac{\ell^2}{\lambda T^2}\left[(\nabla\mathbf{q})\cdot(\nabla\mathbf{q})^T + 2\,(\nabla\cdot\mathbf{q})\,(\nabla\cdot\mathbf{q})\right] \qquad \forall \mathbf{X}\in\Omega,\ \forall t\geq 0 \tag{5.49b}$$

in the non-equilibrium temperature approximation [120] and when the relaxation times of the higher-order fluxes are negligible small [59]. In the special case of the problem described previous, Eqs. (5.49) reduce

$$J_s^{\mathrm{GK}} = \frac{q}{T}\left(1 - \frac{\ell^2}{\lambda T}\partial_x q\right) \qquad \forall\, x\in[0,L_x],\ \forall\, t\geq 0 \tag{5.50a}$$

$$\sigma_s^{\mathrm{GK}} = \frac{1}{\lambda}\left[\left(\frac{q}{T}\right)^2 + 3\left(\frac{\ell}{T}\partial_x q\right)^2\right] \qquad \forall\, x\in[0,L_x],\ \forall\, t\geq 0 \tag{5.50b}$$

which finally become

$$j_s^{\mathrm{GK}} = \left(1 - \mathrm{Kn}^2\,\partial_{\mathsf{x}} h\right)\left(\frac{h}{1+\vartheta}\right) \qquad \forall \mathsf{x}\in[0,1],\ \forall \mathsf{t}\in\mathbb{R}^+ \tag{5.51a}$$

$$\Sigma_s^{\mathrm{GK}} = \frac{h^2 + 3\,(\mathrm{Kn}\,\partial_{\mathsf{x}} h)^2}{(1+\vartheta)^2} \qquad \forall \mathsf{x}\in[0,1],\ \forall \mathsf{t}\in\mathbb{R}^+ \tag{5.51b}$$

if we further introduce the following non-dimensional quantities

$$j_s = \left(\frac{L_x}{\lambda}\right) J_s \qquad \Sigma^s = \left(\frac{L_x^2}{\lambda}\right)\sigma^s \tag{5.52}$$

In terms of the above non-dimensional quantities, in the case of the GK model the coupling of Eqs. (5.48) and (5.49) yields the profile of the (non-dimensional) specific-entropy variation

$$\Delta\pi = \frac{L_x^2}{\tau_r\lambda}\,(s - s_0) \qquad \forall \mathsf{x}\in[0,1]\,,\ \forall \mathsf{t}\in\mathbb{R}^+ \tag{5.53}$$

plotted in Fig. 5.30, with s_0 being the equilibrium value of s, that is, its initial value.

From the analysis of Fig. 5.30 it can be inferred that in the case of the GK model the entropy difference $\Delta\pi$, in any $\mathsf{x}\in[0,1]$, reachs its maximum value in an initial very narrow time interval; afterward it only displays small variations. Whatever the generic point of the thin nano-wire is, therefore, we may claim that the entropy tends to its plateau value without displaying sensibly large variations.

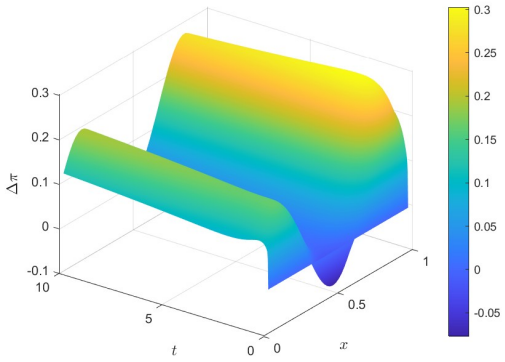

FIGURE 5.30: Behavior of the non-dimensional entropy difference $\Delta\pi\,(x,t)$ in Eq. (5.53) when the GK-model is employed, namely, when Eqs. (5.51) hold.

Chapter 6

Other Applications

This Chapter presents the possible applications of non-Fourier type equations including description of heat transport in biological tissue and laser welding

Firstly, in Section 6.1, a hyperbolic heat transport model for a homogeneously perfused biological tissue irradiated by a laser beam is discussed. The non-Fourier-like bioheat equation thus obtained is solved analytically by using the Laplace transform method., where the òaser heating is considered as internal heat source. The exact solution found here can be used to study the evolution of the temperature within the tissues during thermal therapy. However, the effect of the thermal relaxation phenomena on the temperature profiles in the tissue during and after laser application is investigated.

Subsequentely, in the Section 6.2 the numerical results obtained for a welding laser process on a metal plate using the Fourier law is obtained. Particular attention will be paid to possible future extensions of this model by introducing relaxation times.

6.1 Heat transport in Biological tissue

The study of mathematical models for heat transport in living tissues is an interesting topic for several researchers. The scrupulous description of the thermal interaction between vasculature and tissues is very important also connected with constant improvements of medical technology. In general, all living systems do not exhibit a uniform temperature in organs and blood. This non uniformity of the temperature induces an energy transfer among organs, tissues and the perfused blood. Heat transport in biological tissues, usually modeled with the *bioheat equation*, is not simple to analyze since it involves thermal conduction in tissues, convection and perfusion of blood, and metabolic heat generation. In fact, several authors have introduced various mathematical models of bioheat transfer generalizing the classic Pennes's bioheat equation [160]. This equation describes the thermal behavior of tissue by taking into account several terms influencing the heat transfer at the tissue surface: the heat exchange between the tissue surface and the environment, the conduction through the tissue, the energy transfer due to blood circulation in the tissue, and the heat generation due to local metabolism. Pennes [160], investigating the thermal behavior in forearm skin, proposed the equation

$$\rho_t \, c_t \, \partial_t T = k \, \partial_{xx} T + \rho_b \, c_b \, w_b (T - T_a) + q_{met}, \tag{6.1}$$

where ρ_t, c_t, k, ρ_b and c_b are the density, the specific heat, and the thermal conductivity of skin tissue, the density and specific heat of blood, respectively. Moreover, the quantities w_b, T and T_a are the blood perfusion rate, the skin tissue and arterial blood temperatures, respectively, whereas q_{met} is the metabolic heat generated by the

skin tissue. Since temperature variations in biological tissues depend on many phenomena, various generalizations of this equation have been proposed. Among these extensions, a relevant role is played by models of bioheat transfer where the living tissues are assumed to be deformable porous media [161–166]. This approach implies the necessity of introducing two energy equations for the tissue and the blood. In such a framework, important effects such as the vascular geometry and size, the blood flow and direction, the thermal diffusion and the local thermal nonequilibrium between the blood and peripheral tissues are included.

In the modelization of transport phenomena in porous media, it is possible to describe the living structure composed by a fluid phase (the blood) and a solid matrix (the tissues). Because of the metabolism, a volumetric heat generation in the solid part occurs. Recently, Xuan and Roetzel [167, 168], applied this approach to human tissues, where the porous medium models the tissue cells and the interlinked voids where arterial or venous blood flows.

By using the principle of local thermal nonequilibrium between the tissue and the blood, the thermal energy exchange between the tissue and the blood in a given volume element is formulated as follows [167]:

$$(1-\phi)\rho_t c_t \partial_t T_t = \nabla\cdot((1-\phi)k_t\nabla T_t) + h_{bt}(T_b - T_t) + (1-\phi)q_{met}, \tag{6.2a}$$

$$\phi\rho_b c_b \partial_t T_b = \nabla\cdot(\phi k_b \nabla T_b) - h_{bt}(T_b - T_t) + \phi\rho_b c_b \mathbf{v}_b\cdot\nabla T_b, \tag{6.2b}$$

ϕ, T_t, t_b, k_t, k_b, $\mathbf{v}_b$ and h_{bt} being the porosity of the tissue, the local arterial blood averaged temperature, the local tissue averaged temperature, the tissue thermal conductivity tensor, the blood thermal conductivity tensor, the blood velocity vector and the interstitial convective heat transfer coefficient, respectively. Moreover, the energy equations for both phases are coupled by the interstitial convective heat transfer, representing the heat transfer to the tissue due to blood convection, i.e. the heat exchange rate through the boundary surface between the blood phase and the solid matrix due the local thermal nonequilibrium, [166].

Although the bioheat equation can be valid in several situations, a model that considers a finite speed of propagation of thermal energy is crucial in surgical or therapeutic procedures (such as radiofrequency heating, irradiation, ...) where short heating times occur. In such cases, a non-Fourier type model should be considered by introducing a hyperbolic heat transfer equation by introducing a thermal relaxation time τ_R of the tissue. The hyperbolicity guarantees a finite speed of heat propagation [1–3], which is inversely proportional to τ_R. In many medical treatments, the laser heating of biological tissues is widely used. Consequently, the details of the heat transfer and of the related thermo-mechanical properties of tissues are essential from a medical viewpoint.

Since the thermomechanical response of the skin to various therapeutic temperatures during laser irradiation is not completely known. It is important to investigate the thermal behaviour of tissues during laser heating. Many mathematical models of heat conduction in biological tissues irradiated with laser are described in the literature [169–173]. In most of these contributions, the temperature distribution in the tissues were obtained by using the heat transfer equation proposed by Pennes. Here, we focus on the analysis of a non-Fourier bioheat transfer model describing the laser heating of skin tissue, the solutions will be found by means of the Laplace transform.

6.1.1 Formulation of heat transport model for blood perfused tissues

We consider a semi-infinite fragment of homogenous isotropic biological tissue. Let us suppose that the whole tissue surface is influenced by the laser energy; thus, we will solve the heat transfer equation in a one-dimensional setting, where the unique spatial variable x follows the direction of the laser beam. Furthermore, since blood vessels have small sizes, an acceptable approximation consists in assuming the equality between the tissue and blood temperature in a given volume element, i.e., $T_t = T_b = T$. Hence, the two equations (6.2) reduce to a single equation, say

$$\begin{aligned}[(1-\phi)\rho_t\, c_t + \phi\, \rho_b\, c_b]\, \partial_t T = \nabla \cdot \{[(1-\phi)\, k_t + \phi\, k_b]\, \nabla T\} - \phi\, \rho_b\, c_b \mathbf{v}_b \cdot \nabla T \\ + (1-\phi) q_{met}.\end{aligned} \tag{6.3}$$

Let us remark that the second term on the right hand side in (6.3) expresses the contribution to heat transfer due to blood perfusion. In the following, we suppose that the latter corresponds to the perfusion source term that in Pennes equation (6.1) was taken equal to $\rho_b c_b w_b (T - T_a)$, being w_b the flow rate of blood in the tissue per unit volume. This term is derived under the assumptions that in equilibrium conditions between the capillary tube and the tissue, locally the venous temperature is equal to the tissue temperature. Moreover, the arterial temperature is considered uniform throughout the tissue.

Our mathematical model turns out to be hyperbolic since we introduce a relaxation time τ_R for the tissue. In fact, if we substitute the Fourier' law used in equation (6.3) with the Cattaneo equation for heat flux $\mathbf{q}$, i.e.

$$\tau_R\, \partial_t \mathbf{q} + \mathbf{q} = -[(1-\phi)\, k_t + \phi\, k_b]\, \nabla T,$$

we obtain

$$\begin{aligned}[(1-\phi)\rho_t\, c_t + \phi\, \rho_b\, c_b]\, \partial_t T = -\nabla \cdot \mathbf{q} - \phi\, \rho_b\, c_b\, w_b (T - T_a) + (1-\phi) q_{met}, \\ \tau_R\, \partial_t \mathbf{q} + \mathbf{q} = -[(1-\phi)\, k_t + \phi\, k_b]\, \nabla T.\end{aligned}$$

and considering an additional term which is responsible for the effect of laser heat source on skin tissue, the resulting hyperbolic bioheat transfer equation (6.3), in a semi-infinite domain $\Omega = [0, +\infty)$, reads

$$\begin{aligned}\tau_R\, [(1-\phi)\rho_t\, c_t + \phi\, \rho_b\, c_b]\, \partial_{tt} T + [(1-\phi)\rho_t\, c_t + \phi\, \rho_b\, c_b + \tau_R\, \phi\, \rho_b\, c_b\, w_b]\, \partial_t T = \\ = [(1-\phi) k_t + \phi\, k_b]\, \partial_{xx} T + \phi\, \rho_b\, c_b\, w_b (T_a - T) + (1-\phi) q_{met} \\ + (1-\phi)\, [q_{laser} + \tau_R\, \partial_t q_{laser}]\,,\end{aligned} \tag{6.4}$$

Let us model the effect of laser as an internal heat source q_{laser}, and assign the following initial conditions

$$\begin{aligned}T(x,0) &= T_0 \\ \partial_t T(x,0) &= 0.\end{aligned}$$

and boundary conditions

$$\begin{aligned}\partial_x T(0,t) &= 0, \\ \lim_{x\to\infty} \partial_x T(x,t) &= 0,\end{aligned}$$

where T_0 is the initial temperature, i.e., the tissue temperature before heating. Moreover, let us suppose that, for the small values of the absorption coefficient of tissue a, ($[a] = m^{-1}$), the laser effect is described by the Beer-Lambert's law [174]

$$q_{laser} = a\, I_0\, \exp(-ax)\, H(t_{laser} - t),$$

representing the energy absorption of the laser irradiation. Here, I_0 is the constant irradiation intensity at the skin surface ($[q_{laser}] = Wm^{-2}$), $H(t)$ is the Heaviside function, t_{laser} is the instant the laser is removed, and x is the depth of the tissue.

6.1.2 Analytic solution

Here, we determine the analytic solution of the hyperbolic bioheat model 6.4 by applying the Laplace transform. It is convenient to write the system in the dimensionless form, choosing the following dimensionless variables

$$\eta = A\, t, \qquad \xi = B\, x, \qquad \theta(\xi, \eta) = C\,(T - T_a), \tag{6.5}$$

wherein A, B, C are suitably chosen, can be rewritten the equation (6.4) in the following form

$$\partial_{\eta\eta}\theta + \partial_\eta\theta = \partial_{\xi\xi}\theta - \gamma\theta + \Gamma q_{met} + \lambda \exp\left(-a\frac{\xi}{B}\right) g(\eta), \tag{6.6}$$

for the details see Appendix C.1. The dimensionless initial and boundary conditions are expressed by:

$$\begin{aligned} \theta(\xi, 0) &= \theta_0, \\ \partial_\eta\theta(\xi, 0) &= 0, \end{aligned}$$

and

$$\begin{aligned} \partial_{\tilde{\xi}}\theta(0, \eta) &= 0, \\ \lim_{\xi\to\infty} \partial_{\tilde{\xi}}\theta(\xi, \eta) &= 0, \end{aligned}$$

respectively, where

$$\theta_0 = \frac{(1 + \tilde{\beta} + \Lambda)^2}{T_0(1 + \tilde{\beta})}(T_0 - T_a).$$

By taking Laplace transform with respect to t [175], and defining

$$\begin{aligned} \hat{\theta}(\xi, s) &:= \mathcal{L}[\theta(\xi, \eta)], \\ \hat{g}(s) &:= \mathcal{L}[g(\eta)], \end{aligned}$$

after multiplying the equation (6.6) by $\exp(-s\eta)$ and integrating in $[0, +\infty)$, one gets:

$$\partial_{\xi\xi}\hat{\theta}(\xi, s) - (s^2 + s + \gamma)\hat{\theta}(\xi, s) = -(1 + s)\theta_0 - s\Gamma q_{met} - \lambda \exp\left(-a\frac{\xi}{B}\right)\hat{g}(s); \tag{6.7}$$

moreover, the Laplace transform of the boundary conditions yields:

$$\partial_{\xi}\hat{\theta}(0,s) = 0, \tag{6.8}$$

$$\lim_{\xi\to\infty} \hat{\theta}(\xi,s) = 0. \tag{6.9}$$

Solving the homogeneous equation associated of (6.7), and testing with a particular solution $\hat{\theta}_{part}$, one gets the general solution:

$$\hat{\theta}(\xi,s) = \hat{\theta}_{hom}(\xi,s) + \hat{\theta}_{part}(\xi,s), \tag{6.10}$$

having the following explicit form:

$$\begin{aligned}\hat{\theta}(\xi,s) = c_1 \exp\left(\sqrt{s^2+s+\gamma}\,\xi\right) + c_2 \exp\left(-\sqrt{s^2+s+\gamma}\,\xi\right)\\ + \frac{(1+s)\,\theta_0 + s\Gamma q_{met}}{s^2+s+\gamma} - \frac{\lambda\hat{g}(s)\,B^2}{a^2 - B^2\,(s^2+s+\gamma)} \exp\left(-\frac{a}{B}\,\xi\right).\end{aligned} \tag{6.11}$$

Substituting the boundary conditions (6.8) in the derivative respect to ξ of the general solution, the expression of the coefficients c_1, c_2 are determined

$$c_1 = 0, \quad c_2 = \frac{\lambda\, a\, \hat{g}(s)\, B}{[a^2 - B^2(s^2+s+\gamma)]\sqrt{s^2+s+\gamma}}. \tag{6.12}$$

Moreover, by substituting the relations (6.12) into equation (6.11), the function $\hat{\theta}(\xi,s)$ on the Laplace domain becomes:

$$\begin{aligned}\hat{\theta}(\xi,s) = \frac{\lambda a \hat{g}(s) B}{[a^2 - B^2\,(s^2+s+\gamma)]\sqrt{s^2+s+\gamma}} + \exp\left(-\sqrt{s^2+s+\gamma}\,\xi\right)\\ + \frac{(1+s)\,\theta_0 + s\Gamma q_{met}}{s^2+s+\gamma} - \frac{\lambda\hat{g}(s)\,B^2}{a^2 - B^2(s^2+s+\gamma)} \exp\left(-\frac{a}{B}\xi\right).\end{aligned} \tag{6.13}$$

In order to get the wanted temperature, it is necessary to compute the inverse of the Laplace transform

$$\theta(\xi,\eta) = \mathcal{L}^{-1}\left\{\hat{\theta}(\xi,s)\right\};$$

this computation is not easy and involves different steps. For this reason we split the calculation of each addend, and use the inverse Laplace tables [175], for the details see Appendix C.2.

Finally, by introducing the inverse Laplace transform of all the addends, i.e. (C.5)-(C.6)-(C.7)-(C.8) calculated in Appendix C.2, in the relation (6.13), the temperature $\theta(\xi,\eta)$ reads

$$\begin{aligned}\theta(\xi,\eta) = \mathcal{L}^{-1}\left\{\frac{\lambda\, a\, \hat{g}(s)\, B}{[a^2 - B^2\,(s^2+s+\gamma)]\sqrt{s^2+s+\gamma}} \exp\left(-\sqrt{s^2+s+\gamma}\,\xi\right)\right\} +\\ + \mathcal{L}^{-1}\left\{\frac{1+s}{s^2+s+\gamma}\theta_0\right\} +\\ + \mathcal{L}^{-1}\left\{\frac{s}{s^2+s+\gamma}\Gamma q_{met}\right\} + \mathcal{L}^{-1}\left\{\frac{-\lambda\,\hat{g}(s)\,B^2}{a^2 - B^2\,(s^2+s+\gamma)} \exp\left(-\frac{a}{B}\xi\right)\right\}.\end{aligned}$$

Finally, coming back to the original physical variables, the following solution for $\theta(x, y)$ is obtained

$$T(x,t) = \frac{T_0(1+\tilde{\beta})}{(1+\tilde{\beta}+\Lambda)^2} \cdot \theta(B\,x, A\,t) + T_a.$$

6.1.3 Results and discussion

We analyze the analytic solution obtained before, in order to discuss the distribution of the temperature in a biological tissue as a function of the thermal relaxation time τ_R, also considering different values for blood perfusion ω_b. Thus, the effects of laser irradiation time, laser intensity on the temperature distributions in the layered skin during the laser beam can be described. During the action of the laser it is necessary to control the growth of the temperature. In fact, too high temperatures could cause undesirable and often irreversible damages to the surrounding tissues. A rise in temperature during the laser session of course depends on the irradiation time, laser intensity and type of the exposed tissue.

In Figure 6.1, is shown the non Fourier-type temperature evolution equation as a function of relaxation time τ_R. Let us remark that τ_R plays an important role in the temperature evolution, as expected, whereas the thermal delay time has a major influence on the temperature distribution, i.e., as t_R increases the tissue temperature decreases more slowly. In particular, increasing the value of the relaxation time, the action of laser provides higher values for the temperature, while once the laser action is stopped (after 30 seconds), it is observed a decrease of temperature fluctuations. The temperature profile, from a natural state around $T_b = 37^0C$, during the process of irradiation increases until a maximum acceptable value is attained.

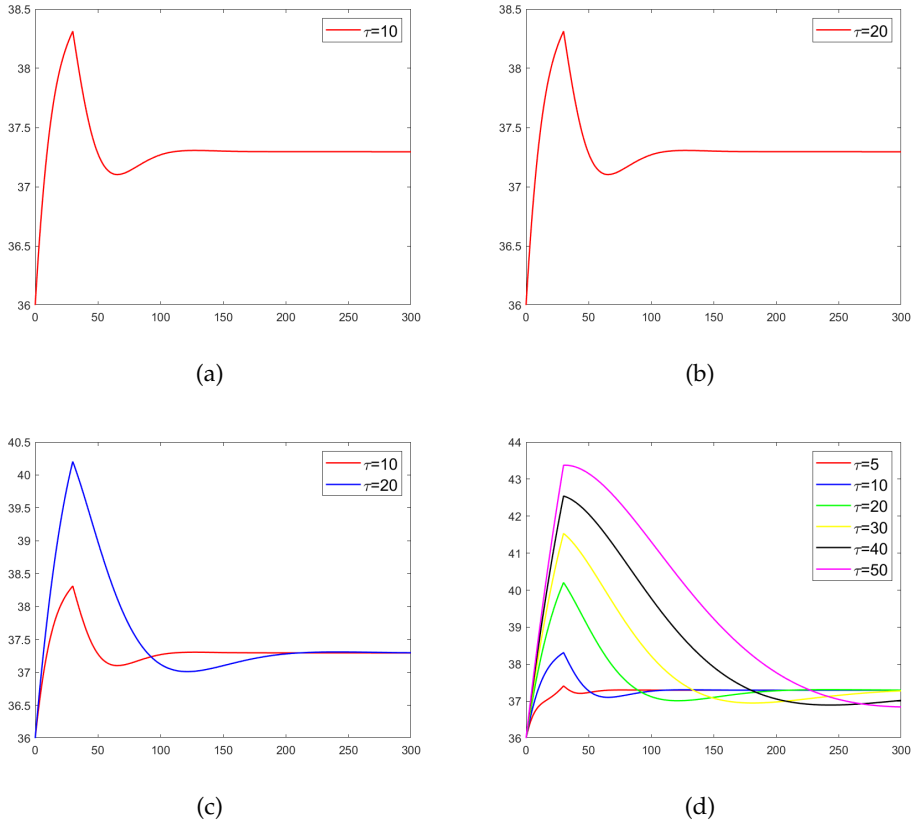

(a) (b)

(c) (d)

FIGURE 6.1: $\phi = 0.3$, $w_b = 0.03\,s^{-1}$, $I_0 = 2.0\,Wmm^{-2}$. (a) $\tau_R = 10s$, (b) $\tau_R = 20s$, (c) Temperature distribution as a function of relaxation times $\tau_R = 10s, \tau_R = 20s$, (d) The skin surface temperature over time vs relaxation times.

In Figure 6.2, the effects of the rate of blood perfusion ω_b under bioheat model with a fixed relation time on the temperature variation are represented. Higher values of the rate of blood perfusion have the effect of increasing the convective heat loss due to faster blood flow, this allows the skin to exhibit lower values of surface temperature.

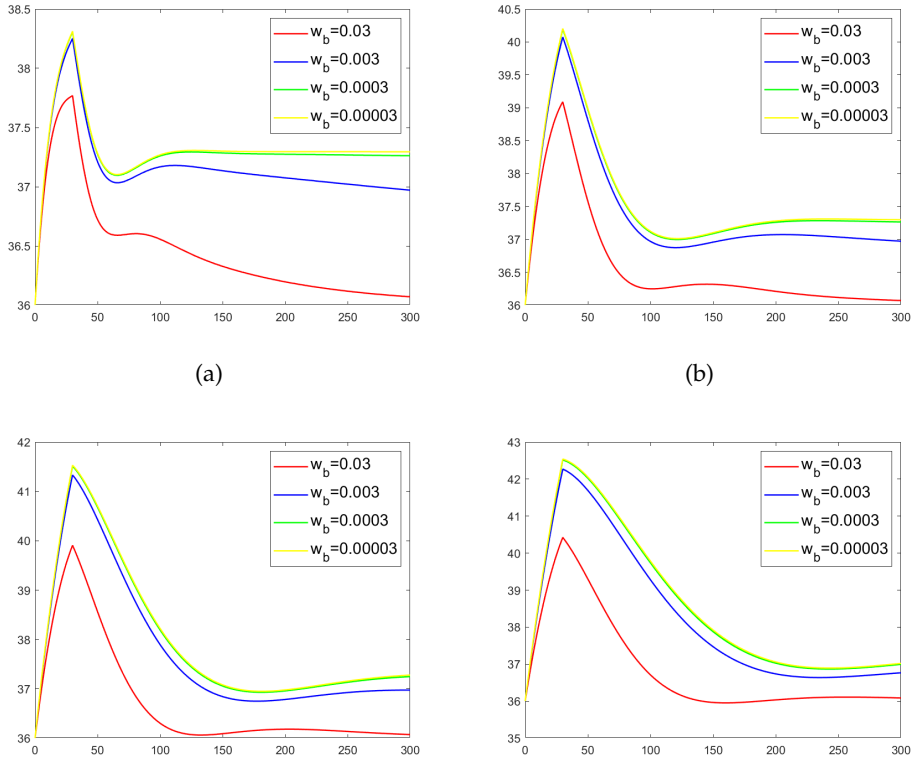

FIGURE 6.2: $\phi = 0.3$, $I_0 = 2.0\, Wmm^{-2}$. Temperature profile over time with: (a) $\tau_R = 10s$, (b) $\tau_R = 20s$, (c) $\tau_R = 30s$, (d) $\tau_R = 40s$.

Finally, Figure 6.3 clearly shows the influence of porosity on the evolution of the skin surface temperature. Higher values of porosity determine smaller temperatures variations. In Figure 6.4, the trend of the temperature is represented varying the intensity of the laser.

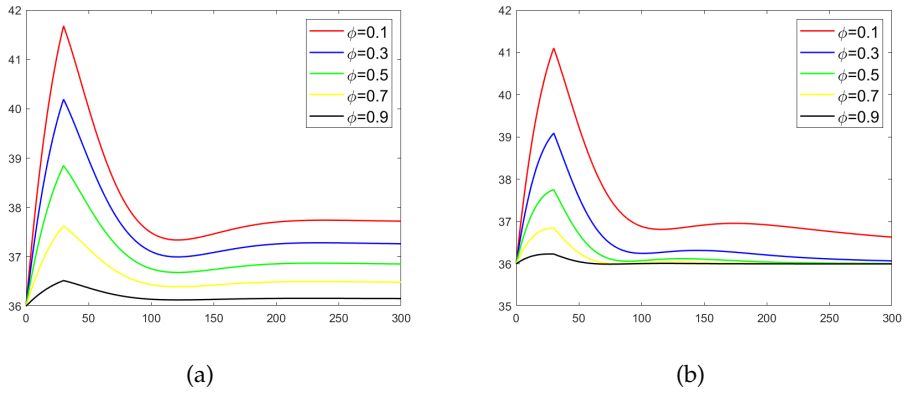

FIGURE 6.3: (a) Temperature profile over time vs porosity with $\tau_R = 20s$, $w_b = 0.0003s^{-1}$, $I_0 = 2.0\, Wmm^{-2}$, (b) Temperature profile over time vs porosity with $\tau_R = 20s$, $w_b = 0.03s^{-1}$, $I_0 = 2.0 \cdot 10^6\, Wm^{-2}$.

In a future work we will consider a more realistic situation, in order to develop a theoretical model including in the generalized bioheat equation (6.4) the

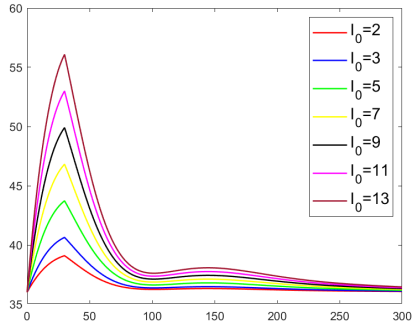

FIGURE 6.4: Temperature distribution changing laser intensity with $\tau_R = 20s$, $w_b = 0.03s^{-1}$, $\phi = 0.3$

non-linearity, as for example a temperature-dependent relaxation time and blood perfusion.

6.2 An Inhomogeneous Model for Laser Welding of Industrial Interest

In this Section, an innovative non-homogeneous dynamic model is presented, for the recovery of temperature during the industrial laser welding process of Al-Si 5% alloy plates. It considers that, metallurgically, during welding, the alloy melts with the presence of solid/liquid phases until total melting, and afterwards re-solidifies with the reverse process. Further, a polynomial substitute thermal capacity of the alloy has been chosen, based on experimental evidence, so that the volumetric solid-state fraction is identifiable. Moreover, to the usual radiative/convective boundary conditions, the contribution due to the positioning of the plates on the workbench is considered (endowing the model with Cauchy-Stefan-Boltzmann boundary conditions). Having verified the well-posedness of the problem, a Galerkin-FEM approach has been implemented to recover the temperature maps, obtained by modeling the laser heat sources with formulations depending on the laser sliding speed. The results achieved have shown good adherence to the experimental evidence, opening up interesting future scenarios for technology transfer.

6.2.1 Introduction to the Problem

As is known, laser welding makes it possible to obtain thin, deep and very resistant welds [176, 177]. This is because, unlike other welding, laser welding does not add material to the sheet metal, and hardly produces obvious defects and residues. High-frequency laser welding locally melts metallic elements, creating a very strong, thin and deep weld [178–181]. Moving at a certain speed v, the laser beam is conveyed over a small section; ensuring welding precision, power concentration on a limited surface without additional materials to the element to be welded (avoiding unsightly residues that are often dangerous because they are harmful to the mechanical strength of the weld) [176, 182]. Although laser welding is a consolidated technique, there remains a strong need to develop new and more complete physical-mathematical models in the recovery of the absolute temperature distributions, T, in materials that are subject to welding. This would identify any a priori thermal problems both in the welding area and in its immediate vicinity. Furthermore, if

$T = T(\mathbf{x}, t)$, with $\mathbf{x} \in \Omega \subset \mathbb{R}^3$, where Ω is the spatial domain and t represents the time instant, it is easy to evaluate the elimination of thermal overload due to welding, highlighting any mechanical anomalies of the welded products [183, 184]. In the past, many dynamic models have been studied to recover $T(\mathbf{x}, t)$ in metallic products subjected to laser welding, starting from the following non-linear, non-homogeneous parabolic heat equation [185]:

$$\mathcal{C}(T(\mathbf{x}, t))\partial_t T(\mathbf{x}, t) = \nabla \cdot [\lambda(T(\mathbf{x}, t))\nabla T(\mathbf{x}, t)] + Q_l(\mathbf{x}, t), \tag{6.14}$$

where $\mathcal{C}(T(\mathbf{x}, t))$ is the volumetric specific heat, $\lambda(T(\mathbf{x}, t))$ is the thermal conductivity, $\nabla T(\mathbf{x}, t)$ is the temperature gradient; and Q_l is the volumetric heat source due to the laser [179, 185–188]; formulated in parabolic frontiers with suitable boundary and initial conditions [185–191]. When the laser moves from an initial temperature T_0, $T(\mathbf{x}, t)$ raises for which the material, initially solid, begins to melt highlighting the co-presence of solid-liquid (intermediate state) until the occurrence of the total melting of the material [192]. The laser, as it moves, melts new areas of the material while the previous ones, due to the reduction of $T(\mathbf{x}, t)$, re-solidify, passing from a liquid to an intermediate state (co-presence of solid and liquid) until only the solid phase is obtained. Further, many models lack the fact that they do not consider convective terms, terms due to irradiation [188, 193] and terms due to practical purposes (i.e., taking into account that the welding is done on a workbench) [191, 194].

Here, we present a non-homogeneous parabolic model for the dynamic temperature recovery during the laser welding of two Al-Si 5% alloy plates that, usually, compared to pure aluminum, offer high mechanical resistance when subjected to welding, as evidenced by the industrial activity of IRIS s.r.l (a leading Italian company in the laser welding sector). Unlike pure Al (which melts at a specific value of the temperature), the binary alloy melts and re-solidifies at a certain range of temperature, in which the material forms a mushy zone, governing $T(\mathbf{x}, t)$ in the welding area. The equation is written in terms of the substitute thermal capacity, $C(T(\mathbf{x}, t))$, of the binary alloy, here formulated as a polynomial [195]. This is chosen to take into account only the presence of liquid, solid, or both depending on the temperature of the material, obtaining a volumetric solid state fraction that is strictly dependent on the volumetric latent heat. The equation was used to simulate a thin strip of 3D laser welding of two Al-Si 5% alloy plates with perfectly smooth surfaces (to avoid voids), made up of two portions of material belonging to each plate. For the parts of the plates not affected by the welding, since the laser source is not present on them, a classic Fourier model of heat transmission has been hypothesized. Neumann boundary conditions have also been formulated to make the heat fluxes from the weld strip (at a higher temperature) to the areas not subject to welding (at a lower temperature) compatible. Further, to make the approach more realistic, boundary conditions due to both contact with the air and contact with the workbench have been added for the surfaces in question, finally achieving Cauchy-Stefan-Boltzmann boundary conditions.

Once verified that the proposed model is well-posed (via hypothesis testing of a well-known result of the recent literature [196]) and reinforced by the fact that it does not allow the explicit recovery of $T(\mathbf{x}, t)$, an optimized Galerkin-FEM approach (to reduce the computational load useful for any real-time applications) has been implemented in the MatLab R2022 PDE Tool and tested for the resolution of the problem by also selecting appropriate formulations of laser heat source, according to known experimental evidence [197].

6.2.2 Melting-Resolidification Process

As neglecting the overheating temperature phenomena of liquid metal (for which convective phenomena lose their meaning), the equation describing the cooling and following solidification process in metals is writable as [198]

$$\mathcal{C}(T(\mathbf{x},t))\,\partial_t T(\mathbf{x},t) = \nabla\cdot[\lambda(T(\mathbf{x},t))\nabla T(\mathbf{x},t)] + Q_l(\mathbf{x},t) + Q_m(\mathbf{x},t), \tag{6.15}$$

where $T(\mathbf{x},t)$ is assumed to be continuous, and $Q_m(\mathbf{x},t)$ is the capacity of volumetric internal heat sources derived from the melting phase change process. During the melting and re-solidification process, both solid and liquid volumetric fractions, $f_S(T(\mathbf{x},t))$ and $f_L(T(\mathbf{x},t))$, respectively, such that

$$f_S(T(\mathbf{x},t)) + f_L(T(\mathbf{x},t)) = 1$$

(for the solid and liquid state, $f_S(T(\mathbf{x},t))$ and $f_L(T(\mathbf{x},t))$ are the constant values (1 or 0)), coexist in the material at the neighborhood of the points considered. Therefore, an appropriate internal heat source, $Q_m(\mathbf{x},t)$, is formulate in terms of $f_S(T(\mathbf{x},t))$ or $f_L(T(\mathbf{x},t))$. In particular, if L_v is the volumetric latent heat of fusion, the heat source due to the solidification becomes [198]

$$Q_m(\mathbf{x},t) = L_v\,\partial_t f_S(T(\mathbf{x},t) = -L_v\,\partial_t f_L(T(\mathbf{x},t) \tag{6.16}$$

highlighting the experimental fact according to which $Q_m(\mathbf{x},t)$ takes non-zero values only at the solidification stage [198–200].

Then, equation (6.15), exploiting (6.16), becomes

$$\mathcal{C}(T(\mathbf{x},t))\,\partial_t T(\mathbf{x},t) = \nabla\cdot[\lambda(T(\mathbf{x},t))\nabla T(\mathbf{x},t)] + Q_l(\mathbf{x},t) + L_v\partial_t f_S(T(\mathbf{x},t)),$$

that, exploiting

$$L_v\,\partial_t f_S(T(\mathbf{x},t)) = \frac{df_S(T(\mathbf{x},t))}{dT}\partial_t T(\mathbf{x},t),$$

becomes

$$\underbrace{\left(\mathcal{C}(T(\mathbf{x},t)) - L_v\frac{df_S(T(\mathbf{x},t))}{dT}\right)}_{C(T(\mathbf{x},t))}\partial_t T(\mathbf{x},t) = \nabla\cdot[\lambda(T(\mathbf{x},t))\nabla T(\mathbf{x},t)] + Q_l(\mathbf{x},t), \tag{6.17}$$

where $C(T(\mathbf{x},t))$, represents the substitute thermal capacity of an artificial mushy zone sub-domain. Unlike pure metals where melting (and resolidification) occurs at a particular temperature value, binary alloys (such as Al-Si 5% here considered) melt and resolidify in a temperature range $[T_S, T_L]$ (i.e., the temperature field across the entire conventionally homogeneous melt domain) in which the material forms a mushy zone. Therefore, it makes sense to write [198]:

$$\begin{aligned}
&f_S = 1, \quad T(\mathbf{x},t) < T_S \quad \text{(solid state)},\\
&f_S \in (0,1), \quad T_S \le T(\mathbf{x},t) \le T_L \quad \text{(mushy zone)},\\
&f_S = 0, \quad T(\mathbf{x},t) > T_L \quad \text{(molten metal)}.
\end{aligned}$$

Recently, important results have been obtained, starting from the knowledge of f_S and then obtaining the behavior of $C(T(\mathbf{x},t))$ [198]. However, the reverse approach is also feasible: a plausible trend of $C(T(\mathbf{x},t))$ can be assumed, from which f_S can be obtained [195]. Here, we consider the inverse approach, and we suppose that a

good approximation for $C(T(\mathbf{x},t))$ is a polynomial one [195]:

$$C(T(\mathbf{x},t)) = a_0 + a_1 T(\mathbf{x},t) + a_2 T^2(\mathbf{x},t) + \tag{6.18a}$$
$$+ a_3 T^3(\mathbf{x},t) + a_4 T^4(\mathbf{x},t), \qquad T(\mathbf{x},t) \in [T_S, T_L], \tag{6.18b}$$

whose coefficients a_i, with $i \in \{0,1,2,3,4\}$, are selected in order that both $C(T(\mathbf{x},t))$ and its first derivative are continuous. For this reason, the following physical constraints are met:

$$C(T_L) = \mathcal{C}(T_L) \equiv \mathcal{C}_L, \tag{6.19a}$$
$$C(T_S) = \mathcal{C}(T_S) \equiv \mathcal{C}_S, \tag{6.19b}$$
$$\frac{dC(T_L)}{dT} = \frac{dC(T_S)}{dT} = 0, \tag{6.19c}$$

also satisfying

$$\int_{T_S}^{T_L} C(T(\mathbf{x},t))\mathrm{d}T = \mathcal{C}_m \Delta T + L_v, \tag{6.20}$$

where $\Delta T = T_L - T_S$ and $\mathcal{C}_m$ is the mushy zone volumetric specific heat (usually, $\mathcal{C}_m = \frac{1}{2}(\mathcal{C}_S + \mathcal{C}_L)$), but other formulations could be taken into account). We note that conditions (6.19) and (6.20) allow construction of a bell-shaped trend for $C(T(\mathbf{x},t))$ [195].

Therefore, after calculations, the coefficients a_i become

$$a_0 = \frac{(\mathcal{C}_L - \mathcal{C}_S) T_L T_S (T_L + T_S)}{(\Delta T)^3} + \frac{30\, T_L^2, T_S^2, L_v}{(\Delta T)^5},$$
$$a_1 = -\frac{6(\mathcal{C}_L - \mathcal{C}_S) T_L T_S}{(\Delta T)^3} - \frac{60\, T_L\, T_S (T_L + T_S) L_v}{(\Delta T)^5},$$
$$a_2 = \frac{3(\mathcal{C}_L - \mathcal{C}_S)(T_L + T_S)}{(\Delta T)^3} + \frac{30\,(T_L^2 + 4\, T_L\, T_S + T_S^2) L_v}{(\Delta T)^5},$$
$$a_3 = -\frac{2(\mathcal{C}_L - \mathcal{C}_S)}{(\Delta T)^3} + \frac{60\,(T_L + T_S)\, L_v}{(\Delta T)^5},$$
$$a_4 = \frac{30 L_v}{(\Delta T)^5},$$

depending on L_v. Furthermore, from (6.17) and (6.18), we can write

$$\mathcal{C}(T(\mathbf{x},t)) - L_v \frac{df_S(T(\mathbf{x},t))}{dT} = a_0 + a_1 T(\mathbf{x},t) + a_2 T^2(\mathbf{x},t) + a_3 T^3(\mathbf{x},t) + \tag{6.21}$$
$$+ a_4 T^4(\mathbf{x},t),$$

with $T(\mathbf{x},t) \in [T_S, T_L]$. But introducing the following definition of $\mathcal{C}(T(\mathbf{x},t))$

$$\mathcal{C}(T(\mathbf{x},t)) = \begin{cases} \mathcal{C}_S & \text{if} \quad T < T_S, \\ \mathcal{C}_m & \text{if} \quad T_S \leq T \leq T_L, \\ \mathcal{C}_L & \text{if} \quad T > T_L, \end{cases}$$

we obtain

$$\mathcal{C}_m - L_v \frac{df_S(T(\mathbf{x},t))}{dT} = a_0 + a_1 T(\mathbf{x},t) + a_2 T^2(\mathbf{x},t) + a_3 T^3(\mathbf{x},t) + \\ + a_4 T^4(\mathbf{x},t),$$

with $T(\mathbf{x},t) \in [T_S, T_L]$. From which we obtain

$$f_s(T(\mathbf{x},t)) = \frac{(\mathcal{C}_m - a_0)T(\mathbf{x},t)}{L_v} - \frac{a_1 T^2(\mathbf{x},t)}{2L_v} - \frac{a_2 T^3(\mathbf{x},t)}{2L_v} - \\ - \frac{a_3 T^4(\mathbf{x},t)}{4L_v} - \frac{a_4 T^5(\mathbf{x},t)}{5L_v} + K, \tag{6.22}$$

where the constant of integration K is determined by imposing $f_s(T_L) = 0$. Finally, (6.22) becomes

$$f_S(T(\mathbf{x},t)) = \frac{(a_0 - \mathcal{C}_m)[T_L - T(\mathbf{x},t)]}{L_v} + \frac{a_1[T_L^2 - T^2(\mathbf{x},t)]}{2L_v} + \frac{a_2[T_L^3 - T^3(\mathbf{x},t)]}{3L_v} + \\ + \frac{a_3[T_L^4 - T^4(\mathbf{x},t)]}{4L_v} + \frac{a_4[T_L^5 - T^5(\mathbf{x},t)]}{5L_v}. \tag{6.23}$$

with $T(\mathbf{x},t) \in [T_S, T_L]$. Furthermore, (6.23) satisfies $f_S(T_S) = 1$ predicting the solidification kinetics of the casting.

6.2.3 Governing Equation

Material and geometries

The specimen consists of two Al-Si 5% alloy plates (without surface oxides which drastically raise the melting temperature), P_1 and P_2, of equal size ($100\,mm \times 40\,mm \times 4\,mm$) (dimensions suggested by IRIS s.r.l.), juxtaposed along the largest dimension, such that the respective faces (perfectly smooth) adhere to favor welding. The absence of voids between the plates allows, on one hand, to simulate a better weld quality and, on the other hand, avoids air between the parts to be welded. For our purposes, we divide the domain Ω into three subdomains: Ω_1 and Ω_2 consisting of the plates placed side by side net of the Ω portion subject to melting and then resolidifying (welding strip); Ω_3 ($100\,mm \times 2\,mm \times 4\,mm$) corresponding to the welding strip, such that $\Omega_i = P_i \setminus \Omega_3$ with $i = 1, 2$, in which the heat transfer is modeled according to the melting/resolidification of the material in the interval of temperature $[T_S, T_L]$. Figure 6.5 shows the partition of Ω into P_1 and P_2 while Figure 6.6 displays Ω_1, Ω_2 and Ω_3; moreover, Table 6.1 and Table 6.2 highlight the geometry of each Ω_i. Finally, for implementation aims, we label the sixteen faces of $\partial\Omega$ by F_i ($i = 1, ..., 16$), so that $\partial\Omega = \left(\bigcup_{i=1}^{16} F_i\right) \setminus (F_2 \cup F_7)$ (see Figure 6.7), whose dimensions are specified in Table 6.3.

Ω_i	**length** (mm)	**width** (mm)	**tickness** (mm)
Ω_1	39	100	4
Ω_2	39	100	4
Ω_3	2	100	4

TABLE 6.1: Dimensions of Ω_1, Ω_2 and Ω_3.

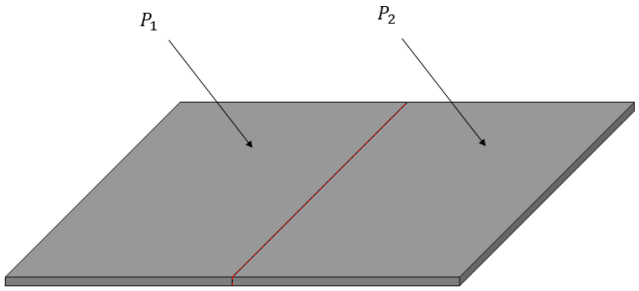

FIGURE 6.5: Al-Si 5% specimen: Ω divided into P_1 and P_2.

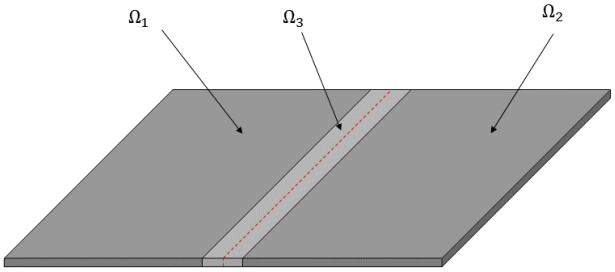

FIGURE 6.6: Al-Si 5% specimen: Ω divided into Ω_1, Ω_2 and Ω_3.

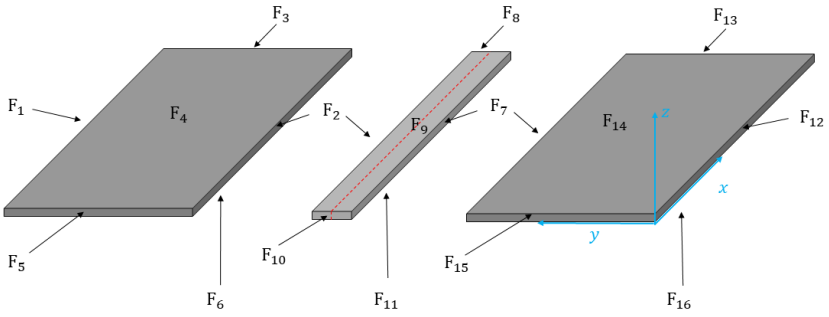

FIGURE 6.7: Al-Si 5% specimen: labels associated with each surface.

Ω_i	**length** (mm)	$\overset{\circ}{\Omega}_i$	**length** (mm)
Ω_1	$[0,100] \times [0,39] \times [0,4]$	$\overset{\circ}{\Omega}_1$	$(0,100) \times (0,39) \times (0,4)$
Ω_2	$[0,100] \times [41,80] \times [0,4]$	$\overset{\circ}{\Omega}_2$	$(0,100) \times (41,80) \times (0,4)$
Ω_3	$[0,100] \times [39,41] \times [0,4]$	$\overset{\circ}{\Omega}_3$	$(0,100) \times (39,41) \times (0,4)$

TABLE 6.2: Geometric characterizations of Ω_1, Ω_2 and Ω_3.

Label	Dimensions	Label	Dimensions
F_{12}	$[0,100]\times\{0\}\times[0,4]$	F_2	$[0,100]\times\{41\}\times[0,4]$
F_7	$[0,100]\times\{39\}\times[0,4]$	F_1	$[0,100]\times\{80\}\times[0,4]$
F_5	$\{0\}\times[41,80]\times[0,4]$	F_4	$[0,100]\times[41,80]\times\{4\}$
F_3	$\{100\}\times[41,80]\times[0,4]$	F_6	$[0,100]\times[41,80]\times\{0\}$
F_{10}	$\{0\}\times[39,41]\times[0,4]$	F_9	$[0,100]\times[39,41]\times\{4\}$
F_8	$\{100\}\times[39,41]\times[0,4]$	F_{11}	$[0,100]\times[39,41]\times\{0\}$
F_{15}	$\{0\}\times[0,39]\times[0,4]$	F_{14}	$[0,100]\times[0,39]\times\{4\}$
F_{13}	$\{100\}\times[0,39]\times[0,4]$	F_{16}	$[0,100]\times[0,39]\times\{0\}$

TABLE 6.3: Geometric characterizations of $\partial\Omega_1$, $\partial\Omega_2$ and $\partial\Omega_3$.

Concerning both Ω_1 and Ω_2, since the laser beam does not pass over them, a model exploiting (6.14) without a laser heat source is sufficient for recovering $T(\mathbf{x},t)$. Concerning Ω_3, since the presence of the laser beam, we propose a model where the equation considers the melting/re-solidification of the material in its melting range, ΔT, on which the replacement heat capacity of the alloy can be formulated according to the known experimental evidence, and from which the volume fraction of the solid state can be easily obtained.

Domains not belonging to the laser welding domain: model, initial and boundary conditions

Starting from (6.14), with $Q_l(\mathbf{x},t)=0$ (absence of the laser), and considering thermal conductivity λ_i independent on the temperature $T_i(\mathbf{x},t)$ supposed to be continuous (it makes sense because the thermal conductivity of the AlSi 5%, during the laser welding, can be considered, in the first approximation, as a constant), we write

$$\mathcal{C}_S\,\partial_t T_i(\mathbf{x},t)=\lambda_i\nabla^2 T_i(\mathbf{x},t),\quad \forall\mathbf{x}\in\overset{\circ}{\Omega}_i \text{ with } i=1,2,\quad \forall t>0,$$

to which the following initial conditions can be associated:

$$T_i(\mathbf{x},0)=T_0\quad \forall\mathbf{x}\in\Omega_i \text{ with } i=1,2.$$

Moreover, since the sides of the surfaces are next to the air conduction heat flux $h^{air}[T_{air}-T_i(\mathbf{x},t)]$, and radiation flux, $\epsilon\,\sigma_B[T_{air}^4-T_i^4(\mathbf{x},t)]$, occur, where h_{air} is the convection coefficient of air, ϵ is the emissivity and σ_B the Boltzmann constant. We identify $\hat{\mathbf{n}}$ the outward unit normal vector to generical faces. Therefore, $\forall\mathbf{x}\in F_j$, $j\in\{1,3,4,5,12,13,14,15\}$ and $\forall t>0$

$$\lambda_i\,\partial_{\hat{\mathbf{n}}}T_i(\mathbf{x},t)=h^{air}[T_{air}-T_i(\mathbf{x},t)]+\epsilon\,\sigma_B[T_{air}^4-T_i^4(\mathbf{x},t)].$$

Furthermore, for the surfaces in contact with the workbench (faces F_6 and F_{16}), we introduce the following boundary condition:

$$\lambda_i\,\partial_{\hat{\mathbf{n}}}T_i(\mathbf{x},t)=h^{bench}[T_{bench}-T_i(\mathbf{x},t)],\quad \forall\mathbf{x}\in F_6\cup F_{16}\quad \forall t>0.$$

with h^{bench} the convection coefficient of the workbench. Finally, it is necessary to consider the heat flow coming from Ω_3 toward both Ω_1 and Ω_2, at a certainly higher temperature the reverse heat flow can be considered as negligible because it will not noticeably modify the numerical solution. Considering this heat flow, negligible means a software design "for the benefit of safety" because, strictly speaking, the

miniscule heat dissipation that goes from the plates towards the welding.

$$\lambda_i \, \partial_{\hat{\mathbf{n}}} T_i(\mathbf{x}, t) = \lambda_3 \, \partial_{\hat{\mathbf{n}}} T_3(\mathbf{x}, t) \quad \forall \mathbf{x} \in F_2 \cup F_7 \quad \forall t > 0,$$

Therefore, the model for Ω_1 and Ω_2 can be compactly written as

$$\mathcal{C}_S \, \partial_t T_i(\mathbf{x}, t) = \lambda_i \, \nabla^2 T_i(\mathbf{x}, t), \qquad \forall \mathbf{x} \in \mathring{\Omega}_i \text{ with } i = 1, 2 \quad \forall t > 0 \tag{6.24a}$$

$$T_i(\mathbf{x}, 0) = T_0, \qquad \forall \mathbf{x} \in \Omega_i \text{ with } i = 1, 2 \tag{6.24b}$$

$$\lambda_i \, \partial_{\hat{\mathbf{n}}} T_i(\mathbf{x}, t) = h^{air} \left(T_{air} - T_i\right) + \epsilon \, \sigma_B \left(T_{air}^4 - T_i^4\right), \qquad \forall \mathbf{x} \in F_4 \cup F_{14} \quad \forall t > 0, \tag{6.24c}$$

$$\lambda_i \, \partial_{\hat{\mathbf{n}}} T_i(\mathbf{x}, t) = h^{air} \left(T_{air} - T_i\right) + h^{bench} \left(T_{bench} - T_i\right), \qquad \forall \mathbf{x} \in F_6 \cup F_{16} \quad \forall t > 0, \tag{6.24d}$$

$$\lambda_i \, \partial_{\hat{\mathbf{n}}} T_i(\mathbf{x}, t) = h^{air} \left(T_{air} - T_i\right), \qquad \forall \mathbf{x} \in F_1 \cup F_3 \cup F_5 \cup F_{12} \cup F_{13} \cup F_{15} \quad \forall t > 0, \tag{6.24e}$$

$$\lambda_i \, \partial_{\hat{\mathbf{n}}} T_i(\mathbf{x}, t) = \lambda_3 \partial_{\hat{\mathbf{n}}} T_3(\mathbf{x}, t), \qquad \forall \mathbf{x} \in F_2 \cup F_7 \quad \forall t > 0. \tag{6.24f}$$

Laser welding domain: the model

When the laser beam flows on the plates, starting from T_0, the temperature $T(\mathbf{x}, t)$ increases, raising the melted material, obtaining the following phase transitions:

$$solid \rightarrow \underbrace{solid + liquid}_{intermediate} \rightarrow liquid.$$

Furthermore, the laser beam, moving again, melts material further while the previously melted material, due to the lowering of $T(\mathbf{x}, t)$, re-solidifies as follows:

$$liquid \rightarrow \underbrace{solid + liquid}_{intermediate} \rightarrow solid.$$

To model this process, we start from [198] in which melting and re-solidification processes for a metallurgical problem have been considered at a temperature interval ΔT. Then, in our case, equation (6.17) is valid, to whose right-hand side we add $Q_l^{(v)}(\mathbf{x}, t)$, which models the volumetric moving laser heat source:

$$\mathcal{C}(T_3(\mathbf{x}, t)) \, \partial_t T_3(\mathbf{x}, t) = \lambda_3 \, \nabla^2 T_3(\mathbf{x}, t)) + Q_l^{(v)}(\mathbf{x}, t), \quad \forall \mathbf{x} \in \mathring{\Omega}_3 \quad \forall t > 0,$$

with the following initial condition

$$T_3(\mathbf{x}, 0) = T_0 \quad \forall \mathbf{x} \in \Omega_3.$$

Concerning the boundary conditions, a first Robin condition concerns the heat flow, which flows from Ω_3 towards the workbench (face F_{11})

$$\lambda_3 \, \partial_{\hat{\mathbf{n}}} T_3(\mathbf{x}, t) = h^{bench} [T_{bench} - T_3(\mathbf{x}, t)] \quad \forall \mathbf{x} \in F_{11} \quad \forall t > 0.$$

Furthermore, the upper side (face F_9), is in contact with the air; so, the following Cauchy-Stefan-Boltzmann boundary condition makes sense:

$$\lambda_3 \, \partial_{\hat{\mathbf{n}}} T_3(\mathbf{x}, t) = h^{air} [T_{air} - T_3(\mathbf{x}, t)] + \epsilon \, k_B [T_{air}^4 - T_3^4(\mathbf{x}, t)] + Q_l^{(s)}(\mathbf{x}, t) \quad \forall \mathbf{x} \in F_9 \quad \forall t > 0,$$

in which the contribution due to irradiation is present ($Q_l^{(s)}(\mathbf{x},t)$, laser beam heat source). Finally, lateral surfaces of Ω_3 in contact with the internal lateral surfaces of Ω_1 and Ω_2 are only affected by conduction flows; therefore,

$$\lambda_3\,\partial_{\hat{\mathbf{n}}}T_3(\mathbf{x},t)=\lambda_i\,\partial_{\hat{\mathbf{n}}}T_i(\mathbf{x},t),\quad \forall\mathbf{x}\in F_2\cup F_7\quad \forall t>0.$$

So, the model for Ω_3 assumes the following compact form

$$\mathcal{C}(T_3(\mathbf{x},t))\,\partial_t T_3(\mathbf{x},t)=\lambda_3\nabla^2 T_3(\mathbf{x},t)+Q_l^{(v)}(\mathbf{x},t),\quad \forall\mathbf{x}\in\overset{\circ}{\Omega}_3\quad \forall t>0 \tag{6.25a}$$
$$T_3(\mathbf{x},0)=T_0,\quad \forall\mathbf{x}\in\Omega_3 \tag{6.25b}$$
$$\lambda_3\,\partial_{\hat{\mathbf{n}}}T_3(\mathbf{x},t)=Q_l^{(s)}(\mathbf{x},t)+ \tag{6.25c}$$
$$+h^{air}\,(T_{air}-T_3)+\epsilon\,\sigma_B\left(T_{air}^4-T_3^4\right),\quad \forall\mathbf{x}\in F_9\quad \forall t>0, \tag{6.25d}$$
$$\lambda_3\,\partial_{\hat{\mathbf{n}}}T_3(\mathbf{x},t)=h^{air}\,(T_{air}-T_3)+h^{bench}\,(T_{bench}-T_3),\quad \forall\mathbf{x}\in F_{11}\quad \forall t>0, \tag{6.25e}$$
$$\lambda_3\,\partial_{\hat{\mathbf{n}}}T_3(\mathbf{x},t)=h^{air}\,(T_{air}-T_3),\quad \forall\mathbf{x}\in F_8\cup F_{10}\quad \forall t>0, \tag{6.25f}$$
$$\lambda_3\partial_{\hat{\mathbf{n}}}T_3(\mathbf{x},t)=\lambda_i\partial_{\hat{\mathbf{n}}}T_i(\mathbf{x},t),\quad \forall\mathbf{x}\in F_2\cup F_7\quad \forall t>0. \tag{6.25g}$$

Full Model in the Domain

Finally, for Ω, the model is compactly written as:

$$\mu\,\partial_t T(\mathbf{x},t)=\lambda\nabla^2 T(\mathbf{x},t)+\eta\,Q_l^{(v)}(\mathbf{x},t),\quad \forall\mathbf{x}\in\overset{\circ}{\Omega}\quad \forall t>0 \tag{6.26a}$$
$$T(\mathbf{x},0)=T_0,\quad \forall\mathbf{x}\in\Omega \tag{6.26b}$$
$$\lambda\partial_{\partial\hat{\mathbf{n}}}T(\mathbf{x},t)=\eta Q_l^{(s)}(\mathbf{x},t)+h^{air}\,(T_{air}-T)+\epsilon\,\sigma_B\left(T_{air}^4-T^4\right), \tag{6.26c}$$
$$\forall\mathbf{x}\in F_4\cup F_9\cup F_{14}\quad \forall t>0, \tag{6.26d}$$
$$\lambda\partial_{\partial\hat{\mathbf{n}}}T(\mathbf{x},t)=h^{air}\,(T_{air}-T)+h^{bench}\,(T_{bench}-T), \tag{6.26e}$$
$$\forall\mathbf{x}\in F_6\cup F_{11}\cup F_{16}\quad \forall t>0, \tag{6.26f}$$
$$\lambda\partial_{\partial\hat{\mathbf{n}}}T(\mathbf{x},t)=h^{air}\,(T_{air}-T),\quad \forall\mathbf{x}\in F_1\cup F_3\cup F_5\cup F_8\cup F_{10}\cup F_{12}\cup F_{13}\cup F_{15}\quad \forall t>0, \tag{6.26g}$$

compactly assumes the form

$$\mu\,\partial_t T(\mathbf{x},t)=\lambda\nabla^2 T(\mathbf{x},t)+\eta\,Q_l^{(v)}(\mathbf{x},t),\quad \forall\mathbf{x}\in\overset{\circ}{\Omega}\quad \forall t>0 \tag{6.27a}$$
$$T(\mathbf{x},0)=T_0,\quad \forall\mathbf{x}\in\Omega \tag{6.27b}$$
$$\lambda\partial_{\partial\hat{\mathbf{n}}}T(\mathbf{x},t)+h^{air}\,(T-T_{air})+\beta h^{bench}\,(T-T_{bench})+\alpha\epsilon\,\sigma_B\left(T^4-T_{air}^4\right)= \tag{6.27c}$$
$$=\eta Q_l^{(s)}(\mathbf{x},t),\quad \forall\mathbf{x}\in\partial\Omega\quad \forall t>0. \tag{6.27d}$$

where

$$T(\mathbf{x},t))=\begin{cases}T_1(\mathbf{x},t))&\text{if}\quad \mathbf{x}\in\Omega_1,\\ T_2(\mathbf{x},t))&\text{if}\quad \mathbf{x}\in\Omega_2,\\ T_3(\mathbf{x},t))&\text{if}\quad \mathbf{x}\in\Omega_3,\end{cases}$$

$$\mu=\begin{cases}\mathcal{C}_S&\text{if}\quad \mathbf{x}\in\Omega_1\cup\Omega_2,\\ \mathcal{C}(T)&\text{if}\quad \mathbf{x}\in\Omega_3,\end{cases}$$

$$\lambda = \begin{cases} \lambda_1 & \text{if} \quad \mathbf{x} \in \Omega_1, \\ \lambda_2 & \text{if} \quad \mathbf{x} \in \Omega_2, \\ \lambda_3 & \text{if} \quad \mathbf{x} \in \Omega_3, \end{cases}$$

$$\eta = \begin{cases} 0 & \text{if} \quad \mathbf{x} \in \Omega_1 \cup \Omega_2, \\ 1 & \text{if} \quad \mathbf{x} \in \Omega_3, \end{cases}$$

$$\alpha = \begin{cases} 1 & \text{if} \quad \mathbf{x} \in F_6 \cup F_{16} \cup F_{11}, \\ 0 & \text{if} \quad \mathbf{x} \in \partial\Omega \setminus (F_6 \cup F_{16} \cup F_{11}), \end{cases}$$

$$\beta = \begin{cases} 1 & \text{if} \quad \mathbf{x} \in F_4 \cup F_{14} \cup F_9, \\ 0 & \text{if} \quad \mathbf{x} \in \partial\Omega \setminus (F_4 \cup F_{14} \cup F_9). \end{cases}$$

The model simulates the welding process of 5% Al-Si alloy plates, which are widely used in industry, without adding any extra material. This is critical as it eliminates unwanted thickening and adheres to regulatory standards. Even if the collaboration with IRIS s.r.l. required the use of 5% Al-Si alloy, the model can get results for other materials, which, for their laser welding, do not require extra material.

Realistic Formulations for both Volumetric and Superficial Laser Heat Sources

To recover $T(\mathbf{x}, t)$, it is necessary to define precisely the shape of the “melting hole" and the subsequent solidification scheme. Then, according to the final mechanical properties of the welding, we should mathematically formalize both $Q_l^{(v)}(\mathbf{x}, t)$ and $Q_l^{(s)}(\mathbf{x}, t)$.

Classical Gaussian laser heat source
To model the moving heat source, as a first approach, we use the established volumetric and superficial Gaussian formulation [197]:

$$Q_l^{(v)}(\mathbf{x},t) = \frac{R_f I_0}{r_U} \exp\left(-\frac{(x-x_0)^2+(y-y_0)^2+(z-z_0)^2}{r_U^2}\right),$$
$$Q_l^{(s)}(\mathbf{x},t) = R_f I_0 \exp\left(-\frac{(x-x_0)^2+(y-y_0)^2}{r_U^2}\right),$$

displayed in Figure 6.8, where $(x_0, y_0, z_0) = (vt, y_0, z_0)$ are the coordinates of the point where the laser beam starts, v denoting the laser speed, r_U is the laser radius, I_0 is the laser intensity (which contributes to give the laser power) and R_f is the reflexivity. It basically just means that on the surface that it's interacting with, they define a heat flux proportional to a Gaussian distribution.

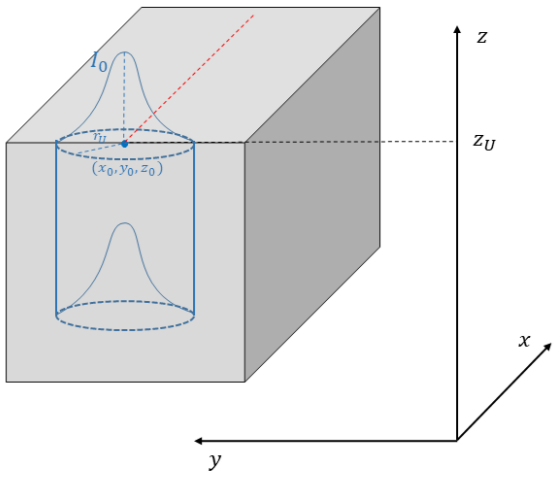

FIGURE 6.8: Representation of Gaussian laser heat source.

Conical laser heat source
As a term of comparison, we will also use the conical laser heat source (see Figure 6.9) deriving from a Gaussian heat distribution. This allowed the following formulations to be used [197]:

$$Q_l^{(v)}(\mathbf{x},t) = \frac{R_f I_0}{r_U} \exp\left(-\frac{(x-vt)^2+(y-y_0)^2+(z-z_0)^2}{r(z)^2}\right),$$
$$Q_l^{(s)}(\mathbf{x},t) = R_f I_0 \exp\left(-\frac{(x-vt)^2+(y-y_0)^2}{r_U^2}\right),$$

where $r(z)$, representing the action radius of the laser on z, is formulable as

$$r(z) = r_U - (r_U - r_L) \cdot \frac{z_U - z}{z_U - z_L},$$

in which r_U and r_L represent the radius on $z = z_U$ (upper) and $z = z_L$ (lower), respectively.

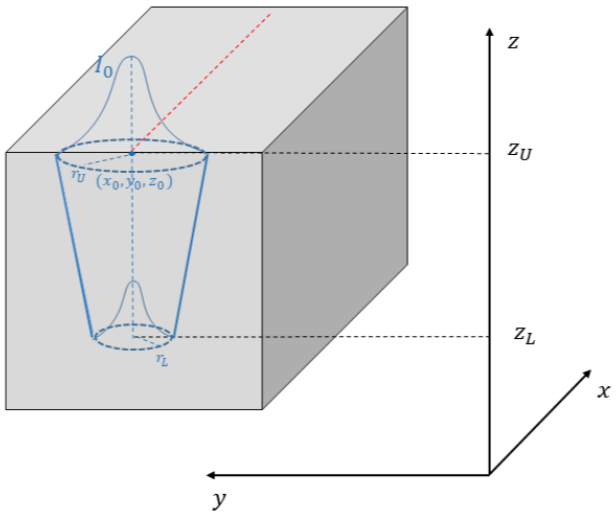

FIGURE 6.9: Representation of the conical laser heat source.

Ellipsoid laser heat source
As a further term of comparison, we exploit this interesting formulation, depicted in Figure 6.10, formulated as [201]

$$Q_l^{(v)}(\mathbf{x}, t) = R_f \frac{\sqrt{3}P}{abc\pi\sqrt{\pi}} \cdot \exp\left(-\left[\frac{(x - vt)^2}{a^2} + \frac{(y - y_0)^2}{b^2} + dfrac(z - z_0)^2 c^2\right]\right),$$
$$Q_l^{(s)}(\mathbf{x}, t) = R_f \frac{\sqrt{3}P}{ab\pi\sqrt{\pi}} \cdot \exp\left(-\left[\frac{(x - vt)^2}{a^2} + \frac{(y - y_0)^2}{b^2}\right]\right),$$

where a, b, c are the length, the width, the depth respectively [201–203].

Remark 17. *The solution $T(\mathbf{x}, t)$ of (6.26) is implicitly linked to I_0 which, generating the laser beam, represents the primary cause of distribution of $T(\mathbf{x}, t)$ in the plates.*

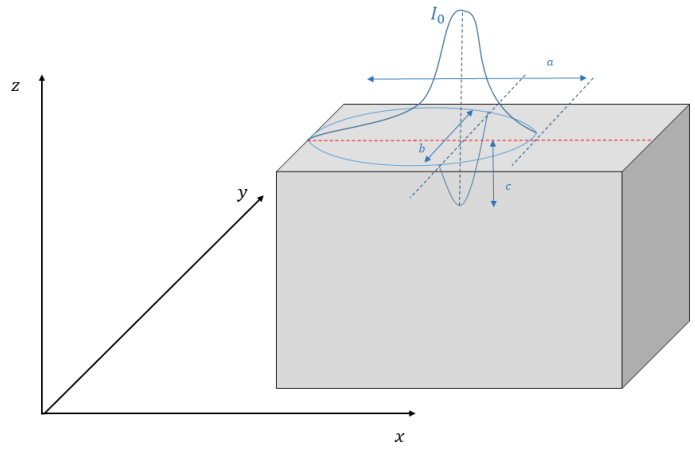

FIGURE 6.10: Representation of ellipsoidal laser heat source.

6.2.4 The Galerkin-FEM Approach

Some remarks on existence, uniqueness and regularity of the solution

We focus our attention on numerical techniques for solving (6.26) after verifying that it is a well-posed one. Thus we recall the following

Theorem 7 (Miranville-Morosanu). *Let $\Omega \subset \mathbb{R}^n$ bounded domain, with a C^2 boundary $\partial\Omega$. For a finite time $\tilde{t} > 0$, we consider the following nonlinear parabolic second-order PDE boundary value problem [196]:*

$$\partial_t T(\mathbf{x},t) = \Phi(T(\mathbf{x},t))\nabla\cdot(K(T(\mathbf{x},t))\,\nabla T(\mathbf{x},t)) + \Psi(T(\mathbf{x},t))r^{(v)}(\mathbf{x},t), \quad in \quad (0,\tilde{t}\,]\times\Omega, \tag{6.28a}$$

$$K(T(\mathbf{x},t))\partial_{\hat{\mathbf{n}}}T(\mathbf{x},t) + p_1[T(\mathbf{x},t)-\theta_1] + p_2[T(\mathbf{x},t)-\theta_2] + \tag{6.28b}$$

$$+ p_3[T^4(\mathbf{x},t)-\theta_3^4] = p_4\, r^{(s)}(\mathbf{x},t), \quad on \quad (0,\tilde{t}\,]\times\partial\Omega, \tag{6.28c}$$

$$T(\mathbf{x},0) = T_0(\mathbf{x}) \quad on \quad \Omega. \tag{6.28d}$$

where $\Phi(T(\mathbf{x},t))$ controls the speed of the diffusion process; $K(T(\mathbf{x},t))$ represent the mobility attached to the solution $T(\mathbf{x},t)$; $r^{(v)}(\mathbf{x},t)$ and $r^{(s)}(\mathbf{x},t)$ are distributed control and boundary control, respectively. Furthermore, ∇ denotes the gradient, $\hat{\mathbf{n}} = \hat{\mathbf{n}}(\mathbf{x})$ is the outward unit normal vector to Ω as a point $\mathbf{x} \in \partial\Omega$ and $\dfrac{\partial}{\partial\hat{\mathbf{n}}}$ denotes differentiation along $\hat{\mathbf{n}}$.
If the following conditions are satisfied:

1) *p_1, p_2, p_3, p_4, are non-negative constants;*

2) *$\Phi(T(\mathbf{x},t))$, is a positive and bounded real function of class $C^1((0,\tilde{t}\,]\times\Omega)$, with bounded derivative;*

3) *$K(T(\mathbf{x},t))$ assumed to satisfy the following inequality*

$$0 < K_m \le K(T(\mathbf{x},t)) \le K_M, \quad \forall(\mathbf{x},t) \in (0,\tilde{t}\,]\times\Omega;$$

where K_m, K_M are constants;

4) $\Psi(T(\mathbf{x},t))$, *is a positive bounded real function;*

5) $r^{(v)}(\mathbf{x},t) \in L^p((0,\tilde{t}\,]\times\Omega)$ *with* $p \geq 2$;

6) $r^{(s)}(\mathbf{x},t) \in W_p^{1-\frac{1}{2p},2-\frac{1}{p}}((0,\tilde{t}\,]\times\partial\Omega)$;

7) $T_0(\mathbf{x}) \in W_\infty^{2-\frac{2}{p}}(\Omega)$, *verifying*

$$K(T_0(\mathbf{x}))\frac{\partial T_0(\mathbf{x})}{\partial \hat{\mathbf{n}}} + p_1[T_0(\mathbf{x})-\theta_1] + p_2[T_0(\mathbf{x})-\theta_2] + p_3[T_0^4(\mathbf{x})-\theta_3^4] = p_4\, r^{(s)}(\mathbf{x},0);$$

then problem (6.28) *is well-posed.*

Proof of Theorem 1. For the proof of this theorem refer to [196]. □

Remark 18. *It is worth noting that Theorem 7 requires that* $\Phi(T(\mathbf{x},t))$ *is a positive real function, bounded and, above all, of* $C^1((0,\tilde{t}\,]\times\Omega)$ *requiring the continuity of* $T(\mathbf{x},t)$.

Theorem 7 can be successfully applied in our laser welding process setting

$$\begin{aligned}
&\Phi(T(\mathbf{x},t)) = \frac{1}{\mu(T(\mathbf{x},t))},\\
&K(T(\mathbf{x},t)) = \lambda, \quad K_m \leq K \leq K_M,\\
&\Psi(T(\mathbf{x},t)) = \frac{\eta}{\mu(T(\mathbf{x},t))},
\end{aligned}$$

and

$$\begin{aligned}
&p_1 = h^{air}, \quad p_2 = \beta h^{bench}, \quad p_3 = \alpha\epsilon\sigma_B, \quad p_4 = \eta,\\
&\theta_1 = T_{air}, \quad \theta_2 = T_{bench}, \quad \theta_3 = T_{air},\\
&r^{(v)}(\mathbf{x},t) = Q_l^{(v)}(\mathbf{x},t), \quad r^{(s)}(\mathbf{x},t) = Q_l^{(s)}(\mathbf{x},t).
\end{aligned}$$

Thus, the non-linear inhomogeneous parabolic model (6.27) is achieved. It is easy to prove that $Q_l^{(v)}(\mathbf{x},t) \in L_p((0,\tilde{t}\,]\times\partial\Omega)$, $Q_l^{(s)}(\mathbf{x},t) \in W_p^{1-\frac{1}{2p},2-\frac{1}{p}}((0,\tilde{t}\,]\times\partial\Omega)$. So, Theorem 7 guarantees the well-posedness of solutions to the problem (6.27).

Galerkin-FEM basics

According to the Subsection 6.2.3, we rewrite both the equation and boundary conditions of (6.26) as follows [112]:

$$\begin{aligned}
R_1 &: \mu\frac{\partial T(\mathbf{x},t)}{\partial t} - \lambda\nabla^2 T(\mathbf{x},t) - \eta Q_l^{(v)}(\mathbf{x},t) = 0,\\
R_2 &: \lambda\frac{\partial T(\mathbf{x},t)}{\partial \hat{\mathbf{n}}} - \beta h^{bench}[T_{bench} - T(\mathbf{x},t)] - h^{air}[T_{air} - T(\mathbf{x},t)] +\\
&\quad - \alpha\epsilon\sigma_B[T_{air}^4 - T^4(\mathbf{x},t)] - \eta Q_l^{(s)}(\mathbf{x},t) = 0.
\end{aligned} \tag{6.29}$$

If w_1 and w_2 are two weight functions, from both (6.29), we can write

$$\int_\Omega w_1\, R_1\, \mathrm{d}\Omega + \int_{\partial\Omega} w_2\, R_2 \mathrm{d}(\partial\Omega) = 0, \tag{6.30}$$

The first integral in (6.30), becomes

$$\int_\Omega w_1\, R_1 \mathrm{d}\Omega = \int_\Omega w_1\, (\mu \partial_t T(\mathbf{x},t))\, \mathrm{d}\Omega - \int_\Omega w_1\, \lambda \nabla^2 T(\mathbf{x},t) \mathrm{d}\Omega - \int_\Omega w_1\, \eta Q_l^{(v)}(\mathbf{x},t) \mathrm{d}\Omega. \tag{6.31}$$

Integrating by parts, the second integral of the right side in (6.31) becomes

$$\int_\Omega w_1\, \lambda \nabla^2 T(\mathbf{x},t) \mathrm{d}\Omega = \int_{\partial\Omega} \lambda\, w_1\, \partial_{\hat{\mathbf{n}}} T(\mathbf{x},t) \mathrm{d}(\partial\Omega) - \int_\Omega \lambda \nabla w_1 \cdot \nabla T(\mathbf{x},t) \mathrm{d}\Omega. \tag{6.32}$$

Therefore, the equation (6.31), by means of (6.32), is writable as

$$\begin{aligned} \int_\Omega w_1\, R_1 \mathrm{d}\Omega = \int_\Omega w_1\, \mu \partial_t T(\mathbf{x},t) \mathrm{d}\Omega - \int_{\partial\Omega} \lambda w_1 \partial_{\hat{\mathbf{n}}} T(\mathbf{x},t) \mathrm{d}(\partial\Omega) + \\ + \int_\Omega \lambda\, \nabla w_1 \cdot \nabla T(\mathbf{x},t) \mathrm{d}\Omega - \int_\Omega w_1\, \eta Q_l^{(v)}(\mathbf{x},t) \mathrm{d}\Omega = 0, \end{aligned} \tag{6.33}$$

from which

$$\begin{aligned} \int_{\partial\Omega} \lambda w_1 \frac{\partial T(\mathbf{x},t)}{\partial \hat{\mathbf{n}}} d(\partial\Omega) = \int_\Omega w_1 \Big(\mu \frac{\partial T(\mathbf{x},t)}{\partial t} - \eta Q_l^{(v)}(\mathbf{x},t) \Big) d\Omega + \\ + \int_\Omega \lambda \nabla w_1 \cdot \nabla T(\mathbf{x},t) d\Omega. \end{aligned} \tag{6.34}$$

The second integral in (6.30), $\forall i \in \{1,2,3\}$ and $\forall j \in \{1,2,...,16\}$, becomes

$$\begin{aligned} \int_{\partial\Omega} w_2 R_2 d(\partial\Omega) = \int_{\partial\Omega} w_2 \Big\{ \lambda \frac{\partial T(\mathbf{x},t)}{\partial \hat{\mathbf{n}}} - \beta h^{bench} [T_{bench} - T(\mathbf{x},t)] + \\ - h^{air} [T_{air} - T(\mathbf{x},t)] - \alpha \epsilon \sigma_B [T_{air}^4 - T^4(\mathbf{x},t)] + \\ - \eta Q_l^{(s)}(\mathbf{x},t) \Big\} d(\partial\Omega) = 0, \end{aligned} \tag{6.35}$$

from which

$$\begin{aligned} \int_{\partial\Omega} \lambda w_2 \frac{\partial T(\mathbf{x},t)}{\partial \hat{\mathbf{n}}} d(\partial\Omega) = \int_{\partial\Omega} w_2 \eta Q_l^{(s)}(\mathbf{x},t) d(\partial\Omega) + \\ + \int_{\partial\Omega} w_2 \beta h^{bench} [T_{bench} - T(\mathbf{x},t)] d(\partial\Omega) + \\ + \int_{\partial\Omega} w_2 h^{air} [T_{air} - T(\mathbf{x},t)] d(\partial\Omega) + \\ + \int_{\partial\Omega} w_2 \alpha \epsilon \sigma_B [T_{air}^4 - T^4(\mathbf{x},t)] d(\partial\Omega). \end{aligned} \tag{6.36}$$

For $w_1 = w_2 = w$, both (6.34) and (6.36) have the same left side, so that, subtracting side-by-side, we can write:

$$\begin{aligned} \int_\Omega w \Big(\mu \frac{\partial T(\mathbf{x},t)}{\partial t} - \eta Q_l^{(v)}(\mathbf{x},t) \Big) d\Omega + \int_\Omega \lambda w \nabla w \cdot \nabla T(\mathbf{x},t) d\Omega + \\ - \int_{\partial\Omega} w \eta Q_l^{(s)}(\mathbf{x},t) d(\partial\Omega) - \int_{\partial\Omega} w \beta h^{bench} [T_{bench} - T(\mathbf{x},t)] d(\partial\Omega) + \\ - \int_{\partial\Omega} w h^{air} [T_{air} - T(\mathbf{x},t)] d(\partial\Omega) - \int_{\partial\Omega} w \alpha \epsilon \sigma_B [T_{air}^4 - T^4(\mathbf{x},t)] d(\partial\Omega) = 0. \end{aligned} \tag{6.37}$$

We discretize Ω into n nodes, on each of which the temperature is indicated with T_k ($k = 1, ..., n$). If N_k are the shape functions, then

$$T = \sum_{k=1}^{n} N_k T_k = N_1 T_1 + N_2 T_2 + ... + N_n T_n, \tag{6.38}$$

$$\begin{aligned} &T = [N]\{T\} = \sum_{i=1}^{n} N_i T_i, \quad T^4 = [N]\{T^4\}, \quad \frac{\partial T}{\partial t} = [N]\{\dot{T}\}, \\ &\frac{\partial T}{\partial x} = [N_x]\{T\}, \quad \frac{\partial T}{\partial y} = [N_y]\{T\}, \quad \frac{\partial T}{\partial z} = [N_z]\{T\}. \end{aligned} \tag{6.39}$$

Assuming that the weight functions are equal to the shape functions, the following makes sense

$$\frac{\partial w}{\partial x} = [N_x], \quad \frac{\partial w}{\partial y} = [N_y], \quad \frac{\partial w}{\partial z} = [N_z], \tag{6.40}$$

so that (6.37) becomes

$$\begin{aligned} &\int_\Omega \mu([N]\{T\})[N]\{\dot{T}\}d\Omega + \int_\Omega \lambda\Big([N_x][N_x] + [N_y][N_y] + [N_z][N_z]\Big)\{T\}d\Omega = \\ &= \int_\Omega [N]\eta Q_l^{(v)}(\mathbf{x}, t)d\Omega + \int_{\partial\Omega} [N]\{T^4\}d(\partial\Omega) + \int_{\partial\Omega} \eta Q_l^{(s)}(\mathbf{x}, t)d(\partial\Omega) + \\ &+ \int_{\partial\Omega} [N]\beta h^{bench} T_{bench} d(\partial\Omega) + \int_{\partial\Omega} [N]h^{air} T_{air} d(\partial\Omega) + \\ &+ \int_{\partial\Omega} [N]\alpha\epsilon\sigma_B T_{air}^4 d(\partial\Omega) - \int_{\partial\Omega} [N]\beta h^{bench}[N]\{T\}d(\partial\Omega) + \\ &- \int_{\partial\Omega} [N]h^{air}[N]\{T\}d(\partial\Omega) - \int_{\partial\Omega} [N]\alpha\epsilon\sigma_B[N]\{T^4\}d(\partial\Omega). \end{aligned} \tag{6.41}$$

Therefore, indicating by

$$\begin{aligned} [Z] &= \int_\Omega \mu[N]d\Omega, \\ [\tilde{Y}] &= [K] + [Y], \\ [K] &= \int_\Omega \lambda\left([N_x][N_x] + [N_y][N_y] + [N_z][N_z]\right)d\Omega, \\ [Y] &= \int_{\partial\Omega} \Big(\beta h^{bench}[N][N] + h^{air}[N][N]d(\partial\Omega)\Big), \\ [H] &= \int_{\partial\Omega} \alpha\epsilon\sigma_B[N][N]d(\partial\Omega), \\ \{F\} &= \int_\Omega [N]\eta Q_l^{(v)}(\mathbf{x}, t)d\Omega + \int_{\partial\Omega} \eta Q_l^{(s)}(\mathbf{x}, t)d(\partial\Omega) + \int_{\partial\Omega} \Big(\beta h^{bench} T_{bench}[N] + \\ &\quad + h^{air} T_{air}[N] + \alpha\epsilon\sigma_B T_{air}^4[N]\Big)d(\partial\Omega). \end{aligned} \tag{6.42}$$

(6.41) is writable as

$$[Z]\{\dot{T}\} + [\tilde{K}]\{T\} + [H]\{T^4\} = \{F\}, \tag{6.43}$$

whose integrals are computed by the Crank-Nicholson procedure. The FEM approach, according to (6.43), has been numerically implemented on an Intel Core 2 CPU 1.45 GHz machine and MatLab R2022 PDE tool, testing them on different kinds of laser sources as described in Subsection 6.2.3.

6.2.5 Results of Computations

Here, the results obtained using the laser heat source as detailed above are presented and discussed. The physical parameter of the alloy Al-Si 5%, kindly provided by IRIS s.r.l., are listed in Table 6.4, and the laser physical parameters related to a typical welding process for alloy Al-Si 5% are listed in Table 6.5 (the laser intensity is computed by $I_0 = P/\pi r_U^2$).

parameter	value	unit
$\mathcal{C}_S$	$2.943 \cdot 10^6$	$J/(m^3K)$
$\mathcal{C}_L$	$3.07 \cdot 10^6$	$J/(m^3K)$
λ	290	$W/(m\,K)$
L_v	$990.6 \cdot 10^6$	$J/(m^3)$
T_S	850.15	K
T_L	923.15	K
ϵ	0.8	

TABLE 6.4: Physical parameters of Al-Si 5% alloy.

parameter	significance	value	unit
v	velocity	40	mm/s
P	power	2400	W
r_U	radius	1.5	mm
R_f	reflexsivity	0.9	
I_0	intensity	340	W/mm^2

TABLE 6.5: Laser parameters.

Furthermore, we set $\sigma_B = 1.35 \cdot 10^{-23} J/K$, $T_0 = T_{air} = T_{bench} = 298K$ (typical environmental temperature in welding forge [204, 205]); $h^{air} = 15 \cdot 10^{-6} W/(mm^2K)$ and $h^{bench} = 20h^{air}$ (as experimentally suggested from metallurgical experiments [206, 207] to guarantee both the correct penetration without favoring the thermal degradation of the alloy structure and is such that it produces significant effects even at depth).

Galerkin-FEM procedure applied to (6.26), described above and implemented in MatLab, optimizes a mesh with tetrahedral elements. To obtain reliable and superimposable results with experimental evidence, Ω has been discretized by a mesh with 3500 finite elements (4522 nodes, 3924 edges), which thicken in the vicinity and especially in correspondence of Ω_3 (welding area) where the melting process takes place (Figure 6.11(a)). Moreover, the mesh refinement at Ω_3 has also been slightly extended in Ω_1 and Ω_2 to perform the temperature reduction in passing from the welding area to the remaining part of Ω. Furthermore, the quality of the mesh was confirmed by computing the indices presented in Subsection 6.2.5 whose values obtained fall within the respective ranges of admissible values for good-quality meshes.

The lasting of the considered welding process is $2.5s$, as is the usual practice for laser welding of plates of dimensions compatible with those fixed in this work [208] (see Figure 6.11(b), where the red point represents the impact point of the laser beam). Once the laser has melted the material. advancing further along the joining line of the plates, the molten material re-solidifies, thanks to the significant drop in temperature (blue area, see Figure 6.11(b)).

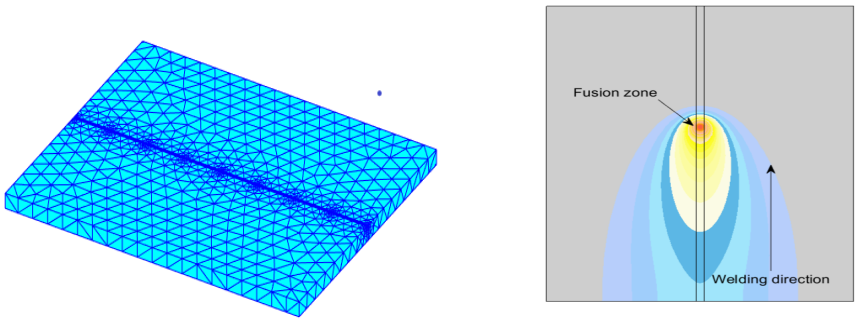

(a) (b)

FIGURE 6.11: (a) Mesh creation: 3500 finite element (4522 nodes, 3924 edges); (b) Fusion zone and welding direction.

Mesh creation

We create the mesh ($\overline{T} = \{E_k\}$) where E_k is the generic finite element and such that $E_k \cap E_{k'} = \emptyset, k \neq k', \forall k \neq k'$ (is either empty or consists of exactly one node or of one edge), obtained with triangulation techniques to obtain tetrahedral finite elements. We have discretized Ω in order that ($\Omega = \cup_{k=1}^{N_{\overline{T}}} E_k$), with $N_{\overline{T}} = |\overline{T}|$. Moreover, the size of the mesh h, $h(E_k)$, is quantifiable as [112] $h(E_k) = \sup_{x,y \in E_k} \|x - y\|$ so that $h = \max_{E_k \in \overline{T}}(E_k)$. Particularly, the volume of each E_k, indicated by V_k, is computable as

$$V_k = \frac{1}{6} \begin{vmatrix} x_2 - x_1 & x_3 - x_1 & x_4 - x_1 \\ y_2 - y_1 & y_3 - y_1 & y_4 - y_1 \\ z_2 - z_1 & z_3 - z_1 & z_4 - z_1 \end{vmatrix}$$

where x_i, y_i, z_i are the coordinates of the vertices P_i of E_k. Moreover, for each triangle of E_k, the surface is

$$S_k = 0.5 \begin{vmatrix} x_2 - x_1 & x_3 - x_1 \\ y_2 - y_1 & y_3 - y_1 \end{vmatrix}.$$

Therefore, a face of E_k is an ordered triad (allowing all possible combinations), while the edges are considered, not as elements of the faces, but as separate entities and are implicitly defined in terms of ordered pairs of vertices. To each E_k we associate the sphere circumscribed at its vertices whose radius, C_k, and its center can be obtained by solving the equation:

$$C_k = \begin{vmatrix} l_1^2 - l^2 & l_2^2 - l_1^2 & l_3^2 - l_1^2 & l_4^2 - l_1^2 \\ x_1 - x & x_2 - x_1 & x_3 - x_1 & x_4 - x_1 \\ y_1 - y & y_2 - y_1 & y_3 - y_1 & y_4 - y_1 \\ z_1 - z & z_2 - z_1 & z_3 - z_1 & z_4 - z_1 \end{vmatrix}$$

where $l^2 = x^2 + y^2 + z^2$ and $l_i^2 = x_i^2 + y_i^2 + z_i^2$ ($i = 1, ..., 4$), or solving a system of linear equation for achieving the center. As in two dimensions, there is a formula that allows you to calculate the radius and that allows you to avoid calculating C_k:

$$r_k = (24V_k)^{-1}((m + n + s)(m + n - s)(n + s - m)(m - n + s))^{0.5}$$

where m, n and s are the products of the lengths of two opposite edges. Finally, the radius of the inscribed sphere can be evaluated as

$$\gamma_k = 3V_k(S_1 + S_2 + S_3 + S_4)^{-1},$$

where S_i is the surface of the triangle i of E_k. Since the simulations require rather long execution times, we have previously evaluated the quality of the meshes obtained. In particular, three well-established quality indices have been exploited: aspect ratio, Jacobian ratio, maximum corner angle and skewness [112]. For each triangular element, the aspect ratio values obtained, an index that guarantees good numerical accuracy if all sides of an element are of equal length, they are all very close to 1. In parallel, for each tetrahedron, the value obtained for the Jacobian ratio, which quantifies whether each average node is positioned in the center with respect to two adjacent nodes, are also very close to 1. The maximum angles between two sides of each element were also evaluated, obtaining values much smaller than 2π rad; this cautions us from possible degradation of performance. Finally, the asymmetries were also evaluated, which resulted to be very close to the zero value. These obtained values highlight the excellent quality of the constructed meshes. Furthermore, the ToolBox uses automatic generation techniques of high quality meshes in relation to the type of problem to be solved. Also, using the "MeshQuality" ToolBox further controlled the quality of the mesh. Finally, during the simulation campaign, we compared the results obtained with similar cases known in the literature.

Exploiting classical Gaussian laser heat source

As already specified, the duration of the welding process is equal to $2.5s$, in accordance with the executive practice of laser welding for plates whose dimensions are compatible with those specified in this [208] paper. Figure 6.12 displays the welding process implemented in MatLab; once the material has melted, the laser advances along the joint line of the slabs, melting further material while the previously melted material solidifies as the temperature drops drastically. Figures 6.13(a)-6.14(a), relating to the final point of the weld, offers greater evidence of this phenomenon, emphasizing that, already in the numerical simulation phase, (6.26) models the underlying of the proposed approach. As highlighted in Figure 6.11(a), the mesh is not capillary over Ω but only over Ω_3 and its immediate vicinity because (6.26) does not consider any delay times for the distribution of $T(\mathbf{x}, t)$ during the passage of the laser beam. Therefore, considering this distribution throughout Ω instantaneous, the cooling in both Ω_1 and Ω_2 is immediate, also considering that the thermal conduction between the plates and the workbench has also been taken into account.

Both Figures 6.15(a) and 6.15(b) depict this aspect because they show the distribution of $T(\mathbf{x}, t)$ both in the initial point and in five different points of the welding wire from which it can be seen that once the temperature peak has been reached, as the laser beam advances, the cooling is locally evident. Furthermore, the final point of the welding path is affected both by the presence of the laser beam and by the conduction of the other points where the welding has already taken place. In fact, the peaks increase as the weld progresses toward the endpoint. However, we observe that this remark does not affect the quality of the proposed model because, regardless of any delay times in the distribution of $T(\mathbf{x}, t)$, Ω_3 remains the most thermally stressed area where, after the laser welding process, checks the mechanical properties. In confirmation of the above, the thermal cycles were obtained transversally to the welding line (in correspondence with its midpoint) from which it is once again

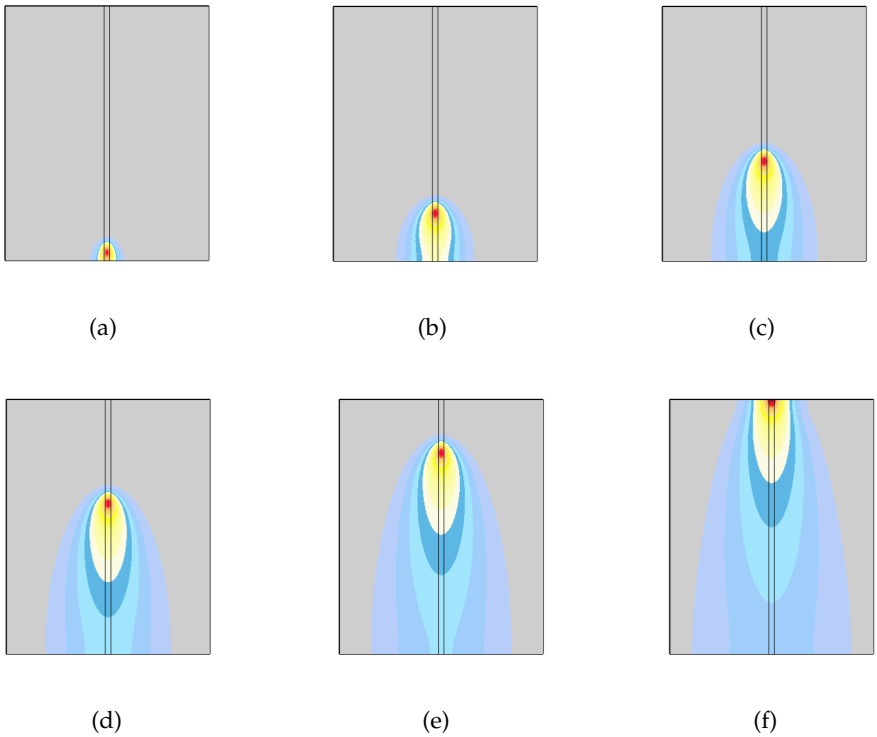

FIGURE 6.12: Welding process. The red point represents the impact area of the laser beam. Initial zone: (a)-(b); central zone: (c)-(d)-(e) and final zone: (f).

highlighted how, moving away from the welding line, the cooling of the plates is drastic (see Figure 6.16(a)). On the other hand, moving along the welding line, the thermal cycles show behaviors that are qualitatively/quantitatively similar to each other (see Figure 6.16(b)). Particularly, during the welding process, the temperature peaks are well above the melting range of the alloy, as required by the welding execution practice, to guarantee the melting of the material along the entire depth of the plates.

Exploiting conical 3D laser heat source

Here, we set all parameters, as in Subsection 6.2.5. Moreover, here $z_U = 4\ mm$ and $z_L = 0\ mm$, as often happens in many aluminum alloy plate welding processes. Therefore, the $T(\mathbf{x}, t)$ distribution in Ω as highlighted in Figures 6.13(b)-6.14(b) (when the laser beam reaches the final position of the welding path), simulating a laser welding of the same duration as the one simulated in subsection 6.2.5. Further in this case, in Ω_3, $T(\mathbf{x}, t)$, throughout the welding process, settles on values, ensuring the fusion of the aluminum even in depth, although the temperatures reached are higher than when a classical Gaussian 3D laser head source is considered, risking carrying out a melting and re-solidification process that does not meet the required quality standards. As regards the thermal cycles both transversely and longitudinally of the welding line, they appear qualitatively superimposable to those obtained in Figures 6.16(a) and 6.16(b). Thus, (6.26) does not consider any thermal losses (as well as any time-lag that slows down the temperature distribution), the Conical 3D laser head source could not be suitable to model the

laser beam because the real $T(\mathbf{x}, t)$ in Ω_3, being oversized, could not guarantee the total melting of the alloy without compromising the internal structure of the material. This phenomenon is more evident by analyzing Figures 6.13(b)-6.14(b) where the aforementioned drop in temperatures is most apparent. However, as highlighted in Subsection 6.2.5, the weld bead still has a truncated cone shape whose geometric parameters are still potentially compatible with those required by current legislation on laser welding. Furthermore, the surface temperature during the welding process is characterized by peaks that largely exceed the melting range of the alloy (see Figures 6.15(c) and 6.15(d)) with consequent marked degradation of the surface itself. It follows that (6.26), together with the joint use of the 3D heat source conic and the values chosen for both P and I_0, does not represent a reliable tool for dynamic mapping of the temperature in the process of laser welding under study, as metallurgically recently proved [204, 205].

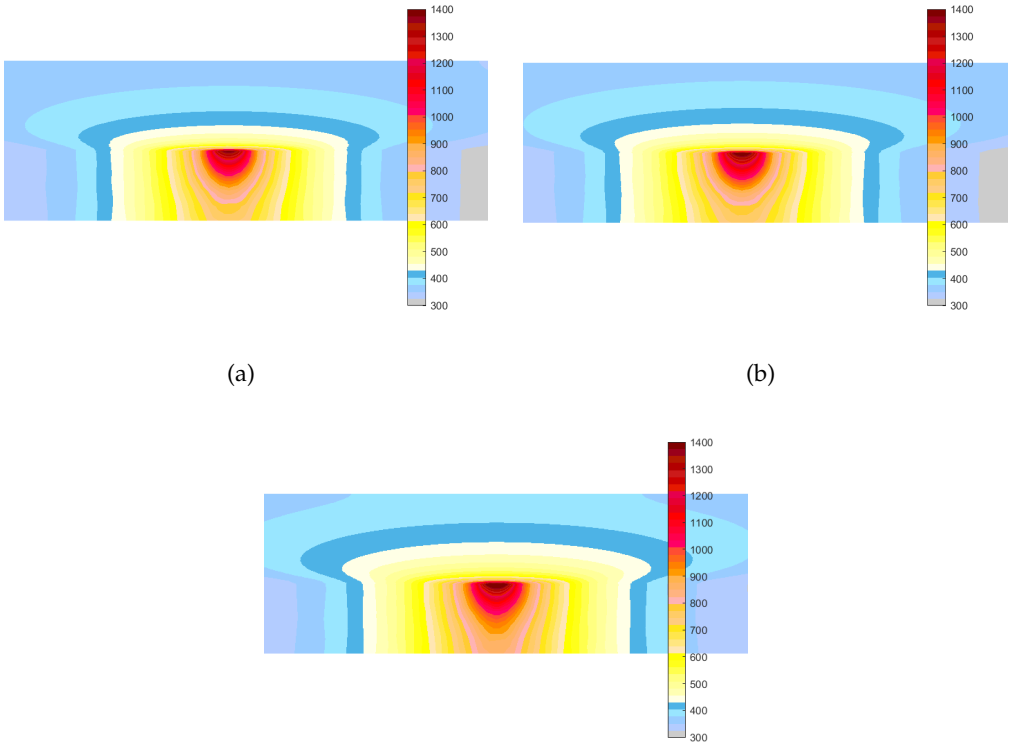

(a) (b)

(c)

FIGURE 6.13: Distribution of $T(\mathbf{x}, t)$ in Ω when the laser beam, modeled using: (a) Gaussian formulation, (b) conical formulation and (c) ellisoidal formulation has reached the final point of the welding path.

Exploiting ellipsoid laser heat source

As a further confirmation of the precision of using the classical 3D Gaussian formulation for laser beam modeling, here we present the results obtained using the ellipsoid formulation as specified in Subsection 6.2.3. Here, too, as for the previous subsections, we have simulated the welding of the same duration using the same physical parameters for the alloy (Table 6.4) while, concerning the ellipsoid laser heat source parameters, as the literature suggests, we set $a_f = 1\ mm$, $a_r = 5\ mm$, and

(a) (b)

(c)

FIGURE 6.14: Distribution of $T(\mathbf{x}, t)$ in Ω when the laser beam, modeled using: (a) Gaussian formulation, (b) conical formulation and (c) ellisoidal formulation.

$b = c = 1\ mm$. In this case, we also used the same mesh exploited in the previous cases since its refinement did not produce appreciable improvements (compared to a conspicuous increase in computational complexity). As depicted in Figures 6.13(c)-6.14(c), the distribution of $T(\mathbf{x}, t)$ in Ω_3 highlights high values of temperature that melting the material only on the surface, without eliminating the risk of local damage in the structure, but without producing deep fusion. This is also evidenced in both Figures 6.15(e) and 6.15(f), which show the same qualitative behavior highlighted using the other laser sources, but with different peaks of temperature. We finally observe that, also in this case, both transversal and longitudinal thermal cycles are qualitatively superimposable with those obtained using the other formulations of heat laser sources. Therefore, the proposed model, assisted by this formulation of the heat source laser and with appropriate power output, appears suitable for industrial and iron and steel applications, which require superficial and sub-surface fusions of the material [192, 209–212].

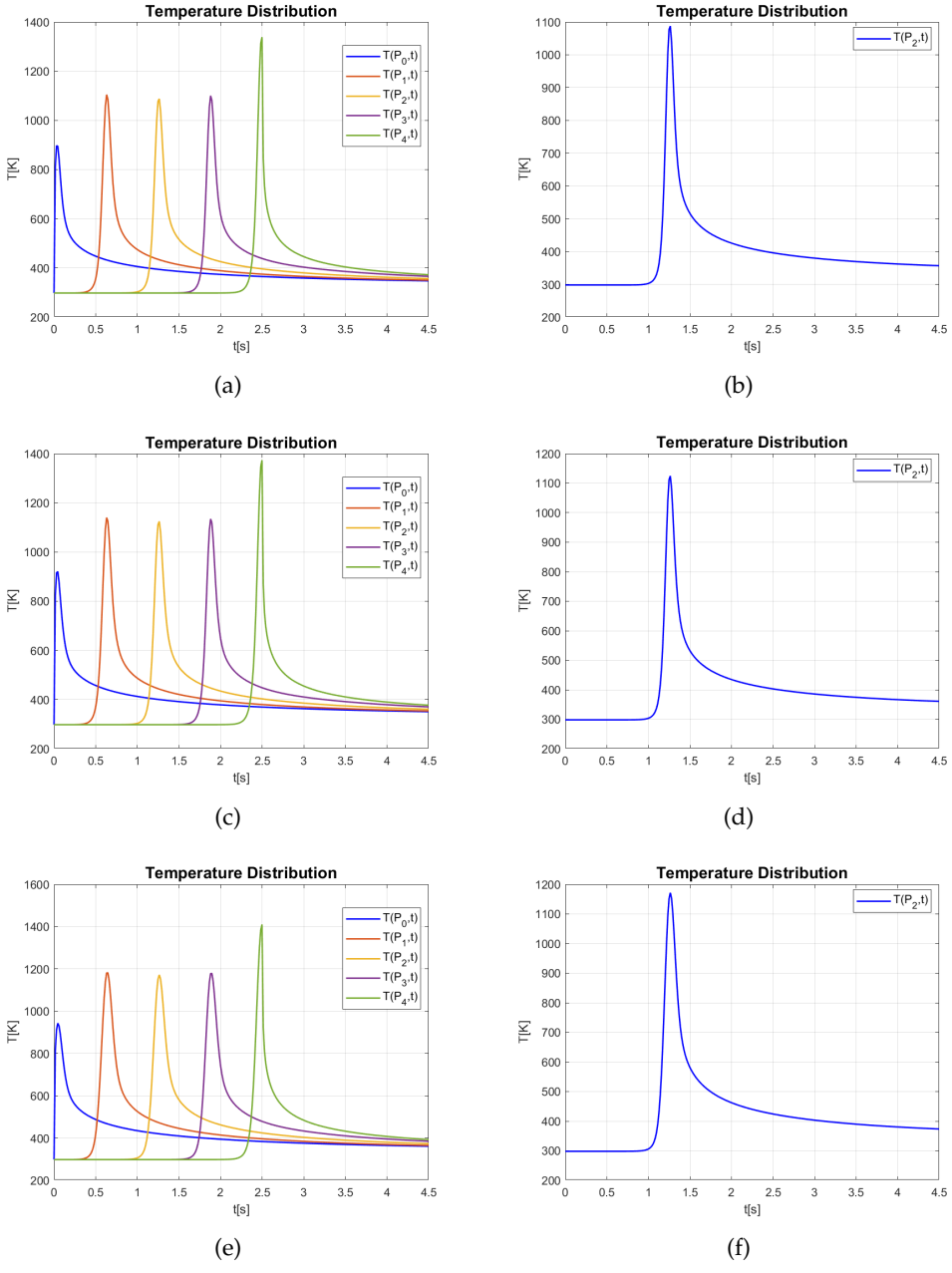

FIGURE 6.15: Distribution of $T(\mathbf{x}, t)$ in five different points on the welding wire ($P_0 = (0, 40.5, 4), P_1 = (25, 40.5, 4), P_2 = (50, 40.5, 4)$, $P_3 = (75, 40.5, 4)$, $P_4 = (100, 40.5, 4)$) (a)-(b)-(c) and in the middle point P_1 of the welding wire (b)-(d)-(f), with Gaussian 3D laser heat source in (a)-(b), Conical 3D laser heat source in (c)-(d) and Ellipsoid 3D laser heat source in (e-(f)

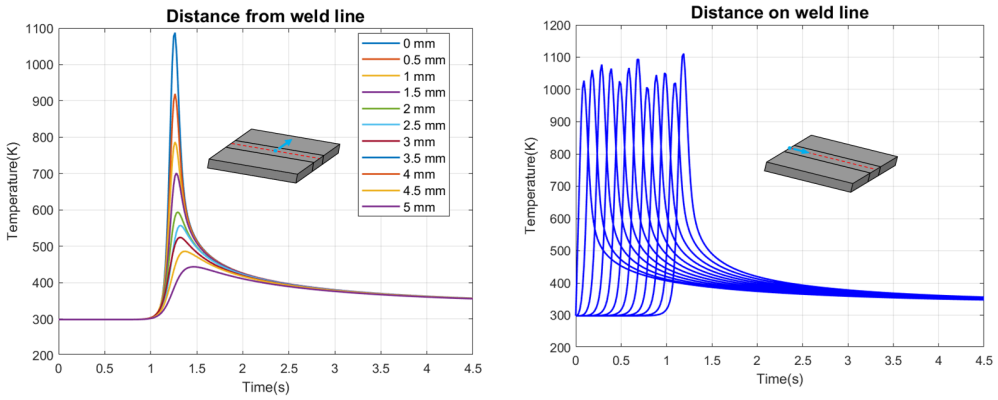

(a) (b)

FIGURE 6.16: Thermal cycles in: (a) transverse direction, (b) longitudinal direction, with Gaussian 3D laser heat source.

The proposed model does not exhaust the phenomenon of laser welding, and several studies must be conducted to optimize the proposed process and evaluate it with experimental tests. In particular, non-linearity can be included, as for the thermal conductivity, where it is assumed that the latter depends on temperature. This would better reflect real world conditions and contribute to more accurate forecasts.

Furthermore, although the laser power is high, it must be borne in mind that it takes time for the electrical power, converted into thermal equivalent, to penetrate the material and cause it to melt. In this case it would be appropriate to consider the material response time before the thermal input of the laser penetrates deep, and introduce one/two relaxation times, considering a model of type Maxwell-Cattaneo-Vernotte/Dual-Phase-lag or another extension of Fourier's law.

Finally, to better simulate the real behaviour of laser welding, phenomena such as the production of vapour bubbles (closing holes), surface tension imbalances caused by temperature gradients (Marangoni effect) could be taken into account..

Conclusions and Future Perspectives

In this thesis, we derived Fourier's law and its generalizations from the framework of Extended Thermodynamics and discussed comparisons with other theories. Particular emphasis was placed on the role of non-Fourier heat conduction, focusing on the temperature dependence of thermal conductivity and relaxation time. We first explored the thermodynamic origin of the Fourier (F), Maxwell-Cattaneo-Vernotte (MCV), and Guyer-Krumhansl (GK) equations, showing how these derivations are based solely on the first and second laws of thermodynamics, and highlighting the connection between material parameters.

In Chapter 3, we investigated the effects of nonlinearities in thermal conductivity within the Fourier framework. Specifically, we examined cases where the thermal conductivity increases or decreases with rising temperature. Such nonlinear effects are particularly relevant in situations where material properties vary significantly with temperature, and their impact must be accounted for in both theoretical models and experimental settings.

In Chapter 4, we investigated the nonlinearities in the MCV model, particularly in the context of heat pulse experiments. We found that even a simple linear temperature dependence in both the relaxation time and thermal conductivity can induce temperature-dependent mass density. This implies that mechanical effects, such as thermal expansion, might need to be considered in future models to obtain a more realistic description of the system. However, the primary objective here was to demonstrate the effectiveness of a staggered numerical scheme in solving nonlinear heat conduction problems in one and two dimensions. We analyzed the scheme's stability and convergence properties, finding that while stability estimates using a linearized version of the problem are useful, they are not fully reliable for predicting the maximum temperature field in nonlinear scenarios. Despite this, the approach allowed for efficient simulations. Our results showed that temperature-dependent material parameters significantly affect the steepness of the temperature wavefront, which could serve as an indicator of nonlinearity in experimental contexts. Moreover, these parameters often produced opposite effects, complicating the identification of specific nonlinearities in measurements. In two-dimensional problems, we observed delays and oscillations in the heat pulse reflections, which are not artifacts of the method but rather a result of the heat conduction dynamics. These effects, along with our method's dispersion properties, could prove valuable for future experimental work on nonlinear heat conduction.

In the future, the study of more complex geometries, potentially using finite element or finite volume methods, will be necessary to extend these results to real-world applications. Although the current method could handle more complicated domains, its implementation in such cases presents challenges.

In the last part of the Chapter 4, we compared two nonlinear formulations of the MCV equation: one assuming temperature-dependent material coefficients, and another using a conservation-dissipation framework to describe the evolution of the thermodynamic conjugate of the heat flux. By focusing on the propagation of short temperature pulses, we examined how nonlinear effects in the thermal conductivity, $\lambda(T)$, and relaxation time, $\tau(T)$, influenced the velocity and shape of the thermal signal. Future research should focus on applying these results to specific materials and experimental setups, as well as comparing nonlinear MCV models with experimental data. Additionally, exploring soliton propagation in wires and nanowires using nonlinear MCV models could be of significant interest, especially in the context of information transmission via thermal pulses.

The Guyer-Krumhansl (GK) model was the focus of Chapter 5, as it is a promising candidate for future engineering applications. We studied the nonlinear effects of temperature-dependent material parameters within the GK framework, finding that the behavior of nonlinear terms, particularly in relaxation time and thermal conductivity, exhibited similar trends to those observed in the MCV model. Specifically, increasing thermal conductivity enhanced heat propagation, while increasing relaxation time delayed it.

Our analysis of the GK model showed that nonlocal terms, which measure the departure from the hyperbolic regime, are significantly affected by nonlinearities. Nonlinearity in thermal conductivity, in particular, reduced the temperature peak and slowed heat propagation. Interestingly, when the nonlocal term was defined as a generic temperature-dependent function, increasing the nonlinearity initially delayed heat propagation, but at higher values, wave-like behavior reemerged, revealing the model's hyperbolic nature.

By employing a staggered numerical scheme, we solved a two-dimensional heat conduction problem with space- and time-dependent boundary conditions. We introduced a second-order tensor $\mathbf{Q}$ as an auxiliary quantity to facilitate boundary condition implementation, which helped in reproducing Fourier-like solutions under specific resonance conditions. Additionally, when rotational terms dominated heat flux evolution, significant local temperature reductions were observed, though this effect is distinct from negative temperatures and occurs only briefly. These results could be useful in future studies involving heterogeneous materials and nanoscales, where adjusting the parameters allows the model to extend beyond the scope of phonon hydrodynamics.

Chapter 6 explored the potential applications of non-Fourier heat conduction models, particularly in biological and medical fields such as bioheat transfer and laser surgery. Predicting tissue temperature during laser irradiation is a critical factor in medical treatments. Here, the Maxwell-Cattaneo-Vernotte equation proves useful for accurately modeling heat transfer in living tissues, especially in scenarios where finite heat propagation speeds are important. Non-Fourier models are also more reliable than classical Fourier models for capturing the thermal response of tissues with long thermal relaxation times. Our analytical solution of a hyperbolic bioheat equation, including terms for blood perfusion and laser irradiation, provided valuable insights into how thermal relaxation time and perfusion rates affect temperature distributions in tissues during thermal therapy. These results suggest that increased blood perfusion lowers local temperature, while long relaxation times concentrate heat at the surface, leading to higher temperatures. Future work will aim to

incorporate temperature-dependent relaxation times and perfusion rates to further improve these models.

Finally, our analysis has shown that non-Fourier heat conduction models have significant potential for a variety of practical applications, from laser welding to bioheat transport. A key area of future research will involve developing more comprehensive nonlinear models that can be applied to real-world materials and geometries, with the goal of improving both the theoretical understanding and the practical implementation of non-Fourier heat conduction in advanced engineering and medical contexts.

Appendix A

Dissipation and Dispersion Errors of NL-MCV

A.1 Two-dimensional case

The investigation of the dissipation (artificial decrease of the amplitude) and dispersion errors (artificial oscillations) is an important task as the simulation outcomes can be significantly distorted by these errors.

As it is possible to see from the Fig. A.2, using non-homogeneous boundary conditions the solution is affected by more evident oscillations. In both situations the significant oscillations highlighted in the figures A.1 (c)-(d) and A.2 (c)-(d) leading to the instability of the solution are the consequence of the fact that the time step is higher than the threshold value of time step that guarantees the stability of the solution.

More insight is provided by Figures A.3, A.4, A.5 and A.6.

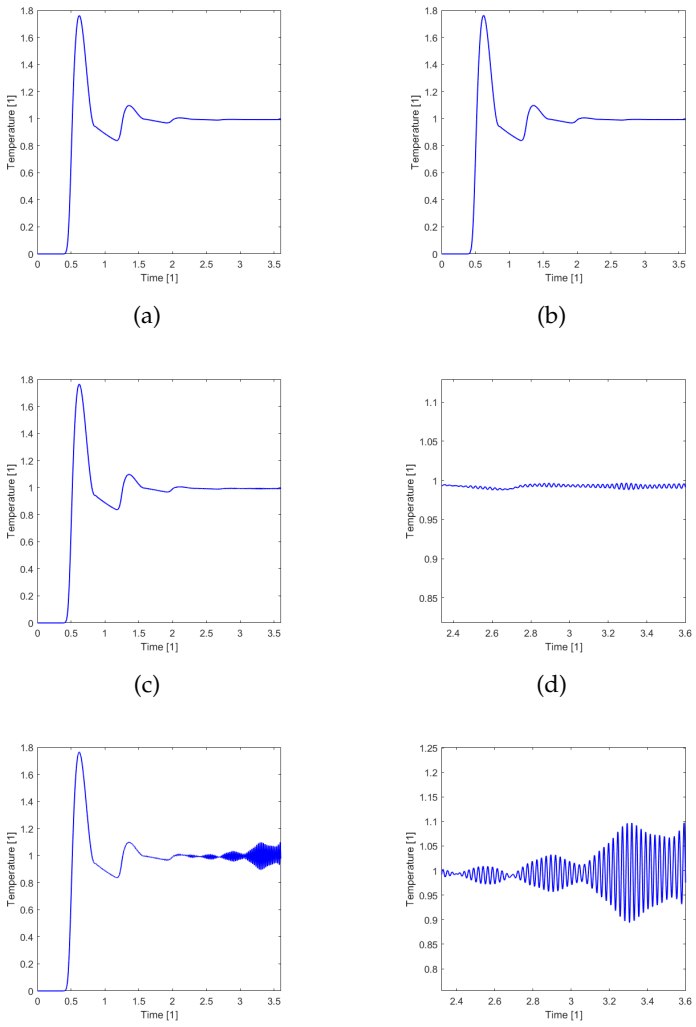

FIGURE A.1: Temperature distribution on the rear face with homogeneous boundary conditions in space, $\Delta x = \Delta y = 0.02, \Delta t_{min} = 5.0367 \cdot 10^{-5}$ (a) $\Delta t = 10^{-5}$, (b) $\Delta t = \Delta t_{min}$, (c)-(d) $\Delta t = 1.2 \cdot 10^{-4}$ and (e)-(f) $\Delta t = 1.5 \cdot 10^{-4}$.

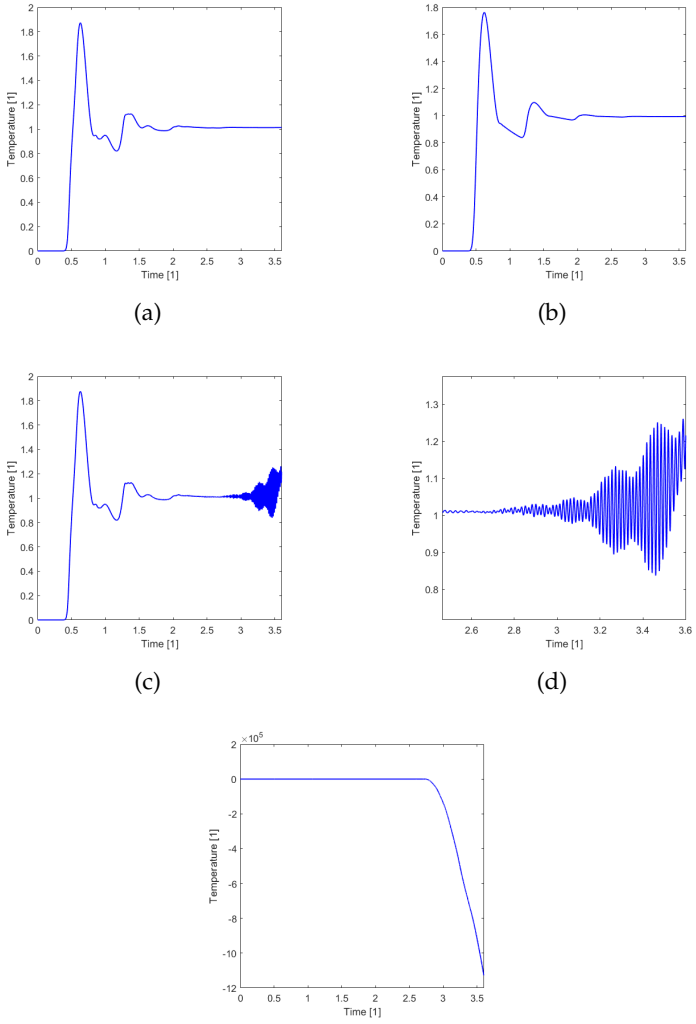

FIGURE A.2: Temperature distribution on the rear face with non-homogeneous boundary conditions in space, $\Delta x = \Delta y = 0.02, \Delta t_{min} = 5.0367 \cdot 10^{-5}$ (a) $\Delta t = 10^{-5}$, (b) $\Delta t = \Delta t_{min}$, (c)-(d) $\Delta t = 1.2 \cdot 10^{-4}$ and (e) $\Delta t = 1.5 \cdot 10^{-4}$.

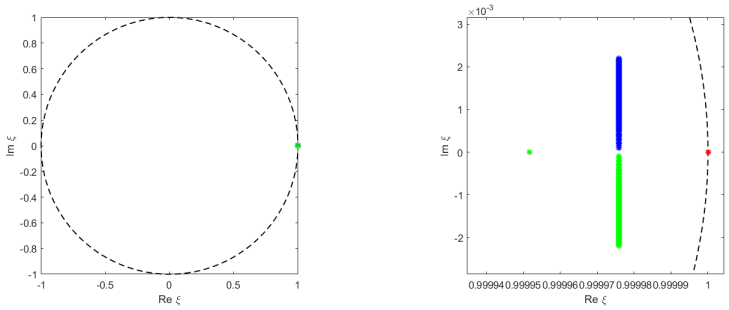

(a) (b)

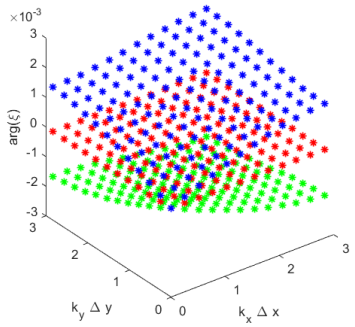

(c)

FIGURE A.3: (a)-(b) The roots of $p(\xi)$ and (c) their argument, with $\Delta x = \Delta y = 0.02, \Delta t = 10^{-5} \leq \Delta t_{min} = 5.0367 \cdot 10^{-5}$. The maximum is choose $Z = 3$. The maximum of the modulus of each roots is: $\max|\xi_1| = 1.00000, \max|\xi_2| = 0.99998, \max|\xi_3| = 0.99998$.

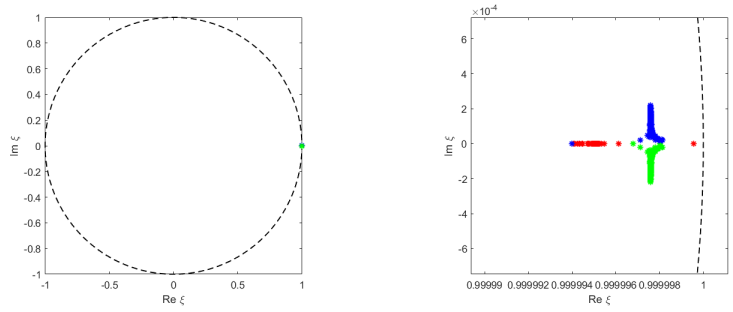

(a) (b)

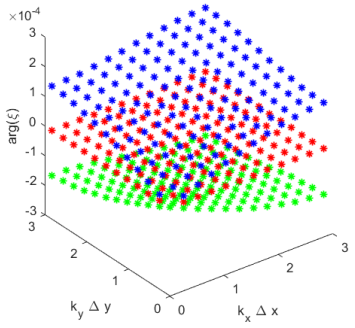

(c)

FIGURE A.4: (a)-(b) The roots of $p(\xi)$ and (c) their argument, with $\Delta x = \Delta y = 0.02, \Delta t = 10^{-6} \leq \Delta t_{min} = 5.0367 \cdot 10^{-5}$. The maximum is choose $Z = 3$.The maximum of the modulus of each roots is: $\max |\xi_1| = 1.00000, \max |\xi_2| = 1.00000, \max |\xi_3| = 1.00000$.

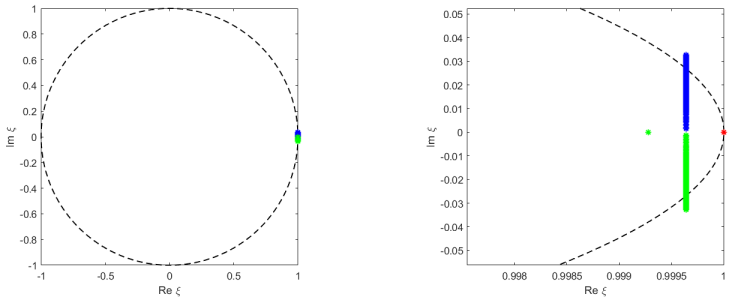

(a) (b)

FIGURE A.5: The roots of $p(\xi)$ with $\Delta x = \Delta y = 0.02, \Delta t = 1.5 \cdot 10^{-4} \geq \Delta t_{min} = 5.0367 \cdot 10^{-5}$. The maximum is choose $Z = 3$. The maximum of the modulus of each roots is: $\max|\xi_1| = 1.0000, \max|\xi_2| = 1.00018, \max|\xi_3| = 1.00018$.

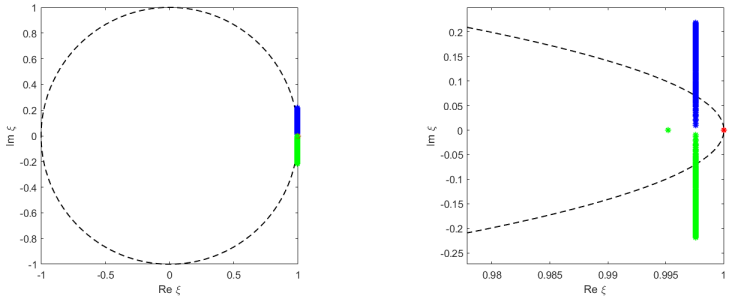

(a) (b)

FIGURE A.6: The roots of $p(\xi)$ with $\Delta x = \Delta y = 0.02, \Delta t = 10^{-3} \geq \Delta t_{min} = 5.0367 \cdot 10^{-5}$. The maximum is choose $Z = 3$. The maximum of the modulus of each roots is: $\max|\xi_1| = 1.0000, \max|\xi_2| = 1.02131, \max|\xi_3| = 1.02131$.

Accuracy order of nonlinear model

It is possible to estimate the accuracy order of the numerical scheme (in powers of $\Delta x, \Delta y$ and Δt). The error of the prediction for $(q_x)^{n+1}_{i+1/2,j}$ reads

$$
\begin{aligned}
(q_x)^{n+1}_{i+1/2,j} - q_x(x_j, y_{i+1/2}, t_{n+1}) &= \left(\frac{\Delta t}{\tau_{q_1} + \tau_{q_2} T^n_{i+1/2,j+1/2}} - 1 \right) (q_x)^n_{i+1/2,j} \\
&- \frac{\left(\tau^{q_x}_{p_1} + \tau^{q_x}_{p_2} T^n_{i+1/2,j+1/2} \right)}{\left(\tau_{q_1} + \tau_{q_2} T^n_{i+1/2,j+1/2} \right)} \cdot \frac{\Delta t}{\Delta x} \cdot \left(T^n_{i+1/2,j+1/2} - T^n_{i+1/2,j-1/2} \right) - q_x(x_j, y_{i+1/2}, t_{n+1}) \\
&\simeq \left(\frac{\Delta t}{\tau_{q_1} + \tau_{q_2} T(x_{j+1/2}, x_{i+1/2}, t_n)} - 1 \right) q_x(x_j, y_{i+1/2}, t_n) - q_x(x_j, y_{i+1/2}, t_{n+1}) - \\
&- \frac{\left(\tau^{q_x}_{p_1} + \tau^{q_x}_{p_2} T^n_{i+1/2,j+1/2} \right)}{\left(\tau_{q_1} + \tau_{q_2} T(x_{j+1/2}, x_{i+1/2}, t_n) \right)} \cdot \frac{\Delta t}{\Delta x} \cdot \left[T(x_{j+1/2}, y_{i+1/2}, t_n) - T(x_{j-1/2}, x_{i+1/2}, t_n) \right] \\
&= - \left[q_x(x_j, y_{i+1/2}, t_{n+1}) - q_x(x_j, y_{i+1/2}, t_n) \right] + \Delta t \cdot \frac{q_x(x_j, y_{i+1/2}, t_n)}{\tau_{q_1} + \tau_{q_2} T(x_{j+1/2}, x_{i+1/2}, t_n)} \\
&- \frac{\left(\tau^{q_x}_{p_1} + \tau^{q_x}_{p_2} T^n_{i+1/2,j+1/2} \right)}{\left(\tau_{q_1} + \tau_{q_2} T(x_{j+1/2}, x_{i+1/2}, t_n) \right)} \cdot \frac{\Delta t}{\Delta x} \cdot \left[T(x_{j+1/2}, y_{i+1/2}, t_n) - T(x_{j-1/2}, x_{i+1/2}, t_n) \right] \\
&= -\Delta t \cdot \frac{\partial q_x}{\partial t}(x_j, y_{i+1/2}, t_n) + o(\Delta t^2) + \Delta t \cdot \frac{q_x(x_j, y_{i+1/2}, t_n)}{\tau_{q_1} + \tau_{q_2} T(x_{j+1/2}, x_{i+1/2}, t_n)} \\
&- \frac{\left(\tau^{q_x}_{p_1} + \tau^{q_x}_{p_2} T^n_{i+1/2,j+1/2} \right)}{\left(\tau_{q_1} + \tau_{q_2} T(x_{j+1/2}, x_{i+1/2}, t_n) \right)} \cdot \frac{\Delta t}{\Delta x} \cdot \left[\Delta x \cdot \frac{\partial T}{\partial x}(x_j, x_{i+1/2}, t_n) + o(\Delta x^3) \right] \\
&= o(\Delta t^2) + o(\Delta x^2).
\end{aligned}
$$

after Taylor series expansion, simplification, and use of equation (4.59b).
Analogously, after executing the same calculations, for the second component of heat flux we obtain

$$(q_y)^{n+1}_{i,j+1/2} - q_y(x_{j+1/2}, y_i, t_{n+1}) = o(\Delta t^2) + o(\Delta y^2).$$

The error of the prediction for $T^{n+1}_{i+1/2,j+1/2}$ is expressed as

$$
\begin{aligned}
&T^{n+1}_{i+1/2,j+1/2} - T(x_{j+1/2}, y_{i+1/2}, t_{n+1}) = T^{n}_{i+1/2,j+1/2} \\
&\quad - \hat{L}\frac{\left[(q_x)^n_{i+1/2,j+1} - (q_x)^n_{i+1/2,j}\right]}{\tau_d\left(1+\frac{\tau_{q_2}}{\tau_{q_1}}T^n_{i+1/2,j+1/2}\right)}\cdot\frac{\Delta t}{\Delta x} - \frac{\left[(q_y)^n_{i+1,j+1/2} - (q_y)^n_{i,j+1/2}\right]}{\tau_d\left(1+\frac{\tau_{q_2}}{\tau_{q_1}}T^n_{i+1/2,j+1/2}\right)}\cdot\frac{\Delta t}{\Delta y} \\
&\quad - T(x_{j+1/2}, y_{i+1/2}, t_{n+1}) \\
&\simeq -\left[T(x_{j+1/2}, y_{i+1/2}, t_{n+1}) - T(x_{j+1/2}, y_{i+1/2}, t_n)\right] \\
&\quad - \hat{L}\frac{\left[q_x(x_{j+1}, y_{i+1/2}, t_n) - q_x(x_j, y_{i+1/2}, t_n)\right]}{\tau_d\left(1+\frac{\tau_{q_2}}{\tau_{q_1}}(x_{j+1/2}, y_{i+1/2}, t_n)\right)}\cdot\frac{\Delta t}{\Delta x} \\
&\quad - \frac{\left[q_y(x_{j+1/2}, y_{i+1}, t_n) - q_y(x_{j+1/2}, y_i, t_n)\right]}{\tau_d\left(1+\frac{\tau_{q_2}}{\tau_{q_1}}T(x_{j+1/2}, y_{i+1/2}, t_n)\right)}\cdot\frac{\Delta t}{\Delta y} \\
&= -\Delta t\cdot\frac{\partial T}{\partial t}(x_{j+1/2}, y_{i+1/2}, t_n) + o(\Delta t^2) \\
&\quad - \frac{\hat{L}}{\tau_d\left(1+\frac{\tau_{q_2}}{\tau_{q_1}}T^n_{i+1/2,j+1/2}\right)}\cdot\frac{\Delta t}{\Delta x}\cdot\left[\frac{\partial q_x}{\partial x}(x_j, y_{i+1/2}, t_n)\Delta x + o(\Delta x^2)\right] \\
&\quad - \frac{1}{\tau_d\left(1+\frac{\tau_{q_2}}{\tau_{q_1}}T^n_{i+1/2,j+1/2}\right)}\cdot\frac{\Delta t}{\Delta y}\cdot\left[\frac{\partial q_y}{\partial y}(x_{j+1/2}, y_i, t_n)\Delta y + o(\Delta y^2)\right] \\
&= o(\Delta t^2) + o(\Delta x) + o(\Delta y).
\end{aligned}
$$

after Taylor series expansion, cancellation and use of equation (4.59a).
Finally

$$
\begin{aligned}
T^{n+1}_{i+1/2,j+1/2} - T(x_{j+1/2}, y_{i+1/2}, t_{n+1}) &= o(\Delta t^2) + o(\Delta x) + o(\Delta y), \\
(q_x)^{n+1}_{i+1/2,j} - q_x(x_j, y_{i+1/2}, t_{n+1}) &= o(\Delta t^2) + o(\Delta x^2), \\
(q_y)^{n+1}_{i,j+1/2} - q_y(x_{j+1/2}, y_i, t_{n+1}) &= o(\Delta t^2) + o(\Delta y^2).
\end{aligned} \tag{A.1}
$$

hence is proved the numerical scheme is second order accurate in time and first order in space, globally it is of order one.

A.2 One-dimensional case

Similarly to the two-dimensional case, the analysis of the dissipation and dispersion errors is shown in the Figures A.7, A.8, A.9, A.10.

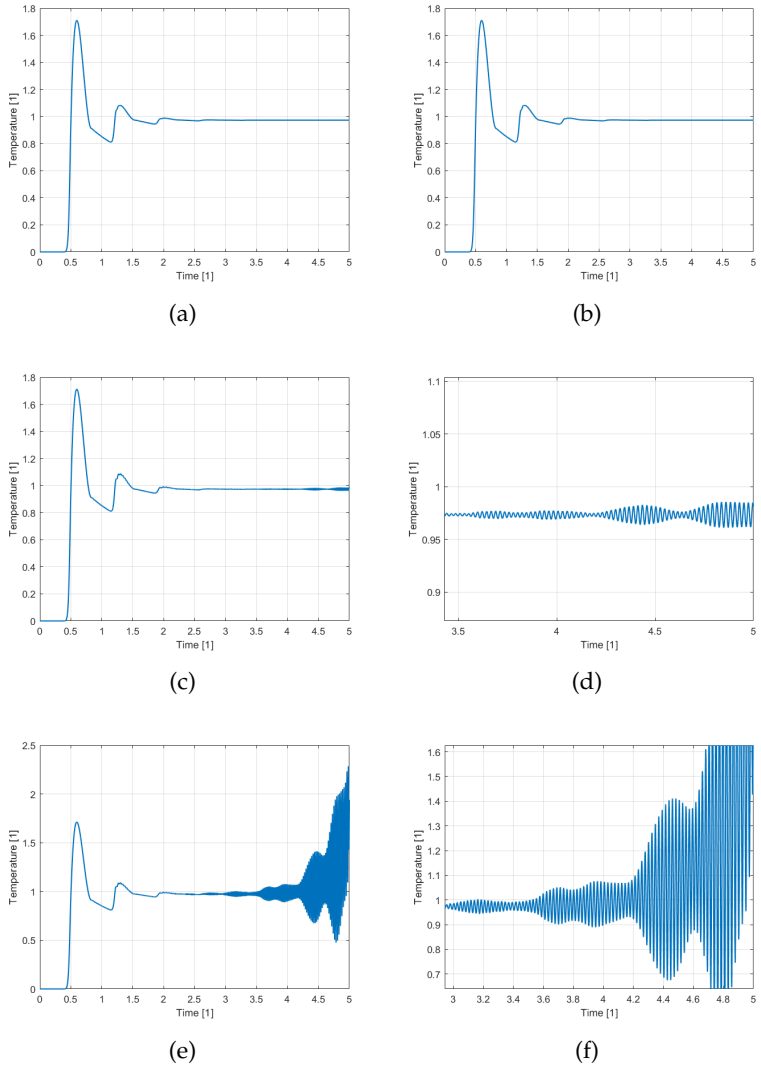

FIGURE A.7: Temperature distribution of rear face in 1D, with $\Delta x = 0.02, \Delta t_{min} = 9.8015 \cdot 10^{-5}$ (a) $\Delta t = 10^{-6}$, (b) $\Delta t = 10^{-5}$, (c)-(d) $\Delta t = \Delta t_{min}$ and (e)-(f) $\Delta t = 1.2 \cdot 10^{-4}$.

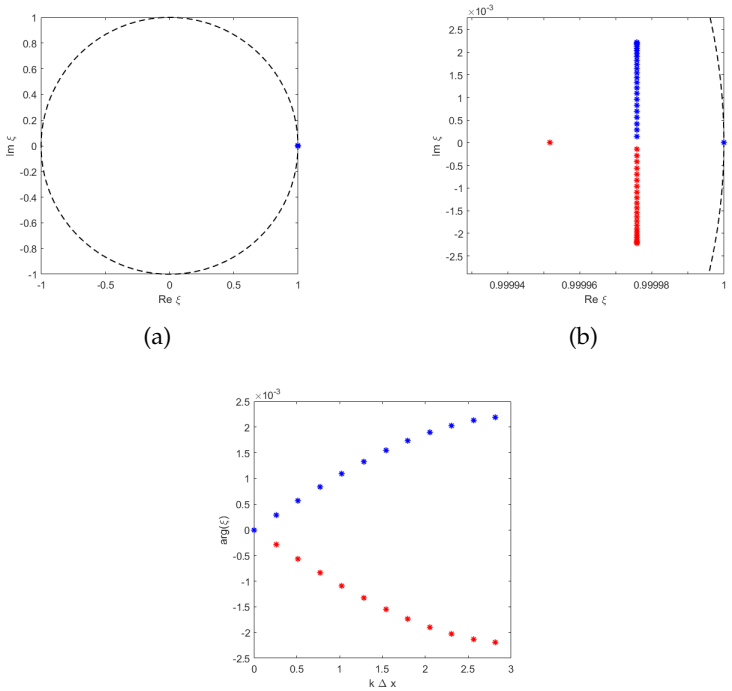

(a) (b)

(c)

FIGURE A.8: (a)-(b) The roots of $p(\xi)$ and (c) the argument, with $\Delta x = 0.02, \Delta t = 10^{-5} \leq \Delta t_{min} = 9.8015 \cdot 10^{-5}$. The maximum is choose $Z = 3$. The maximum of the modulus of each roots is: $\max|\xi_1| = 1.00000, \max|\xi_2| = 1.00000$.

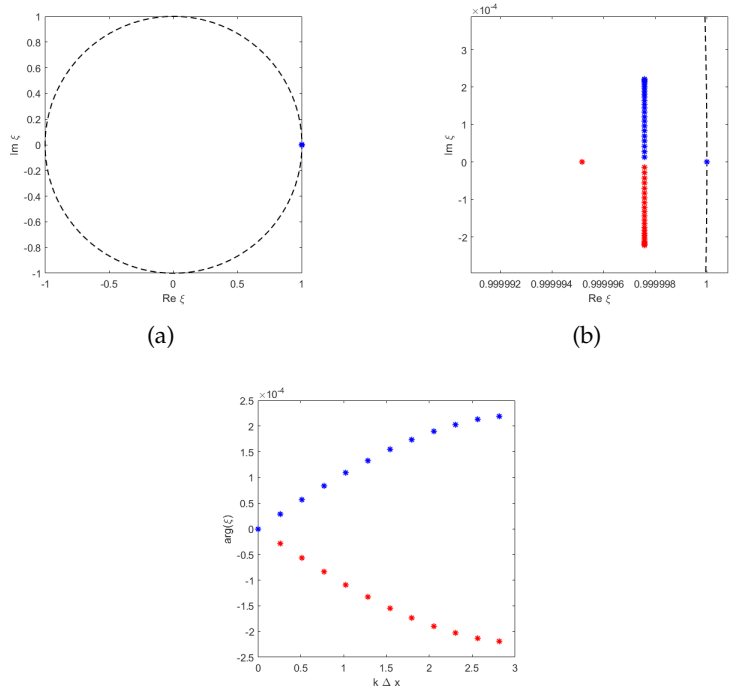

(a) (b)

(c)

FIGURE A.9: (a)-(b) The roots of $p(\xi)$ and (c) the argument, with $\Delta x = 0.02, \Delta t = 10^{-6} \leq \Delta t_{min} = 9.8015 \cdot 10^{-5}$. The maximum is choose $Z = 3$. The maximum of the modulus of each roots is: $\max|\xi_1| = 1.00000, \max|\xi_2| = 1.00000$.

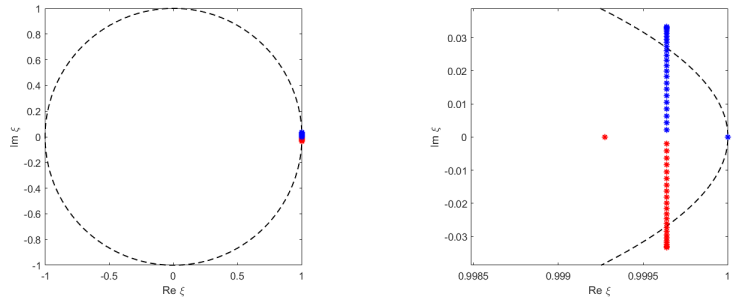

(a) (b)

FIGURE A.10: (a)-(b) The roots of $p(\xi)$ and (c) the argument, with $\Delta x = 0.02, \Delta t = 1.5 \cdot 10^{-4} \geq \Delta t_{min} = 9.8015 \cdot 10^{-5}$. The maximum is choose $Z = 3$. The maximum of the modulus of each roots is: $\max|\xi_1| = 1.00019, \max|\xi_2| = 1.00019$.

Appendix B

Numerical scheme of GK-1D with slip BCs

B.0.1 Numerical scheme

All the main results of Section 5.4 have been obtained by numerical approaches. Here we briefly comment them.

The numerical solution of the problem given by Eqs. (5.47) can be obtained by using the explicit finite difference method (FDM): let us, therefore, consider the one dimensional spatial domain $\Omega_x = [0,1]$ and the time interval $\Omega_t = [0, t_{max}]$. The solutions $\vartheta(x,t), h(x,t)$ are consequently defined as

$$\begin{aligned} \vartheta,\, h,\, : \Omega_x \times \Omega_t &\longrightarrow \mathbb{R} \\ (x,t) &\longmapsto \vartheta(x,t), h(x,t) \end{aligned}$$

From a numerical point of view, we discretize the Cartesian product $\Omega_x \times \Omega_t$ as: for the geometric domain

$$\Omega_x : \{x_1, x_2, \ldots, x_{i-1}, x_i, x_{i+1}, \ldots x_N, x_{N+1}\}$$

and for the temporal interval

$$\Omega_t : \left\{t^1, t^2 \ldots, t^{n-1}, t^n, t^{n+1}, \ldots t^F, t^{F+1}\right\},$$

where the discrete space and time values are obtained as

$$x_i = x_1 + (i-1)\cdot \Delta x \quad i = 1, ..., N+1 \tag{B.1a}$$

$$t^n = t_1 + (n-1)\cdot \Delta t \quad n = 1, ..., F+1 \tag{B.1b}$$

with Δx and Δt, spatial and time steps respectively (here are assumed to be constant values). Hence, as in [29, 30, 98], the heat flux h is computed in the nodes $x_1, x_2 ... x_N, x_{N+1}$, while the temperature ϑ is computed in the center of the computation cell $\Omega_i = [x_i, x_{i+1}]$, i.e., in the nodes $x_{i+1/2}$: the temperature, therefore, is shifted by half space step $\Delta x/2$, as it is shown in Fig. B.1. Furthermore, no boundary conditions will be prescribed for the temperature.

Then we approximate the solutions as

$$\begin{aligned} \vartheta(x_{i+1/2}, t^n) &\simeq \vartheta^n_{i+1/2}, \\ h(x_i, t^n) &\simeq h^n_i \end{aligned}$$

We have used an forward finite difference for the time derivatives and for the prime spatial derivatives of the heat flux, while we have used an backward finite difference

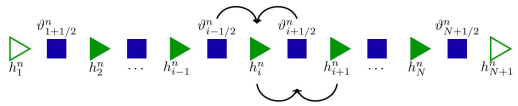

FIGURE B.1: Representation of numerical scheme of "staggered fields". The filled squares represent the temperature ϑ, and the filled triangles represent the heat flux h. Empty symbols denote boundary conditions (only for the heat flux).

for the prime spatial derivatives of the temperature and central finite difference for the second spatial derivatives of the heat flux.

Then, under this approximations we obtain the following FDM for the GK model (5.47a)-(5.47b)

$$\frac{\vartheta_{i+1/2}^{n+1}-\vartheta_{i+1/2}^{n}}{\Delta t}+\frac{Kn^2}{3}\cdot\frac{h_{i+1}^{n}-h_{i}^{n}}{\Delta x}=0$$
$$\frac{h_{i}^{n+1}-h_{i}^{n}}{\Delta t}+h_{i}^{n}+\frac{\vartheta_{i+1/2}^{n}-\vartheta_{i-1/2}^{n}}{\Delta x}-3Kn^2\cdot\frac{h_{i+1}^{n}-2h_{i}^{n}+h_{i-1}^{n}}{(\Delta x)^2}=0$$

After some rearrangements, we obtain for $i=2,...,N$

$$\vartheta_{i+1/2}^{n+1}=\vartheta_{i+1/2}^{n}-\mathcal{A}\cdot\left[h_{i+1}^{n}-h_{i}^{n}\right] \tag{B.2a}$$
$$h_{i}^{n+1}=(1-\Delta t)\,h_{i}^{n}-\nu_x\cdot\left(\vartheta_{i+1/2}^{n}-\vartheta_{i-1/2}^{n}\right)+\mathcal{B}\cdot\left[h_{i+1}^{n}-2h_{i}^{n}+h_{i-1}^{n}\right] \tag{B.2b}$$

where

$$\mathcal{A}=\nu_x\frac{Kn^2}{3},\quad \mathcal{B}=3\,Kn^2\nu_{xx},\qquad \nu_x=\frac{\Delta t}{\Delta x},\qquad \nu_{xx}=\frac{\Delta t}{(\Delta x)^2} \tag{B.3}$$

For the boundary conditions ($i=1$ and $i=N+1$), we use for the approximations of the first/second spatial derivatives: for $i=1$ an forward finite difference and for $i=N+1$ an backward finite difference. After some rearrangement we obtain

$$h_1^n=\frac{C\mathcal{D}h_2^n-\alpha\mathcal{D}^2\left[h_3^n-2h_2^n\right]}{1+C\mathcal{D}+\alpha\mathcal{D}^2}, \tag{B.4a}$$
$$h_{N+1}^n=\frac{C\mathcal{D}h_N^n-\alpha\mathcal{D}^2\left[h_{N-1}^n-2h_N^n\right]}{1+C\mathcal{D}+\alpha\mathcal{D}^2} \tag{B.4b}$$

with

$$\mathcal{D}=\frac{Kn}{\Delta x} \tag{B.5}$$

Entropy

For the entropy we have

$$\partial_t\Delta\pi+\partial_x j_s=\Sigma_s$$
$$\Delta\pi(x,0)=0$$

with $j_s=j_s(\vartheta,h)$ and $\Sigma_s=\Sigma_s(\vartheta,h)$. From a numerical point of view we compute the entropy in the internal nodes (filled squares) in Fig. B.1 and the entropy flux in the triangles. After using the forward finite difference for the time interval of the entropy and the forward finite difference for the spatial derivative of the entropy

flux, we obtain

$$\frac{\Delta\pi^{n+1}_{i+1/2} - \Delta\pi^{n}_{i+1/2}}{\Delta t} + \frac{(j_s)^n_{i+1} - (j_s)^n_i}{\Delta x} = (\Sigma_s)^n_{i+1/2}$$

from which

$$\Delta\pi^{n+1}_{i+1/2} = \Delta\pi^{n}_{i+1/2} - \nu_x \left[(j_s)^n_{i+1} - (j_s)^n_i\right] + \Delta t \cdot (\Sigma_s)^n_{i+1/2}$$

with

$$(j_s)^n_i = j_s(\vartheta^n_i, h^n_i) = j_s(\overline{\vartheta^n_i}, h^n_i)$$
$$(\Sigma_s)^n_{i+1/2} = \Sigma_s(\vartheta^n_{i+1/2}, h^n_{i+1/2}) = \Sigma_s(\vartheta^n_{i+1/2}, \overline{h^n_{i+1/2}})$$

where we replace the unknown values of $\vartheta^n_i, h^n_{i+1/2}$ with the average between the values in the nearby nodes as follow

$$\vartheta^n_i \longmapsto \overline{\vartheta^n_i} := \frac{\vartheta^n_{i+1/2} + \vartheta^n_{i-1/2}}{2}$$
$$h^n_{i+1/2} \longmapsto \overline{h^n_{i+1/2}} := \frac{h^n_{i+1} + h^n_i}{2}$$

Appendix C

Dimensionless form of bioheat model and inverse Laplace transform

C.1 Dimensionless form of bioheat model

We choose the following dimensionless variables, in order to obtain the dimensionless form of the equation (6.4)

$$\eta = A\,t, \qquad \xi = B\,x, \qquad \theta(\xi,\eta) = C\,(T - T_a), \tag{C.1}$$

wherein A, B, C are suitably chosen. Hence, the dimensionless thermal wave-like bioheat transfer equation during laser irradiation becomes

$$\frac{\tau_R^2 A^2(1+\tilde{\beta})}{T_0\,C}\cdot\partial_{\eta\eta}\theta + \frac{\tau_R A(1+\tilde{\beta}+\Lambda)}{T_0\,C}\cdot\partial_{\eta}\theta = \frac{\tau_R B^2(\alpha_t+\alpha_b)}{T_0\,C}\cdot\partial_{\xi\xi}\theta - \frac{\tau_R\tilde{\beta}w_b}{T_0\,C}\cdot\theta$$
$$+\frac{\tau_R}{T_0\,\rho_t\,c_t}q_{met} + \frac{\tau_R a I_0}{T_0\,\rho_t\,c_t}\cdot\exp\left(-a\frac{\xi}{B}\right)\cdot\left[H\left(\frac{\eta_{laser}}{A}-\frac{\eta}{A}\right)+\tau_R A\,\partial_\eta\left(H\left(\frac{\eta_{laser}}{A}-\frac{\eta}{A}\right)\right)\right], \tag{C.2}$$

where

$$\tilde{\beta} = \frac{\phi\,\rho_b\,c_b}{(1-\phi)\rho_t\,c_t}, \quad \Lambda = \tau_R\,w_b\,\tilde{\beta}, \quad \alpha_t = \frac{k_t}{\rho_t\,c_t}, \quad \alpha_b = \frac{k_b}{(1-\phi)\rho_t\,c_t}, \quad \eta_{laser} = A\,t_{laser} \tag{C.3}$$

with $[\alpha_t] = [\alpha_b] = m^2 s^{-1}$. Moreover, without loss of generality, we can assume that the coefficients of the derivatives of the temperature are equal to 1, i.e.,

$$\frac{\tau_R^2 A^2(1+\tilde{\beta})}{T_0\,C} = 1, \qquad \frac{\tau_R A(1+\tilde{\beta}+\Lambda)}{T_0\,C} = 1, \qquad \frac{\tau_R B^2(\alpha_t+\alpha_b)}{T_0\,C} = 1, \tag{C.4}$$

this imply the following expressions for the coefficients A, B and C:

$$A = \frac{1+\tilde{\beta}+\Lambda}{\tau_R\,(1+\tilde{\beta})},$$
$$B = \frac{1+\tilde{\beta}+\Lambda}{\sqrt{\tau_R\,(\alpha_t+\alpha_b)(1+\tilde{\beta})}},$$
$$C = \frac{(1+\tilde{\beta}+\Lambda)^2}{T_0\,(1+\tilde{\beta})}.$$

Using the previous coefficients in the relations (C.4), leads us to the further positions:

$$\gamma = \frac{\tau_R w_b \tilde{\beta}(1+\tilde{\beta})}{(1+\tilde{\beta}+\Lambda)^2}, \quad \Gamma = \frac{\tau_R}{T_0\,\rho_t\,c_t}, \quad \lambda = \frac{\tau_R\, a\, I_0}{T_0\,\rho_t\,c_t}, \quad g(\eta) = F(\eta) + A\tau_R \partial_\eta F(\eta),$$

with

$$F(\eta) = H\left(\frac{\eta_{laser} - \eta}{A}\right).$$

C.2 Inverse Laplace Transform

The inverse Laplace transform of the first term of equation (6.13) is obtained by applying the convolution theorem of Laplace transform,

$$\mathcal{L}^{-1}\{F(s)G(s)\} = \int_0^\eta \mathcal{L}^{-1}\left\{F(s)\right\}_{s\to u}\mathcal{L}^{-1}\{G(s)\}_{s\to\eta-u}\mathrm{d}u = \int_0^\eta F(u)\,G(\eta-u)\mathrm{d}u,$$

leading to:

$$\begin{aligned}
&\mathcal{L}^{-1}\Big\{\frac{\lambda a\hat{g}(s)B}{[a^2 - B^2(s^2+s+\gamma)]\sqrt{s^2+s+\gamma}}\exp\left(-\sqrt{s^2+s+\gamma}\,\xi\right)\Big\} = \\
&= \lambda aB\int_0^\eta \exp\left(-\frac{\eta-v}{2}\right) I_0\Big(\frac{1}{2}i\sqrt{4\gamma-1}\cdot\sqrt{(\eta-v)^2-\xi^2}\Big) H(\eta-v-\xi)\times \\
&\times \int_0^v F(u)\exp\left(-\frac{v-u}{2}\right)\Big[-\frac{A\tau_R}{B^2}\cosh\Big(\frac{\sqrt{-4B^2\gamma+4a^2+B^2}}{2B}(v-u)\Big) \\
&+ \frac{A\tau_R - 2}{\sqrt{-4B^2\gamma+4a^2+B^2}}\sinh\Big(\frac{\sqrt{-4B^2\gamma+4a^2+B^2}}{2B}(v-u)\Big)\Big]dudv \\
&- \lambda aB\int_0^\eta \exp\left(-\frac{\eta-v}{2}\right) I_0\Big(\frac{1}{2}i\sqrt{4\gamma-1}\cdot\sqrt{(\eta-v)^2-\xi^2}\Big) H(\eta-v-\xi)\times \\
&\times \Big[\frac{2A\tau_R F(0)\exp\left(-\frac{v}{2}\right)}{B\sqrt{-4B^2\gamma+4a^2+B^2}}\exp\left(-\frac{\eta}{2}\right)\sinh\Big(\frac{v}{2}\frac{\sqrt{-4B^2\gamma+4a^2+B^2}}{B}\Big)\Big]dv,
\end{aligned} \tag{C.5}$$

with

$$\hat{g}(s) = (1 + A\tau_R s)\hat{F}(s) - A\tau_R H\left(\frac{\eta_{laser}}{A}\right).$$

The inverse Laplace transform of the second term of (6.13)

$$\begin{aligned}
\mathcal{L}^{-1}\left\{\frac{1+s}{s^2+s+\gamma}\theta_0\right\} = \theta_0\exp\left(\frac{\eta}{2}\right)\Big[&\cos\Big(\frac{\eta}{2}\sqrt{4\gamma+1}\Big) + \\
&+\frac{1}{\sqrt{4\gamma+1}}\sin\Big(\frac{\eta}{2}\sqrt{4\gamma+1}\Big)\Big]
\end{aligned} \tag{C.6}$$

The inverse Laplace transform of the third term of (6.13) is given by

$$\begin{aligned}
\mathcal{L}^{-1}\left\{\frac{s}{s^2+s+\gamma}\Gamma q_{met}\right\} = \Gamma q_{met}\,\exp\left(-\frac{\eta}{2}\right)\Big[&\cos\Big(\frac{\eta}{2}\sqrt{4\gamma+1}\Big) - \\
&-\frac{1}{\sqrt{4\gamma+1}}\sin\Big(\frac{\eta}{2}\sqrt{4\gamma+1}\Big)\Big].
\end{aligned} \tag{C.7}$$

Moreover, the inverse Laplace transform of the fourth term of (6.13) is:

$$\mathcal{L}^{-1}\left\{\frac{-\lambda\,\hat{g}(s)\,B^2}{a^2-B^2\,(s^2+s+\gamma)}\exp\left(-\frac{a}{B}\xi\right)\right\}=-\lambda\,B\exp\left(-\frac{a}{B}\xi\right)\int_0^{\eta}F(u)\exp\left(-\frac{\eta-u}{2}\right)\times$$
$$\times\left[-\frac{A\tau_R}{B}\cosh\left(\frac{\sqrt{-4B^2\,\gamma+4a^2+B^2}}{2B}(\eta-u)\right)+\right.$$
$$\left.+\frac{A\tau_R-2}{\sqrt{-4B^2\,\gamma+4a^2+B^2}}\sinh\left(\frac{\sqrt{-4B^2\,\gamma+4a^2+B^2}}{2B}(\eta-u)\right)\right]\mathrm{d}u+$$
$$+\frac{2\lambda\,B\exp\left(-\frac{a}{B}\xi\right)A\,\tau_R\,F(0)}{\sqrt{-4B^2\,\gamma+4a^2+B^2}}\exp\left(-\frac{\eta}{2}\right)\sinh\left(\frac{\eta}{2}\frac{\sqrt{-4B^2\,\gamma+4a^2+B^2}}{B}\right). \tag{C.8}$$

Bibliography

[1] C. Cattaneo. “Sulla conduzione del calore”. In: *Atti del Seminario Matematico e Fisico dell’Università di Modena* 3 (1948), pp. 3–21.

[2] M. P. Vernotte and C. R. Hebd. “Les paradoxes de la theorie continue de l’equation de la chaleur”. In: *Comptes rendus* 246.22 (1958), p. 3154.

[3] J. C. Maxwell. “IV. On the dynamical theory of gases”. In: *hilosophical Transactions of the Royal Society of London* 157 (1867), pp. 49–88.

[4] R. A. Guyer and J. A. Krumhansl. “Dispersion relation for second sound in solids”. In: *Physical Review* 133.5A (1964), A1411.

[5] R. A. Guyer and J. A. Krumhansl. “Solution of the linearized phonon Boltzmann equation”. In: *Physical Review* 148.2 (1966), p. 766.

[6] R. A. Guyer and J. A. Krumhansl. “Thermal conductivity, second sound, and phonon hydrodynamic phenomena in nonmetallic crystals”. In: *Physical Review* 148.2 (1966), p. 778.

[7] D. D. Joseph and L. Preziosi. “Heat waves”. In: *Reviews of modern physics* 61.1 (1989), p. 41.

[8] A. E. Green and P. M. Naghdi. “A re-examination of the basic postulates of thermomechanics”. In: *Proceedings of the Royal Society of London. Series A: Mathematical and Physical Sciences* 432.1885 (1991), pp. 171–194.

[9] L. Onsager. “Reciprocal relations in irreversible processes. I.” In: *Physical review* 37.4 (1931), p. 405.

[10] L. Tisza. “Transport phenomena in helium II”. In: *Nature* 141.3577 (1938), pp. 913–913.

[11] L. D. Landau. “Theory of the superfluidity of Helium II”. In: *Physical Review* 60.4 (1941), 356—358.

[12] V. Peshkov. “The second sound in Helium II”. In: *Journal of Physics (Moscow)* 8 (1944), 381—389.

[13] C. T. Lane, H. A. Fairbank, and W. M. Fairbank. “Second sound in liquid helium II”. In: *Physical Review* 71.9 (1947), p. 600.

[14] R. D. Maurer and M. A. Herlin. “Second sound velocity in helium II”. In: *Physical Review* 76.7 (1949), p. 948.

[15] J. R. Pellam. “Investigations of pulsed second sound in liquid helium II”. In: *Physical Review* 75.8 (1949), p. 1183.

[16] V. Narayanamurti and R. C. Dynes. “Observation of second sound in bismuth”. In: *Physical Review Letters* 28.22 (1972), p. 1461.

[17] V. Narayanamurti and R. C. Dynes. “Ballistic phonons and the transition to second sound in solid He 3 and He 4”. In: *Physical Review B* 12.5 (1975), p. 1731.

[18] V. Narayanamurti, R. C. Dynes, and K. Andres. "Propagation of sound and second sound using heat pulses". In: *Physical Review B* 11.7 (1975), p. 2500.

[19] T. F. McNelly et al. "Heat pulses in NaF: onset of second sound". In: *Physical Review Letters* 24.3 (1970), pp. 100–102.

[20] H. E. Jackson, C. T. Walker, and T. F. McNelly. "Second sound in NaF". In: *Physical Review Letters* 25.1 (1970), pp. 26–29.

[21] H. E. Jackson and C. T. Walker. "Thermal conductivity, second sound, and phonon-phonon interactions in NaF". In: *Physical Review B* 3.4 (1971), pp. 1428–1439.

[22] A. Fehér and R. Kovács. "Analytical evaluation of non-Fourier heat pulse experiments on room temperature". In: *IFAC-PapersOnLine* 55.18 (2022), pp. 87–92.

[23] A. Fehér et al. "Size effects and beyond-Fourier heat conduction in room-temperature experiments". In: *Journal of Non-Equilibrium Thermodynamics* 46.4 (2021), pp. 403–411.

[24] A. Fehér and R. Kovács. "On the dynamic thermal conductivity and diffusivity observed in heat pulse experiments". In: *Journal of Non-Equilibrium Thermodynamics* 49.2 (2024), pp. 161–170.

[25] H. Herwig and K. Beckert. "Fourier versus non-Fourier heat conduction in materials with a nonhomogeneous inner structure". In: *Journal of Heat Transfer* 122.2 (2000), pp. 363–365.

[26] E. P. Scott, M. Tilahun, and B. Vick. "The question of thermal waves in heterogeneous and biological materials". In: *ASME International Mechanical Engineering Congress and Exposition* 16431 (1999), pp. 145–152.

[27] J. L. Auriault. "Acoustic and heat waves in Fourier thermoelastic materials". In: *International Journal of Engineering Science* 81 (2014), pp. 100–106.

[28] J. L. Auriault. "Cattaneo–Vernotte equation versus Fourier thermoelastic hyperbolic heat equation". In: *International Journal of Engineering Science* 101 (2016), pp. 45–49.

[29] R. Kovács and P. Rogolino. "Numerical treatment of nonlinear Fourier and Maxwell-Cattaneo-Vernotte heat transport equations". In: *International Journal of Heat and Mass Transfer* 150 (2020), p. 119281.

[30] C. F. Munafò, P. Rogolino, and R. Kovács. "Nonlinear thermal analysis of two-dimensional materials with memory". In: *International Journal of Heat and Mass Transfer* 219 (2024), p. 124847.

[31] K. Frischmuth and V. A. Cimmelli. "Coupling in thermo-mechanical wave propagation in NaF at low temperature". In: *Archives of Mechanics* 50.4 (1998), pp. 703–713.

[32] G. Balassa et al. "New perspectives for modelling ballistic-diffusive heat conduction". In: *Continuum Mechanics and Thermodynamics* 33 (2021), pp. 2007–2026.

[33] T. F. McNelly. "Second sound and anharmonic processes in isotopically pure alkali-halides". PhD thesis. 1974.

[34] M. Szücs. "Irreversible Thermodynamical Study of Elastic, Thermal Expansion, Rheological and Heat Conduction Processes in Solids". PhD thesis. Budapest University of Technology and Economics (Hungary), 2022.

[35] P. Ván, R. Kovács, and T. Fülöp. "Thermodynamic hierarchies of evolution equations". In: *Proceedings of the Estonian Academy of Sciences* 64.3S (2015), pp. 389–395.

[36] C. T. Walker. "Thermal conductivity of some alkali halides containing F centers". In: *Physical Review* 132.5 (1963).

[37] R. Kovács and P. Ván. "Second sound and ballistic heat conduction: NaF experiments revisited". In: *International Journal of Heat and Mass Transfer* 117 (2018), pp. 682–690.

[38] K. Mitra et al. "Experimental evidence of hyperbolic heat conduction in processed meat". In: *Journal of Heat Transfer* 117.3 (1995).

[39] W. Kaminski. "Hyperbolic heat conduction equation for materials with a nonhomogeneous inner structure". In: *Journal of Heat Transfer (Transactions of the ASME (American Society of Mechanical Engineers), Series C);(United States)* 112.3 (1990).

[40] H. Herwig and K. Beckert. "Experimental evidence about the controversy concerning Fourier or non-Fourier heat conduction in materials with a nonhomogeneous inner structure". In: *Heat and Mass Transfer* 36.5 (2000), pp. 387–392.

[41] TJ Bright and ZM Zhang. "Common misperceptions of the hyperbolic heat equation". In: *Journal of Thermophysics and Heat Transfer* 23.3 (2009), pp. 601–607.

[42] P. Ván et al. "Guyer-Krumhansl–type heat conduction at room temperature". In: *Europhysics Letters* 118.5 (2017), p. 50005.

[43] W. J. Parker et al. "Flash method of determining thermal diffusivity, heat capacity, and thermal conductivity". In: *Journal of applied physics* 32.9 (1961), pp. 1679–1684.

[44] G. I. Gróf. "Measurement of the thermal diffusivity of single- and two-layered specimens by the flash method". PhD thesis. Budapest University of Technology and Economics (Hungary), 2002.

[45] M. Fabrizio and B. Lazzari. "Stability and second law of thermodynamics in dual-phase-lag heat conduction". In: *International Journal of Heat and Mass Transfer* 74 (2014), pp. 484–489.

[46] M. Fabrizio, B. Lazzari, and V. Tibullo. "Stability and thermodynamic restrictions for a dual-phase-lag thermal model". In: *Journal of Non-Equilibrium Thermodynamics* 42.3 (2017), pp. 243–252.

[47] S. A. Rukolaine. "Unphysical effects of the dual-phase-lag model of heat conduction". In: *International Journal of Heat and Mass Transfer* 78 (2014), pp. 58–63.

[48] R. Kovács and P. Ván. "Thermodynamical consistency of the dual-phase-lag heat conduction equation". In: *Continuum Mechanics and Thermodynamics* 30.6 (2018), pp. 1223–1230.

[49] R. Kovács. "Analytic solution of Guyer-Krumhansl equation for laser flash experiments". In: *International Journal of Heat and Mass Transfer* 127 (2018), pp. 631–636.

[50] R. Kovács. "Transient non-Fourier behavior of large surface bodies". In: *International Communications in Heat and Mass Transfer* 148 (2023), p. 107028.

[51] A. J. A. Ramos et al. “Mathematical analysis and numerical simulation of the Guyer–Krumhansl heat equation”. In: *Applied Mathematical Modelling* 115 (2023), pp. 191–202.

[52] A. J. A. Ramos et al. “Non-negativity and maximum principle: Revisiting the Guyer–Krumhansl heat equation”. In: *International Journal of Heat and Mass Transfer* 211 (2023), p. 124288.

[53] R. Kovács. “Heat equations beyond Fourier: From heat waves to thermal metamaterials”. In: *Physics Reports* 1048 (2024), pp. 1–75.

[54] T. Ruggeri. “Extended thermodynamics”. In: *Springer Tracts in Natural Philosophy 37* (1993).

[55] I. Müller and T. Ruggeri. *Rational Extended Thermodynamics*. Springer Verlag, 1998.

[56] I. Müller and T. Ruggeri. *Rational extended thermodynamics*. Vol. 37. Springer Science & Business Media, 2013.

[57] W. Dreyer and H. Struchtrup. “Heat pulse experiments revisited”. In: *Continuum Mechanics and Thermodynamics* 5 (1993), pp. 3–50.

[58] D. Jou, J. Casas-Vázquez, and Georgy G. Lebon. *Extended irreversible thermodynamics*. Springer, 1996.

[59] D. Jou, G. Lebon, and J. Casas-Vázquez. *Extended irreversible thermodynamics: non-equilibrium equations of state*. Springer, 2010.

[60] G. Lebon and D. Jou J. Casas-Vázquez. *Understanding non-equilibrium thermodynamics*. Vol. 295. Springer, 2008.

[61] J. Verhás. “On the entropy current”. In: *Journal of Non-Equilibrium Thermodynamics* 8 (1983), pp. 201–206.

[62] B. Nyíri. “On the entropy current”. In: *Journal of Non-Equilibrium Thermodynamics* 16 (1991), pp. 179–186.

[63] P. Ván and T. Fülöp. “Universality in heat conduction theory: weakly nonlocal thermodynamics”. In: *Annalen der Physik* 524.8 (2012), pp. 470–478.

[64] R. Kovács and P. Ván. “Generalized heat conduction in heat pulse experiments”. In: *International Journal of Heat and Mass Transfer* 83 (2015), pp. 613–620.

[65] A. Berezovski and P. Ván. *Internal variables in thermoelasticity*. Vol. 243. Springer, 2017.

[66] M. Grmela and H. C. Öttinger. “Dynamics and thermodynamics of complex fluids. I. Development of a general formalism”. In: *Physical Review E* 56.6 (1997), p. 6620.

[67] H. C. Öttinger. “Nonequilibrium thermodynamics for open systems”. In: *Physical Review E—Statistical, Nonlinear, and Soft Matter Physics* 73.3 (2006), p. 036126.

[68] H. C. Öttinger and M. Grmela. “Dynamics and thermodynamics of complex fluids. II. Illustrations of a general formalism”. In: *Physical Review E* 56.6 (1997), p. 6633.

[69] M. Pavelka, V. Klika, and M. Grmela. *Multiscale thermo-dynamics: introduction to GENERIC*. Walter de Gruyter GmbH & Co KG, 2018.

[70] M. Szücs et al. “A case study of non-Fourier heat conduction using internal variables and GENERIC”. In: *Journal of Non-Equilibrium Thermodynamics* 47.1 (2022), pp. 31–60.

[71] V. A. Cimmelli et al. “Entropy principle and recent results in non-equilibrium theories”. In: *Entropy* 16.3 (2014), pp. 1756–1807.

[72] B. D. Coleman and W. Noll. “The thermodynamics of elastic materials with heat conduction and viscosity”. In: *Archive for Rational Mechanics and Analysi* 13 (1963), pp. 145–156.

[73] I. S. Liu. “Method of Lagrange multipliers for exploitation of the entropy principle”. In: *Archive for Rational Mechanics and Analysis* 46 (1972), pp. 131–148.

[74] V. Triani et al. “Exploitation of the second law: Coleman–Noll and Liu procedure in comparison”. In: *Journal of non-equilibrium thermodynamics* 33 (2008), pp. 47–60.

[75] V. A. Cimmelli, F. Oliveri, and V. Triani. “Exploitation of the entropy principle: Proof of Liu theorem if the gradients of the governing equations are considered as constraints”. In: *Journal of mathematical physics* 52.2 (2011).

[76] S. R. De Groot and P. Mazur. *Non-equilibrium thermodynamics*. Courier Corporation, 2013.

[77] C. Truesdell. *Rational Thermodynamics*. (McGraw-Hill New York, 1969.

[78] I. Müller. “On the entropy inequality”. In: *Archive for Rational Mechanics and Analysis* 26 (1967), pp. 118–141.

[79] I. Müller. “Zum paradoxon der wärmeleitungstheorie”. In: *Zeitschrift für Physik* 198.4 (1967), pp. 329–344.

[80] T. Ruggeri. “Symmetric-hyperbolic system of conservative equations for a viscous heat conducting fluid”. In: *Acta Mechanica* 47.3 (1983), pp. 167–183.

[81] I. S. Liu and I. Müller. “Extended thermodynamics of classical and degenerate ideal gases”. In: *Archive for rational mechanics and analysis* 83.4 (1983), pp. 285–332.

[82] T. Ruggeri, I. S. Liu, and I. Müller. “Relativistic thermodynamics of gases”. In: *Annals of Physics* 169 (1986), p. 191.

[83] H. Grad. “On the kinetic theory of rarefied gases”. In: *Communications on pure and applied mathematics* 2.4 (1949), pp. 331–407.

[84] D. Jou, J. Casas-Vázquez, and G. Lebon. “Extended irreversible thermodynamics of heat transport: A brief introduction”. In: *Proceedings of the Estonian Academy of Sciences* 57.3 (2008).

[85] J. Casas-Vázquez and D. Jou. “Temperature in non-equilibrium states: a review of open problems and current proposals”. In: *Reports on Progress in Physics* 66.11 (2003), p. 1937.

[86] G. Lebon et al. “Weakly Nonlocal and Nonlinear Heat Transport in Rigid Solids”. In: *Journal of Non-Equilibrium Thermodynamics* 23 (1998), pp. 176–191.

[87] G. Lebon et al. “Heat conduction at low temperature: A non-linear generalization of the Guyer-Krumhansl equation”. In: *Periodica Polytechnica Chemical Engineering* 41.2 (1997), pp. 185–196.

[88] D. Jou and V. A. Cimmelli. “Constitutive equations for heat conduction in nanosystems and nonequilibrium processes: an overview”. In: *Communications in Applied and Industrial Mathematics* 7.2 (2016), pp. 196–222.

[89] G. A. Maugin and W. Muschik. “Thermodynamics with internal variables. Part I. General concepts”. In: (1994).

[90] W. Muschik. "Internal Variables in Non-Equilibrium Thermodynamics". In: *Journal of non-equilibrium thermodynamics* 15.2 (1990), pp. 127–137.

[91] G. A. Maugin. "On the thermomechanics of continuous media with diffusion and/or weak nonlocality". In: *Archive of applied mechanics* 75 (2006), pp. 723–738.

[92] J. R. Rice. "Inelastic constitutive relations for solids: an internal-variable theory and its application to metal plasticity". In: *Journal of the Mechanics and Physics of Solids* 19.6 (1971), pp. 433–455.

[93] J. Kestin. "Internal variables in the local-equilibrium approximation". In: *Journal of non-equilibrium thermodynamics (Print)* 18.4 (1993), pp. 360–379.

[94] W. Muschik. "Comment to J. Kestin: Internal variables in the local-equilibrium approximation". In: (1993).

[95] V. A. Cimmelli. "On the causality requirement for diffusive-hyperbolic systems in non-equilibrium thermodynamics". In: *J. Non-Equilib. Thermodyn* 29 (2004), pp. 125–139.

[96] S. Salsa. *Equazioni a derivate parziali: Metodi, modelli e applicazioni*. Vol. 98. Springer, 2016.

[97] H. M. James. "Some extensions of the flash method of measuring thermal diffusivity". In: *Journal of Applied Physics* 51.9 (1980), pp. 4666–4672.

[98] A. Rieth, R. Kovács, and T. Fülöp. "Implicit numerical schemes for generalized heat conduction equations". In: *International Journal of Heat and Mass Transfer* 126 (2018), pp. 1177–1182.

[99] J. Weickert, B. M. T. H. Romeny, and M. A. Viergever. "Efficient and reliable schemes for nonlinear diffusion filtering". In: *IEEE transactions on image processing* 7.3 (1998), pp. 398–410.

[100] J. Weickert. "Nonlinear diffusion scale-spaces: From the continuous to the discrete setting". In: *ICAOS'96: 12th International Conference on Analysis and Optimization of Systems Images, Wavelets and PDEs Paris, June 26–28, 1996*. Springer. 1996, pp. 111–118.

[101] J. Weickert. "A review of nonlinear diffusion filtering". In: *International conference on scale-space theories in computer vision*. Springer. 1997, pp. 1–28.

[102] W. H. Press. *Numerical recipes 3rd edition: The art of scientific computing*. Cambridge university press, 2007.

[103] E. I. Jury, L. Stark, and V. V. Krishnan. "Inners and stability of dynamic systems". In: *IEEE Transactions on Systems, Man, and Cybernetics* 10 (1976), pp. 724–725.

[104] C. I. Christov and P. M. Jordan. "Heat conduction paradox involving second-sound propagation in moving media". In: *Physical review letters* 94.15 (2005), p. 154301.

[105] C. I. Christov. "On frame indifferent formulation of the Maxwell–Cattaneo model of finite-speed heat conduction". In: *Mechanics research communications* 36.4 (2009), pp. 481–486.

[106] A. Morro. "Modelling of elastic heat conductors via objective rate equations". In: *Continuum Mechanics and Thermodynamics* 30 (2018), pp. 1231–1243.

[107] P. L. Kapitza. "Heat transfer and superfluidity of helium II". In: *Physical Review* 60.4 (1941), p. 354.

[108] L. Dresner. "Transient heat transfer in superfluid helium—part II". In: *Advances in Cryogenic Engineering: Volume 29*. Springer, 1984, pp. 323–333.

[109] KR Atkins and DV Osborne. "The velocity of second sound below 1 K". In: *The London, Edinburgh, and Dublin Philosophical Magazine and Journal of Science* 41.321 (1950), pp. 1078–1081.

[110] T. Fülöp et al. "Thermodynamical extension of a symplectic numerical scheme with half space and time shifts demonstrated on rheological waves in solids". In: *Entropy* 22.2 (2020), p. 155.

[111] A. Pozsár et al. "Four spacetime dimensional simulation of rheological waves in solids and the merits of thermodynamics". In: *Entropy* 22.12 (2020), p. 1376.

[112] A. Quarteroni and S. Quarteroni. *Numerical models for differential problems*. Vol. 2. Springer, 2009.

[113] B. Straughan. *Heat waves*. Vol. 177. Springer Science & Business Media, 2011.

[114] V. A. Cimmelli. "Different Thermodynamic Theories and Different Heat Conduction Laws." In: *Journal of Non-Equilibrium Thermodynamics* 34.4 (2009), pp. 299–333.

[115] G. Lebon. "Heat conduction at micro and nanoscales: a review through the prism of extended irreversible thermodynamics". In: *Journal of Non-Equilibrium Thermodynamics* 39.1 (2014), pp. 35–59.

[116] G. Chen. "Non-Fourier phonon heat conduction at the microscale and nanoscale". In: *Nature Reviews Physics* 3.8 (2021), pp. 555–569.

[117] G. Benenti et al. "Non-Fourier heat transport in nanosystems". In: *La Rivista del Nuovo Cimento* 46.3 (2023), pp. 105–161.

[118] A. Sellitto, V. A. Cimmelli, and D. Jou. *Mesoscopic theories of heat transport in nanosystems*. Vol. 6. Springer, 2016.

[119] H. Machrafi. *Extended non-equilibrium thermodynamics: from principles to applications in nanosystems*. CRC Press, Boca Raton (USA), 2019.

[120] M. Di Domenico, D. Jou, and A. Sellitto. "Nonlinear heat waves and some analogies with nonlinear optics". In: *International Journal of Heat and Mass Transfer* 156 (2020), p. 119888.

[121] M. Di Domenico, D. Jou, and A. Sellitto. "Heat-flux dependence of the speed of nonlinear heat waves: Analogies with the Kerr effect in nonlinear optics". In: *International Journal of Thermal Sciences* 161 (2021), p. 106719.

[122] Y. Guo and M. Wang. "Phonon hydrodynamics and its applications in nanoscale heat transport". In: *Physics Reports* 595 (2015), pp. 1–44.

[123] M. Sciacca et al. "Heat solitons and thermal transfer of information along thin wires". In: *International Journal of Heat and Mass Transfer* 155 (2020), p. 119809.

[124] M. Sỳkora et al. "Multiscale heat transport with inertia and thermal vortices". In: *Physica Scripta* 98.10 (2023), p. 105234.

[125] J. Tur-Prats et al. "Microscopic origin of heat vorticity in quasi-ballistic phonon transport". In: *International Journal of Heat and Mass Transfer* 226 (2024), p. 125464.

[126] S. L. Sobolev. "Heat conduction equation for systems with an inhomogeneous internal structure". In: *Journal of engineering physics and thermophysics* 66.4 (1994), pp. 436–440.

[127] S. L. Sobolev. "Local non-equilibrium transport models". In: *Physics-Uspekhi* 40.10 (1997), p. 1043.

[128] S. L. Sobolev. "Nonlocal two-temperature model: Application to heat transport in metals irradiated by ultrashort laser pulses". In: *International Journal of Heat and Mass Transfer* 94 (2016), pp. 138–144.

[129] X. Chen et al. "Thermal storage analysis of a foam-filled PCM heat exchanger subjected to fluctuating flow conditions". In: *Energy* 216 (2021), p. 119259.

[130] A. NematpourKeshteli et al. "Enhancing PCMs thermal conductivity: A comparison among porous metal foams, nanoparticles and finned surfaces in triplex tube heat exchangers". In: *Applied Thermal Engineering* 212 (2022), p. 118623.

[131] S. Zhang et al. "Experimental study on heat transfer characteristics of metal foam/paraffin composite PCMs in large cavities: Effects of material types and heating configurations". In: *Applied Energy* 325 (2022), p. 119790.

[132] M. S. Mongiovì, D. Jou, and M. Sciacca. "Non-equilibrium thermodynamics, heat transport and thermal waves in laminar and turbulent superfluid helium". In: *Physics Reports* 726 (2018), pp. 1–71.

[133] M. Sỳkora et al. "On the relations between large-scale models of superfluid helium-4". In: *Physics of Fluids* 33.12 (2021).

[134] D. Jou, M. S. Mongiovì, and M. Sciacca. "Hydrodynamic equations of anisotropic, polarized and inhomogeneous superfluid vortex tangles". In: *Physica D: Nonlinear Phenomena* 240.3 (2011), pp. 249–258.

[135] M. Y. Shang et al. "Heat vortex in hydrodynamic phonon transport of two-dimensional materials". In: *Scientific Reports* 10.1 (2020), p. 8272.

[136] T. Rossing. *Springer handbook of acoustics*. Springer Science & Business Media, 2007.

[137] K K. Zhukovsky. "Violation of the maximum principle and negative solutions for pulse propagation in Guyer–Krumhansl model". In: *International Journal of Heat and Mass Transfer* 98 (2016), pp. 523–529.

[138] P. Ván. "Weakly nonlocal irreversible thermodynamics—the Guyer–Krumhansl and the Cahn–Hilliard equations". In: *Physics Letters A* 290.1-2 (2001), pp. 88–92.

[139] B. Y. Cao and Z. Y. Guo. "Equation of motion of a phonon gas and non-Fourier heat conduction". In: *Journal of Applied Physics* 102.5 (2007).

[140] D. Y. Tzou. *Macro-to microscale heat transfer: the lagging behavior*. John Wiley & Sons, 2014.

[141] D. G. Cahill et al. "Nanoscale thermal transport. II. 2003–2012". In: *Applied physics reviews* 1.1 (2014).

[142] Y. Dong. *Dynamical analysis of non-Fourier heat conduction and its application in nanosystems*. Springer, 2015.

[143] A. Sellitto, V. A. Cimmelli, and D. Jou. "Linear and Nonlinear Heat-Transport Equations. In: Mesoscopic Theories of Heat Transport in Nanosystems. SEMA SIMAI Springer Series". In: vol. 6. Cham: Springer International Publishing, 2016, pp. 31–51.

[144] S. Lepri, R. Livi, and A. Politi. "Heat conduction in chains of nonlinear oscillators". In: *Physical review letters* 78.10 (1997), p. 1896.

[145] C. W. Chang et al. "Breakdown of Fourier's law in nanotube thermal conductors". In: *Physical review letters* 101.7 (2008), p. 075903.

[146] Y. C. Hua and B. Y. Cao. "The effective thermal conductivity of ballistic–diffusive heat conduction in nanostructures with internal heat source". In: *International Journal of Heat and Mass Transfer* 92 (2016), pp. 995–1003.

[147] Y. Guo and M. Wang. "Phonon hydrodynamics for nanoscale heat transport at ordinary temperatures". In: *Physical Review B* 97.3 (2018), p. 035421.

[148] G. Fugallo et al. "Ab initio variational approach for evaluating lattice thermal conductivity". In: *Physical Review B—Condensed Matter and Materials Physics* 88.4 (2013), p. 045430.

[149] W. Li et al. "ShengBTE: A solver of the Boltzmann transport equation for phonons". In: *Computer Physics Communications* 185.6 (2014), pp. 1747–1758.

[150] J. H. Zou and B. Y. Cao. "Phonon thermal properties of graphene on h-BN from molecular dynamics simulations". In: *Applied Physics Letters* 110.10 (2017).

[151] J. He et al. "Orbitally driven giant thermal conductance associated with abnormal strain dependence in hydrogenated graphene-like borophene". In: *npj Computational Materials* 5.1 (2019), p. 47.

[152] A. Sellitto, V. A. Cimmelli, and D. Jou. "Mesoscopic Description of Boundary Effects and Effective Thermal Conductivity in Nanosystems: Phonon Hydrodynamics. In: Mesoscopic Theories of Heat Transport in Nanosystems. SEMA SIMAI Springer Series". In: vol. 6. Cham: Springer International Publishing, 2016, pp. 53–89.

[153] A. Beardo et al. "Phonon hydrodynamics in frequency-domain thermoreflectance experiments". In: *Physical Review B* 101.7 (2020), p. 075303.

[154] I. Bochicchio, F. Giannetti, and A. Sellitto. "Heat transfer at nanoscale and boundary conditions". In: *Zeitschrift für angewandte Mathematik und Physik* 73.4 (2022), p. 147.

[155] G. Chen. *Nanoscale energy transport and conversion: a parallel treatment of electrons, molecules, phonons, and photons*. Oxford university press, 2005.

[156] A. Sellitto, F. X. Alvarez, and D. Jou. "Second law of thermodynamics and phonon-boundary conditions in nanowires". In: *Journal of Applied Physics* 107.6 (2010).

[157] A. Sellitto, F. X. Alvarez, and D. Jou. "Temperature dependence of boundary conditions in phonon hydrodynamics of smooth and rough nanowires". In: *Journal of Applied Physics* 107.11 (2010).

[158] L. Wu. "A slip model for rarefied gas flows at arbitrary Knudsen number". In: *Applied Physics Letters* 93.25 (2008).

[159] W. Muschik and H. Ehrentraut. "An Amendment to the Second Law". In: *Journal of Non-Equilibrium Thermodynamics* 21.2 (1996), pp. 175–192.

[160] H. H. Pennes. "Analysis of tissue and arterial blood temperatures in the resting human forearm". In: *Journal of applied physiology* 1.2 (1948), pp. 93–122.

[161] K. Khanafer et al. "Flow and heat transfer in biological tissues: application of porous media theory". In: *Emerging Topics in Heat and Mass Transfer in Porous Media: From Bioengineering and Microelectronics to Nanotechnology* (2008), pp. 237–259.

[162] M. M. Chen and K. R. Holmes. "Microvascular contributions in tissue heat transfer". In: *Annals of the New York Academy of Sciences* 335.1 (1980), pp. 137–150.

[163] M. Wulff. "The energy conservation equation for living tissue". In: *IEEE transactions on biomedical engineering* 6 (1974), pp. 494–495.

[164] H. G. Klinger. "Heat transfer in perfused biological tissue—I: General theory". In: *Bulletin of Mathematical Biology* 36 (1974), pp. 403–415.

[165] . Nakayama, F. Kuwahara, and W. Liu. "A macroscopic model for countercurrent bioheat transfer in a circulatory system". In: *Journal of Porous Media* 12.4 (2009).

[166] A. Nakayama and F. Kuwahara. "A general bioheat transfer model based on the theory of porous media". In: *International Journal of Heat and Mass Transfer* 51.11-12 (2008), pp. 3190–3199.

[167] Y. Xuan and W. Roetzel. "Bioheat equation of the human thermal system". In: *Chemical Engineering & Technology: Industrial Chemistry-Plant Equipment-Process Engineering-Biotechnology* 20.4 (1997), pp. 268–276.

[168] Ping P. Yuan. "Numerical analysis of temperature and thermal dose response of biological tissues to thermal non-equilibrium during hyperthermia therapy". In: *Medical engineering & physics* 30.2 (2008), pp. 135–143.

[169] R. Brinkmann et al. "Investigations on laser thermokeratoplasty". In: *Lasers and Light in Ophthalmology* 6.4 (1994), pp. 259–270.

[170] J. A. L. Molina et al. "Effect of the thermal wave in radiofrequency ablation modeling: an analytical study". In: *Physics in Medicine & Biology* 53.5 (2008), p. 1447.

[171] M. K. Loze and C. D. Wright. "Temperature distributions in laser-heated biological tissue with application to birthmark removal". In: *Journal of Biomedical Optics* 6.1 (2001), pp. 74–85.

[172] H. Ahmadikia et al. "Analytical solution of non-Fourier and Fourier bioheat transfer analysis during laser irradiation of skin tissue". In: *Journal of mechanical science and technology* 26 (2012), pp. 1937–1947.

[173] P. Wongchadakul, P. Rattanadecho, and T. Wessapan. "Implementation of a thermomechanical model to simulate laser heating in shrinkage tissue (effects of wavelength, laser irradiation intensity, and irradiation beam area)". In: *International Journal of Thermal Sciences* 134 (2018), pp. 321–336.

[174] R. W. Waynant. *Lasers in medicine*. CRC press, 2011.

[175] M. Abramowitz and I. A. Stegun. *Handbook of Mathematical Functions with Formulas, Graphs, and Mathematical Tables*. Vol. 55. US Government Printing Office, 1964.

[176] S. Katayama. *Fundamentals and details of laser welding*. Springer, 2020.

[177] K. E. Min, J. W. Jang, and C. Kim. "New Frontiers of Laser Welding Technology." In: *Applied Sciences (2076-3417)* 13.3 (2023).

[178] M. Dal and R. Fabbro. "An overview of the state of art in laser welding simulation". In: *Optics & Laser Technology* 78 (2016), pp. 2–14.

[179] K. M. Hong and Y. C. Shin. "Prospects of laser welding technology in the automotive industry: A review". In: *Journal of Materials Processing Technology* 245 (2017), pp. 46–69.

[180] M. A. Mohr et al. "jYCaMP: an optimized calcium indicator for two-photon imaging at fiber laser wavelengths". In: *Nature methods* 17.7 (2020), pp. 694–697.

[181] V. Rimal, S. Shishodia, and P. K. Srivastava. "Novel synthesis of high-thermal stability carbon dots and nanocomposites from oleic acid as an organic substrate". In: *Applied Nanoscience* 10.2 (2020), pp. 455–464.

[182] X. Na. *Laser welding*. BoD–Books on Demand, 2010.

[183] Z. Ren et al. "State of the art in defect detection based on machine vision". In: *International Journal of Precision Engineering and Manufacturing-Green Technology* 9.2 (2022), pp. 661–691.

[184] L. E. dos Santos Paes et al. "Lack of fusion mitigation in directed energy deposition with laser (DED-L) additive manufacturing through laser remelting". In: *Journal of Manufacturing Processes* 73 (2022), pp. 67–77.

[185] A. Ghosh and H. Chattopadhyay. "Mathematical modeling of moving heat source shape for submerged arc welding process". In: *The International Journal of Advanced Manufacturing Technology* 69 (2013), pp. 2691–2701.

[186] H. Kaplan and F. Alexander. "Influence of the beam profile formulation when modeling fiber-guided laser welding". In: *Journal of Laser Applications* 23.4 (2011).

[187] A. K. Unni and M. Vasudevan. "Determination of heat source model for simulating full penetration laser welding of 316 LN stainless steel by computational fluid dynamics". In: *Materials Today: Proceedings* 45 (2021), pp. 4465–4471.

[188] C. Moroşanu and B. Satco. "Qualitative and quantitative analysis for a nonlocal and nonlinear reaction-diffusion problem with in-homogeneous Neumann boundary conditions." In: *Discrete & Continuous Dynamical Systems-Series S* 16.1 (2023).

[189] K. Oussaid and A. El Ouafi. "A three-dimensional numerical model for predicting the Weld bead geometry characteristics in laser overlap welding of low carbon galvanized steel". In: *Journal of Applied Mathematics and Physics* 7.10 (2019), p. 2169.

[190] m. Ragavendran and M. Vasudevan. "Effect of laser and hybrid laser welding processes on the residual stresses and distortion in AISI type 316L (N) stainless steel weld joints". In: *Metallurgical and Materials Transactions B* 52.4 (2021), pp. 2582–2603.

[191] R. Fakir, N. Barka, and J. Brousseau. "Case study of laser hardening process applied to 4340 steel cylindrical specimens using simulation and experimental validation". In: *Case Studies in Thermal Engineering* 11 (2018), pp. 15–25.

[192] V. K. Sarila et al. "Characterization of microstructural anisotropy in 17–4 PH stainless steel fabricated by DMLS additive manufacturing and laser shot peening". In: *Transactions of the Indian Institute of Metals* 76.2 (2023), pp. 403–410.

[193] V. V. Belyaev and O. B. Kovalev. "Simulation of one method of laser welding of metal plates involving an SHS-reacting powder mixture". In: *International Journal of Heat and Mass Transfer* 52.1-2 (2009), pp. 173–180.

[194] N. C. Giglio and N. M. Fried. "Computational simulations for infrared laser sealing and cutting of blood vessels". In: *IEEE Journal of Selected Topics in Quantum Electronics* 27.4 (2020), pp. 1–8.

[195] E. Majchrzak, B. Mochnacki, and J. Suchy. "Kinetics of casting solidification-an inverse approach". In: *Scientific Research of the Institute of Mathematics and Computer Science* 6.1 (2007), pp. 169–178.

[196] A. Miranville and C. Moroşanu. "A Qualitative Analysis of a Nonlinear Second-Order Anisotropic Diffusion Problem with Non-homogeneous Cauchy–Stefan–Boltzmann Boundary Conditions". In: *Applied Mathematics & Optimization* 84 (2021), pp. 227–244.

[197] A. Mohan, D. Ceglarek, and M. Auinger. "Numerical modelling of thermal quantities for improving remote laser welding process capability space with consideration to beam oscillation". In: *The International Journal of Advanced Manufacturing Technology* 123.3 (2022), pp. 761–782.

[198] M. Ciesielski and B. Mochnacki. "Comparison of approaches to the numerical modelling of pure metals solidification using the control volume method". In: *International Journal of Cast Metals Research* (2019).

[199] E. Nuñez del Prado, N. Challamel, and V. Picandet. "Discrete and nonlocal solutions for the lattice Cattaneo–Vernotte heat diffusion equation". In: *Mathematics and Mechanics of Complex Systems* 9.4 (2022), pp. 367–396.

[200] T. DebRoy et al. "Metallurgy, mechanistic models and machine learning in metal printing". In: *Nature Reviews Materials* 6.1 (2021), pp. 48–68.

[201] C. Pyo et al. "A Study on the Enhanced Process of Elaborate Heat Source Model Parameters for Flux Core Arc Welding of 9% Nickel Steel for Cryogenic Storage Tank". In: *Journal of Marine Science and Engineering* 10.12 (2022), p. 1810.

[202] J. A. Goldak and M. Akhlaghi. *Computational welding mechanics*. Springer Science & Business Media, 2005.

[203] J. Chen et al. "Influence mechanism of process parameters on the interfacial characterization of selective laser melting 316L/CuSn10". In: *Materials Science and Engineering: A* 792 (2020), p. 139316.

[204] R. Escribano-García, P. Álvarez, and D. Marquez-Monje. "Calibration of finite element model of titanium laser welding by fractional factorial design". In: *Journal of Manufacturing and Materials Processing* 6.6 (2022), p. 130.

[205] S. D'Ostuni, P. Leo, and G. Casalino. "FEM simulation of dissimilar aluminum titanium fiber laser welding using 2D and 3D Gaussian heat sources". In: *Metals* 7.8 (2017), p. 307.

[206] S. A. Tsirkas, P. Papanikos, and T. Kermanidis. "Numerical simulation of the laser welding process in butt-joint specimens". In: *Journal of materials processing technology* 134.1 (2003), pp. 59–69.

[207] y. w. Park and s. Rhee. "Process modeling and parameter optimization using neural network and genetic algorithms for aluminum laser welding automation". In: *The International Journal of Advanced Manufacturing Technology* 37 (2008), pp. 1014–1021.

[208] P. Mascenik and S. Pavlenko. "Determination of stress and deformation during laser welding of aluminum alloys with the PC support." In: *MM Science Journal* (2020).

[209] M. Balbaa et al. "A novel post-processing approach towards improving hole accuracy and surface integrity in laser powder bed fusion of IN625". In: *The International Journal of Advanced Manufacturing Technology* 119.9 (2022), pp. 6225–6234.

[210] T. Xu et al. "Significant reinforcement of mechanical properties in laser welding aluminum alloy with carbon nanotubes added". In: *Carbon* 191 (2022), pp. 36–47.

[211] D. Ma et al. "Online porosity prediction in laser welding of aluminum alloys based on a multi-fidelity deep learning framework". In: *Journal of Intelligent Manufacturing* 35.1 (2024), pp. 55–73.

[212] H. Ramiarison et al. "Parameter optimization for laser welding of dissimilar aluminum alloy: 5052-H32 and 6061-T6 considering wobbling technique". In: *The International Journal of Advanced Manufacturing Technology* (2022), pp. 1–17.

List of publications

This thesis represents the collection of different works and study topics. The reader can find references to the key documents of the thesis below

1) C. F. MUNAFÒ, P. ROGOLINO, R. KÓVÁC : *Nonlinear thermal analysis of two-dimensional materials with memory*, International Journal of Heat and Mass Transfer, 219, pp. 124847, 2024. https://doi.org/10.1016/j.ijheatmasstransfer.2023.124847

2) R. KÓVÁC, P. ROGOLINO : *Numerical treatment of nonlinear Fourier and Maxwell-Cattaneo-Vernotte heat transport equations*, International Journal of Heat and Mass Transfer, 150, pp. 119281, 2020. https://doi.org/10.1016/j.ijheatmasstransfer.2019.119281

3) C. F. MUNAFÒ, R. KÓVÁC, MÁTYAS SZÜCS: *Investigating the whirling heat current density in the Guyer–Krumhansl equation*, 2024, arXiv preprint https://doi.org/10.48550/arXiv.2405.09199

4) C. F. MUNAFÒ : *Analysis of nonlinear Guyer-Krumhansl heat equation*, submitted in International Journal of Engineering Science.

5) C. F. MUNAFÒ, P. ROGOLINO, D. JOU: *Comparison of two nonlinear formulations of the Maxwell-Cattaneo equation in heat pulse transmission*, accepted to Applied Mathematical Modelling, 2024.

6) C. F. MUNAFÒ, P. ROGOLINO, A. SELLITTO *Heat transfer at nano-scale and boundary conditions: A comparison between the Guyer-Krumhansl model and the Thermomass theory*, preprint submitted to International Journal of Thermal Science, 2024.

7) C. F. MUNAFÒ, A. PALUMBO, M. VERSACI: *An inhomogeneous model for laser welding of industrial interest*, Mathematics, 11(15), pp. 3357, 2023, https://doi.org/10.3390/math11153357

In the following, there is a list of references to other published papers dealing with other topics (mostly related to kinetic theory, Turing patterns in biologic and ecologic models, non-linear heat propagation in volcanic activity and in biological tissue)

1) M. MENALE, C. F. MUNAFÒ: *A kinetic framework under the action of an external force field: Analysis and application in epidemiology*, Chaos, Solitons & Fractals, 174, pp. 113801, 2023. https://doi.org/10.1016/j.chaos.2023.113801

2) M. MENALE, C. F. MUNAFÒ, F. OLIVERI: *A nonconservative kinetic framework with logistic growth for modeling the coexistence in a multi-species ecological system*, submitted in The European Physical Journal Plus.

3) G. INFERRERA, C. F. MUNAFÒ, F. OLIVERI, P. ROGOLINO: *Reaction-diffusion models of crimo-taxis in a street*, Applied Mathematics and Computation, 467, pp. 128504. https://doi.org/10.1016/j.amc.2023.128504

4) R. DELLA MARCA, A. D'ONOFRIO, C. F. MUNAFÒ, R. TRAVAGLINI: *Spatio–temporal chaos induced by all–ages vaccine hesitation in SIR model*, preprint.

5) C. GODANO, C. F. MUNAFÒ, F. OLIVERI: *The birth of a volcano: A nonlinear convective model for rock melting at the asthenosphere—Lithosphere boundary*, Applications in Engineering Science, 18, pp. 100179, 2024. https://doi.org/10.1016/j.apples.2024.100179

6) C. F. MUNAFÒ, P. ROGOLINO: *Analysis of a Hyperbolic Heat Transfer Model in Blood-perfused Biological Tissues with Laser Heating*, Journal of Applied and Computational Mechanics, 8(4), pp. 1398-1406, 2022,https://doi.org/10.22055/jacm.2022.40152.3528

7) M. GORGONE, C.F. MUNAFÒ, A. PALUMBO, P. ROGOLINO: *A thermodynamical suspension model for blood*, Meccanica, pp. 1–13, 2024. https://doi.org/10.1007/s11012-024-01859-2

8) C. F. MUNAFÒ, P. ROGOLINO, R. KÓVÁC: *Non-linear ballistic heat conduction in one dimension*, preprint.